AD NUMBER

AD880348

LIMITATION CHANGES

TO:

Approved for public release; distribution is unlimited.

FROM:

**Distribution authorized to U.S. Gov't. agencies and their contractors;
Administrative/Operational Use; DEC 1970. Other requests shall be referred to Air Force Materials Lab., Wright-Patterson AFB, OH 45433.**

AUTHORITY

AFML ltr 21 May 1973

AFML-TR-70-154

Evaluation Of The Fused Slurry Silicide Coating Considering Component Design And Reuse

BARRY G. FITZGERALD

EUGENE L. RUSERT

MCDONNELL DOUGLAS ASTRONAUTICS COMPANY • EAST

TECHNICAL REPORT AFML-TR-70-154

December 1970

Air Force Materials Laboratory
Air Force Systems Command
Wright-Patterson Air Force Base, Ohio

NOTICE

When Government drawings, specifications, or other data are used for any purpose other than in connection with a definitely related Government procurement operation, the United States Government thereby incurs no responsibility nor any obligation whatsoever; and the fact that the Government may have formulated, furnished, or in any way supplied the said drawings, specifications, or other data, is not to be regarded by implication or otherwise as in any manner licensing the holder or any other person or corporation, or conveying any rights or permission to manufacture, use, or sell any patented invention that may in any way be related thereto.

This document is subject to special export controls and each transmittal to foreign governments or foreign nationals may be made only with prior approval of the Metals and Ceramics Division (MAM), Air Force Materials Laboratory, Wright-Patterson Air Force Base, Ohio 45433.

It contains technology identifiable with items on the strategic embargo lists excluded from export under the United States Export Control Act, as implemented by AFR 310-2 and AFSC 80-20.

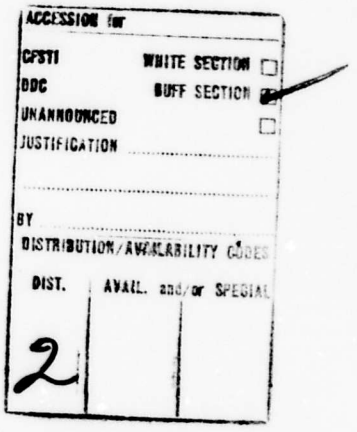

THE DISTRIBUTION OF THIS REPORT IS LIMITED BECAUSE IT CONTAINS TECHNOLOGY IDENTIFIABLE WITH ITEMS ON THE STRATEGIC EMBARGO LISTS EXCLUDED FROM EXPORT UNDER THE U.S. EXPORT CONTROL ACT, AS IMPLEMENTED BY AFR 310-2 AND AFSC 80-20.

Copies of this report should not be returned unless return is required by security considerations, contractual obligations, or notice on a specific document.

BLANK PAGE

Evaluation Of The Fused Slurry Silicide Coating Considering Component Design And Reuse

BARRY G. FITZGERALD

EUGENE L. RUSERT

FOREWORD

This Final Technical Report was prepared by the McDonnell Douglas Astronautics Company - Eastern Division under USAF Contract No. F33(615)-67-C-1574 and covers work performed during the period 1 June 1967 to 31 December 1969. This contract was initiated under Project No. 7312, Task 731201, "Metals Surface Protection". This work was administered under direction of the Air Force Materials Laboratory, Air Force Systems Command, Wright-Patterson Air Force Base, Ohio, with Mr. Norman Geyer (LLP) as the Project Engineer.

The authors wish to acknowledge the contributions of the following personnel that were responsible for the program's efforts that fell in their respective field of endeavor: L. Barton and R. Withers (Manufacturing), F. Hotze and J. Storm (Strength), A. Lopatin (Design), D. Link and D. Jones (Testing), T. Allen and R. Durnil (Emittance Measurements), and R. Wilcox and D. Moore (Metallography). Dr. T. Grimm was the Laboratory Test Manager for this program.

This report was submitted by the authors on 19 June 1970.

This technical report has been reviewed and is approved.

I. Perlmutter
Chief, Metals Branch
Metals and Ceramics Division
Air Force Materials Laboratory

ABSTRACT

The reuse capabilities of coated columbium were investigated. The investigation included: (1) the establishment of baseline coating performance and mechanical properties; (2) the effects of design on the performance of coating columbium; (3) the effects of local coating damage; and (4) the effects of multiple reentry flights on the coating emittance.

The coating used was Sylvania's R-512E and the columbium alloy used was Cb-752. The selected time, temperature, pressure and stress relationships which constitute the test conditions for practically all of the testing performed do not represent a specific vehicle; however, the conditions are representative of classes of high L/D reentry vehicles and missions, which makes the evaluation meaningful.

The major observation from the mechanical property tests was that the R-512E coating has no significant adverse effect on the properties of the Cb-752 base metal. Basic oxidation tests were conducted with results from each substantiating good coating reproducibility.

The coated columbium heat shield specimens proved to have an extensive reuse capability of greater than 100 flights. The effects of design on reuse are directly related to the pressure environment. Designs containing faying surfaces were intolerant to pressure environments representative of external vehicle pressures. Under the test conditions of this program, reuse was limited by creep deformation and not coating failure.

The structural integrity of coated columbium is very tolerant of the local absence of coating.

Using an integral cavity specimen and the temperature-pressure conditions defined in this program, the total normal emittance of R-512E coated Cb-752 at 2400°F was found to decrease from approximately 0.85 to 0.75 after exposure to 20 simulated reentries. A modified R-512E coating with a higher chromium and iron content maintained an emittance of 0.85 or higher.

TABLE OF CONTENTS

LIST OF ILLUSTRATIONS

LIST OF ILLUSTRATIONS (Cont)

LIST OF ILLUSTRATIONS (Cont)

LIST OF ILLUSTRATIONS (Cont)

LIST OF ILLUSTRATIONS (Cont)

LIST OF ILLUSTRATIONS (Cont)

LIST OF ILLUSTRATIONS (Cont)

LIST OF ILLUSTRATIONS (Cont)

LIST OF ILLUSTRATIONS (Cont)

LIST OF TABLES

LIST OF TABLES (Cont)

SECTION I

INTRODUCTION

The fused slurry silicide coatings developed by the Sylvania High Temperature Composites Laboratory under an Air Force-sponsored program are proving to be the best and most useful coating systems developed to date. For coated columbium, long and reproducible coating lives have been obtained in static, reduced pressure and slow cyclic testing. Because the coating is formed from a chemically agressive molten phase, it has a high potential for the reproducible coating of complex parts containing faying surfaces and areas of limited access.

The purpose of this program was the evaulation of Sylvania's fused slurry silicide coating at representative reentry and hypersonic cruise flight conditions.

The major considerations for the evaluation were:

(1) The selection, design and fabrication of test specimens that were truly representative of coated refractory metal heat shields.

(2) The simulation of the important environmental flight conditions simultaneously during the testing phases.

The test specimens were fabricated and coated by the best possible techniques within the state-of-the-art to assure the most accurate results and conclusions.

The most important environmental conditions were temperature, air pressure, stress or load factors, and time. Simultaneous simulation of these conditions appeared particularly important for meaningful testing in cases where coated joints and faying surfaces are "worked" as the structure is loaded and unloaded at the flight pressures and temperatures. Simulation of the important environmental conditions was also important to determine accurately how local coating damage and subsequent breakdown of protection would affect the structural integrity of a flight component.

Sylvania's R-512E (60Si-20Cr-20Fe) fused slurry silicide coating and single annealed Cb-752 columbium alloy were selected as the coating/metal system for evaluation.

Major objectives of this program were:

(a) Establish baseline oxidation resistance data for the coated columbium alloy and mechanical property data for the bare and coated columbium alloy.

(b) Determine the protective life of the coating when applied to specimens having joints and faying surfaces representative of typical advanced flight vehicle hardware.

(c) Determine the effects of local coating damage on the structural integrity of representative hardware.

(d) Evaluate the effectiveness of repair coatings when applied to representative hardware.

(e) Determine the effects of multiple reentry flights on the total normal emittance of R-512E coated Cb-752.

(f) Utilize nondestructive test methods to predict coating performance and assist in interpreting test results.

(g) Identify coating process and hardware design limitations and recommend methods of improvement.

A large number of the representative heat shield specimens were tested at simulated flight conditions which combined temperature, pressure, stress and time profiles to answer the question of reuseability. This was the most complete simulation of flight on specimens representative of hardware conducted to date. A systems approach to failure was utilized which was something new for coated refractory metals. The criteria established for failure was structural deformation rather than the first sighting of columbium oxide. The ability to maintain structural integrity after local loss of coating was investigated which is an aspect that must be fully substantiated for coated columbium to be used with confidence under temperature, pressure, and stress conditions typical for a space vehicle reentry.

The emittance of coated columbium was measured while being subjected to varying temperature-pressure conditions in a profile fashion simulating reentry. The effect of multiple reentry cycles on coating emittance was determined. This was the most complete determination of coated columbium emittance during and under reuse conducted to date. Effects of coating batch to batch, chemistry and thickness variations were also determined.

SECTION II

TEST DEFINITION

This section describes the variables that were defined before the testing began. In this section are: Materials, which includes columbium alloy selection and coating selection; Specimen Design, which includes baseline specimen design and panel design; Test Conditions; and Testing Equipment and Calibration for various tests conducted.

1. MATERIALS

The columbium alloy selected was single annealed Cb-752. This alloy was selected because of industrial experience, availability, fabrication, strength and weldability. The coating selected was Sylvania's R-512E.

(a) Columbium Alloy Selection

Four of the most promising second generation columbium alloys presently being evaluated in the aerospace industry are D-43 (Cb-10W-1Zr-0.1C), Cb-752 (Cb-10W-2.5Zr), FS-85 (Cb-28Ta-10W-1Zr) and C-129Y (Cb-10W-10Hf-0.1Y). These alloys have been used for, or studied for use as, thrust chambers, heat shields and structures for advanced reentry vehicles.

These relatively high strength alloys have presented several fabrication problems because of their susceptibility to embrittlement under various conditions. Included under fabrication are the four categories of: (1) heat treatment, (2) welding, (3) machining and (4) forming.

Unlike steels, for example, heat treatments are not used to improve the strength of these alloys after they have been processed at the mill. Several producers have, though, incorporated annealing treatments which can be used to boost the tensile strength, but when excessive strengths are obtained, the ductility usually decreases to a minimum, and perhaps, to an unacceptable value. Refractory metal producers supply the columbium alloy sheets either in the stress-relieved or recrystallized condition. The fully recrystallized condition is usually specified; and, for this reason, the fully recrystallized properties are used for design purposes.

These alloys can be welded by the tungsten inert gas (TIG) electron beam (EB) and resistance welding processes. The D-43 alloy is the only alloy not readily weldable. The ductile-to-brittle transition temperature (DBTT) for all four alloys is usually increased by tungsten inert gas or electron beam welding. The relatively minor effect TIG or EB welding has on the DBTT of FS-85 and C-129Y compared to that for D-43 and Cb-752 has been demonstrated in several investigations. Usually the slower welding speeds cause a greater increase in the DBTT.

Electron beam welding has been used extensively to weld these four alloys since it offers high speeds and low levels of contamination during welding. As with the TIG process, a vacuum stress relief operation may be necessary after welding to lower the level of residual stresses. These residual stresses are a result of solidification at the weld beads.

Resistance welding of these alloys has been successful, but as with all columbium alloys, great care is required to prevent electrode sticking and contamination during spot welding. Seam welding is feasible, but as yet has not been used extensively. The resultant residual stresses after resistance welding are usually low enough to make a post weld stress relief unnecessary.

All four alloys have equivalent machinability. Ordinary tool steels can be used, but it is necessary to use a lubricant/coolant to reduce the tendency to tear and gall that is characteristic of all columbium base alloys.

Forming such as shearing, blanking, bending, brake forming, drawing, etc., can be accomplished on all four alloys at room temperature, but D-43 is slightly less formable than the other three alloys. Stress-relief annealing may be required after drastic forming of the stronger alloys.

In the process of developing the second generation alloys, various solid solution hardening elements were used to increase the high temperature strength, room temperature formability, weldability or secondary creep properties. These elements also increased the density of these alloys. The density of D-43 (.325 lb/in^3) and Cb-752 (.326 lb/in^3) is relatively low when compared to FS-85 (.383 lb/in^3) and C-129Y (.343 lb/in^3).

Mechanical properties are one of the most important selection factors. Table I gives the baseline room temperature mechanical properties for D-43, Cb-752, FS-85 and C-129Y. This table shows that FS-85 has the lowest strength to density ratio of all the alloys of interest. Figures 1, 2, 3, and 4 show the effects of elevated temperature on the ultimate tensile strength (Ftu), tensile yield strength (Fty), percent elongation (%e), and Young's Modulus (E), respectively. In Figure 1, it is readily apparent that the Ftu of FS-85 goes through a minimum to maximum reversal from 800°F to 1200°F; this is in contrast to the smooth decrease in Ftu of Cb-752. In this figure it is also apparent that the rate of decrease in Ftu of all four alloys is about the same from 1800°F to 2500°F.

Table I
Room Temperature Mechanical Properties

	Condition	Ultimate tensile strength Ftu, ksi	Tensile yield strength Fty ksi	% Elongation	Value Basis	Ftu/ρ ksi/lb in^{-3}	Young's modulus 10^6, psi	Basis for Modulus	Ref.
D-43	Annealed, 18 mil gauge, transverse	85	55	14	Average	261	16.9	-	1
Cb-752	Recrystallized (single annealed)	75	60	15	Min.	230	15.02	Dyn.	2
FS-85	Recrystallized	70	50	20	Min.	182.5	20	-	3
C-129Y	Recrystallized	89.8	75.7	25	Typ.	262	16.3	Static	4

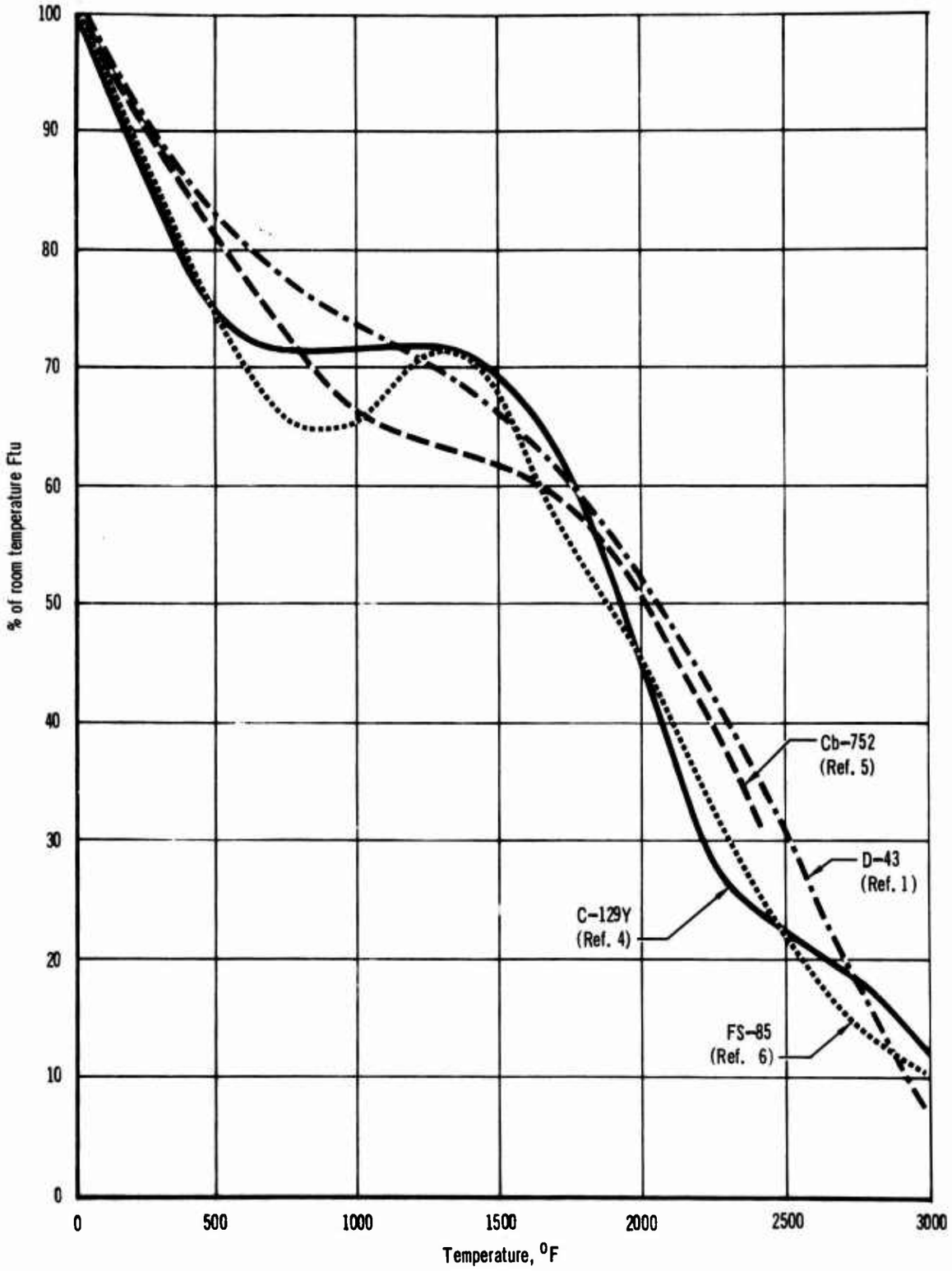

Figure 1 Effect Of Temperature On The Ftu Of D-43, Cb-752, FS-85 And C-129Y

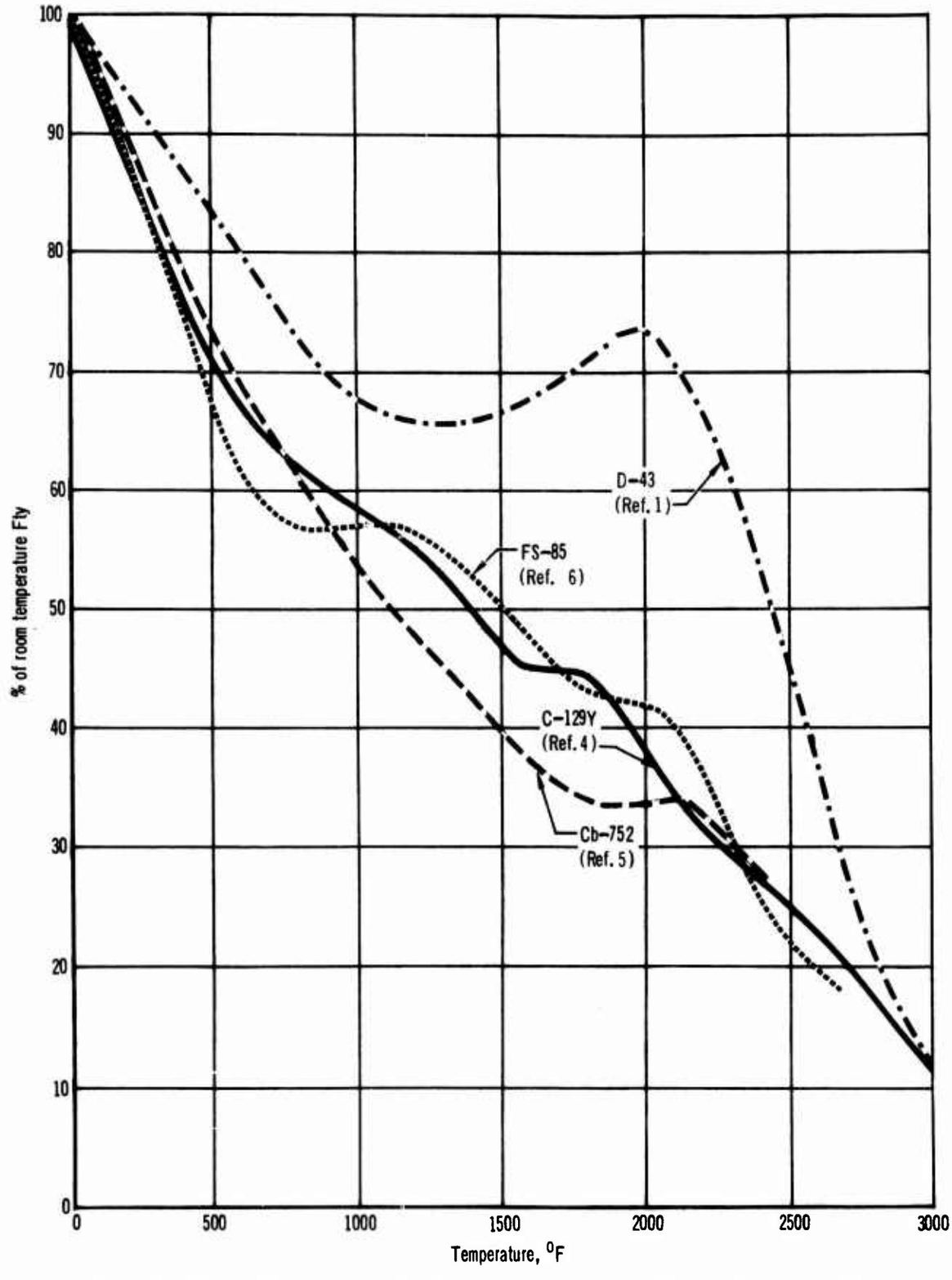

Figure 2 Effect Of Temperature On The Fty Of D–43, Cb–752, FS–85 And C–129Y

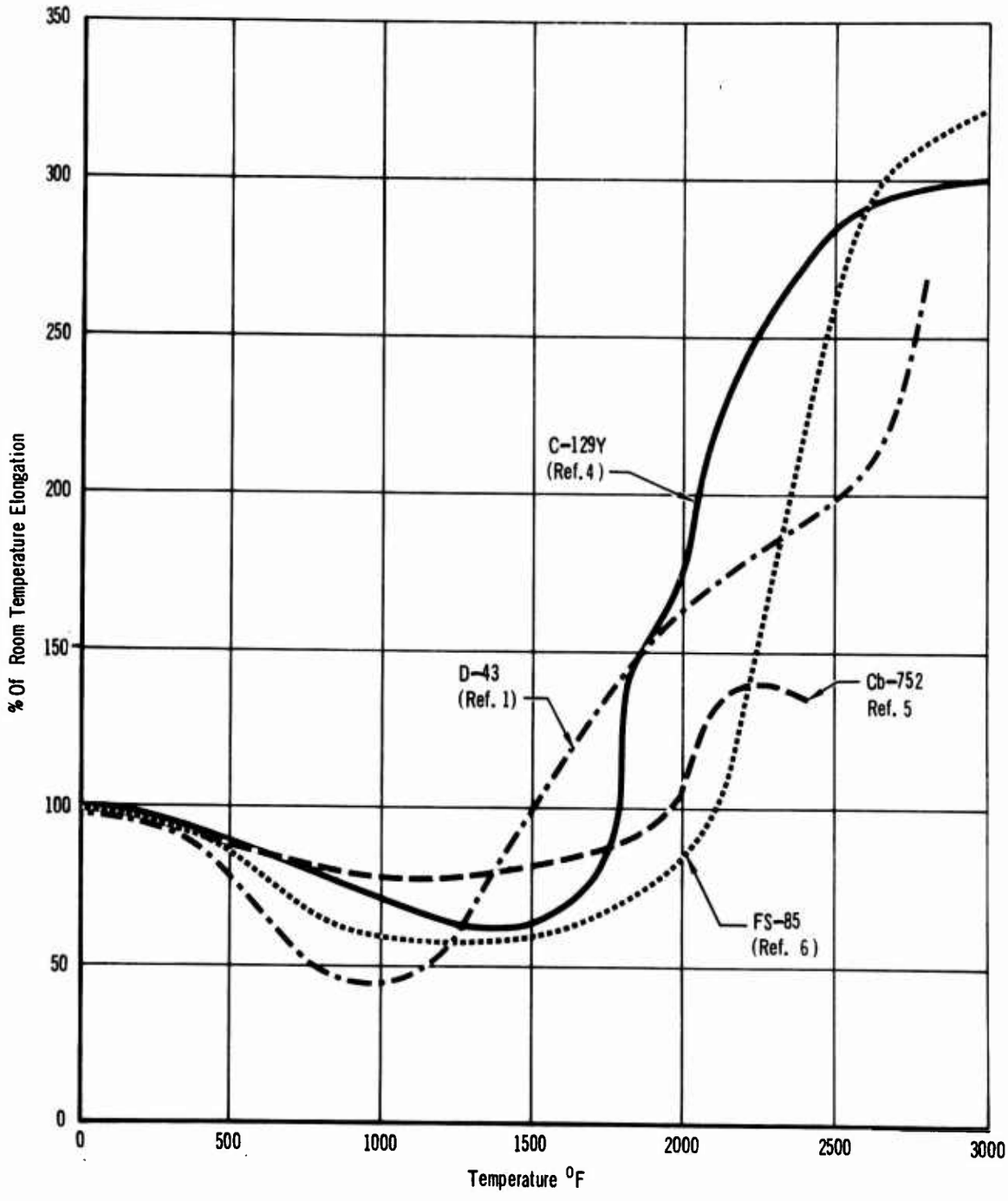

Figure 3 Effect Of Temperature On The Elongation Of D-43, Cb-752, FS-85 And C-129Y

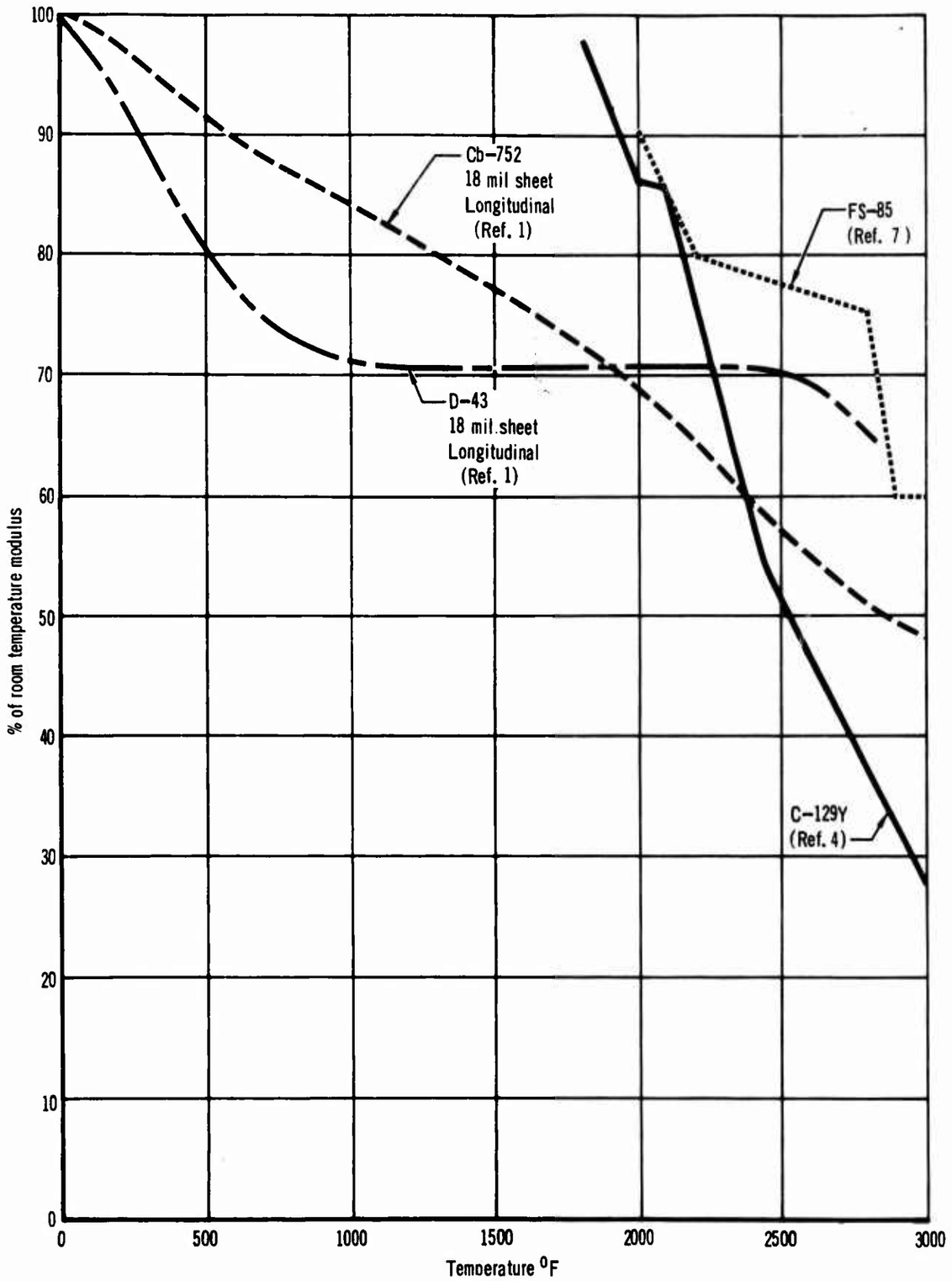

Figure 4 Effect Of Temperature On The Modulus Of D–43, Cb–752, FS–85, And C–129Y

Figure 2 shows the effect of elevated temperature on the Fty of the four alloys of interest. It is apparent that the rate of decrease in Fty is much less for D-43 than for the other three alloys, particularly in the vicinity of 2000°F. The D-43 alloy maintains the highest Fty to about 2700°F.

The effect of elevated temperature on elongation is shown in Figure 3. For all four alloys, the % elongation at first decreases reaching a minimum at 1000 to 1400°F.

The effect of temperature on the moduli of the four alloys is shown in Figure 4.

Of significant importance in the selection of any alloy is the toughness of the material over a range of temperatures. One measure of an alloy's toughness is the notched to unnotched strength ratio; materials with a ratio equal to or greater than one are defined as tough. Figure 5, shows the effect of temperature on the notched to unnotched strength ratio for two different thicknesses of D-43 and Cb-752. The only material which shows low toughness is the 12 mil D-43 sheet. As was shown in Figure 1, the bend ductile to brittle transition temperature of the four alloys can be affected to varying extents by different welding procedures. The bend ductility is also affected by the grain direction and the condition of the material. Table II gives the bend properties of Cb-752 and D-43 at three temperatures. It is apparent that D-43 shows a greater propensity for bend failure than Cb-752.

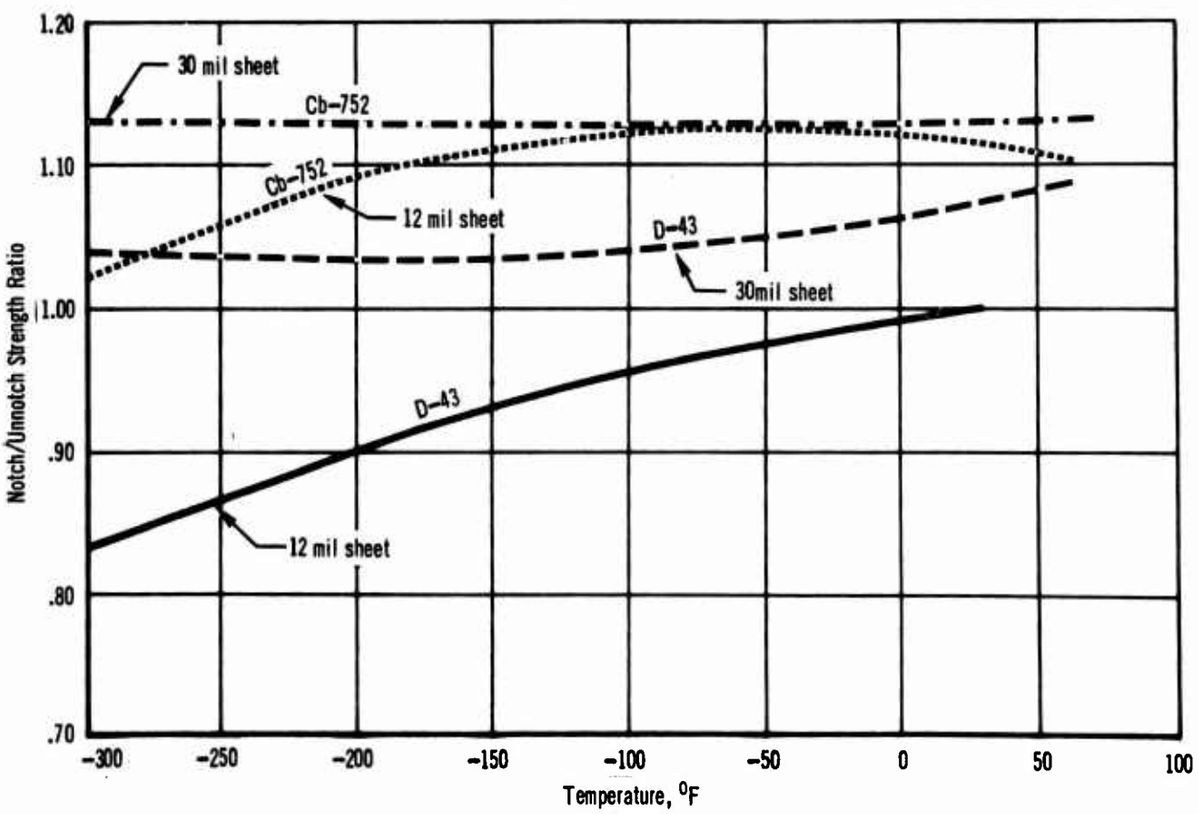

Figure 5 Notch Strength Ratio Of Cb-752 and D-43, K_t = 3 (Ref. 1)

Table II

Bend Properties Of Cb-752 And D-43 (Ref. 1)

Temp. °F	Gauge Mils	Grain Direction	Final Bend Angle After Springback (degrees) Cb-752	D-43
70	12	Trans.	84	84
-110	12	Trans.	70-74	70-71
-320	12	Trans.	44-47	19-28 F*
70	18	Trans.	89	85-87
-110	18	Trans.	83-84	87
-320	18	Trans.	63	66-69
70	18	Long.	93	94-96
-110	18	Long.	88-91	89-91
-320	18	Long.	69-71	25-34 F
70	30	Trans.	78-79	90-91
-110	30	Trans.	78-79	75-93
-320	30	Trans.	52-75 F	83

*F - indicates failure. Tests conducted with 2T radius bend and a ram speed of 1.0 in/min.

For most aerospace applications the short-time creep properties of the refractory alloys are of importance in the selection of a particular alloy. Figure 6 gives the available short time, 1% strain, creep data for D-43, Cb-752 and C-129Y. Although D-43 has better creep strength than Cb-752 it has other properties, as have been mentioned, which are drawbacks to its wide use.

The effect of aging on the mechanical properties of the four alloys is summarized in Table III. Long time exposure or cyclic exposure to temperatures in excess of 2000°F may result in a drastic decrease in the mechanical properties of D-43.

Based on the data presented in this section, Cb-752 was selected at the most promising of the four alloys. When industrial experience is also taken into account the desirability of continuing to use Cb-752 is reinforced. This alloy offers good fabricability, weldability, and machinability along with good elevated temperature strength; and it is readily available. The other three alloys, D-43, C-129Y or FS-85, possess certain individual qualities superior to Cb-752, but usually these better qualities are accompanied by inherent drawbacks such as low weldability, low formability or low strength to density ratio.

(b) Coating Selection

The fused slurry silicide coating developed by the Sylvania High Temperature Composites Laboratory is proving to be one of the best and most useful coating systems developed to date. For coated columbium, long and reproducible coating lives have been obtained in static, reduced pressure and slow cyclic testing. Because the coating is formed from a chemically

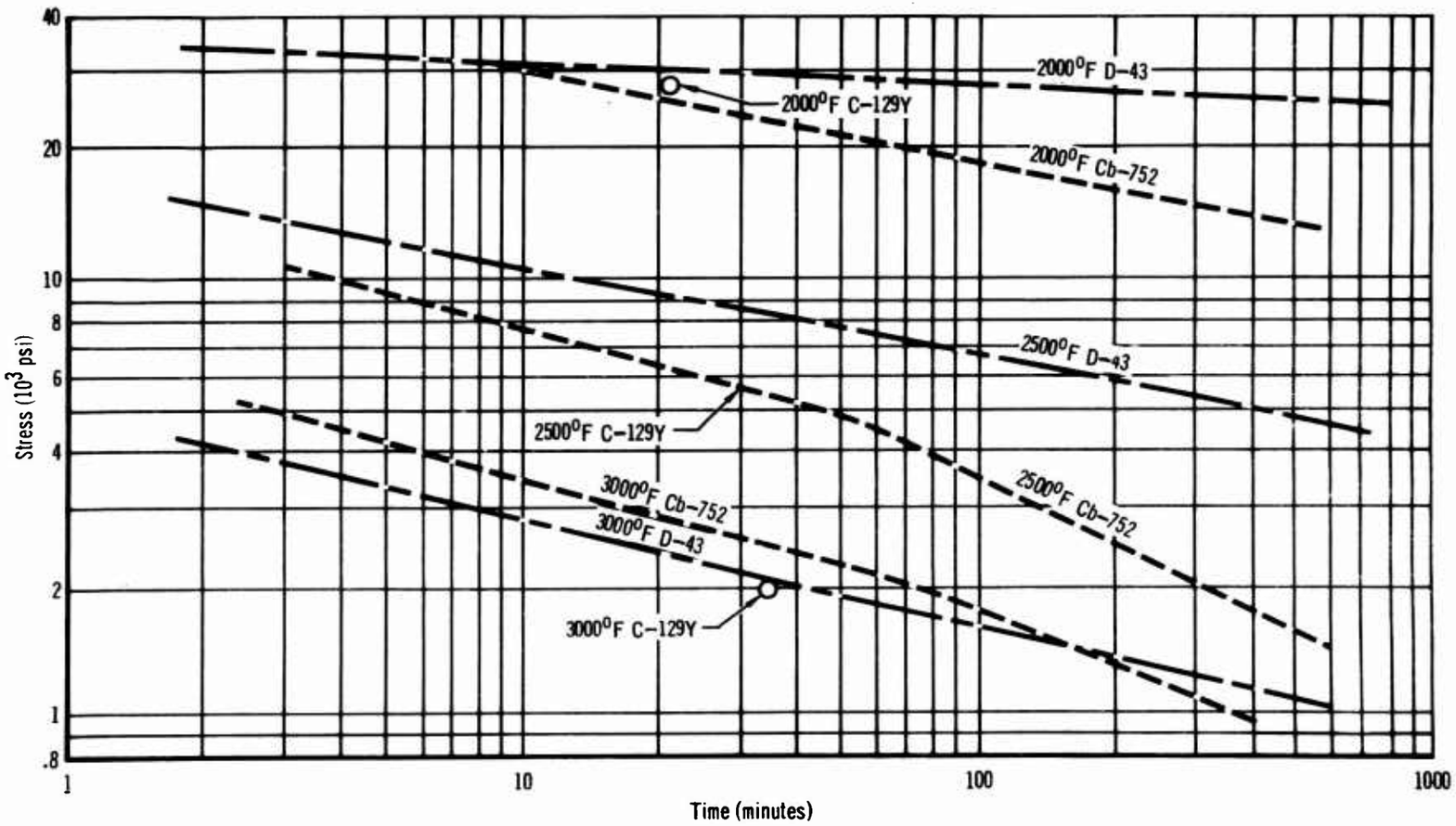

Figure 6 Creep Strength VS Time For 1% Strain For 18 Mil Gauge D-43 And Cb-752 (Ref. 1) And For C-129Y (Ref. 4)

aggressive molten phase, this coating system has a high potential for the reproducible coating of complex parts containing faying surfaces and areas of limited access.

Data generated by Sylvania under Air Force Contract AF33(615)-3272 and by other independent investigators, (References 9, 10 and 11), have established the basic protectiveness of the fused silicide coatings.

Table III

SUMMARY OF TENSILE PROPERTY RESPONSES

TO AGING (TO 1000 HOURS) (REF. 8)

Note: Arrangement is in approximate order of decreasing tensile thermal stability.

I. Little or no Response to Aging

FS-85: Good stability without definite response in tensile or shield strength or elongation in either weld or base metal at ambient or elevated temperature.

C-129Y: Like FS-85

II. Limited, Non-General Responses

Cb-752: Room temperature strength increased for all aging with a modest loss in elevated temperature strength. Yield strength response in room temperature tests imply a complex aging response whereas 1800°F yield strength responded in a classic manner. Base metal elongation did not follow strength changes, but instead became more variable with increased test temperature while weld elongation remained largely unchanged.

III. Classic Overaging and Consequent Loss of Strength for Increasing Time Temperature Exposures

D-43: Similar response for both ultimate and yield strengths. Elongation only slightly increased with decreasing strength. Weld and base metal similar in strength and aging response.

The coating selected for this program was the Si60-20Cr-20Fe composition (R-512E) in the Sylvania R-512 fused slurry silicide series. This selection was made jointly with Sylvania. The R-512E coating was selected because it produces a more uniform coating on the Cb-752 alloy than most of the other fused slurry compositions. The inherent oxidation resistance of the R-512E composition is comparable to any of the fused slurry silicides compositions developed to date. Also, there is more available data on the R-512E/Cb-752 system than on other fused slurry silicide/Cb-752 systems.

The coating and base metal characteristics which influence coating performance, such as coating thickness (maximum and minimum), minimum edge radius, and minimum base metal thickness, were discussed with Sylvania. A mutual decision established the nominal coating thickness and weight as 3.5 mils and 25 mg/cm^2, respectfully. Minimum nominal gauge thickness was established as 12 mils. Sylvania applied all fused slurry silicide coatings because of their thorough knowledge of the coating system, well developed processing techniques, and proven equipment.

A summary of available data on the properties and reliability of the coating on Cb-752 is presented in Figures 7, 8, 9 and Table IV. These data substantiated that the R-512E coating had the basic protectiveness and reuse capabilities for reentry applications.

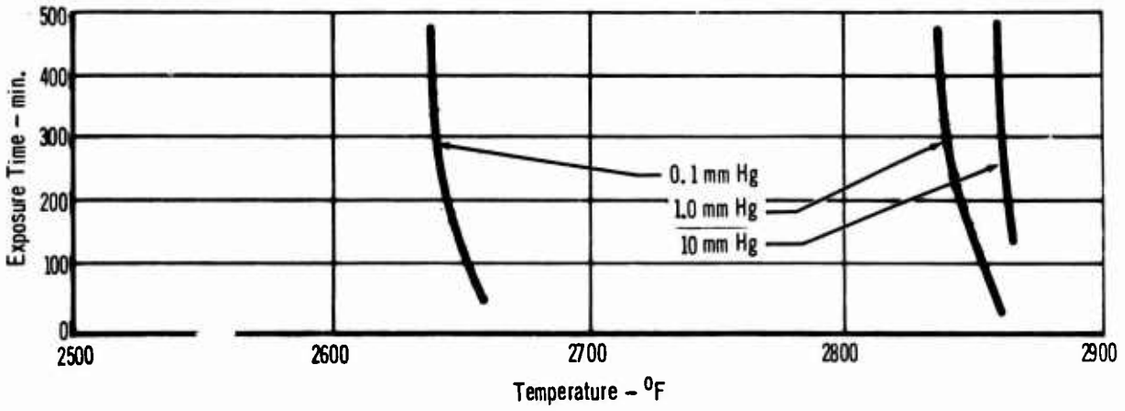

Note: Failure region is to the right of each curve.

Figure 7 Protection of Cb-752 Columbium Alloy by Sylvania R-512E Coating (Ref. 12)

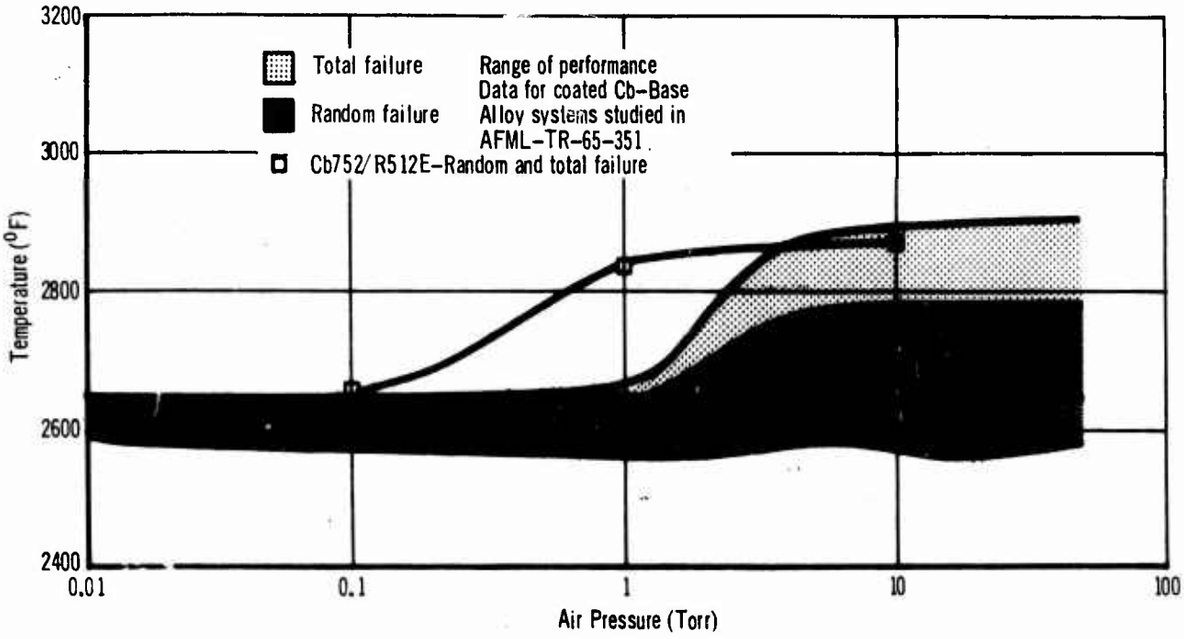

Figure 8 Maximum Temperature for 4-Hour Lifetime for Cb 752/R512E System and Coated Alloys Studied in AFML-TR-65-351

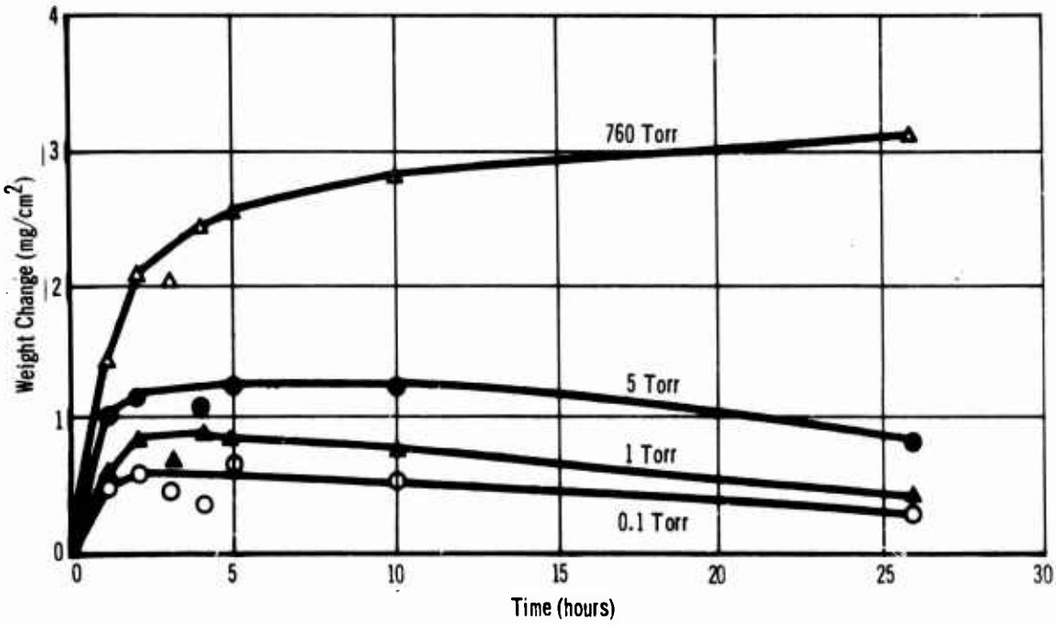

Figure 9 Weight Change vs Time at 2500°F for R512-E Coating on Cb-752 at Various Air Pressures. (Ref. 13)

Table IV

Various Oxidation and Reentry Simulation Test Data for R512-E Coated Cb-752 Columbium Alloy (Ref 13)

Cyclic Oxidation Life at 2800°F (No. 1-Hour Cycles to Failure)	Slow Cyclic Oxidation Life at 1 atm. 2500°F Maximum Temperature (No. 1-Hour Cycles to Failure)	Reentry Simulation Life (No. 1-Hour Cycles to Failure)		
		2500°F Maximum Temperature Internal Surface Profiles	2500°F Maximum Temperature External Surface Profiles	2600°F Maximum Temperature Internal Surface Profiles
9(E)	71(E), 71(E)	40+, 40+, 200+, 200+	40+, 40+, 200+, 200+ 200+,	169 (E)*

+ Test stopped. Samples not failed.
E Edge failure.
* Specimens contaminated by reaction products of first failed specimen

2. SPECIMEN DESIGN

In this section the design of base line specimens and panels is discussed.

(a) Base Line Specimens

Mechanical property and oxidation specimens were used for base line property determinations.

Mechanical property specimen configurations are shown in Figures 10, 11, 12, and 13. The specimens included tensile and elongation, creep, bend, notch sensitivity, and welded lap tensile.

Oxidation specimen designs included small coupons (1 1/2" x 3/4") for slow cycle, static, and time-temperature-pressure oxidation testing. These specimens are identical to the bend specimen shown in Figure 10. For time-temperature-pressure-stress testing 18" x 1" tensile, riveted lap tensile, and threaded fastener lap tensile specimens were used. These specimens are shown in Figures 14, 15, and 16.

All baseline specimens except for the countersunk riveted lap tensile and the threaded fasteners lap tensile were fabricated from .016 gauge Cb-752.

The countersunk riveted lap tensile and the threaded fastner lap tensile were fabricated from .035" gauge Cb-752. All specimens were manufactured in the Advanced Materials Fabrication Facility (AMFF). This facility incorporates the most modern equipment and used the same process specifications and process controls that were successfully used in the manufacturing of columbium flight hardware for the ASSET and BGRV programs.

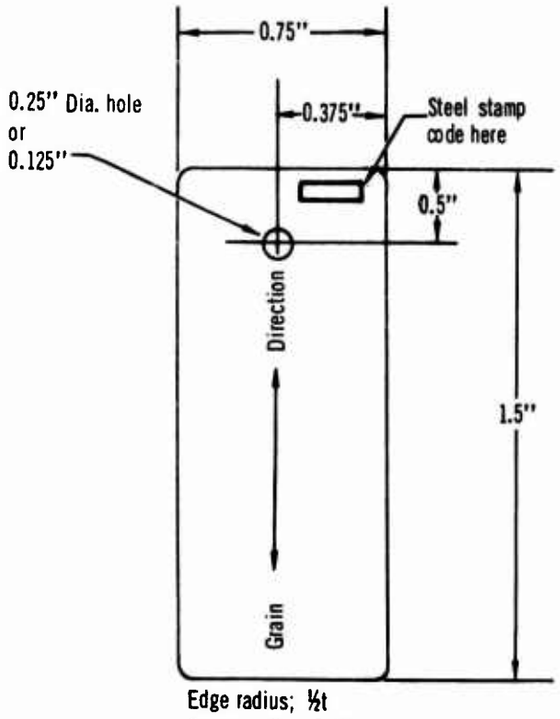

Figure 10 Oxidation And Bend Test Specimens

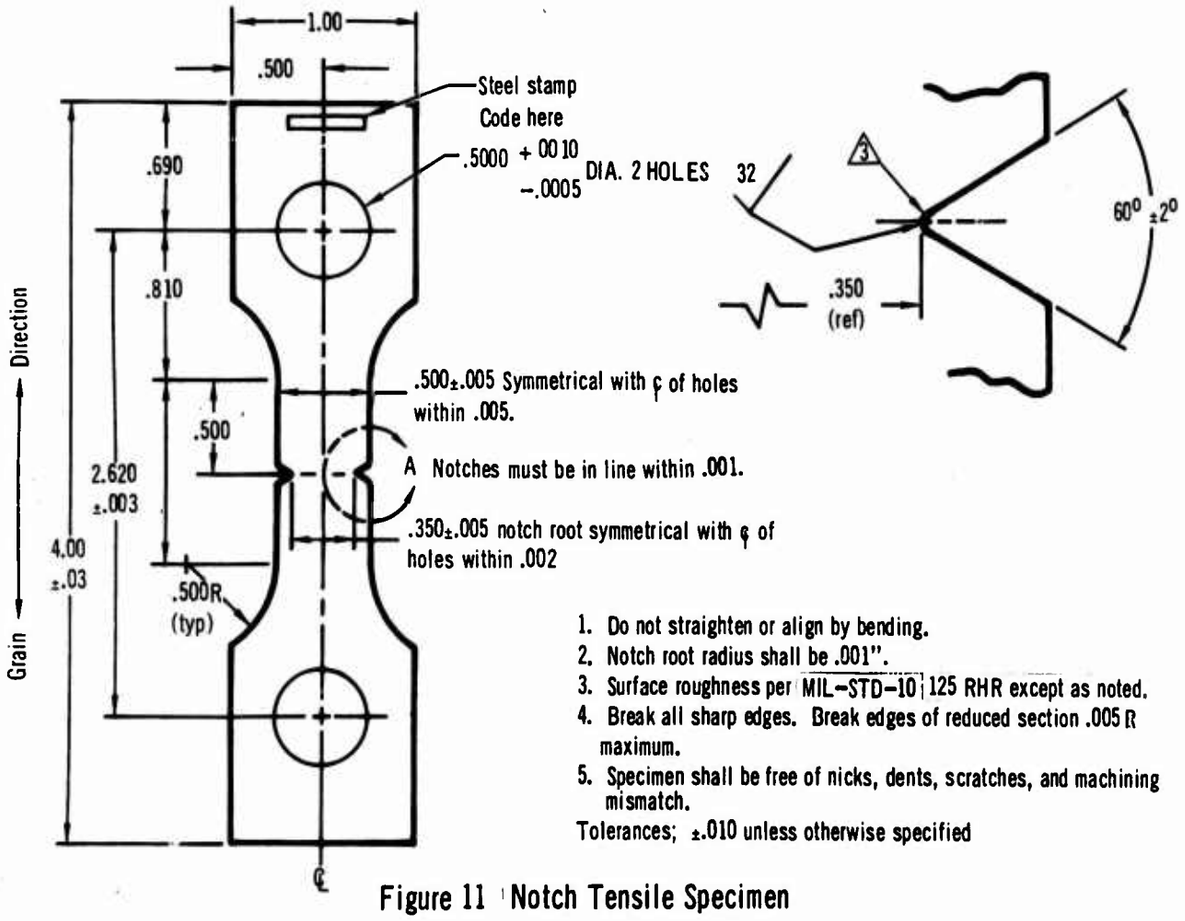

Figure 11 Notch Tensile Specimen

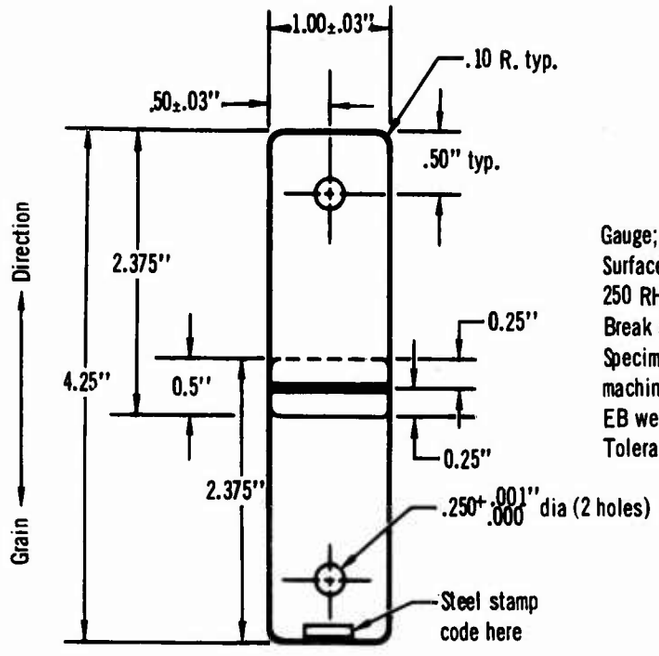

Gauge; .016" and .016"
Surface roughness per MIL-STD-10. Machined edges shall be 250 RHR
Break all sharp edges.
Specimen shall be free of nicks, dents, scratches, and machining mismatch
EB weld per P.S. 22301
Tolerances; ±.010 unless otherwise specified.

Figure 12 EB Weld Lap Tensile Specimen

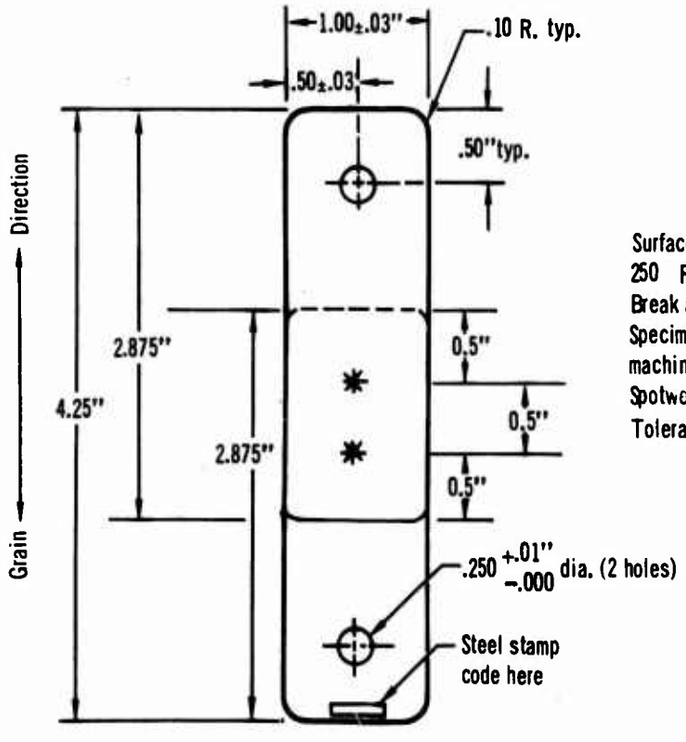

Gauge; .016" and .016"
Surface roughness per MIL-STD-10. Machined edges shall be 250 RHR
Break all sharp edges.
Specimen shall be free of necks, dents, scratches, and machining mismatch.
Spotweld per P.S. 22142
Tolerances; ±.010 unless otherwise specified.

Figure 13 Spotweld Lap Tensile Specimen

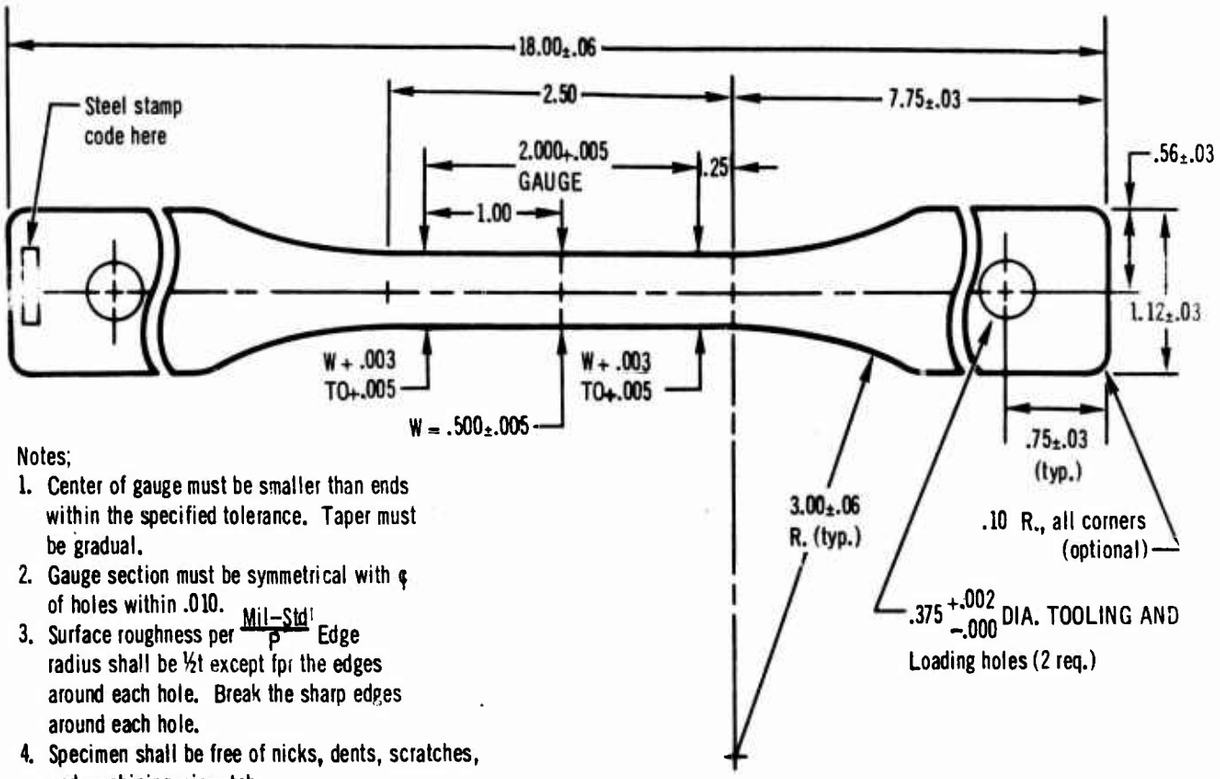

Notes;

1. Center of gauge must be smaller than ends within the specified tolerance. Taper must be gradual.
2. Gauge section must be symmetrical with ℄ of holes within .010.
3. Surface roughness per $\frac{\text{Mil-Std}}{\text{P}}$ Edge radius shall be ½t except fpr the edges around each hole. Break the sharp edges around each hole.
4. Specimen shall be free of nicks, dents, scratches, and machining mismatch

Tolerance; ±.010 unless otherwise specified

Figure 14 Stress Profile Oxidation Specimen

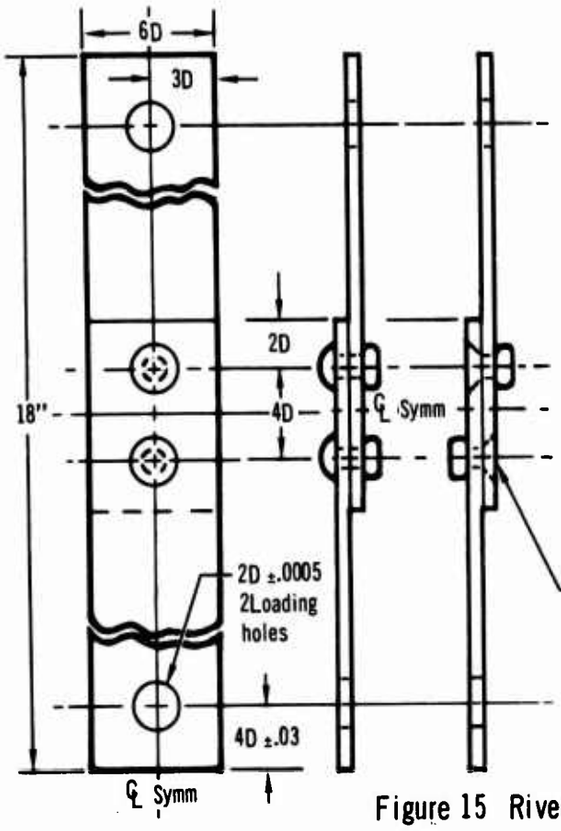

Notes

1. D = Nominal rivet diameter as specified by individual request (.125"
2. Dimensional tolerances are ±010 except as otherwise noted
3. Drill and ream rivet holes per MAC P.S. 19110 (group 2) unless otherwise required by individual request
4. Finish of machined surfaces shall be 125 RMS maximum
5. Break sharp corners and edges
6. Install rivets according to instructions of individual requiest
7. Specimens shall be symmetrical about horizontal and vertical centerlines within .010"
8. Specimens shall be free of nicks, scratches, and machining mismatch.

Alternate countersinks as shown above for flush head rivet installation

Figure 15 Riveted Single Lap–Shear Specimen

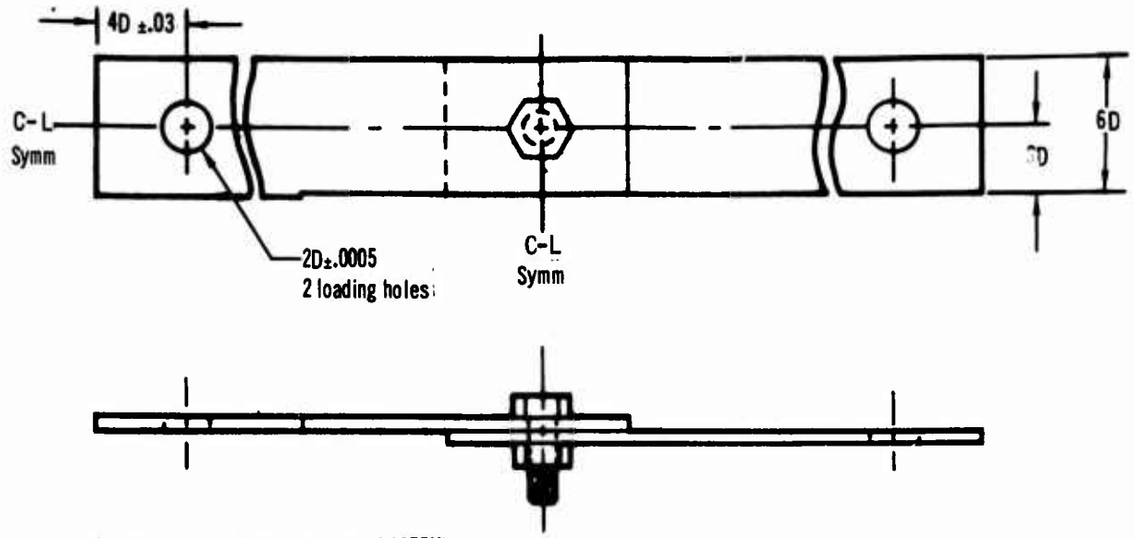

1. D = Nominal fastner diameter (.1875")
2. Dimensional tolerances are ±.010 except as otherwise noted
3. Drill and ream holes.
4. Finish of machined surfaces shall be 125 RMS maximum
5. Break sharp corners and edges
6. Specimens shall be symmetrical about horizontal and vertical centerlines within .010"
7. Specimens shall be free of nicks, scratches, and machining mismatch.

Figure 16 Threaded Fastner Single Lap-Shear Specimen

(b) Heat Shield Panel Design

Heat shield panels and their supporting structure are the components of lifting reentry and hypersonic cruise vehicles that are normally fabricated of coated refractory metals. Heat shield panels may also be the primary structure, but usually the use of cooler primary structure is more efficient. In order to maintain surface smoothness and rigidity with minimum weight, heat shield panels are fabricated from relatively thin gauge material and, almost without exception, are of a stiffened skin design. It is this stiffening that leads to faying surface and joint considerations which must be included in coating performance evaluations. Typical heat shield configurations were closely examined to select representative designs. The five general types of heat shields considered were: sandwich, corrugation-skin, monocoque, sheet-stringer, and integrally stiffened.

Sandwich structures incorporate two facing sheets separated and held in position by a low-weight core. Two commonly used cores are honeycomb and semi-structural or structural corrugations. The sandwich structure has the advantage of being rigid and, with proper support, is able to resist high bending or column compression loads efficiently. The greater limitation of the sandwich is the difficulty and cost of fabrication.

The corrugation-skin structure is also efficient, particularly for applications where the loading is predominately in one direction. It is also relatively easy to fabricate, since the joining of the corrugations to the skin is open and not blind, thus permitting the use of welding or riveting.

The monocoque surface offers economy, simplicity, and ease of fabrication, while suffering from a low strength-to-weight ratio and lack of rigidity.

The sheet-stringer panel, while not as inherently rigid as the sandwich and corrugation-skin, does provide the advantage of simplicity. The stringers are generally arranged to run in one direction only; they can be attached by either rivets or welds.

The integrally stiffened panel is simple and presents no joint or faying surface problems; however, it can be costly because of machining time and material waste. EB welding can reduce cost and material waste of integrally stiffened type designs. Structural efficiency decreases as panel size increases.

The honeycomb sandwich and integrally stiffened configurations have no faying surfaces to be protected by the oxidation resistant coating. The only joints of importance to this program would be those involved in their attachment to substructure which is usually accomplished with threaded fasteners. The coating must, of course, be compatible with the braze alloy in a honeycomb sandwich.

Variations of representative heat shield panel designs were used in determining the protection that the R-512E fused silicide coating will afford to faying surfaces and joints. Variations involve different methods of attaching the stiffener to the skin such as, resistance spot and seam, electron beam, and T.I.G. welding, and riveting.

Consistent with good practices and the state-of-the-art, the representative heat shield panel configurations selected were as follows:

(a) Single faced corrugated panels with flat topped corrugations (resistance spot and electron beam welded).

(b) Single faced corrugated panels with "V" shaped corrugations (electron beam welded).

(c) Skin-stringer panels (resistance spot and electron beam welded).

(d) Skin-Channel panel with riveted joint.

Based on the selected test conditions of stress and temperature, test specimens representative of the above heat shield panel constructions were designed. Table V summarizes the gauge(s), pitch and depth for each specimen type. Because of the restraints imposed by the dimensions of the test facility, heat shield panel specimen size was limited to 4 inches long, 1 inch wide, and up to .25 inch in depth.

In order to design the small test panels, full size panels of representative design were selected, typical loads due to pressure differentials were analytically applied to each design, and the resultant radius of curvature was calculated for each. Then the small test panels were designed with the proper gauge and geometry, and the test loads were selected to produce the same radius of curvature. Therefore, by matching the radius of curvature of the small test panel to the radius for a full size heat shield panel, the small test heat shields experienced skin and stiffener stresses and joint behavior the same as full size flight articles.

Table VI Heat Shield Test Specimen Designs

Specimen Type	Construction Gauge (mils)	Pitch (inch)	Depth (inch)
Single-faced flat corrugation 	Skin 12 Corrugation 12	.180	.160
Single-faced vee corrugation 	Skin 16 Corrugation 16	.450	.250
Skin sheet stringer 	Skin 16 Stringer 34	.500	.250
Skin channel stringer 	Skin 12 Stringer 12	.500	.250
Riveted single-faced flat corrugation 	Skin 12 Corrugation 16	.820	.250

A balance of the existing stresses to the allowable stresses was also an important factor in designing the simply supported test panels. A simply supported full size flight heat shield panel, of optimum design and loaded by pressure differential to produce primarily bending loads, would experience at its maximum loading condition an exact balance between the allowable tensile stress and the actual tensile stress in the stiffener (corrugation, etc.) and between the allowable compressive or buckling stress and the actual compressive stress in the skin. These stresses are balanced by integration of material gauge, and geometry (e.g., depth and pitch or stiffener). Of course, this integration is performed to produce a panel of minimum weight and thickness. The test panels for this program were designed using this typical philosophy; however the exact balance of allowable tensile and compressive stresses, with respect to the actual stresses, could not be attained because of restrictions of minimum gauge, specimen size, and tooling. The maximum unbalance or stress differential is 25 percent, and in most cases, it was on the order of 10 percent.

The use of gauges that would be used on full size panels was considered important for obtaining typical coating behavior at edges and typical mechanical properties of the coated metal composite. Therefore, typical gauges (.0" to .032 before coating) were always used.

Since it was possible for the test panel to have the same radius of curvature and the same tensile stress level as the full size flight panel, the performance of all parts of the coated test panel was considered representative of those experienced on full size panels during flight.

Like the baseline specimens, the heat shield specimens were fabricated in the Advanced Materials Fabrication Facility (AMFF). Panels were manufactured using detail drawings such as that shown in Figure 17 for the Vee corrugation stiffened configuration. Heat shield panel test specimens of the various single faced stiffened configuration approaches used for this program are shown in Figure 18.

3. TEST CONDITIONS

In this section the selection of test conditions is discussed.

The two vehicles of primary interest to this program are (1) lifting spacecraft which will reenter the Earth's atmosphere from a near-earth orbit and make a horizontal landing and (2) the hypersonic cruise vehicle which will fly within the sensible atmosphere. For the lifting reentry spacecraft many trajectories are possible and depend primarily on the reentry path angle, reentry velocity, mode of glide acquisition, and the aerodynamic characteristics of the vehicle. Trajectories for the hypersonic cruise vehicle may also vary considerably and depend, among other things, on mach number, type and amount of fuel, engine performance, and glide descent characteristics.

Diffusion type coatings, including the fused slurry silicides, are sensitive to time profiles of temperature, pressure, and stress. This means that representative test conditions must be used in order to achieve accurate evaluations.

Two sets of test profile conditions, temperature-pressure-stress-time, were selected by reviewing available flight environment data for reentry and hypersonic cruise vehicles. The various flight environmental conditions were studied to determine which of the multitude of combinations of temperature, pressure, stress and time would yield the most meaningful evaluation of the fused slurry silicide coating, while maintaining integrity of the test conditions with respect to actual vehicles.

The test conditions selected are shown in Figure 19. The specific time, temperature, pressure and stress relationships do not represent a specific vehicle and mission; however, the conditions are representative of classes of high L/D vehicles and missions which will provide a meaningful evaluation of coated columbium hardware configurations.

The time-temperature relationship selected was the same for both test profiles. The hypersonic cruise vehicle typically has an appreciable dwell time at the maximum temperature whereas a reentry vehicle is more likely to have one or more short duration peaks or spikes to maximum temperature. Such reentry vehicle temperature peaks can be caused by glide acquisition maneuvers, in-flight maneuvers, or boundary layer transitions, and can occur at any time during the flight. Any combination of such maximum temperature peaks was considered to be included in the selected 12 minute hold at maximum test temperature. The selected dwells at 1400°F will permit coating evaluation in a region where the coating oxidation rate can be high and the Cb-752 ductility can be low.

The atmospheric pressure is an important factor in coating performance. It will be noted that both an internal and an external pressure profile are presented in Figure 19. External pressures are those associated or present on the mold line surfaces of the reentry vehicle. Internal pressures are those associated with the internal surfaces and are normally considered as ambient or equal to altitude.

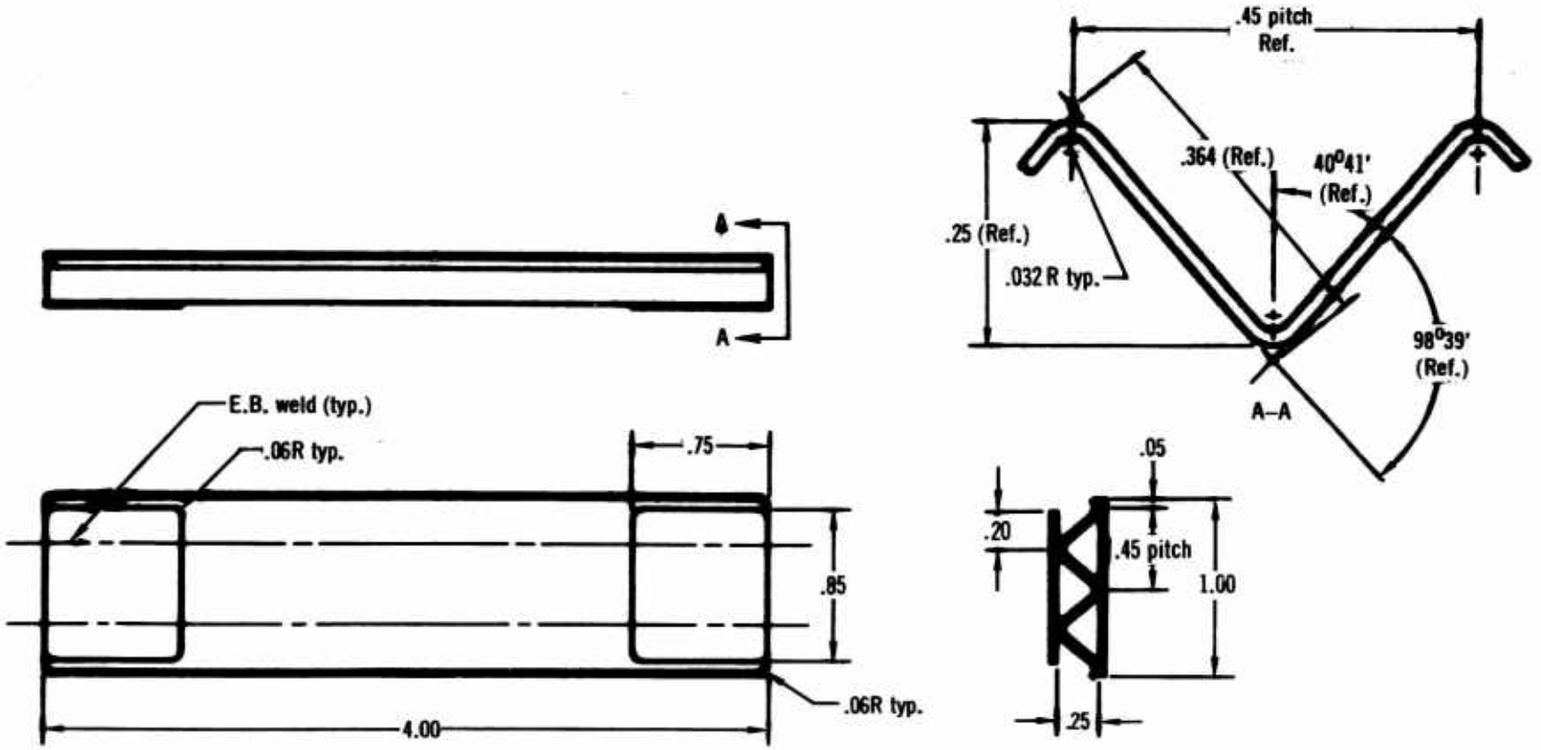

Figure 17 Detailed Drawing of the "V" Shaped Single Faced Corrugation Stiffened Heat Shield Specimen

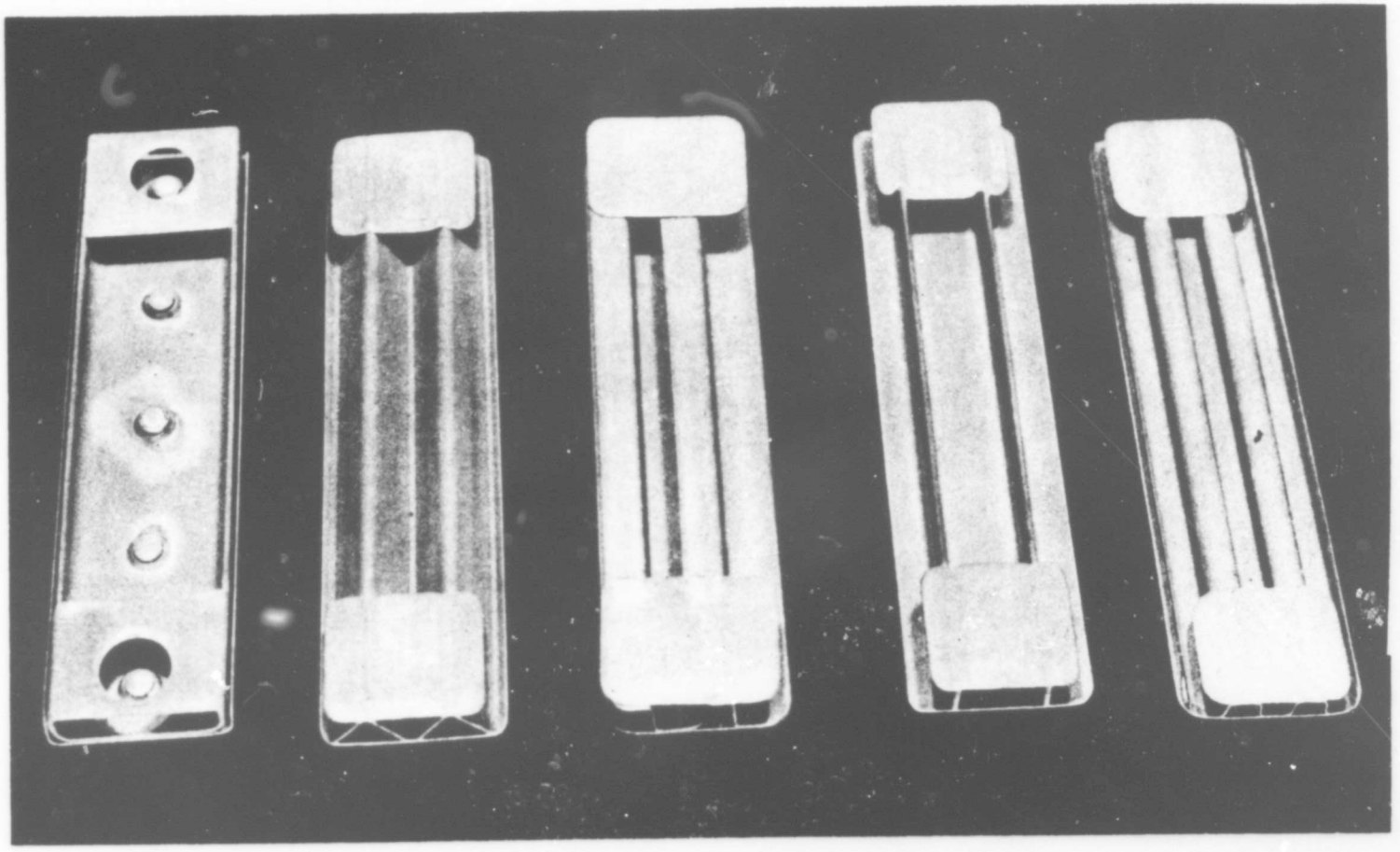

Riveted channel | Vee corrugation | Zee stringer | Rib stringer | Flat corrugation stiffened

Figure 18 Heat Shield Specimens

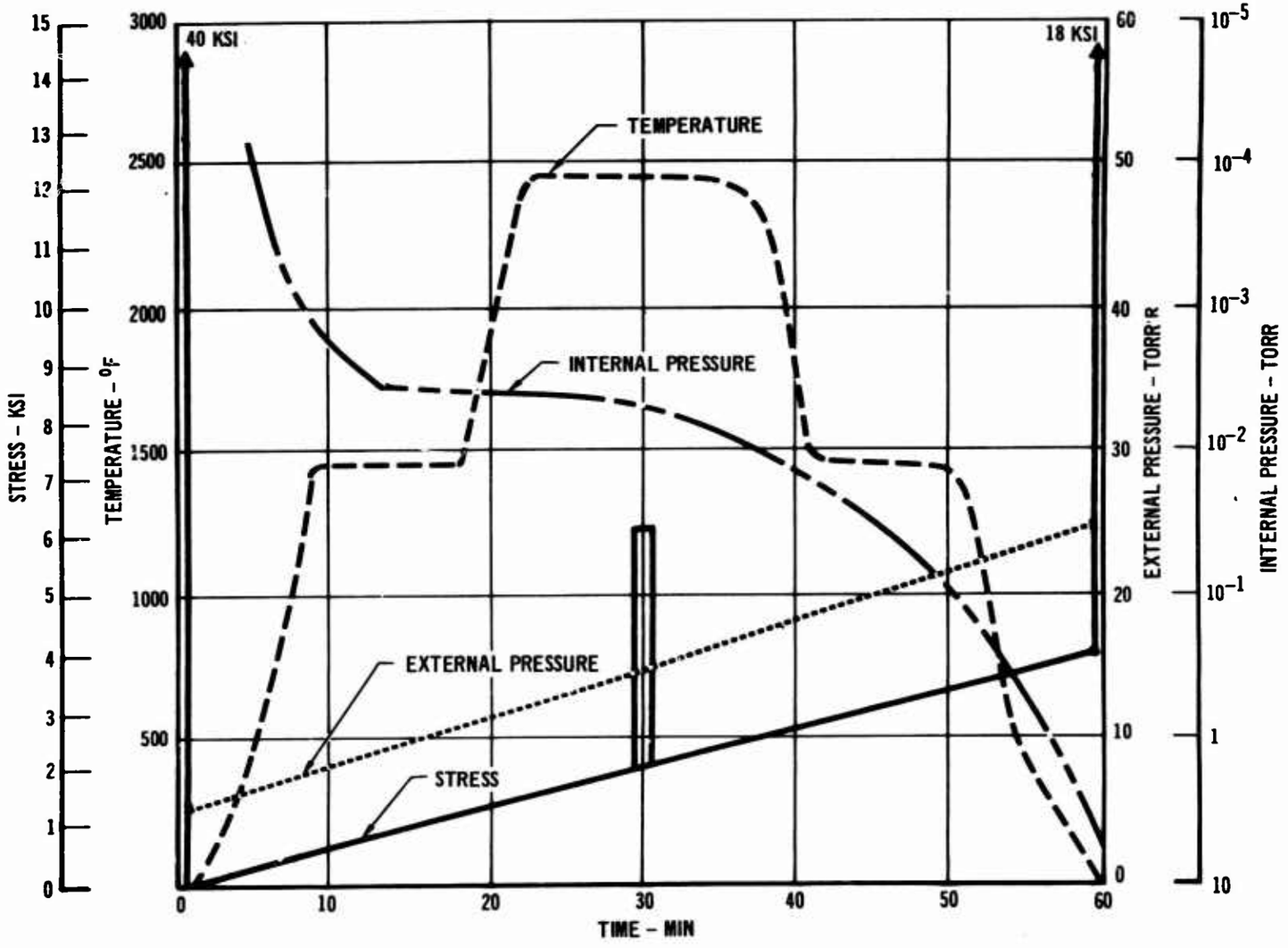

Figure 19 Profile Test Conditions Of Temperature, Pressure, Stress

The effect of stress is the least understood of the parameters included in the evaluation. The critical stress condition can occur at almost any point in the flight - boost, hot maneuvers or terminal maneuvers. High loads at low temperatures are always encountered during landing and takeoff (boost); therefore, the selected stress profile included a realistically high load at room temperature at the beginning and end of the test cycle.

One of the two selected time-stress profiles began with a very low stress which was increased with time at a constant rate to simulate low air loads. The second stress profile employed a similar increasing stress except a high load (6000 psi) was applied for a very short duration (30 sec.) during the maximum temperature plateau to simulate a maneuver.

The maximum temperature of the test profile later in the program was lowered from 2600°F to 2400°F to allow a longer test time before excessive creep deformation occurred on the heat shield panel specimens. All the other test conditions remained the same.

Static and slow cycle (800°F-2500°F-800°F, one atmosphere) oxidation tests were performed. Time-temperature-pressure profile testing was conducted using the profiles in Figure 19 without any stress. These oxidation tests showed the reproducibility of the coating (static and slow cycle) and generated a baseline for later determination of the effect of stress (time, temperature, pressure profile) on coating life.

4. EQUIPMENT AND CALIBRATION

This section includes description of the equipment used for conducting the testing and calibration procedures employed to characterize the test articles and test environments.

(a) Equipment

Standard oxidation test furnaces and universal testing machines were used in generating basic performance data for the bare and R-512E coated Cb-752 alloy, except for an accessory which provided varying loads to specimens being subjected to temperature-pressure-time reentry profile testing.

Oxidation test furnaces including an automatic slow cycle test facility and a reduced pressure oxidation test facility which were used for determining baseline oxidation data are shown in Figures 20, 21, and 22.

Tensile and elongation properties of bare and coated Cb-752 were determined in the facilities shown in Figures 23 and 24. Bend tests were conducted using the fixture shown in Figure 25. Creep tests conducted by Metcut-Research Associates Inc. were performed in a cold wall vacuum furnace set in a conventional creep rack. The specimen was radiant heated to the desired test temperature by a resistance heated tantalum sheet element. The furnace and associated equipment utilized during the creep tests are shown in Figure 26.

The accessory which provided varying loads to specimens being subjected to temperature pressure reentry profile testing is shown in Figure 27 attached to an ASTRO Industries Model 2570C graphite tube furnance. The accessory consisted of a rigid frame, L-605 loading rods to transmit the

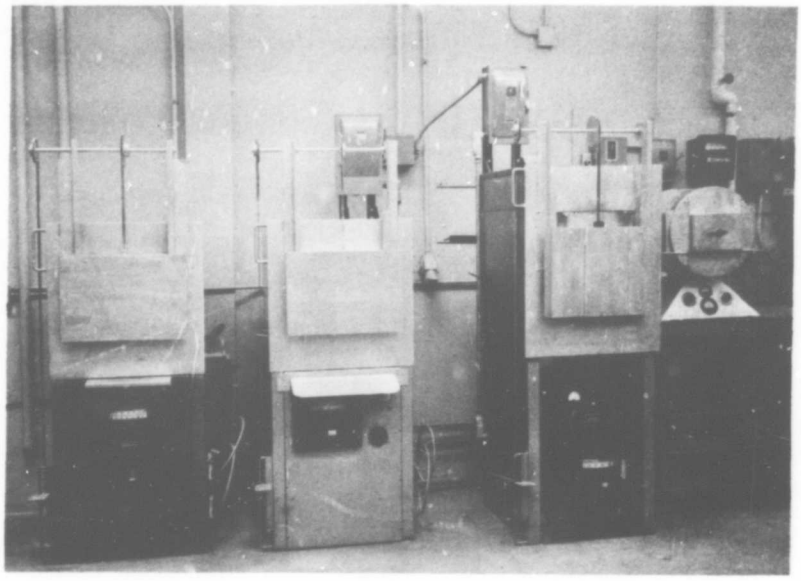

Figure 20 Static Oxidation Test Furnaces

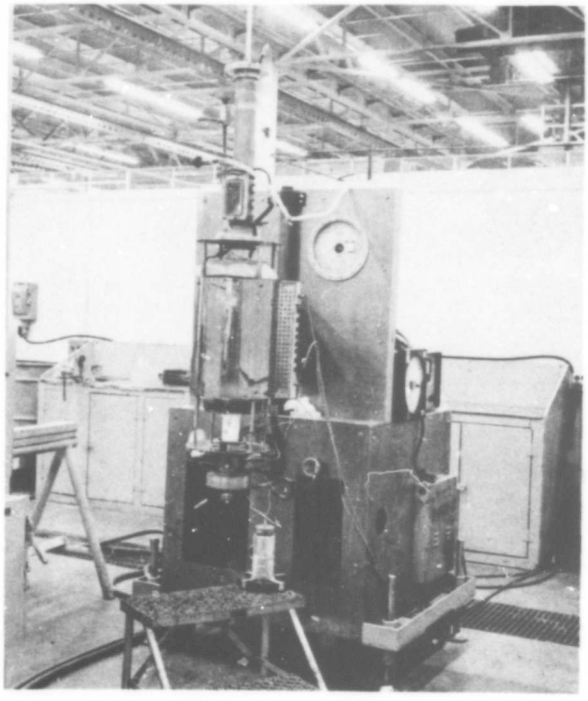

Figure 21 Pressure Temperature Profile Oxidation Test Facility

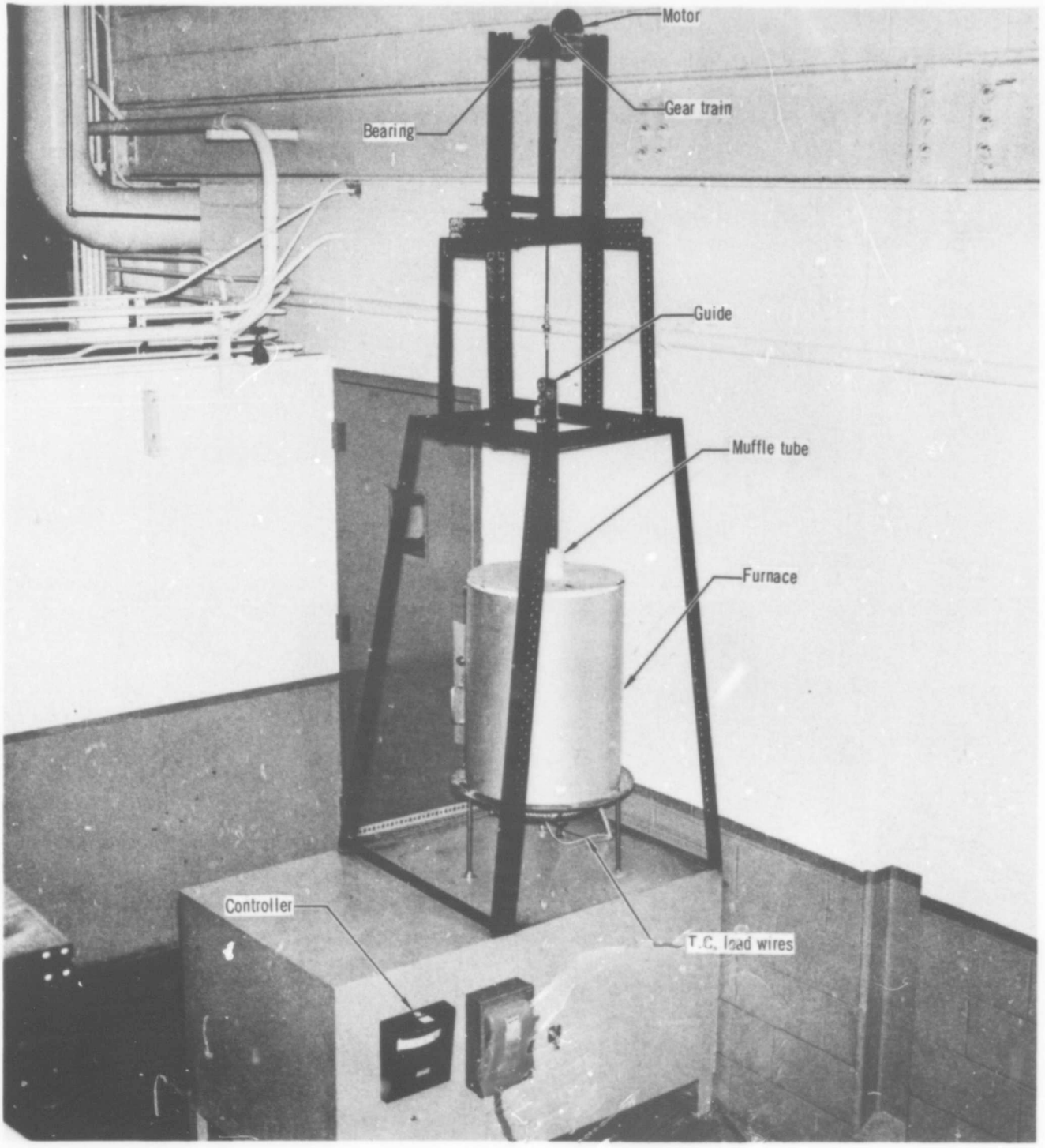

Figure 22 Slow Cycle Oxidation Test Furnace

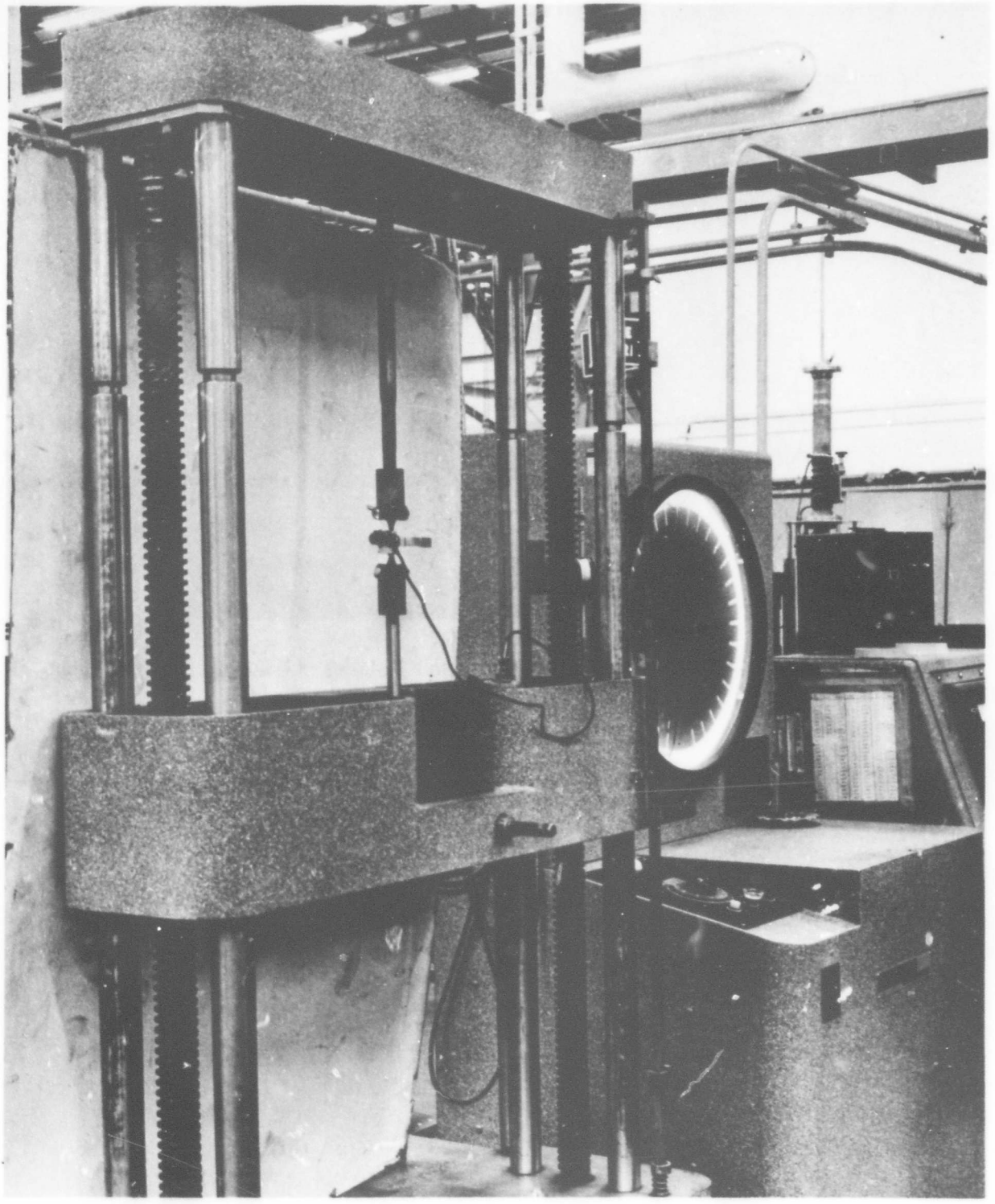

Figure 23 Universal Testing Machine

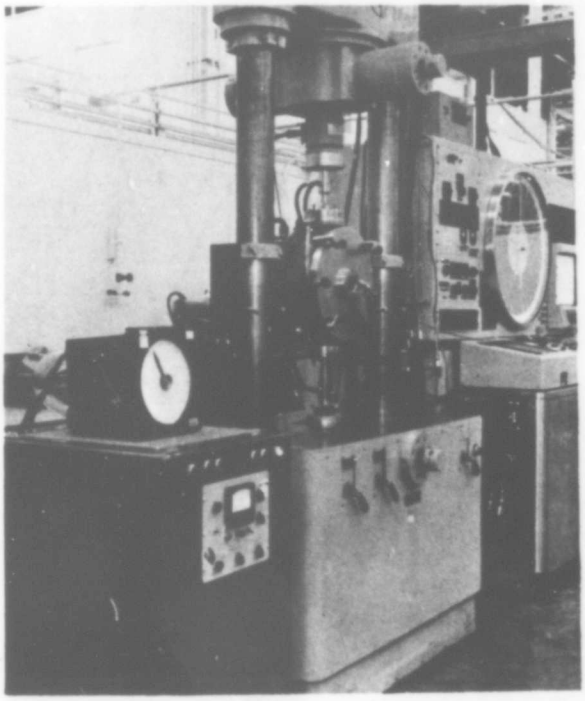

Figure 24 Vacuum Tensile Apparatus Installed in Universal Testing Machine

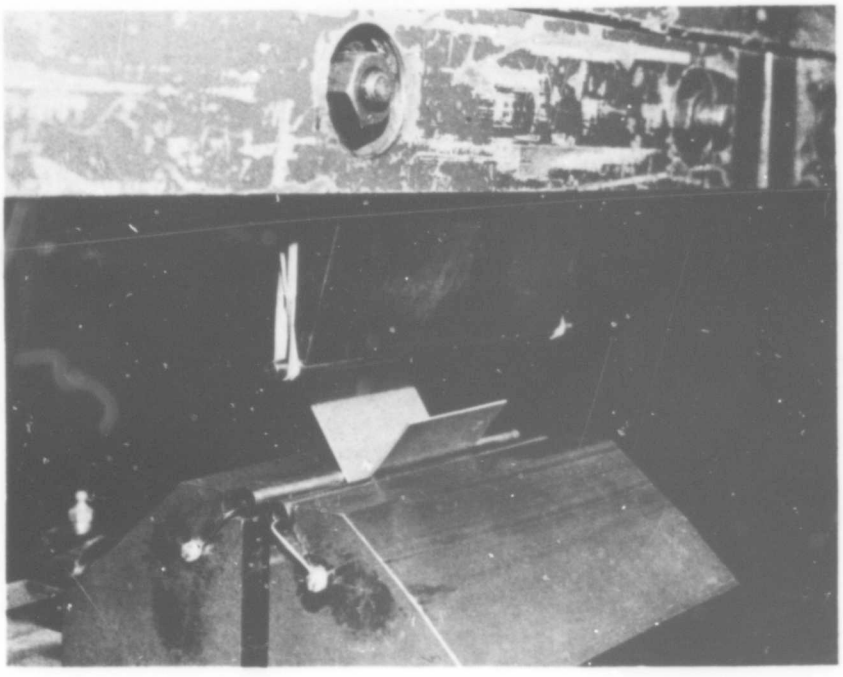

Figure 25 Bend Test Fixture

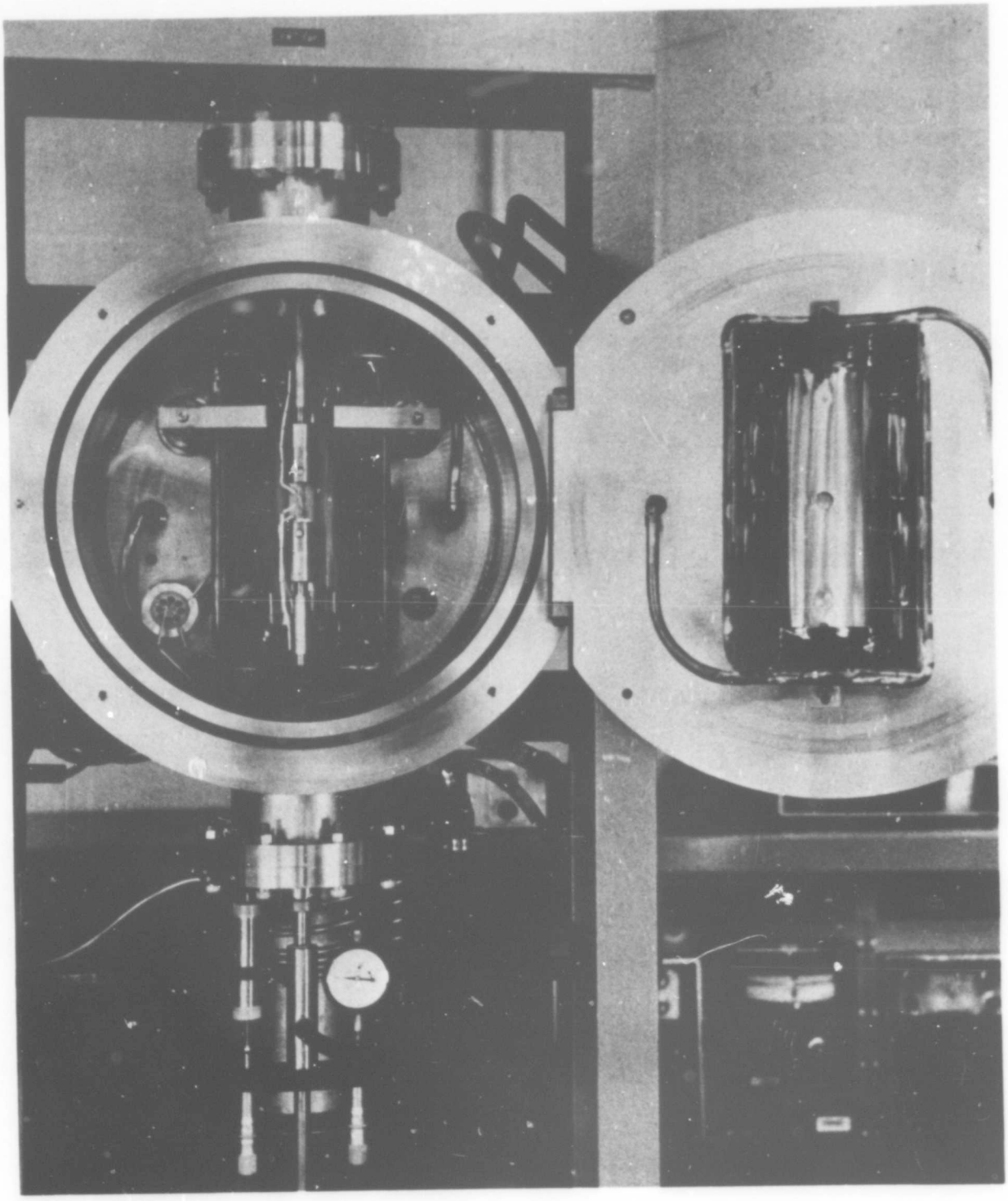

Figure 26 Creep Test Setup (2400^{0} – 2600^{0}F) Metcut Research Associates, Inc.

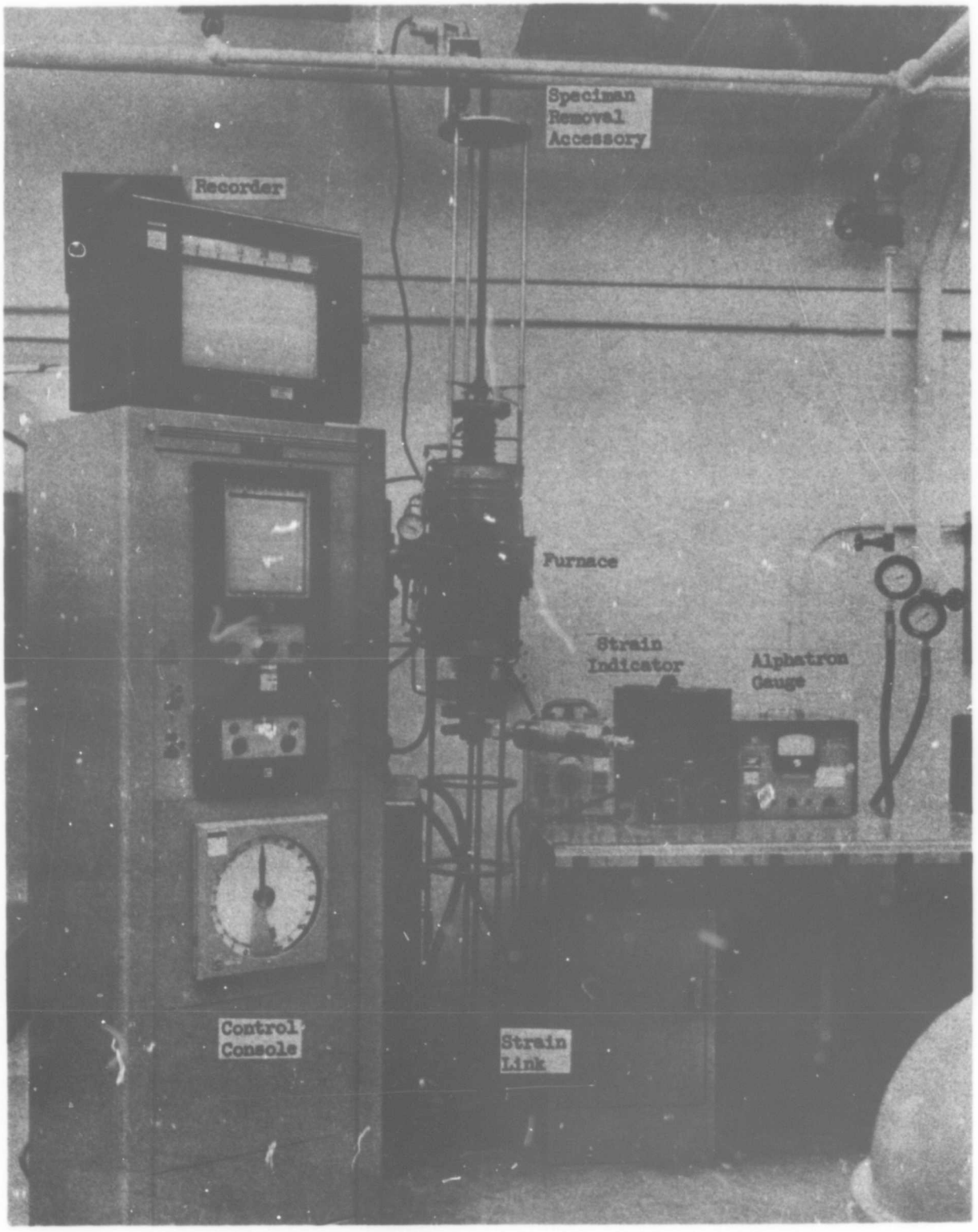

Figure 27 Pressure-Temperature-Stress Profile Oxidation Test Facility

load to the specimen, a motor driven loading mechanism, a strain link for measuring the applied load, and a motor driven accessory for specimen insertion and removal. The high torque-low rpm motor which drives the loading mechanism (a threaded rod-gear arrangement shown in Figure 28) gave the apparatus the capability of producing a tensile load of 450 pounds. The accessory was designed to accommodate automatically programmed temperature and stress profiles. Other accessories used included a mullite tube which contained the specimens for testing, a vacuum pump connected to one end of the tube and a controlled leak on the other end to provide the desired air pressure profile, and temperature sensing equipment (thermocouple). This unique reentry simulator was the workhorse piece of equipment used on this program.

Fixtures were constructed which allowed bending loads to be applied to heatshield test specimens while they are being exposed to reentry conditions of temperature and pressure. Fixtures were constructed from Cb-752 and protected from oxidation with the R-512E coating. A fixture with a heatshield specimen in place is shown in Figure 29. This method of loading places the heat shield specimens in bending which is typical at flight behavior. Therefore, the joints and faying surfaces are "worked" in the same manner as in actual flight where the panel is loaded and unloaded at and by the flight environmental pressures.

To assure that the maximum amount of information was obtained for interpreting and predicting test results, NDT techniques for determining coating thickness were applied. The prominent mode of premature coating failures in the R-512E/CB-752 coating system has previously been determined (References 14 and 15) to be thinly coated edges.

Nondestructive test (NDT) techniques were utilized to determine coating thicknesses before testing, between cyclic exposures, and after oxidation tests. Techniques utilized included "Dermitron" and thermo-electric instruments. The "Dermitron" which works on a eddy current principle was used to measure coating thickness on flat surfaces and is shown in Figure 30. The thermo-electric instrument shown in Figure 31, works on the same principle as a thermocouple. It is sensitive to chemistry change which can be related to coating thickness and was used for coating thickness measurement on edges as well as on flat surfaces.

(b) Calibration

The working zone temperature profile of the Astro test furnace, modified for reentry simulation, was determined with a bare baseline stress oxidation specimen (1" x 18") in place. The temperature profile was determined throughout a complete test temperature-pressure profile by attaching a series of eight (8) thermocouples to the specimen.

The pressure profile was maintained using an inert gas. A uniform temperature ($\pm$ 5°F) was found to exist over a one inch span at the center of the specimen throughout the test profile. Temperatures at the end of a three inch span was 100°F lower than at the center of the specimen. This difference remained fairly constant throughout the test profile. The temperature at the center of the specimen was no more than 5°F higher than the control thermocouple which is adjacent to the center of the test specimen. The test temperature profile could be followed quite closely by controlling the power to the furnace. The constant temperature zone could be lengthened by incorporating radiation shields within the length of the mullite muffle tube. However, since thermal gradients are a reality on actual flight heat shield panels it was felt that the thermal gradients on the baseline specimens as well as on the panel specimens would add rather than detract from the evaluation tests.

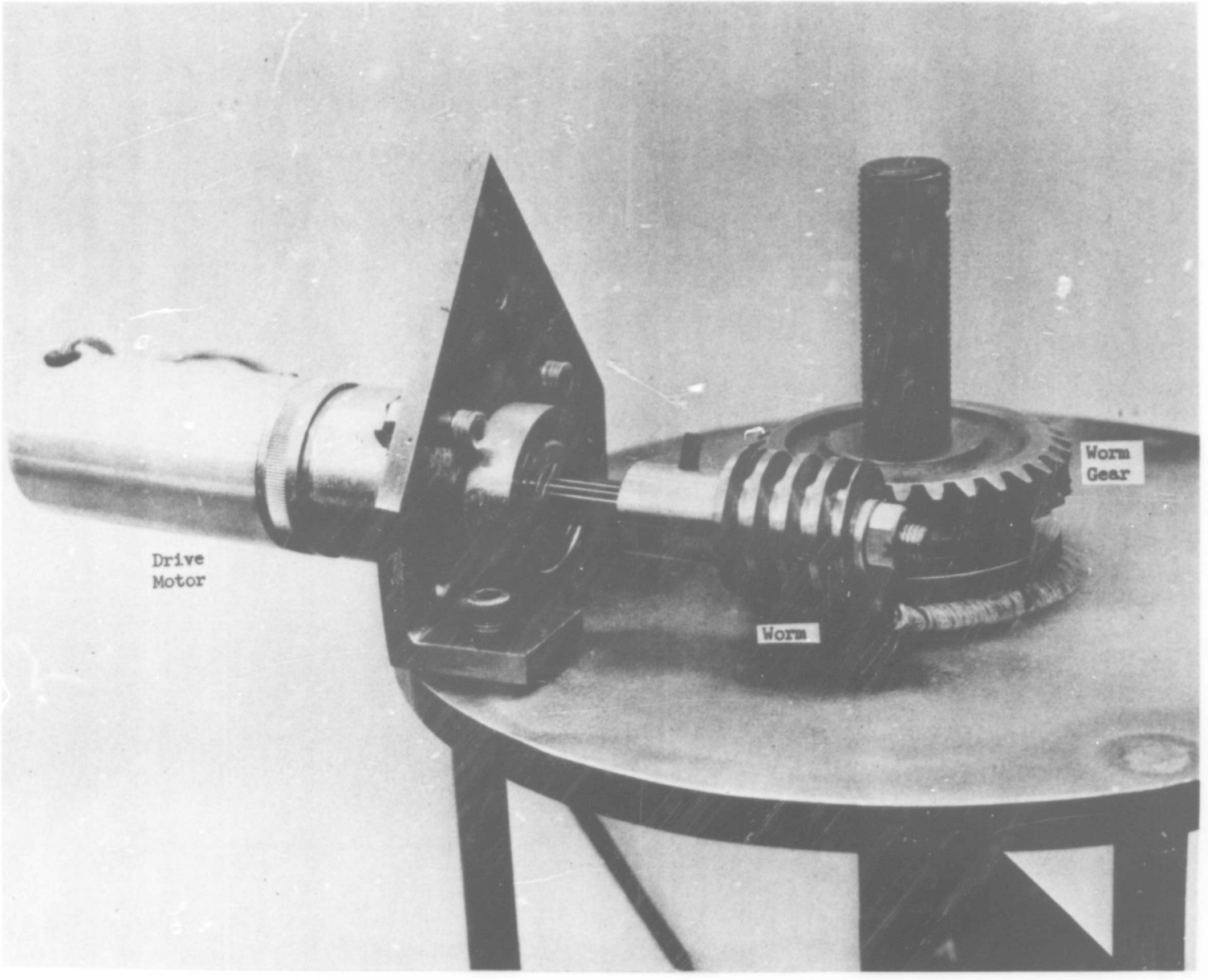

Figure 28 Reentry Simulator Driving Mechanism For Load Application

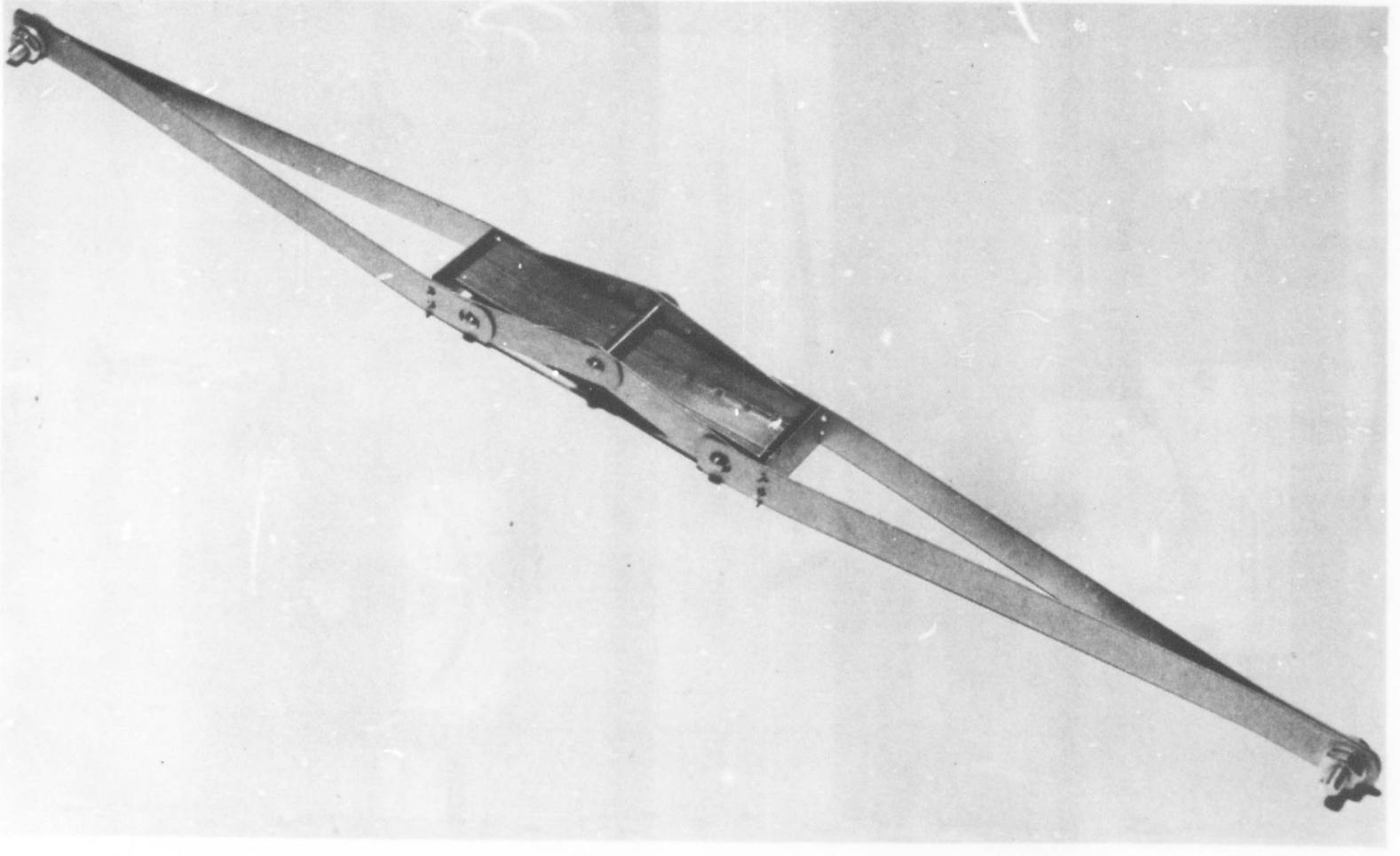

Figure 29 Fixture (with Specimen in Place) for Applying Bending Loads to Specimens Typical of Heat Shield Constructions

Figure 30 Dermitron Eddy Current Instrument

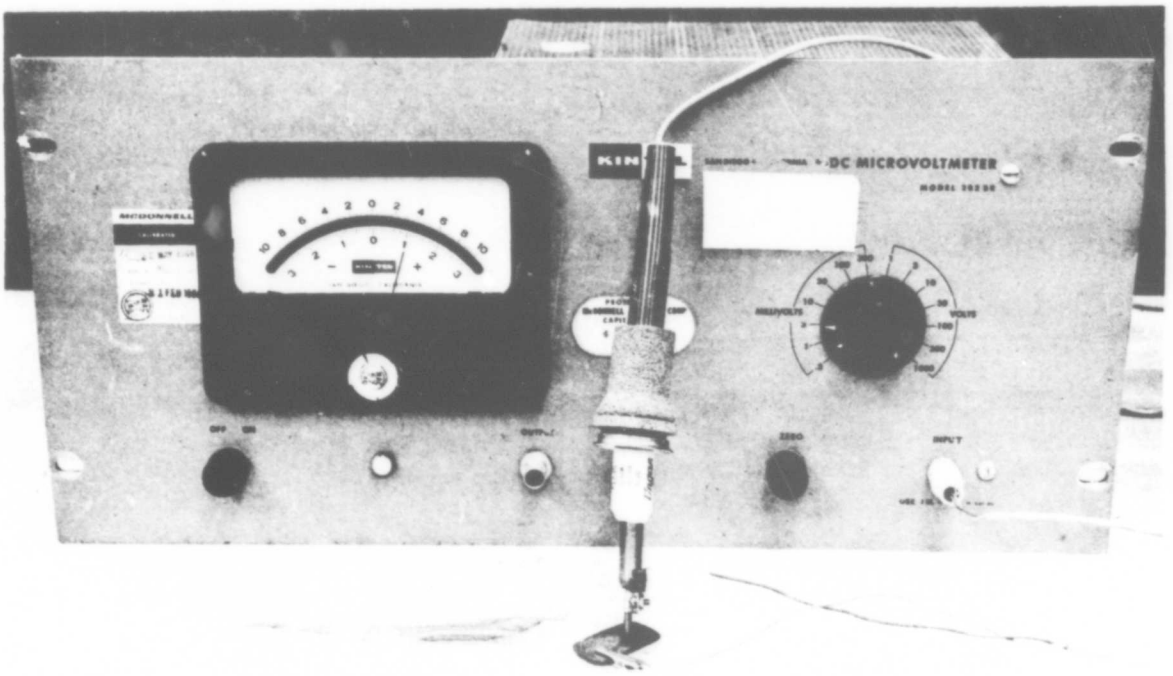

Figure 31 Thermoelectric Test Instrument

Preliminary to starting the stress oxidation tests on the heat shield specimens, temperature gradients and lag during a typical test cycle were determined. Thermocouples (Pt - Pt 10% Rh) were welded to the skin of an uncoated single faced corrugation stiffened heat shield specimen at intervals of 1/4 inch from the center of the specimen. The instrumented specimen was placed into the scissors loading fixture and subjected to the temperature versus time profile. The uniform temperature zone was 1/2 inch and the gradient on either side of this zone was 100°F/in for the first inch on either side of the uniform temperature zone. Thus, the gradient from the uniform temperature zone (center of specimen) to the top and bottom loading pins was 125°F. The temperature difference between the free standing furnace control thermocouple and the adjacent thermocouple attached to the specimen was $\pm$ 5°F at 2600°F. There was a time lag of approximately 1 minute between the furnace control thermocouple and the panel temperature.

The load or stress being applied during testing was determined from a aluminum alloy strain link connected between the lower loading rod and the motor driven loading mechanism. To determine the efficiency of the load train (loss due to friction, etc.) a correlation was made between stress in the specimen and applied load to the load rod at the strain link. This was accomplished by instrumenting a baseline stress oxidation specimen and straining it at room temperature. As shown in Table VI, there was very little energy loss.

To determine if any energy was lost in the loading fixture used to apply bending loads to heat shield panels, a strain gauge was attached to the skin of a single faced corrugation stiffened heat shield panel and load was applied by the load train. The stress in the specimen was then correlated with the stress registered by the strain link used for control. This experiment indicated that very little if any energy was lost due to friction or binding in the loading fixture.

Utilizing this same set-up the loading reproducibility of the strain link was determined. Five different load levels were applied by the load train and at each level the strain in the specimen was recorded. This procedure was repeated 4 times and the results are present in Table VII.

Table VI Loading Mechanism Calibration

Load On Strain Link (Lbs)	Load On Specimen (Lbs)
20.0	19.5
41.5	41.0
49.5	49.0
80.5	81.0
99.0	97.0
109.0	108.0
123.0	121.0
138.0	136.0
152.0	151.0
181.0	180.0
196.0	194.0
209.0	208.0
224.0	223.0
238.0	236.0
252.0	249.0

Table VII Specimen Strain vs Load

Strain on Strain Link (μ In./In.)	Load (lb)	Strain in Specimen (μ In./In.)			
		Cycle* 1	Cycle 2	Cycle 3	Cycle 4
0	0	0	0	0	0
656	3.98	78	77	78	77
1312	7.96	150	151	151	151
1968	11.94	224	225	223	224
2624	15.92	288	292	286	290
3280	19.90	356	356	352	354

*1 Cycle 0 → 20 lb → 0

Notes:

1. No measurable difference in specimen strain between loading and unloading.
2. The strain in the strain link and in the specimen should not be the same.

Calibration of NDT devices proceeded as follows. CB-752 specimens with various R-521E coating thicknesses ranging from 1.5 mils per side to 5.5 mils per side were surveyed with the thermo-electric and eddy current devices. The specimens were prepared for metallographic examination and coating thickness measurements were made at 500X. Using this information, calibration curves for the thermo-electric device and Dermitron were established and are presented in Figures 32 and 33, respectively. These calibration curves are in good agreement, for up to 3 mils of coating thickness, with those developed by AVCO and Sylvania and reported in Reference 16. Above 3 mils of coating thickness the AVCO and Sylvania calibration curves tend to have higher slopes than the ones developed here. However, thinly coated areas are the major concern and these can be readily and accurately detected.

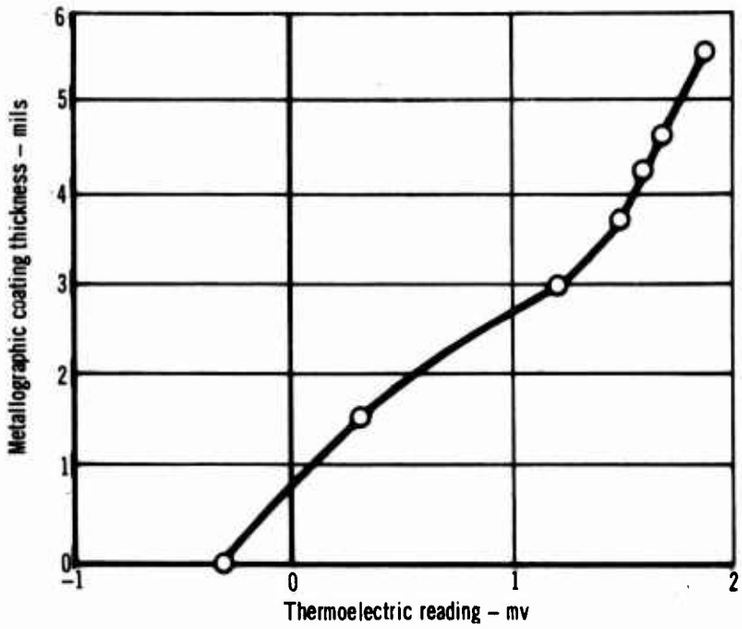

Figure 32 Thermoelectric Emf vs Metallographic Coating Thickness for Cb–752 Alloy with R–512E Coating

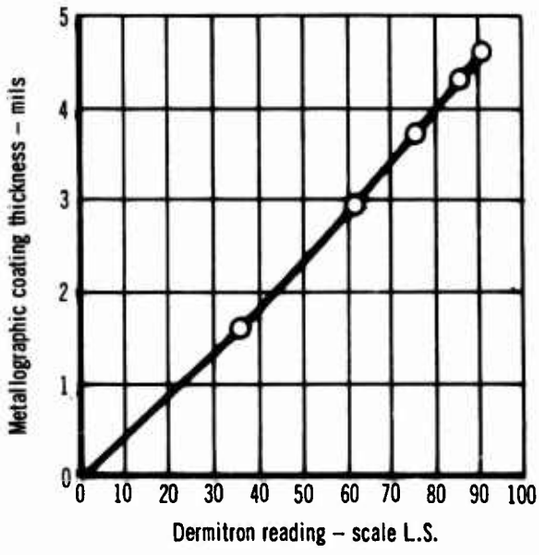

Figure 33 Dermitron Reading vs Metallographic Coating Thickness for Cb–752 Alloy with R–512E Coating

SECTION III

TEST RESULTS

The objectives of the testing were to:

a. Establish baseline oxidation resistance data for the R-512E coating and mechanical property data for the bare and coated Cb-752 columbium alloy.

b. Determine the protective life of the coating when applied to specimens having joints and faying surfaces representative of typical advanced flight vehicle parts.

c. Determine the effects of local coating damage on the structural integrity of representative hardware.

d. Evaluate the effectiveness of repair coatings when applied to representative hardware.

e. Utilize nondestructive test methods to predict performance and interpret results.

To present the test data in a usable form the major parts of this section are:

. Baseline testing

. Heat shield panel testing

. Effects of local coating removal

. Repair coatings

. Non-destructive testing

Included in the baseline testing sections are oxidation resistance performance and mechanical properties. The section on effects of coating removal includes testing performed on baseline and heat shield panel specimens.

1. BASELINE TESTING

Discussed in this section are oxidation performance and mechanical properties.

a. Oxidation Performance

Basic oxidation performance tests which were conducted are summarized in Figure 34. The span of failures observed for each test condition are shown. The low and high stress call-outs represent the two different stress

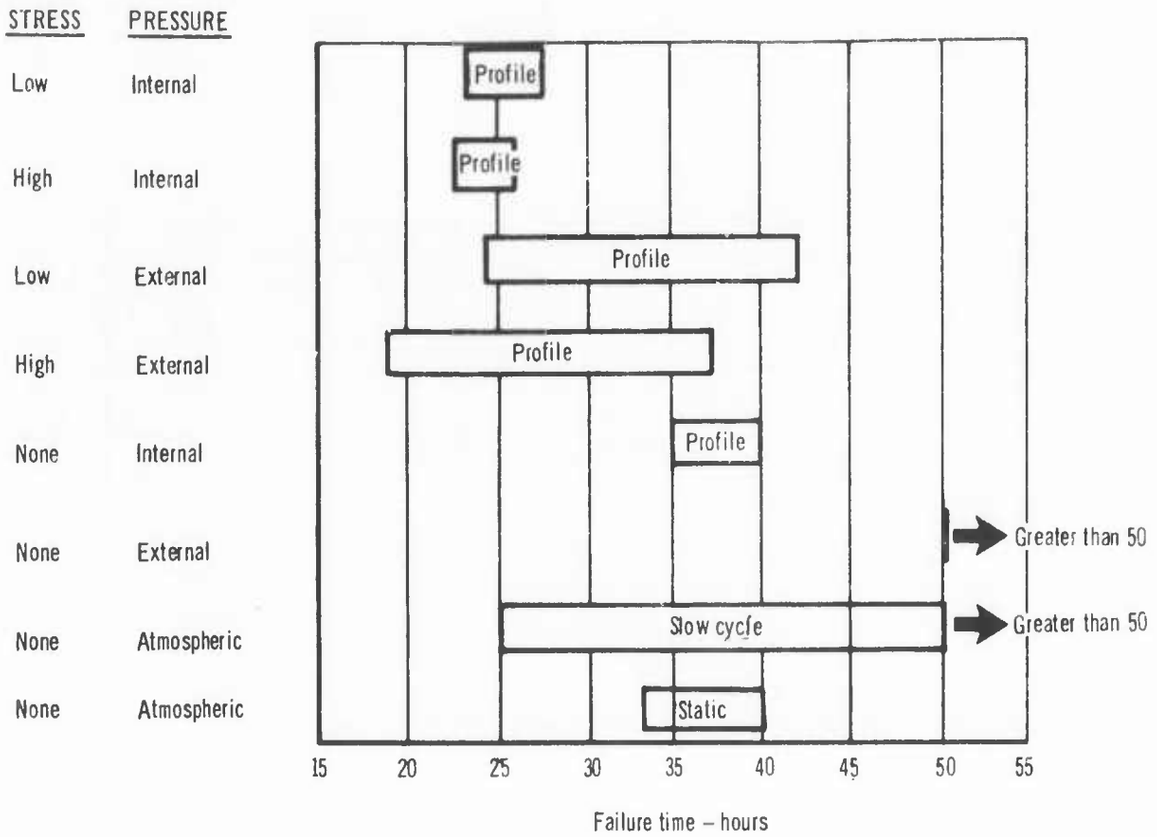

Figure 34 Baseline Oxidation Comparison (2600°F Tmax. For All Tests)

profiles to which the specimens were subjected. The only difference between them is that the low stress profile lacks the 30 second 6000 psi stress peak while at maximum temperature. The internal and external pressure profiles represent conditions typical of internal and external vehicle pressures during reentry. For the non-loaded or un-stressed specimens, failure was the visual evidence of columbium oxide. Failure for the specimens tested under stress was breaking or rupture.

Static (one atmosphere, one hour cycles) and slow cycle (800°F-2500°F-800°F) oxidation tests were for the purpose of determining coating reproducibility. Static tests were conducted at 1400°F, 2000°F, 2400°F, and 2600°F. The specimens which were being tested at 1400°F were accidently dropped on the concrete after 52 hours of exposure which resulted in coating edge chips and testing was terminated. At 2000°F 100 cycles were obtained with no failure. Specimens tested at 2400°F had top edge coating failures after 28 - 37 cycles. Specimen tested at 2600°F had top edge coating failures after 33 - 40 cycles. Slow cycle test produced edge failures after 25 to greater than 50 cycles. The edge failures which were the only made of coating failures displayed are readily related to the thinly coated edges which result from dip application of the slurry coating. The thinly coated edges were detected with the thermoelectric device prior to testing. Upper edges were determined to be the thinnest (See Appendix III). Coating oxidation life demonstrated in the various tests were comparable with results obtained from other investigations (References 11, 12, and 13). The results of the static and slow cycle oxidation tests are presented in Table VIII and Table IX, respectively.

Table VIII

Results of Static Oxidation Tests – R–512E Coated Cb–752

Specimen Number	Test Condition	Test Results	Remarks
1	1400°F for 1 hr	52 Cycles	Dropped specimens coating chipped
2		52	
3		52	
4	1400°F for 1 hr	52	
5	2000°F for 1 hr	100	No failure
6		100	
7		100	
8	2000°F for 1 hr	100	
9	2400°F for 1 hr	28	Edge Failure
10		37	
11		37	
12	2400°F for 1 hr	29	
13	2600°F for 1 hr	33	
14		33	
15		35	
16	2500°F for 1 hr	40	

Table IX

Results of Slow Cycle Oxidation Tests – R–512E Coated Cb–752

Specimen Number	Test Condition	Test Results	Remarks
32	Slow cycle*	35 Cycles	No failure – removed
33		40	Failed
34		45	No failure
35		25	Failure at hole
36		50	Failure, upper edge
37		50	No failure
38		50	Failure, upper edge
39		50	No failure
40		50	No failure

*One hour duration per cycle (800°F–2500°F–800°F)

Metallograpnic examination wereperformed on four specimens that were exposed to 25, 35, 45, and 50 hours of slow cycle oxidation. Photomicrographs of typical coating on these specimens are shown in Figures 35, 36, 37, and 38. The photomicrographs reveal a severe preferential oxidation of the coating. However this is typical of the type of oxidation produced by slow cycle testing. Some edge failures and one surface failure occurred. The performance of the coating in this test was normal in all respects.

Tests were conducted under the time-temperature-pressure profile conditions shown in Section II, Figure 19 to determine the performance of the R-512E coating under these conditions as a baseline for evaluating the effect of stress. Specimens exposed to the external pressure profile condition were removed from testing after 35, 40, and 50 cycles with no failures. Tests were stopped at these cycles to be consistent with failures observed on specimens which were tested under stress conditions. Photomicrographs of typical coating on these three specimens are shown in Figures 39, 40, and 41. There was no base metal contamination evident on any of these specimens. There was preferential oxidation at the thermal expansion microcracks in the coating. There is a definite similarity between the specimens exposed to the external pressure profiles and those exposed to the slow cycle test. The specimens exposed to the slow cycle test show more severe preferential oxidation which can be related to the greater amount of oxygen present. It becomes apparent that temperature cycling is mainly responsible for the preferential oxidation attack of the coating, with pressure having a lesser effect.

Specimens were also exposed to the internal pressure profile conditions for 25, 35, 40 cycles. A visual failure was noted on the surface near the top edge of the specimen exposed for 40 cycles. The coating seemed to spall at the failure site and later metallographic examination revealed contamination of the Cb-752 base metal. The coating was approximately 1.0 mil thick near the point of failure as measured thermoelectrically prior to oxidation testing. No visible failures occurred on the other specimens which were tested for 25 and 35 cycles.

Testing was stopped at these points to enable comparison of the coating/substrate microstructure with the microstructure of specimens profile tested under stress. Photomicrographs of a portion of each of these specimens are shown in Figures 42, 43, and 44. Examination of the specimen which was tested for 25 cycles (Figure 42) shows no substrate contamination at the upper edge. No contamination was noted at any location on the microsection. Examination of the specimens tested for 35 and 40 cycles reveals contamination at the upper edges. The microsection made on the specimen tested for 40 cycles was not from the area of visible coating failure. Preferential oxidation attack is noticeable on all three specimens but the most prevalent mechanism has been a general conversion of the coating to an oxide with some vaproization having taken place. With respect to coating life, the internal pressure environment is more severe than the external pressure environment.

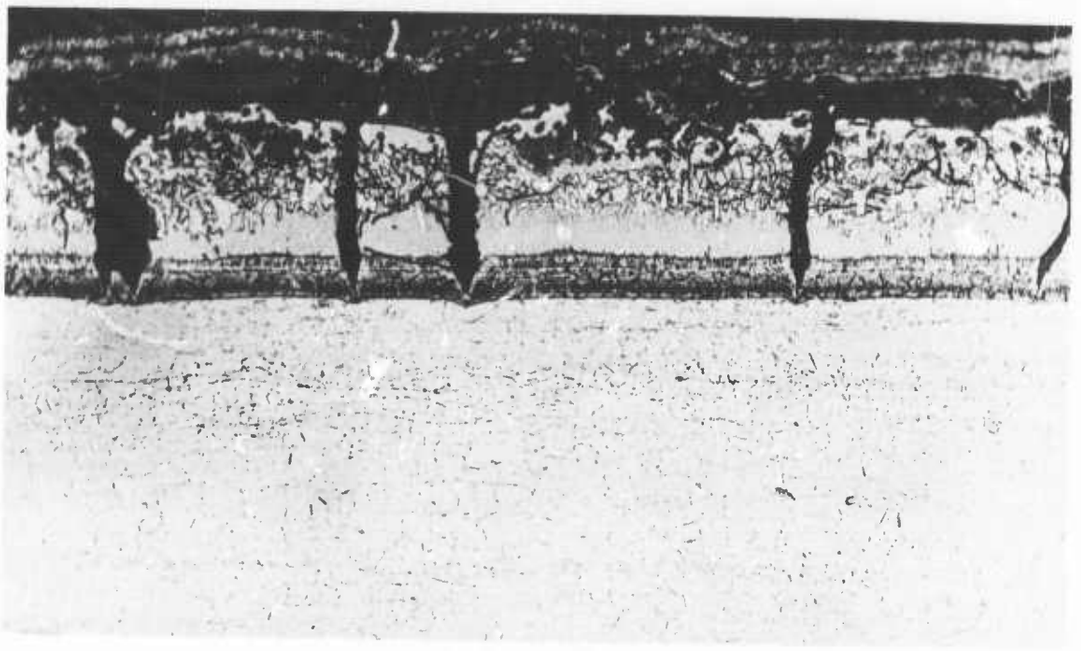

Figure 35 R–512E Coated Cb–752 After 25 Hours of Slow Cycle Oxidation Testing

250X

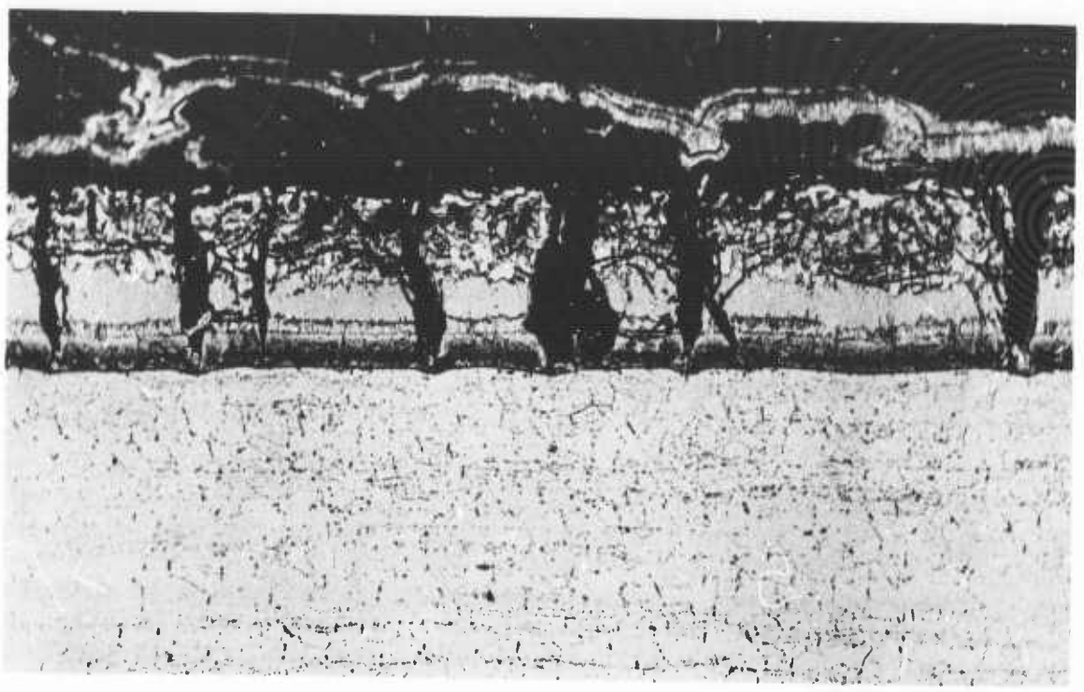

Figure 36 R–512E Coated Cb–752 After 35 Hours of Slow Cycle Oxidation Testing

250X

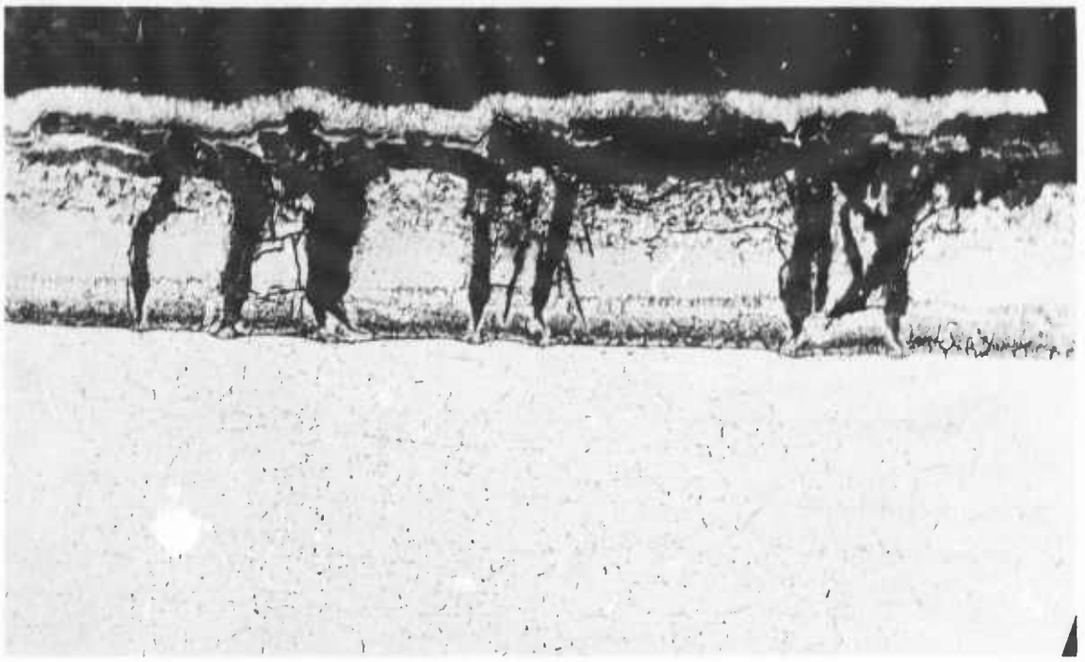

Figure 37 R–512E Coated Cb–752 After 45 Hours of Slow Cycle Oxidation Testing

250X

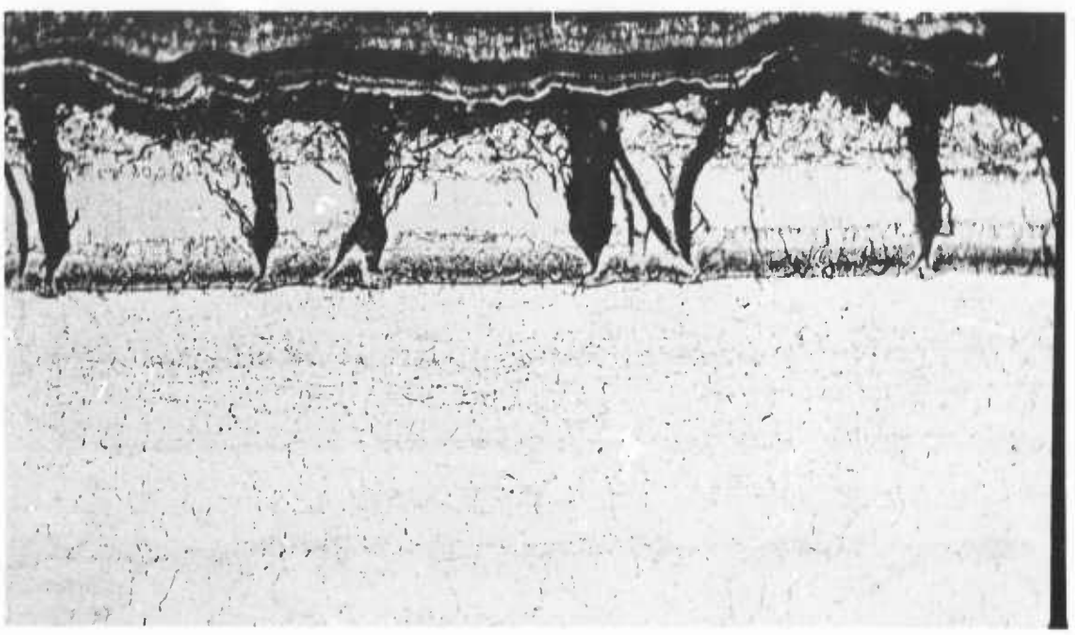

250X

Figure 38 R–512E Coated Cb–752 After 50 Hours of Slow Cycle Oxidation Testing

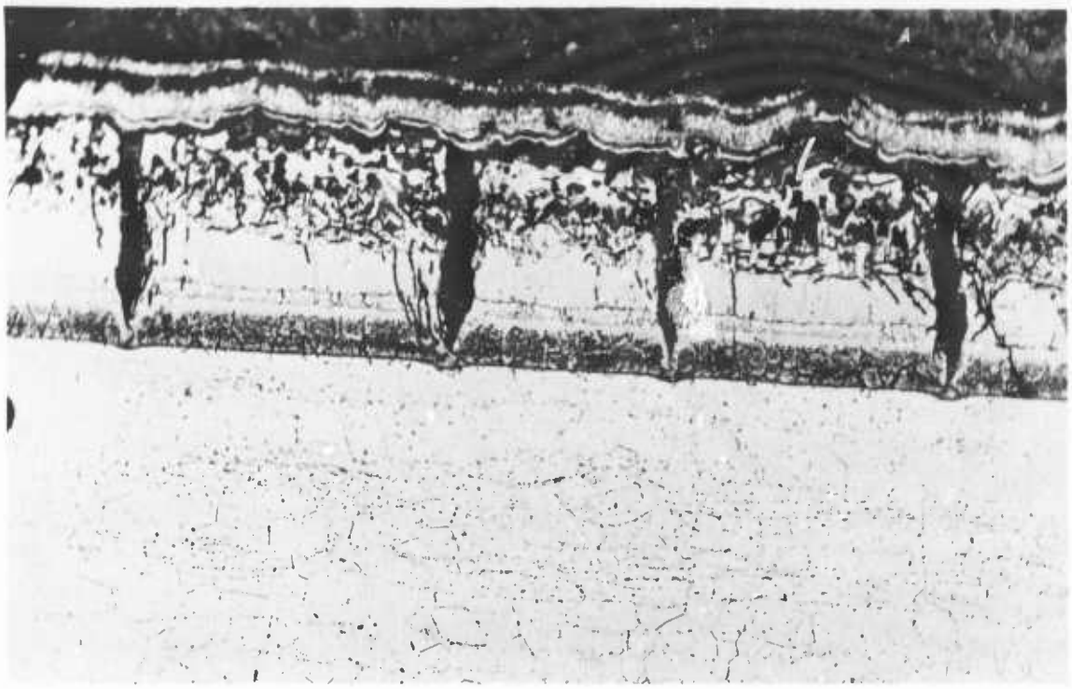

Figure 39 R–512E Coated Cb–752 After 35 External Pressure 2600°F Reentry Profiles 250X

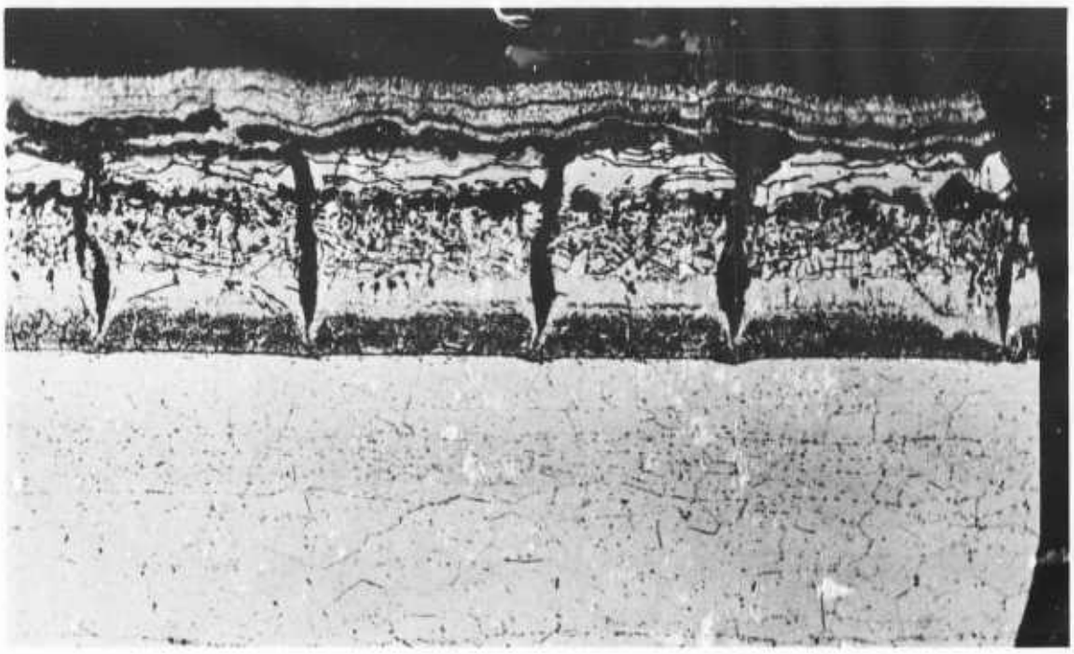

Figure 40 R–512E Coated Cb–752 After 40 External Pressure 2600°F Reentry Profiles 250X

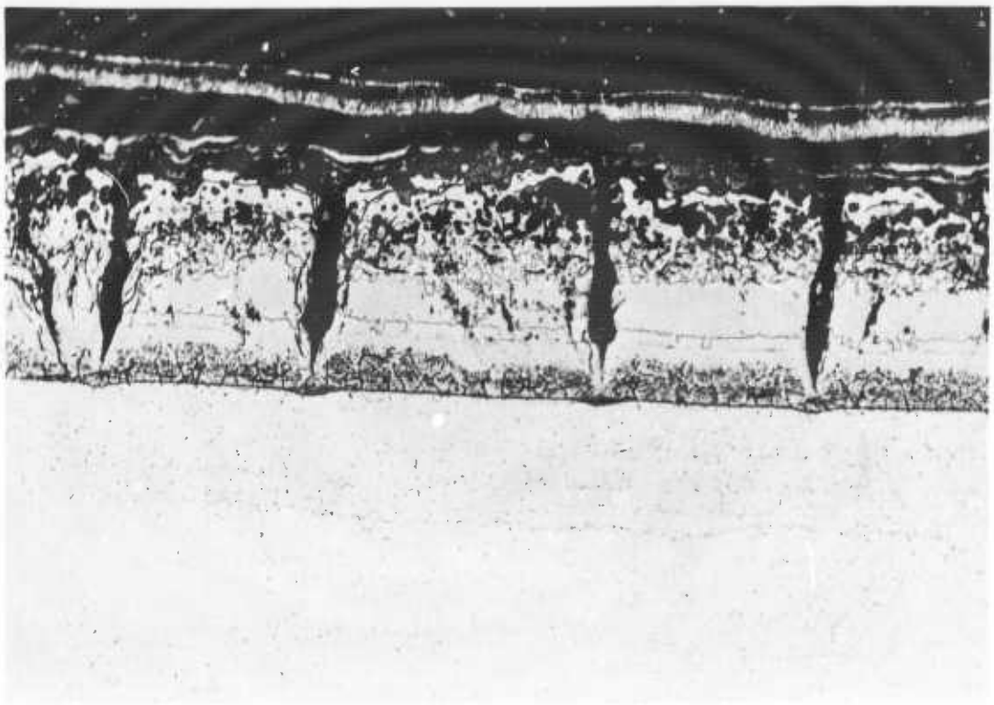

Figure 41 R–512E Coated Cb–752 After 50 External Pressure 2600°F Reentry Profiles

250X

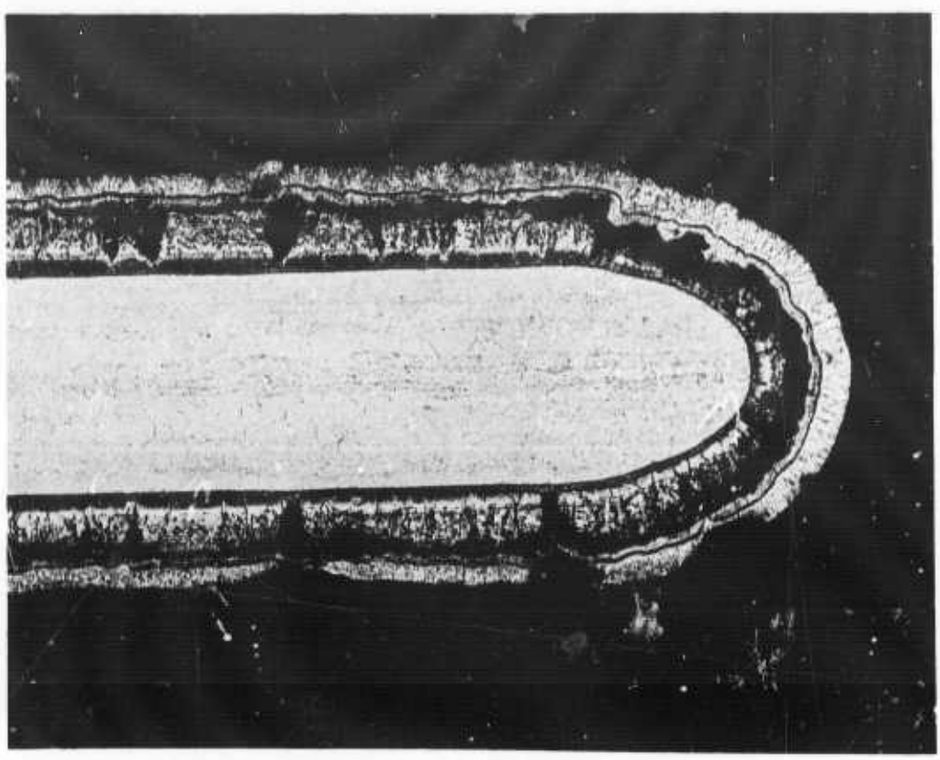

Figure 42 R–512E Coated Cb–752 After 25 Internal Pressure 2600°F Reentry Cycles

100X

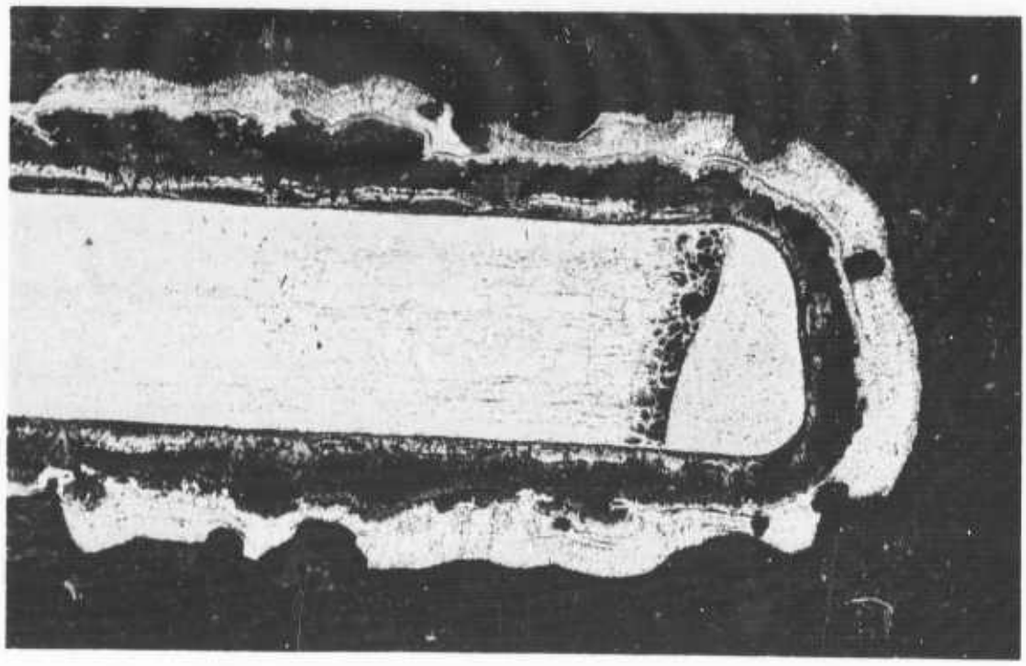

Figure 43 R–512E Coated Cb–752 After 35 Internal Pressure 2600°F Reentry Cycles 100X

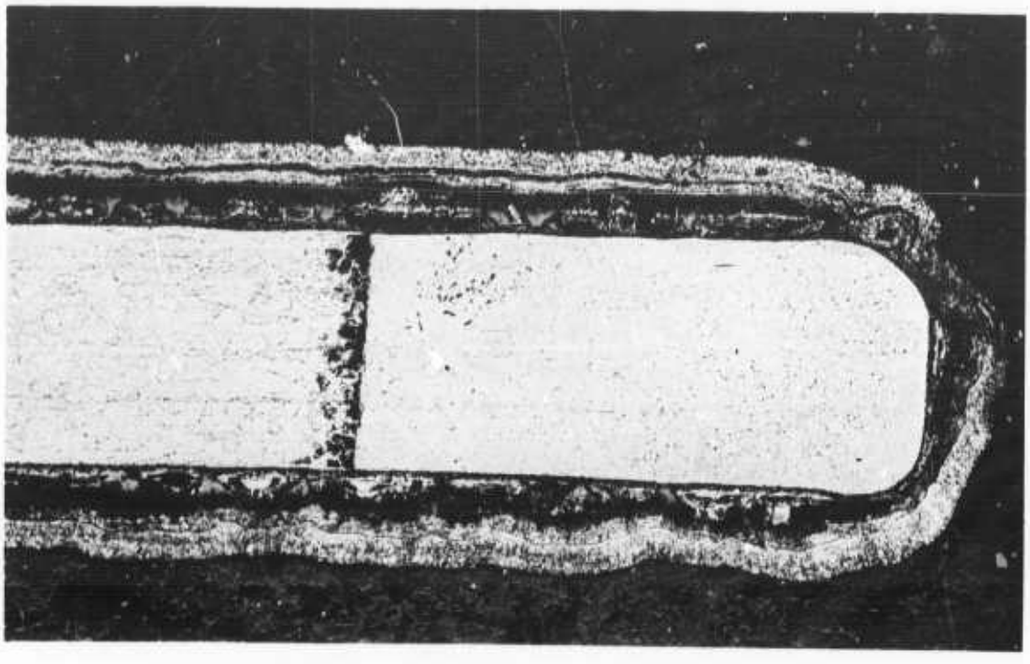

Figure 44 R–512E Coated Cb–752 After 40 Internal Pressure 2600°F Reentry Cycles 100X

The primary baseline test of the coating's performance is the temperature-pressure-stress-time profile test because this test condition is used for the major testing of the coated structural configurations. Profile test conditions of temperature, internal and external pressure, and high and low stress are as presented in Figure 19 of Section III. The low stress profile is differentiated from the high stress profile by the absence of the 6000 psi stress peak in the middle of the profile peak temperature. The loads required to produce the desired stress levels were derived using the calculated cross-sectional area of the metal remaining after coating. From measured coating weights, the amount of base metal consumption due to coating (approximately one mil per side) was obtained from Reference 17. An additional one-half mil per side, based on a 50 cycle exposure, was alloted for consumption due to diffusion zone growth which occurs during testing.

Baseline stress oxidation specimens (also presented in Table X) which were tested at 2600°F are grouped under the test conditions to which they were exposed and are reported in number of test cycles completed before rupture as follows:

EXTERNAL PRESSURE/HIGH STRESS	EXTERNAL PRESSURE/LOW STRESS
19	24
25	28
27	35
31	35
37	42

INTERNAL PRESSURE/HIGH STRESS	INTERNAL PRESSURE/LOW STRESS
23	24
25	26
26	27

Table X
Results of Time-Temperature-Pressure-Stress Profile Tests
R-512E Coated Cb-752

Specimen Number	Test Condition		Test Results	Remarks
	Stress	Press		
1	High	Int	26 Cycles	Fractured
2	Low	Ext	35	
3	Low	Int	24	
4	Low	Int	26	
6	Low	Ext	35	
7	Low	Ext	28	
10	Low	Ext	42	
11	High	Ext	37	Fractured
12	High	Ext	31	Edge oxidation at 29 cycles, fractured 31 cycles
13	High	Ext	27	Fractured
14	Low	Int	27	
15	High	Int	23	
16	High	Int	25	
17	High	Ext	19	Fractured
18	High	Ext	25	Edge oxidation at 23 cycles, fractured 25 cycles
19	Low	Ext	24	Fractured

The high stress profile (6000 psi load at 2600°F) produced no significant effect over the low stress profile in the internal pressure environment. However, the high stress profile does have a moderate effect as more oxygen becomes available in the external pressure environment. Figure 45 is a microsection of a specimen which ruptured after being exposed for 37 cycles to the external pressure/high stress environment. This section was taken perpendicular to the direction of applied load. A slight amount of contamination is evident immediately below the coating. Figure 46 is a microsection of the same specimen taken parallel to the direction of applied load. Contamination is evident beneath the areas of preferential oxidation attack. There are oxide filled cracks in the majority of these areas. Figure 47 is a microsection of a specimen which ruptured after being exposed for 35 cycles to the external pressure/low stress environment. This section was taken parallel to the direction of applied load. The preferential oxidation attack of the coating is present; however, in this particular section there was no evidence of base metal contamination. A comparison of Figures 39, 40, and 41 (specimens exposed to external pressure environments without stress) and specimens exposed to the external pressure with stress (Figures 46 and 47) reveals the significant effect of stress. The stress accelerated the time to produce coating failure by a minimum of 40% in the external pressure environment. Perhaps columbium creep is more definitive of what is really happening to cause the accelerated oxidation. Shown in Figure 48 are baseline stress oxidation specimens "before test" and "after 31 cycles" in the external pressure-high stress-2600°F environment. Note the difference in total length which gives a feel for the amount of creep which took place. Figure 49 is a microsection of a specimen after being exposed for 26 cycles to the internal pressure/high stress environment. This section was taken perpendicular to the direction of applied load and shows one edge of the specimen which is heavily contaminated from oxidation. Figure 50 is a section of the same specimen taken parallel to the direction of applied load. Practically all of the coating has been oxidized and vaporized with large areas of contamination resulting where the coating has failed. The majority of these contaminated areas show fissures or cracks that penetrate up to one-third of the way through the base metal. Figure 51 is a microsection of a specimen which ruptured after being exposed for 24 cycles to the internal pressure/low stress environment. A slight amount of contamination and an associated crack in the base metal is evident. The oxidation attack or loss of the coating is not as uniform as for the specimens exposed to the internal pressure/high stress condition. Comparison of these specimens exposed to the internal pressure-high and low stress conditions with those exposed only to the internal pressure condition show an accelerated loss of coating for the specimens tested under stress. Stress is opening the microcracks in the coating thus exposing a greater surface area of the coating for oxidation and vaporization. Oxidation protective life of the coating is at a minimum reduced by 25% in the internal pressure environment due to the effect of stress.

Failure or rupture in all cases occurred at the beginning of the test cycle when the specimens failed to withstand the programmed 40,000 stress level.

The most probable mode and/or sequence of events which led to tensile failures were: vaporization-oxidation of the coating, contamination in the metal locally where first coating breakthrough occurred, cracks forming in the contaminated metal due to the stress profile, and finally rupture as the stress risers created by the cracks multiplied the stress to a point where the ultimate strength of the base metal was exceeded.

Because of the maximum test temperature reduction from 2600°F to 2400°F, which occurred after baseline stress oxidation tests had been conducted at 2600°F, more baseline tensile type specimens were subjected to 2400°F maximum temperature stress oxidation tests. Using the 2400°F maximum temperature and the external pressure high stress profiles, three specimens were exposed individually for 60, 34, and 10 simulated reentries. No coating failures were detected nor was

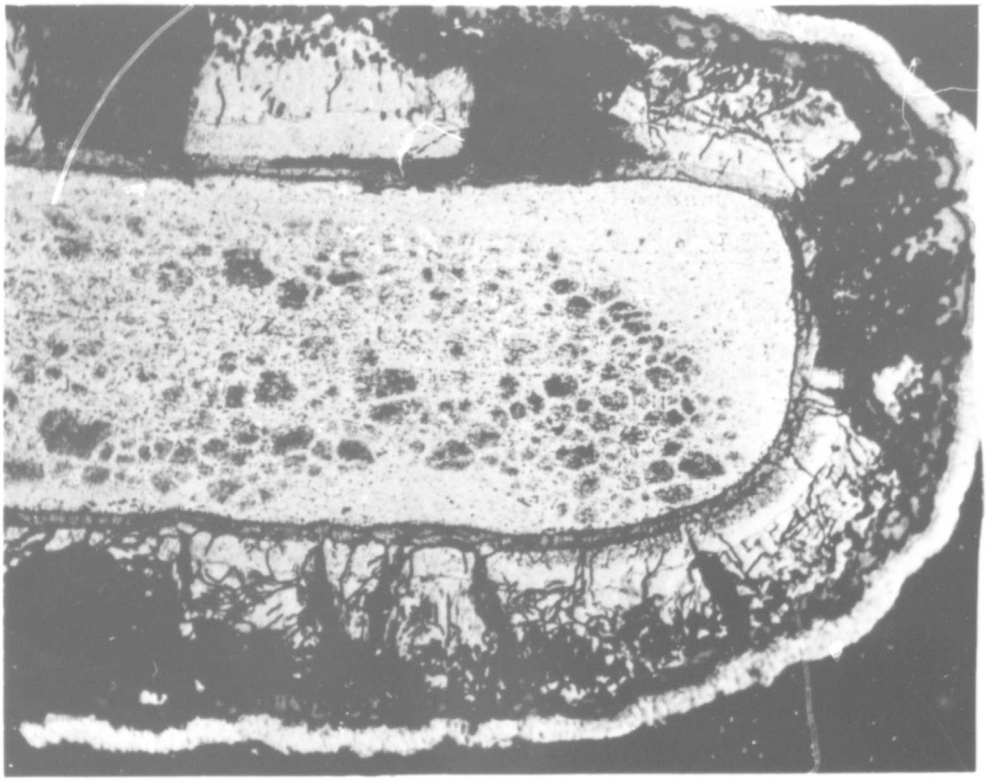

Figure 45 R–512E Coated Cb–752 After 37 Simulated Reentry Cycles Under External Pressure/High Stress Conditions 250X

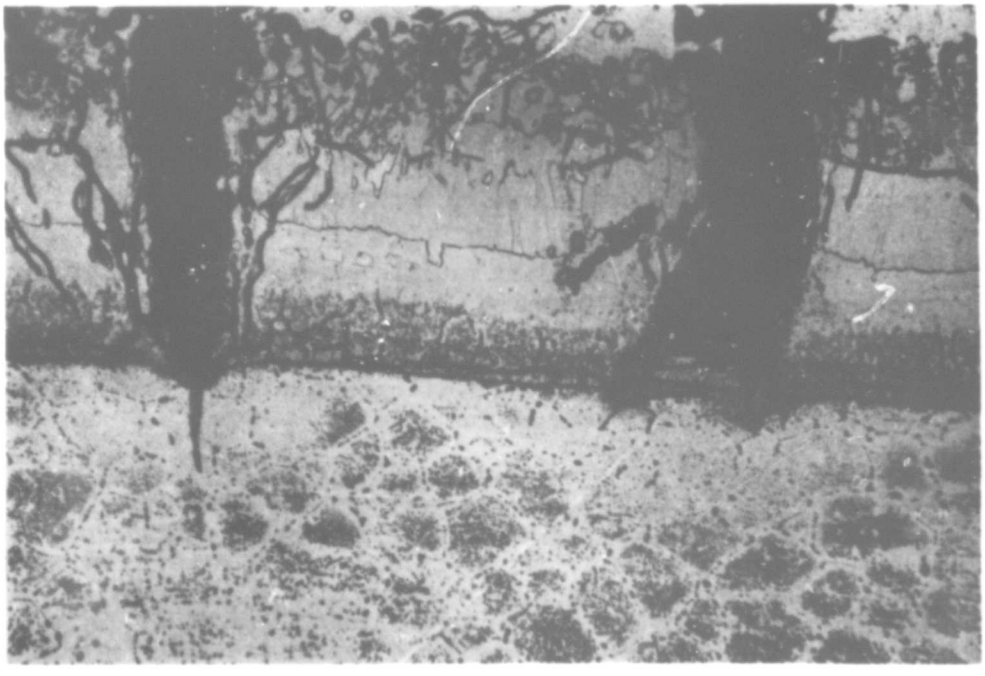

Figure 46 R–512E Coated Cb–752 After 37 Simulated Reentry Cycles Under External Pressure/High Stress Conditions 500X

Figure 47 R-512E Coated Cb-752 After 35 Simulated Reentry Cycles Under External Pressure/Low Stress Conditions 500X

structural integrity lost on any of the specimens. Three specimens were exposed to the internal pressure-high stress profiles for 60, 30, and 10 simulated reentries. Again no coating failures or structural failures occurred. These baseline tests were conducted after completion of the heat shield panel tests and were suspended from testing at 60, 30, and 10 cycles based on duration of heat shield panel testing to allow comparison with the coating on the panels which were stressed under bending loads or biaxial stresses.

By comparison, baseline profile stress oxidation testing at 2600°F produced structural failures in 23 to 26 flights or simulated reentries in the internal pressure environment and 19 to 37 flights or simulated reentries in the external pressure environment. Therefore, the 200°F difference in maximum test temperature had a large affect (greater than 3 fold) on the number of simulated flights for tensile failure.

Figure 52 and 53 are microsections taken parallel and perpendicular respectively, to the direction of applied load of the specimen which was exposed for 60 cycles to the external pressure, high stress, and 2400°F temperature flight simulation profile. Coating deterioration appears to be of the same type and approximate extent of that observed on the specimen exposed to the same pressure - stress conditions at 2600°F but only for 37 cycles (See Figure 45). Figure 54 and 55 are microsections taken parallel and perpendicular, respectively, to the direction of applied load of the specimen which was exposed for 60 cycles to the internal pressure, high stress, and 2400°F temperature profile. The coating oxidation/vaporization was considerably less than that observed on the specimen exposed to the same pressure-stress conditions at 2600°F, but for only 26 cycles (see Figure 50).

Figure 48 Baseline Stress Oxidation Specimens Before And After Testing For 31 Flights In An High Stress External Pressure – 2600°F Environment.

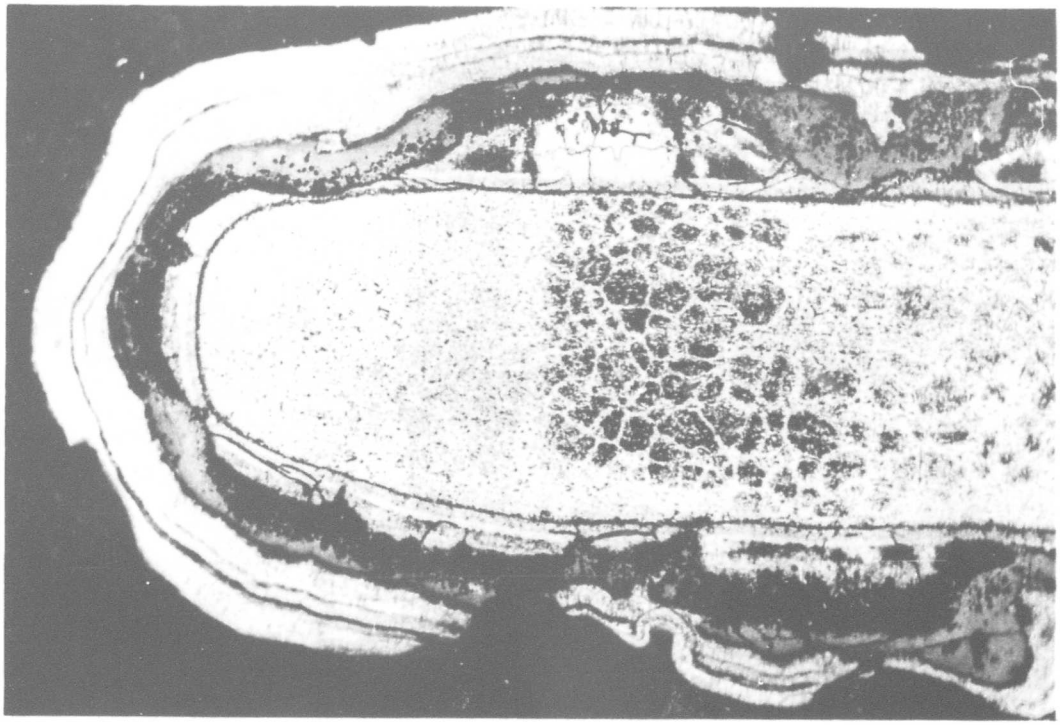

Figure 49 R–512E Coated Cb–752 After 26 Simulated Reentry Cycles Under Internal Pressure/High Stress Conditions 250X

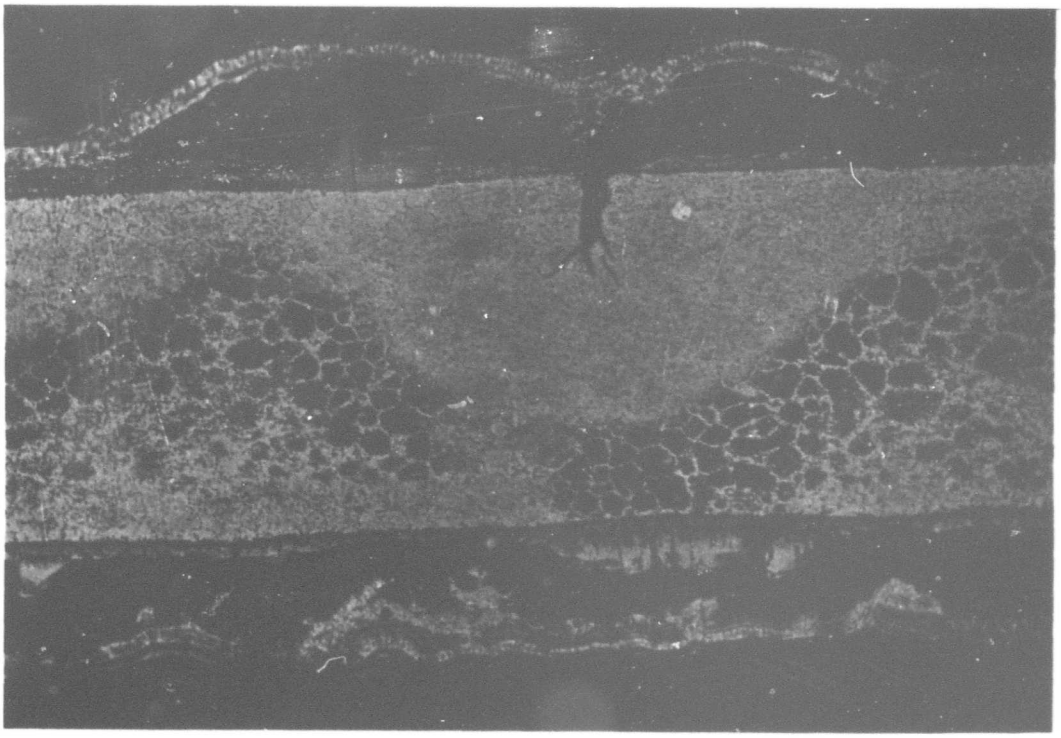

Figure 50 R–512E Coated Cb–752 After 26 Simulated Reentry Cycles Under Internal Pressure/High Stress Conditions 250X

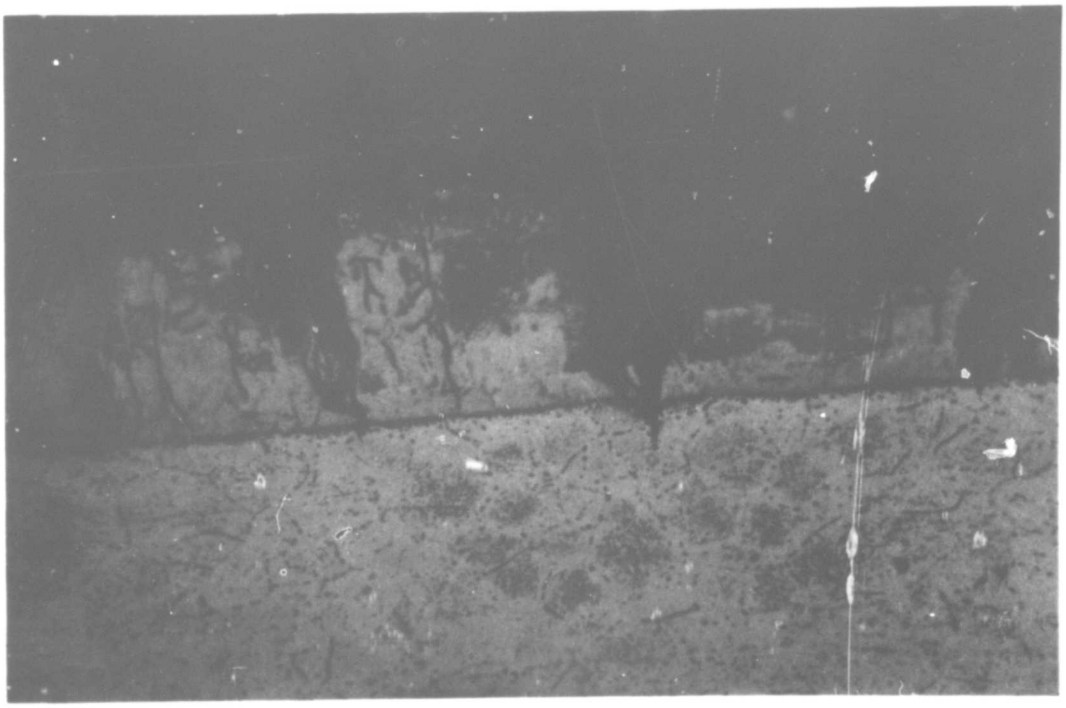

Figure 51 R-512E Coated Cb-752 After 24 Simulated Reentry Cycles Under Internal Pressure/Low Stress Conditions 500X

There is however a certain zone or layer of the coating that has been preferentially removed by the oxidation/vaporization mechanism. The coating has remained entirely protective in spite of the creep and elongation which occurred.

Two fractured baseline tensile specimens were examined by electron fractographic techniques. The specimens were exposed to two different testing environments. Specimen 1 was tested to failure (26 cycles) in an internal pressure, high stress, and 2600°F temperature profile and failed in a brittle manner; metallographic examination indicated that the base metal had been contaminated. Specimen 2 was tested to failure (35 cycles) in an external pressure, low stress and 2600°F temperature profile, and metallographic examination did not show evidence of contamination.

Two areas on each specimen were selected for replication and subsequent electron microscopic examination. Presented in Figure 56 is a photograph of the fractured surfaces of both specimens with the location of the areas replicated.

The microscopic features of the fracture surfaces as observed in the light microscope indicate fracture origin at both edges of Specimen 1 and at one edge of Specimen 2. The remaining areas of both specimens consisted of shear fracture. Electron fractographic examination of Specimen 1 revealed a duplex structure at the origin, Figure 57 Area A. The duplex structure consisted of a mixture of brittle cleavage rupture and ductile dimple rupture. The shear region exhibited elongated dimples typical of a ductile shear rupture, Area B of Figure 57. Both the origin and shear region on Specimen 2 revealed ductile features typical of an overload failure, Figure 58.

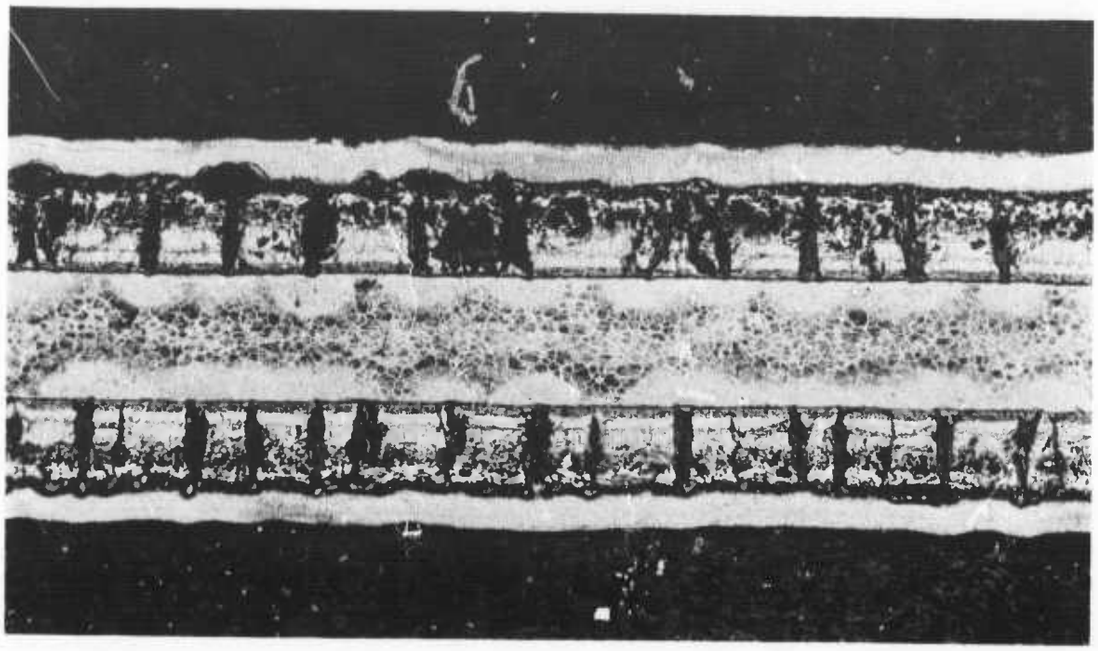

100X

Figure 52 R–512E Coated Cb–752 After 60 Simulated Reentry Cycles (2400°F) Under External Pressure High Stress Conditions

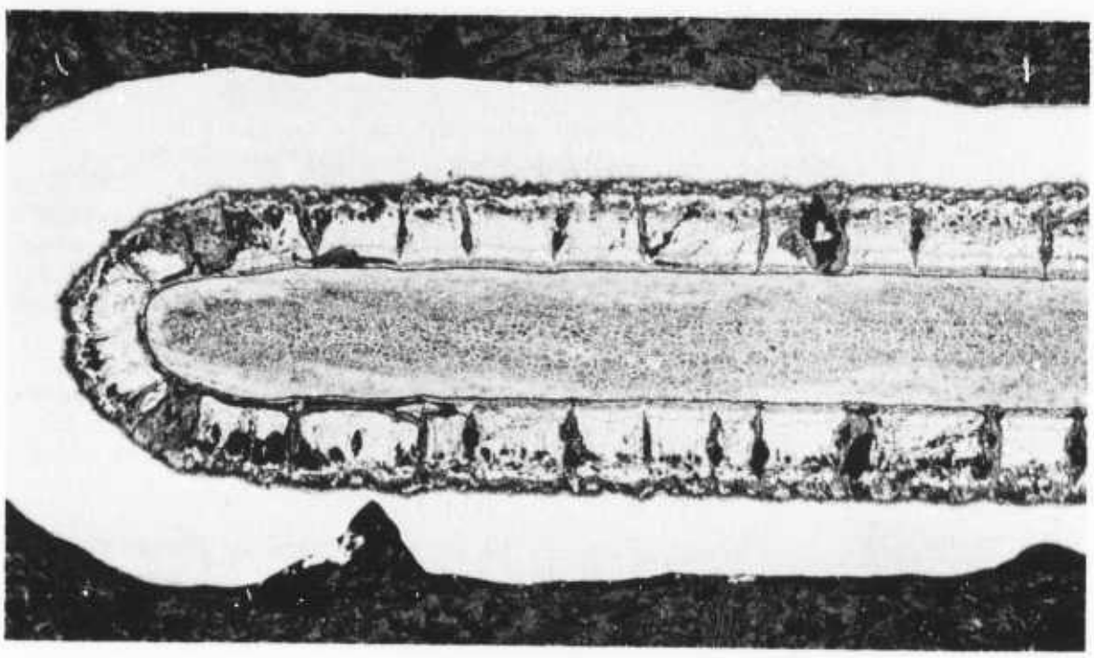

100X

Figure 53 R–512E Coated Cb–752 After 60 Simulated Reentry Cycles (2400°F) Under External Pressure/High Stress Conditions

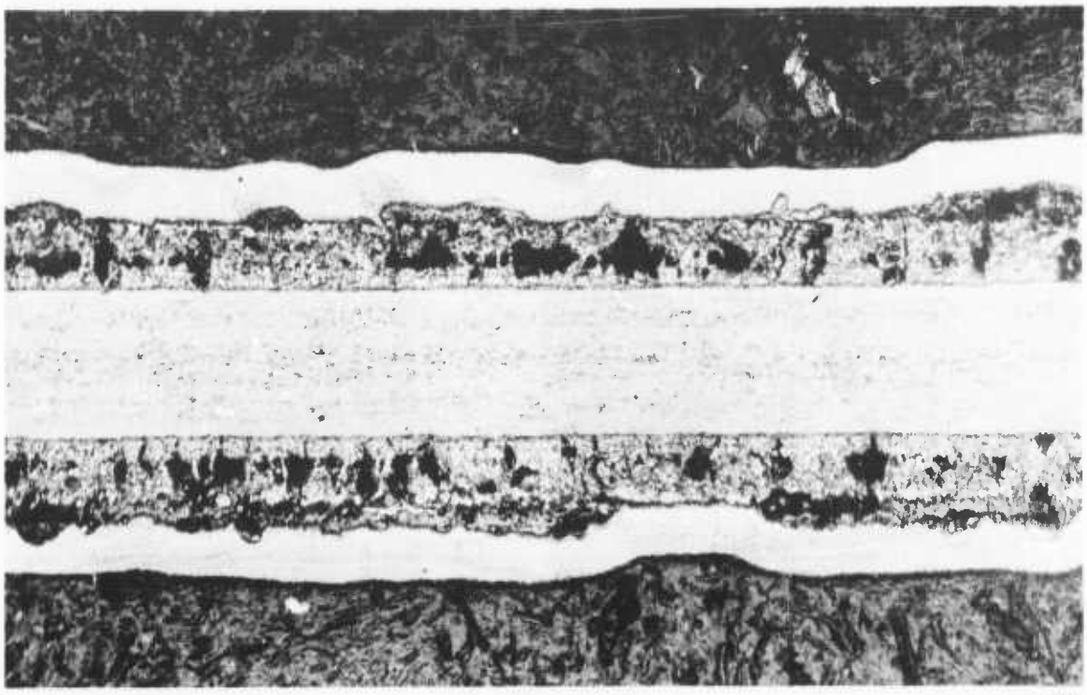

100X

Figure 54 R–512E Coated Cb–752 After 60 Simulated Reentry Cycles (2400°F) Under Internal Pressure/High Stress Conditions

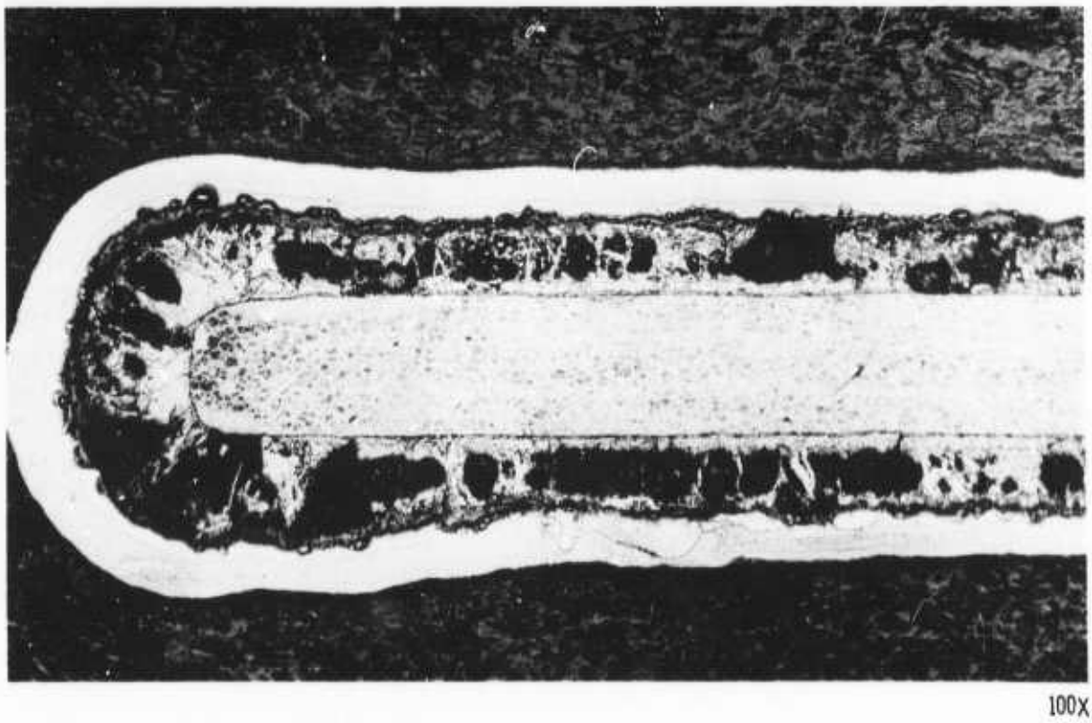

100X

Figure 55 R–512E Coated Cb–752 After 60 Simulated Reentry Cycles (2400°F) Under Internal Pressure/High Stress Conditions

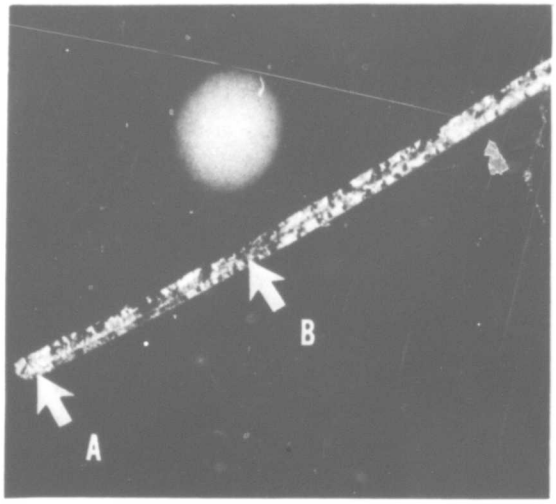

8X

Specimen 1

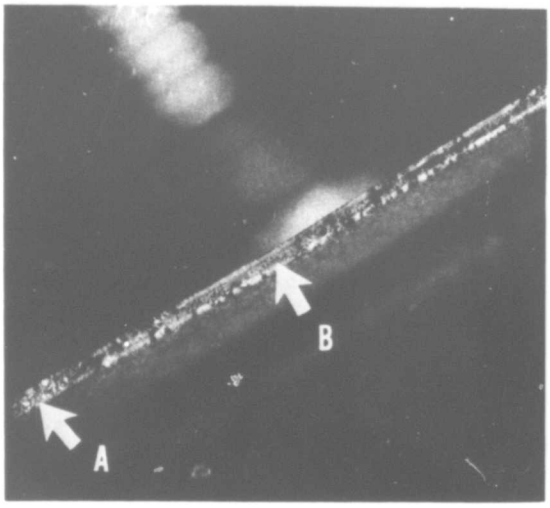

8X

Specimen 2

Figure 56 Fracture Surface Of Both Specimens With The Location Of The Areas Replicated.

Area A 4200X

Area B 4200X

Figure 57 Replicated Fracture Surface Areas Of Specimen 1

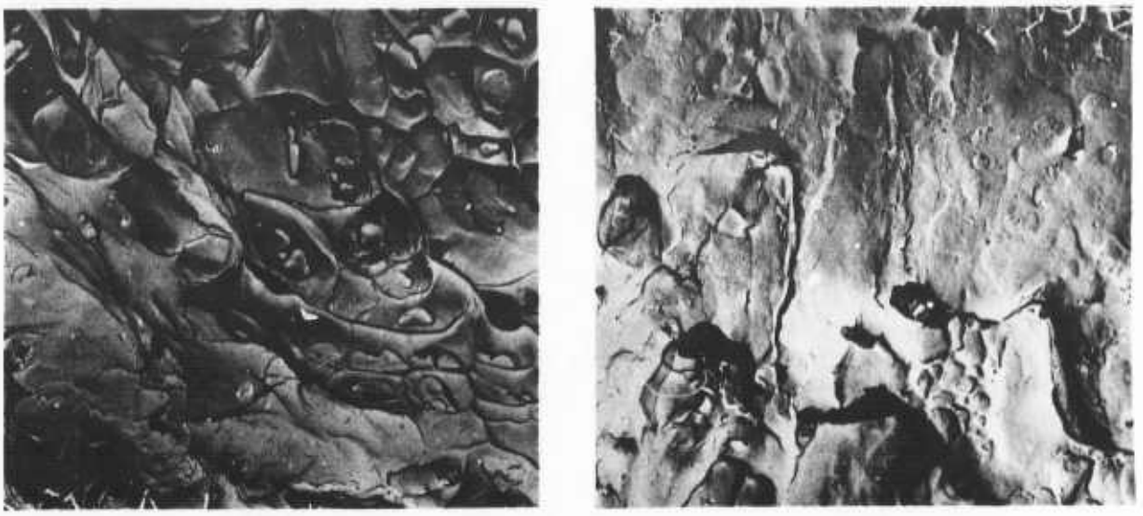

Area A
4200X

Area B
4200X

Figure 58 Replicated Fracture Surface Areas Of Specimen 2

The results of the electron fractographic examination confirmed that the rupture of Specimen 1 initiated at local brittle regions where the base material had been contaminated. It also was confirmed that Specimen 2 ruptured in a completely ductile mode, and that the rupture was not associated with contamination.

All specimens tested to the external pressure condition were not free of contamination and it must be assumed that these specimens did not fracture in a completely ductile mode.

In spite of the considerable contamination and cracks in the base metal due to preferential coating oxidation, the baseline oxidation specimens withstood the 18,000 psi loading at the end of the test cycle, and usually 80% of the load required to produce 40,000 psi, at the beginning of the next cycle, before rupture occurred.

Riveted lap shear specimens, as shown in Figure 15 of Section II, were evaluated under temperature-pressure-stress profile conditions. The 2400°F maximum temperature profile was used.

The riveted lap shear specimens included two types. One type employed two flush head 1/8"dia. rivets fit in counter sunk holes in the .034" Cb-752 material and the other type employed two button head 1/8" dia. rivets in the .016" Cb-752 material. Stress calculations showed that the specimens with the flush head rivets would fail in shear and the specimens with the button head rivets would fail in bearing. Two coated specimens of each type were tested at room temperature to produce failure. The average load required to produce failure for the specimens with flush head rivets and for the specimens with button head rivets was 1190 pounds and 789 pounds, respectively. This corresponds to ultimate shear and bearing stresses of 55,000 psi and 114,000 psi, respectively. Based on shear and bearing

strength data reported by DMIC, yield stresses were calculated for room temperature and 2400°F. A load profile was developed for each type of specimen which would produce, at R.T. and at Tmax., 66 2/3% of the yield stress. For the flush head rivet specimens these stresses were 23,500 psi at R.T. and 7,900 psi at 2400°F. For the button head rivet type specimens these stresses were 69,000 psi at R.T. and 16,500 psi at 2400°F.

The load profile in terms of pounds for the flush head rivet type specimens consists of a steadily increasing load from 0 to 50 pounds over the length of the test. Three load peaks are induced, one at Tmax. equal to 170 pounds and two at R.T., one at the beginning and one at the end of the profile test each equal to 505 pounds. The loading device on our test facility is limited to 475 pounds in order to maintain accuracy. This deficit of 30 pounds amounts to 1400 psi in terms of shear stresses which is 6% less than desired.

The load profile in terms of pounds for the button head rivet type specimens consists of a steadily increasing load from 0 to 50 pounds over the length of the test. Three load peaks are induced, one at Tmax. equal to 114 pounds and two at R.T. one at the beginning and one at the end of the profile test each equal to 475 pounds.

Four of the flush head riveted type specimens were exposed to the external pressure, 2400°F Tmax. profile, and the load profile previously explained. Due to the eccentric loading produced by the lap, which caused the riveted joint to rotate so that true shear loading was not produced, and oxide growth in the faying surface, results of the testing were eratic and not really conclusive. Structural failure was attained for the four specimens in 1 1/2, 3 1/2, 4 and 6 cycles, respectively. Results are summarized in Table XI. Rivet pull-out was responsible for failure in all cases. The specimen which failed in 6 cycles had slurry painted on the faying surfaces prior to riveting; this proceeded the coating cycle. Slurry painting of faying surfaces prior to assembly proved to be an effective method of protecting faying surfaces and also eliminates the need for a second coating cycle to repair damaged rivets.

A riveted lap shear specimen, with countersunk holes to accommodate flush head rivets, was coated before assembly and then locally recoated to refurbish the damaged coating on the rivets. This specimen was tested in the internal pressure environment at a maximum room temperature shear stress of 23,5000 psi and a 2400°F shear stress peak of 7,900 psi. Testing was terminated after 20 profiles with no visible signs of deterioration, except for some rotation of the riveted joint due to the eccentric loading. An identical specimen tested in the external pressure environment survived only 4 profiles before rupture.

Three of the button head riveted type specimens were exposed to the external pressure, 2400°F Tmax. profile and the load profile previously explained for this type of specimen. Again due to the eccentric loading produced by the lap, which caused the riveted joint to rotate so that true bearing loading was not produced, results of the testing were not entirely conclusive. Structural failure was attained for the specimens after 6, 7, and 9 cycles. Rivet tear-out was responsible for failure in all cases.

Table XI
Summary Of Lap Shear Specimen Tests

Type	No.	Test Cond.	No. of cycles tested	Description	Remarks
.034" Stock Flush Head Rivet	4	E.P./H.S.	3 1/2	Assembled and coated	Fracture on mid load of cycle 4
	7	E.P./H.S.	1.1/2	Bare faying surface	Fracture on mid load of cycle 2
	8	E.P./H.S.	6	Slurry coated faying surface	Fracture on initial load of cycle 7
	9	E.P./H.S.	4	Coated and assembled	Fracture on final load of cycle 4
	10	I.P./H.S.	20	Coated and assembled	No failure
.016" Stock Button Head Rivet	6	I.P./H.S.	19	Bare faying surface	Fracture on final load of cycle 19
	7	E.P./H.S.	7	Slurry coated faying surface	Fracture on final load of cycle 7
	9	E.P./H.S.	9	Coated and assembled	Fracture on final load of cycle 9
	10	E.P./H.S.	6	Coated and assembled	Fracture on final load of cycle 6
.034" Stock Double Lap with Threaded Fasterner	N.A.	E.P./H.S.	20	Coated and assembled	Terminated after 20 cycles No failure

E.P. = External pressure
I.P. = Internal pressure
H.S. = High stress

The specimen which failed in 7 cycles had slurry painted on the faying surfaces prior to riveting, this proceeded the coating cycle. The specimens which failed in 6 and 9 cycles were coated prior to riveting and then recoated to refurbish the damaged coating on the rivets. No gross faying surface oxidation was noted in either case.

A button head riveted lap shear specimen with a known bare faying surface was tested to the internal pressure 2400° profile environment at a maximum room temperature bearing stress of 69,000 psi and a 2400°F bearing stress peak of 16,500 psi. The specimens ruptured after 19 profiles. This compares to lap shear specimens with coated faying surfaces which survived 4 to 6 profiles in the external pressure environment.

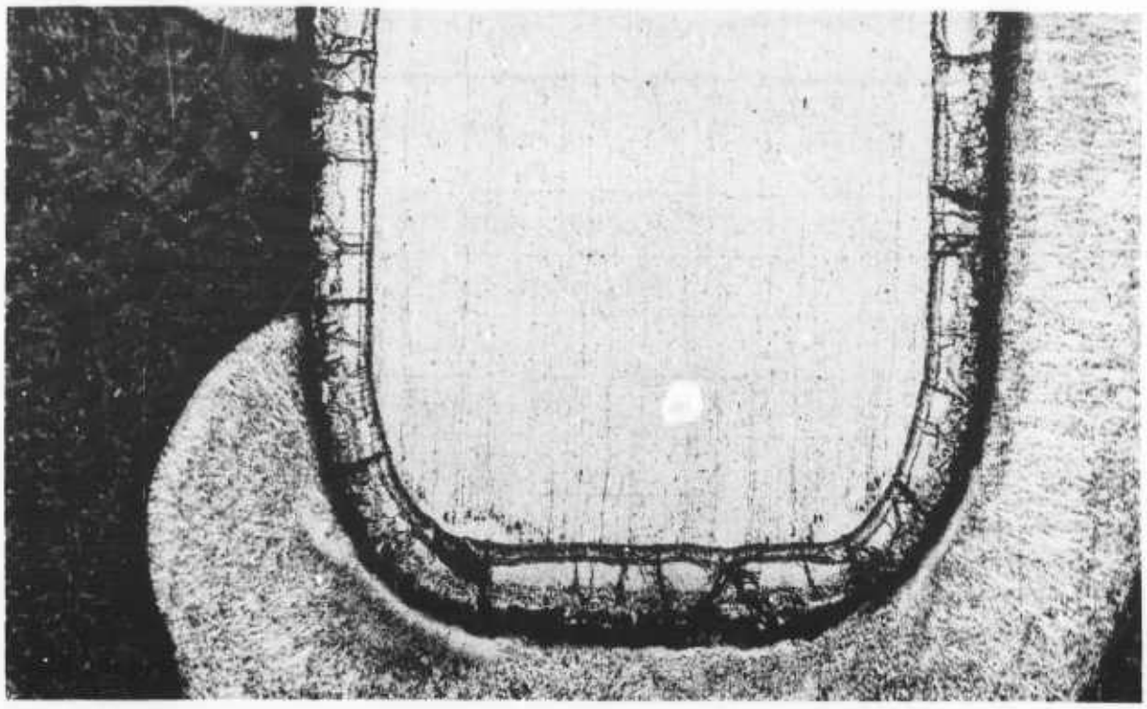

100X

Figure 59 Bearing Area On Sheet Specimen Used In Threaded Fastner Test After 20 Simulated Reentries In An External Pressure Environment

A threaded fastener joint was assembled in a double lap shear arrangement and tested to the external pressure 2400°F profile with a maximum room temperature bearing stress of 69,000 psi and the 2400°F bearing stress peak was 16,500 psi. The specimen was tested for 20 profiles with no signs of oxidation or deterioration. As shown in Figure 59, metallographic examination of the bearing area in the single leg of the joint showed no gross deterioration of the coating due to the bearing load. There appeared to be a partial spalling of the coating at one edge which has allowed a small amount of base metal contamination.

b. Mechanical Properties

Mechanical property data for bare and R-512E coated Cb-752 served as a reference to establish load limits, show the effect of coating on mechanical properties, and help interpret the test results for the heat shield panel specimens.

Tabulated data for the tensile, creep, bend, spot and electron beam (EB) welded lap shear, and notch sensitivity test are presented in Appendix I.

Elevated temperature tests (1300°F to 2600°F) on all bare specimens and tests on coated specimens at 1300°F and 1800°F were conducted at a maximum pressure of 1×10^{-4} Torr. Tests on coated specimens at temperatures of 2400°F and 2600°F were performed in a helium environment at a pressure of 700 Torr. The helium atmosphere was used to prevent contamination of the furnace due to coating vaporization.

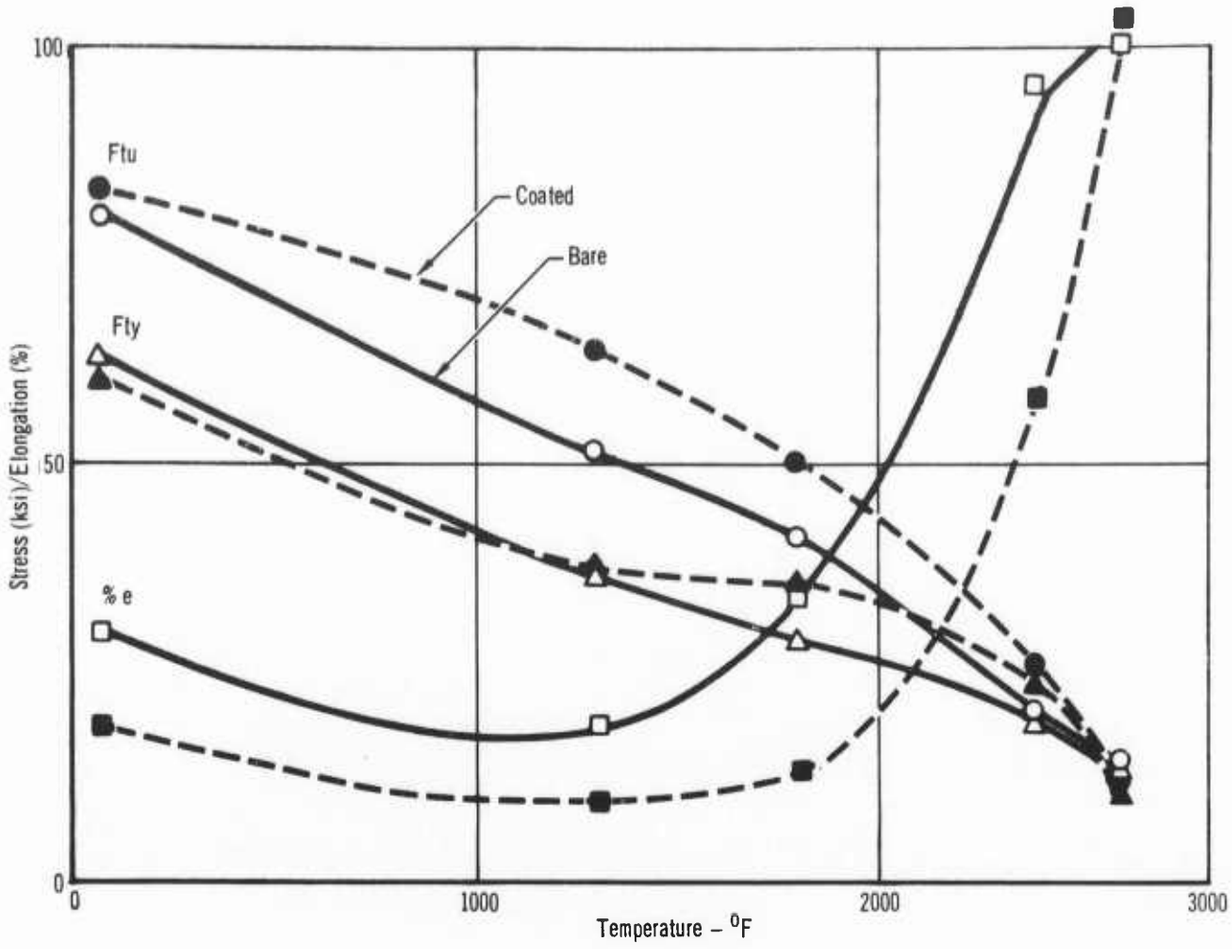

Figure 60 Comparison of Tensile Test Data for Bare and R-512E Coated Cb-752

Test temperatures were measured with a platinum/platinum 10 percent rhodium thermocouple and a Leeds and Northrup pyrometer. The thermocouple was tack-welded directly to the specimen for tests conducted on bare specimens and was tack-welded to a bare dummy specimen, located adjacent to the actual test specimen, for the tests conducted on coated specimens. Room temperature tensile tests were conducted at a strain rate of 0.005 in/in/min to yield (0.6 percent offset) and at 0.050 in/in/min thereafter. Elevated temperature tensile tests were conducted at a head travel rate of 0.050 inch/minute. The cross sectional area of the coated specimens was determined by knowing the original thickness and allowing 0.001 inch/side for base metal consumption during the coating process.

Figure 60 shows graphically a comparison of tensile test data for bare and R-512E coated Cb-752. Each data point represents the average of three specimens tested. The coated specimens displayed a slightly higher Ftu than did the bare specimens (except at 2600°F). The percent elongation of the coated specimens was consistently less (approximately 50%) than the bare coupons. At 2600°F no significant different between the tensile test results of the bare and coated specimens was observed. Notch sensitivity tests were conducted at the same head travel rate as for the tensile specimens.

The comparison of notch tensile strength with ultimate tensile strength for bare and R-512E coated Cb-752 is presented in Figure 61. The comparison was not made at 2400°F and 2600°F, since no drastic notch sensitivity was detected in the low ductility range of 12-1800°F. Each data point represents the average of three specimens tested. The notch root radius after coating is .002". Initial notch root radius before coating was .0006"-.0007". The notch root radius of a coated specimen was determined from a metallographic section as shown in Figure 62. The notch tensile and ultimate strength of the bare alloy is approximately the same, which shows practically no notch sensitivity in the uncoated condition. The percent reduction in strength due to notching was considerably greater for the coated than for the bare alloy. Notches and/or notch effects are a reality in coated refractory metal structures and must not be disregarded. The notch strength of the R-512E coated Cb-752 compared to the coated ultimate strength was high enough (.90 of ultimate) to indicate good material toughness.

Welded lap tensile tests were conducted at a steady loading rate which caused failure in 3±.5 minutes. A comparison of bare and R-512E coated Cb-752 welded lap tensile data is presented in Figure 63. The two types of welded specimens employed in this test were electron beam welded and resistance spot welded. The specimens having a horizontal weld across the one inch width and the spot welded specimens having two welds along the longitudinal center line. Most data points are for an average of two specimens because approximately one-third of the specimens failed through the loading hole during testing. Welded lap tensile tests, because of the eccentric loading, produce tri-axial stresses in the joint and can therefore be used as a sensitive indicator of weld ductility. Weld failures observed in these tests were of a ductile nature. It can be observed that the coating and/or coating process had no adverse effects on weld strengths. The spotweld strength approaches the electron beam weld strength as the temperature increases.

Bend specimens (bare and coated) were formed 120 degrees around a 0.031 inch radius mandrel at room temperature. A die throat opening of 2R + 2-1/2 t and a ram travel rate of 1.0 inch/minute were used. Neither the bare or coated specimens broke during forming and displayed no visual cracking in the metal, although as expected the coated specimens did exhibit cracking of the coating.

Creep tests on bare and coated specimens at 2400°F and 2600°F were conducted by Metcut Research Associates Inc., of Cincinnati, Ohio. The tests were performed in a cold wall vacuum furnace set in a conventional creep rack in which a hanging dead weight was used to load the test specimen. The specimen was radiant heated to the desired test temperature by a resistance heated tantalum sheet element. The furnace was controlled automatically by means of silicon rectifiers operating on a thermocouple signal.

Creep was measured by a linear variable differential transformer which sensed the pull bar motion beneath the creep furnace. This output was fed through a demodulator into a multipoint speedomax recorder. The creep specimen was loaded after a gradual heat up and a fifteen minute stabilization period at the test temperature. The load was applied gradually and continually over a 10-15 second interval by releasing a hydraulic load elevator. The deformation was rezeroed as soon as the specimen was fully loaded and the ensuing creep was automatically recorded. The furnace and associated equipment

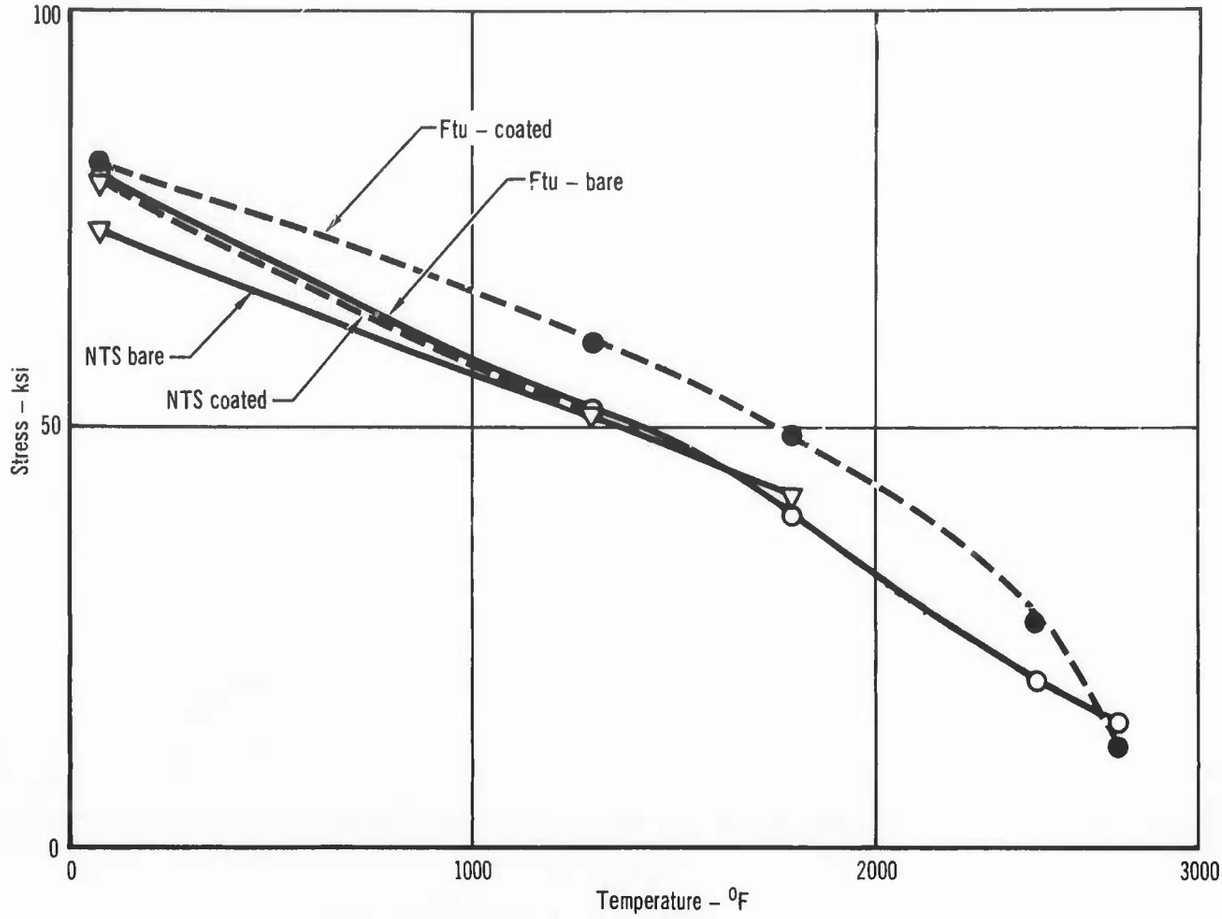

Figure 61 Comparison of Notch Tensile Strength with Ultimate Tensile Strength for Bare and R–512E Coated Cb–752

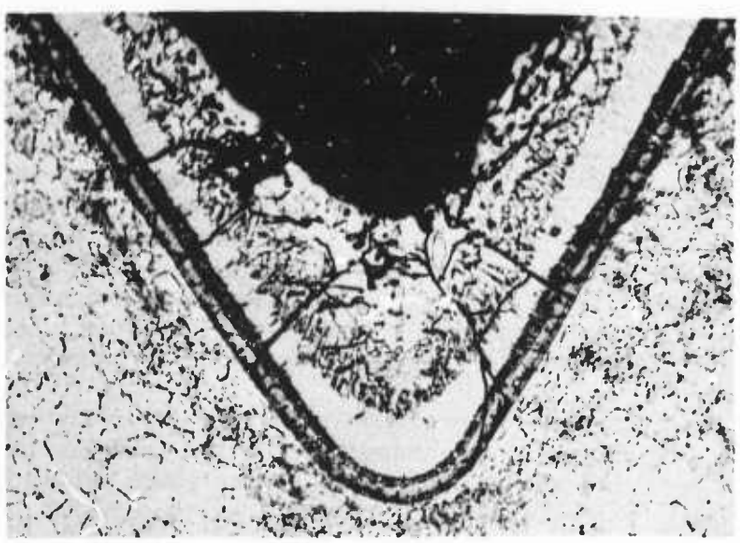

Machined radius (prior to coating) 0.0006/0.0007 **250X**
Radius after coating 0.002

Figure 62 Notch Root of Notched Tensile Specimen after Coating

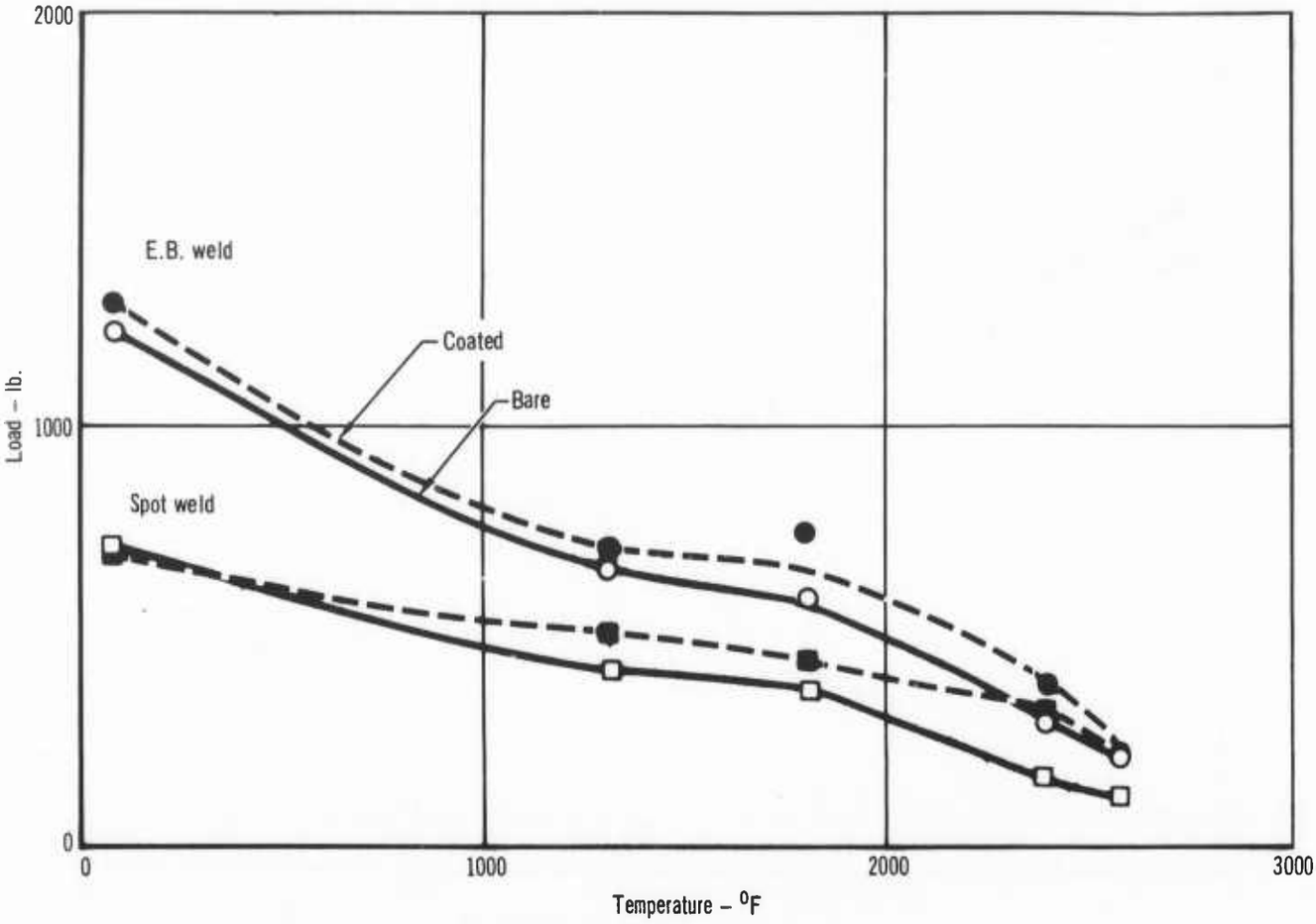

Figure 63 Comparison of Bare and R-512E Coated Cb-752 Welded Lap Tensile Data

utilized during the creep test were shown in Figure 26.

Creep data taken at 2400 and 2600°F is compared in Figure 64 which shows the relationship between stress and the time to creep 2%. There is little difference between the creep properties of the bare and the coated material at either 2400°F or 2600°F. The coating and temperature history of the coating process do not degrade creep properties of the single annealed Cb-752 and, if anything, may slightly improve resistance to creep. The creep rate of bare and coated material is considerably lower at 2400°F than at 2600°F. Figure 64 also shows that there is somewhat more scatter in the 2600°F data than in the 2400°F data. This scatter in the creep data is typical for high temperature creep measurements on columbium alloys.

When designing columbium alloy structures for reuse capabilities, complete characterization of the properties of the material from which the component will be fabricated is essential for reliable performance. This is due to the fact that properties vary from heat to heat of the alloy. Also it has been shown that the fused slurry-silicide coating process essentially has no effect on the mechanical properties of the Cb-752 columbium alloy.

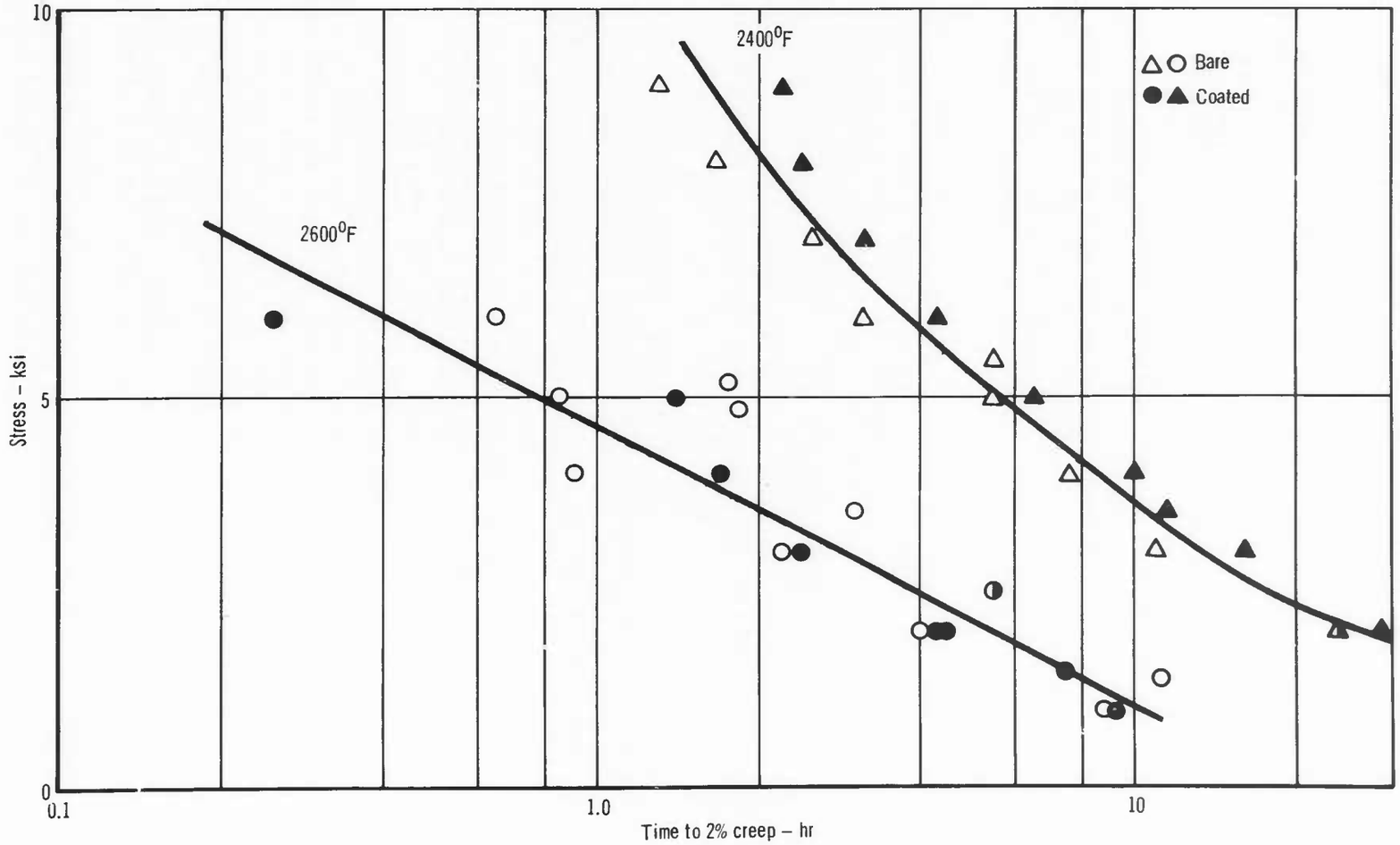

Figure 64 Comparison of Bare and Coated Creep Data

2. HEAT SHIELD PANEL TESTING

Discussed in this section are coating performance results for various heat shield constructions.

Variations of representative heat shield designs were used to determine the protection that the R-512E coating will afford to faying surfaces and joints. These variations involved different methods of attaching the stiffener to the skin, such as, resistance spot and electron beam welding and riveting. Representative heat shield configurations selected for evaluation include single faced flat and vee corrugation stiffened, rib and stringer stiffened, and riveted channel stiffened panels. Based on the selected test conditions of stress and temperature, test specimens representative of the aforementioned variations and configurations were designed, fabricated, coated, and flight simulation tested. Flight simulation testing consisted of the simultaneous temperature, pressure, stress, versus time profiles previously shown in Section II, Figure 19. Results are summarized in Table XII.

Three single faced flat corrugation stiffened heat shield specimens were tested at the internal pressure/high stress 2600°F profile condition. For these specimens, the skin to corrugation joint was made by spot welding. Of the heat shield constructions being evaluated, the spot welded construction should be the most difficult to reliably coat. These specimens were tested through 7 to 12 cycles without coating failure. These tests were stopped because of excessive permanent deflection due to creep of the base metal. The variation in deflection per cycle was also excessive, indicating poor load control.

In order to identify the cause for the unacceptable variation, all calculations and the test apparatus were checked. It was found that strain link, which was used to control the loading of the specimen, was not sufficiently sensitive at the low loads or stress levels. Based on calculations, about two-thirds to three-fourths of the creep was caused by an outer fiber tensile stress of 2000 psi, corresponding to a load of only five pounds (no permanent specimen deflection). Yet the strain link also had to be capable of operating at a load of 200 pounds (after permanent specimen deflection) to provide the 40,000 psi stress at the beginning of a test cycle. (As permanent deflection is induced in the specimen, the load applied to the scissors must be increased to provide a given outer fiber stress because the mechanical advantage of the scissors decreases.) The problem of excessive variation in deflection/test cycle was solved by using two strain links for control. The large one was used when the 40,000 and 18,000 psi stress is applied at the beginning and end of a test cycle. A much more sensitive strain link was used when the zero to 6000 psi stress is applied during the time the specimen is being heated. The small strain link was made so that a 20 pound load would produce approximately 80% of its yield strength. The strain links were dead weight calibrated in series with the strain indicator used in performing the testing. The two strain links can be readily interchanged. This change did not alter the test profile.

Based on the 2600°F creep data, it was calculated that the permanent deflection resulting from the temperature-load test conditions would be approximately .010 inch/cycle, or 0.1 inch after ten cycles. About twice

Table XII

Summary Of Heat Shield Panel Tests

Specimen Type	Spec. No.	Test conditions	Cycles Tested	Total Deflection	Remarks
Spot weld Flat Corrugation	2	I.P. H.S.	8	.045	Furnace failure
	7	I.P. H.S.	12	.040	No Failure
	9	E.P. H.S.	10	.041	Reversed load on cycle 7
	3	I.P. H.S.	12	.209	Tested at 2600^{0}F
	5	I.P. H.S.	7	.209	Tested at 2600^{0}F
	6	I.P. H.S.	10	.184	Tested at 2600^{0}F
E.B Weld Flat Corrugation	3	I.P. H.S.	10	.040	Overstressed on cycles No Failure
	5	I.P. H.S.	17	.040	No Failure
	6	E.P. H.S	15	.042	No Failure
	10	I.P. H.S.	15	.040	No Failure
Vee Corrugation	1	I.P. H.S.	32	.040	No Failure
	2	I.P. H.S.	32	.048	Overload on cycle 18
	3	I.P. L.S.	40	.040	No Failure
	5	I.P. H.S.	16	.029	Furnace failure
	7	E.P. H.S.	8	.026	Furnace failure
	9	E.P. H.S.	10	.034	Furnace failure
	13	E.P. H.S.	29	.041	No Failure
Zee Stringer	1	I.P. H.S.	21	.040	No Failure
	2	I.P. H.S.	23	.040	No Failure
	3	E.P. H.S.	22	.041	Oxidation Failure, Faying surface
	4	I.P. H.S.	19	.041	No Failure
Rib Stiffened	1	I.P. H.S.	38	.040	No Failure
	2	I.P. H.S.	55	.040	No Failure
	3	I.P. H.S.	48	.040	No Failure
	4	E.P. H.S.	61 (100)	.040 (.062)	Tested for an additional 39 flights – no failure
Riveted Channel	2	E.P. H.S.	51	.040	Detail coated, then assembled
	8	E.P. H.S.	26	–	Oxidation and structural fatigue. No deflection reading after cycle 7
	10	I.P. H.S.	54	.041	No Failure

Note;
E.P. – External pressure
I.P. – Internal pressure
H.S. – High stress
L.S. – Low stress

this deflection occurred on the spot welded constructions tested for approximately ten cycles. This indicates that the applied loads (stresses) were greater than planned. In spite of the excessive deflections, there were no coating failures. Considering that these are the most difficult to coat constructions, the performance of the coating is very encouraging. However, if testing to the 2600°F profile was continued, it appeared unlikely that coating failures could be produced at realistic creep deflections.

An important consideration in the design of hot spacecraft heat shield structures, and one which influences structural weight, is the maximum panel deflection which can occur without increasing the heating rates over that for an undeflected smooth surface. In one of our advanced design studies, a permanent deflection criterion had been selected as a guide. For a twenty inch panel, permissible deflection varied from 0.1 inch at body station 12 to 0.5 inch at body station 120. The flight trajectory and lift to drag ratio of the vehicle will also influence permissible deflection. In terms of the three inch loading span on the test panels, this means permissible deflections from 20 mils to 100 mils accounting for the concentrated loading in this test versus the uniform air loading in flight. Since there seems to be no good logic for selecting any certain permissible deflection, 40 mils was arbitrarily selected as the creep deflection limit to which the majority of the test panels would be tested.

Using the 2600°F test conditions, an unacceptable deflection would result after about four cycles. Continuing to test at the 2600°F condition would simply confirm that the columbium alloy had a very high creep rate. Not much would be learned about the ability of the coating to provide protection to the various heat shield constructions. Therefore, the maximum temperature in the profile tests was reduced to 2400°F. All the other test conditions remained the same. This temperature reduction enabled the specimens to withstand considerably more test cycles before a creep deflection of .040 inch was reached.

Twenty-five heat shield specimens were tested at 2400°F Tmax. which produced meaningful data. Several specimens were destroyed as a result of electrical and/or mechanical failure of the testing apparatus. Specimens were tested until a creep deflection of 40 mils was achieved except in cases where the specimen ruptured or where there were initial deflections resulting from fabrication and/or coating processing or where excessive deflections occurred during testing which resulted from a known instance of overloading. In these cases, these deflections were added to the permissible 40 mils. Total specimen deflection versus number of test cycles or flights are presented in Appendix II for each of the tested heat shield specimens. From the four possible profile combinations of stress and pressure, the high stress and internal pressure combination was chosen as the primary testing condition. This combination was selected primarily because joint and faying surface studies were a major objective of the program and joints and faying surfaces will experience internal pressure environments during actual use. Each type of panel design was also tested under external pressure conditions. The large difference in number of flights required to attain 40 mils of creep deflection from one configuration to another is due to the difference in the weight efficiency and in the stress distribution from the outer fibers of the stiffener (tension) to the outer fibers of the skin (compression). In all cases, the outer fibers of the stiffeners of the various configurations

were exposed to the same stress during testing. Due to the different designs and varying distribution of cross-sectional area from the tensile to the compressive side of the panels, the stress distributions were different for different panel configurations. Also none of the configurations were truly optimumly designed because of the constraints of minimum gauge, and allowable specimen size. Therefore with these aforementioned facts in mind, one must know and should remember that the number of cycles required to attain 40 mils of deflection cannot be used to select a superior structural design.

A comparison was made of the performance of the spotwelded flat corrugation type panel when exposed to internal versus external pressure environments. The skin to corrugation joint for this type of panel is made by resistance spot-welding at a spotweld spacing of one-half inch. The panels tested in the internal pressure environment revealed no visible signs of coating failure and structural integrity was maintained up to the creep deflection limit. The panel tested in the external pressure environment was progressing at approximately the same rate of deflection as the panels tested at internal pressure for six cycles. The panel was mistakenly installed backwards in the loading fixture in cycle #7. The panel was apparently damaged structurally because the subsequent deflection rate increased approximately sixfold. Columbium oxide growth could be seen in the faying surface after 9 cycles.

A comparison was made of the performance of the electron beam welded flat corrugation type panel when exposed to the external versus internal pressure environments. The skin to corrugation joint for this type of panel is made by a continuous electron beam weld running the entire length of the panel. The faying surface of the electron beam welded flat corrugation configuration is not as difficult to protect from oxidation as the faying surface of the spot welded configuration because the electron beam welded joint is much more rigid. This rigidity prevents opening of the faying surface when the joint is worked as the loading level changes during flight. During this testing, structural integrity was maintained and no visible coating failures were detected. The 14 cycles required to produce 40 mils of deflection at external pressure compares exactly to the 14 cycle average for the three specimens tested under internal pressure-high stress conditions.

One of the electron beam welded flat top corrugation stiffened panels which was tested for 15 cycles at internal pressure-high stress conditions was examined metallographically. Figures 65 and 66 show the condition of the coating on the external and internal surfaces of the corrugation taken parallel and perpendicular to the corrugation direction, respectively. The first major observable difference is the coating thickness on the exterior versus interior surface. The coating is almost twice as thick on the external surface. However, the two mils of coating on the interior surface was more than adequate to provide oxidation protection for the 15 simulated reentries.

The effects of stress and bending are noted by the pronounced amount of cracks in the coating, running in all directions. Figures 67 and 68 are photomicrographs of the same panel from the perpendicular section, but taken in the area of the skin to corrugation joint. Coating thickness in general is slightly greater (1 mil) in the joint area than on the rest of the skin and corrugation. Base metal contamination can be noted in Figure 67 where the coating has not penetrated and protected the faying surface. This amount of contamination did not affect the structural integrity of the panel.

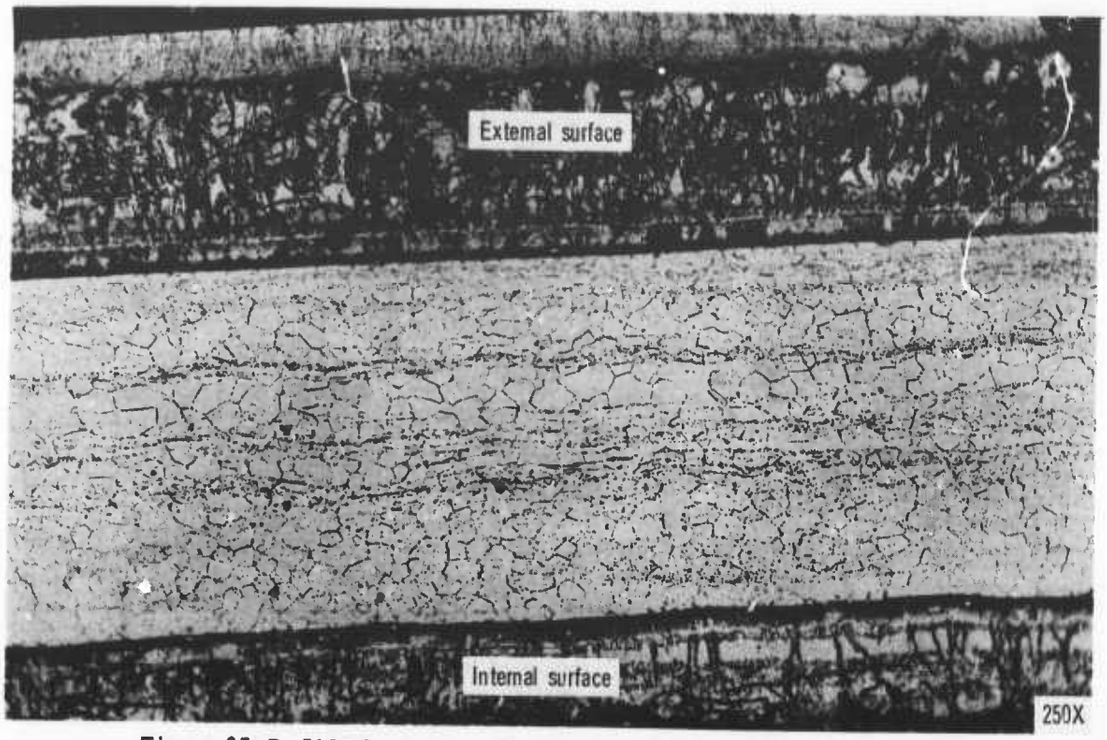

Figure 65 R-512E Coating on Corrugation of Panel After 15 Simulated Reentries Under Internal Pressure/High Stress Conditions (Section Made Parallel to Corrugation Direction)

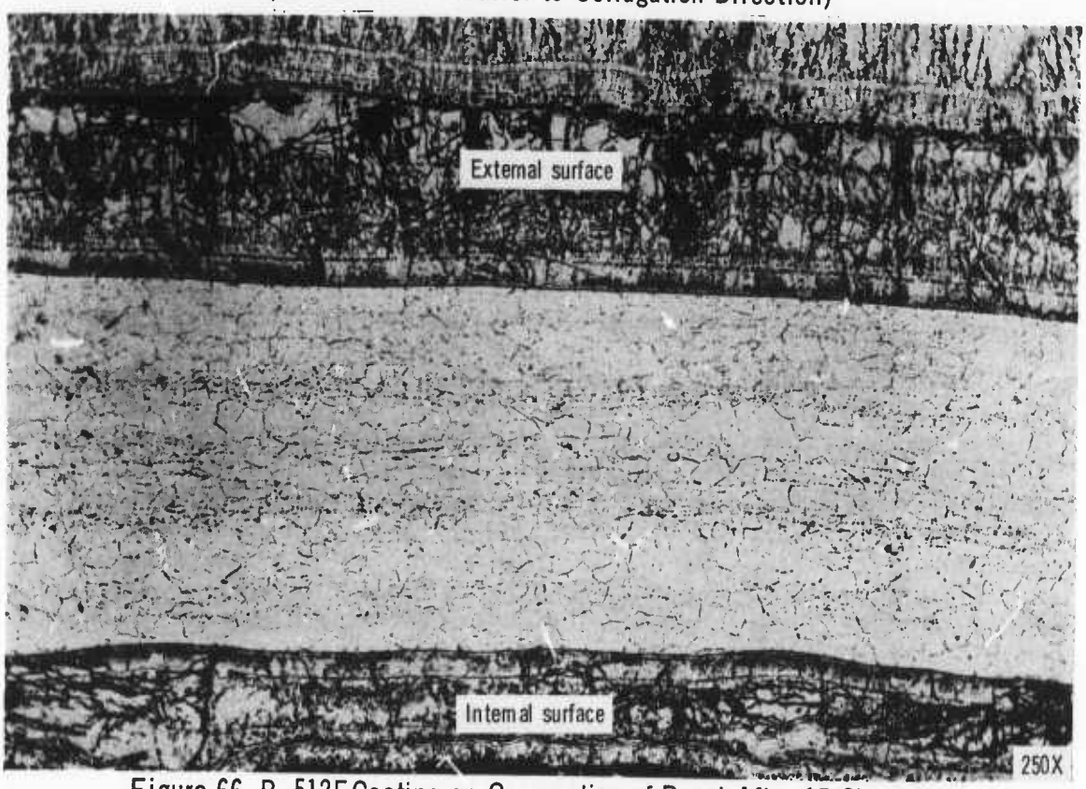

Figure 66 R-512E Coating on Corrugation of Panel After 15 Simulated Reentries Under Internal Pressure/High Stress Conditions (Section Made Perpendicular to Corrugation Direction)

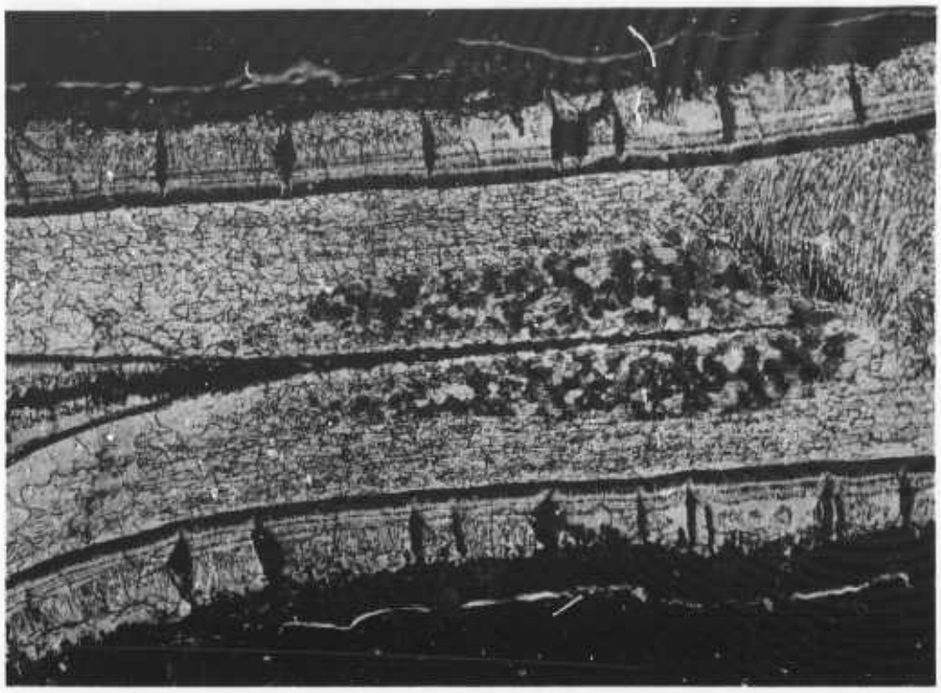

100X

Figure 67 R–512E Coating at Skin and Corrugation Joint of Panel After 15 Simulated Reentries Under Internal Pressure/High Stress Conditions (Note Base Metal Contamination)

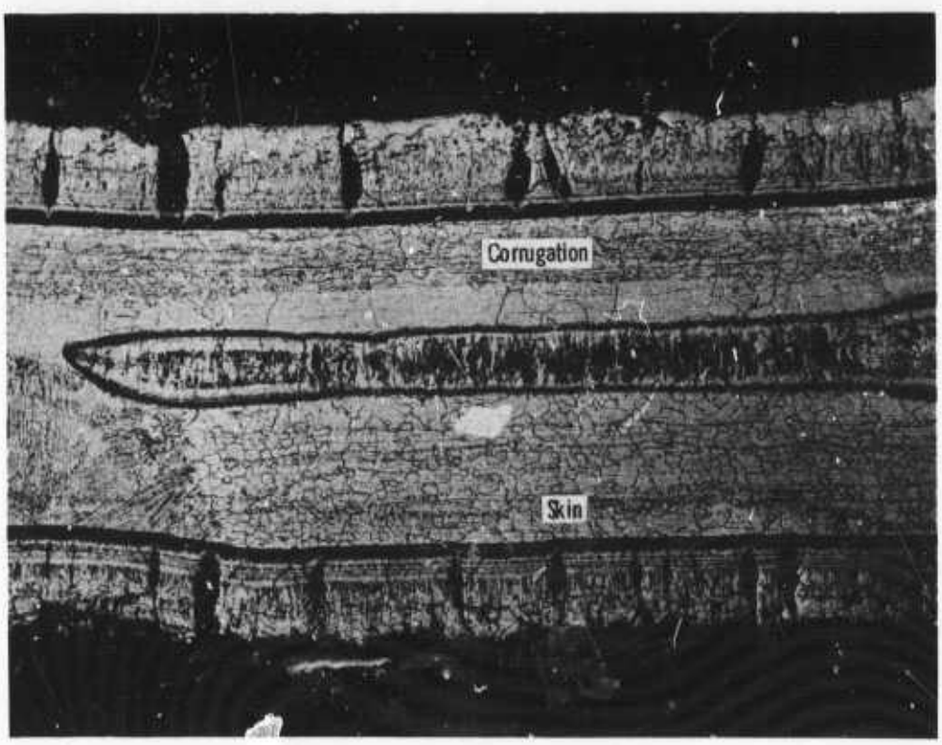

100X

Figure 68 R–512E Coating at Skin and Corrugation Joint of Panel After 15 Simulated Reentries Under Internal Pressure/High Stress Conditions (Note Complete Coating Coverage in Faying Surface)

A complete contrast to the faying surface coating coverage can be seen in Figure 68, which is a section taken from the same panel. The most logical explanation is that the gap between the skin and corrugation must be large enough to allow penetration of the coating. Examination, Metallographic of the EB welded flat corrugation panel which was tested in the external pressure environment revealed large amounts of contamination where the coating has not penetrated and protected the faying surface. However, where there was coating penetration and coverage there was no contamination.

The performance of the rib stiffened type panel was determined when exposed to internal versus external pressure environments. The skin to rib joint was made by electron beam welding. There are no faying surfaces in this panel design. During tests conducted on the rib stiffened panels structural integrity was maintained and no coating failures were observable in either the internal or external pressure environments. Performance in the internal and external pressure environments compares favorably. There was a change in rate of deflection after 25 to 30 cycles of testing for the panel tested is the external pressure environment, which is not truly explainable, but may be related to stability of the rib stiffeners. A cross-section photomicrograph of the joint section of a rib stiffened panel which has been subjected to 48 simulated flights in an internal pressure environment is shown in Figure 69. One of the rib stiffened panels which had been subjected to 61 flights (the point where the .040" permissible deflection was attained) in an external pressure environment was exposed for an additional 39 flights. No coating failures were detectable after the 100 flight exposure.

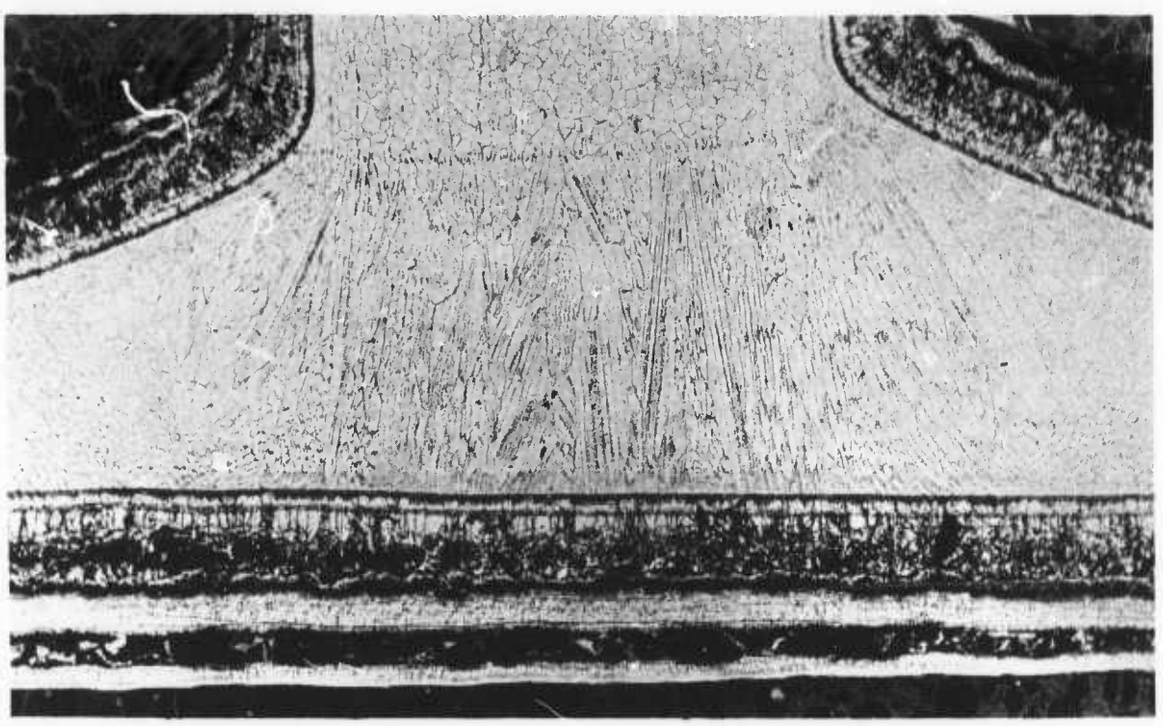

Figure 69 Joint Area Of Rib Stiffened Panel After 48 Flights In An Internal Pressure Environment 100X

A photomicrograph of the joint area of a vee corrugation type panel exposed in an external pressure environment for 29 flights is shown in Figure 70. The skin to corrugation joint was made by electron beam welding in such a way that faying surfaces were eliminated. Structural integrity was maintained and no coating failures were evident during evaluation of this panel. The 37 cycles required to attain 40 mils of deflection compares closely to the 32 cycles required to produce the same amount of deflection in an internal pressure environment. A photomicrograph of the joint area for the panel exposed to 32 flights in the internal pressure environment is shown in Figure 71.

There was no decernible difference in the performance of the vee corrugation stiffened panels when evaluated in the external or internal pressure environments. A vee corrugation stiffened panel was subjected to the low stress profile in the internal pressure environment and 40 cycles were required to produce 40 mils of deflection. This is approximately 25% more cycles than was required under the high stress condition. This corresponds to the calculated 25% increase in creep due to the additional 4000 psi loading at T_{max} in the high stress profile.

The performance of the zee stiffened type panel was studied when exposed in internal versus external pressure environments. The stiffener to skin joint is made by resistance spotwelding at a spotweld spacing of one-half inch. Performance of these panel specimens was very reproducible. Three panels tested in the internal pressure environment required 19, 21 and 23 cycles of exposure to attain 40 mils of deflection, while the panel exposed at external pressure required 22 cycles. The non-uniformity of deflection per cycle for this type of specimen can be attributed to buckling of the skin and resultant movement of the deflection measurement point.

This buckling occurred in the skin on one side of the specimen because the skin was not supported or reinforced by the stiffener along this side. This was a limitation of the design for this size specimen. The zee stiffened specimen exposed to the external pressure environment revealed columbium oxide growth in the faying surface after 8 cycles of testing. After two more cycles of testing the skin was ruptured by the oxide growth. This area gradually increased in size as testing progressed through 22 cycles. This specimen is shown in Figure 72 after the 22 cycles of testing. Note that the specimen did not break in spite of the extensive oxidation of the skin. The specimens exposed in the internal pressure environment showed no visible signs of coating failure nor was structural integrity lost.

The performance of the riveted type panels during exposure in internal and external pressure environments was studied.

The skin to stiffener joint was made by flush head rivets in dimpled holes at a rivet spacing of .9 inch. These specimens were assembled prior to coating. No coating failures were observed and structural integrity was maintained for the specimen exposed to the internal pressure-high stress condition. For the specimen exposed to the external pressure-high stress condition, visible coating failures developed in the faying surface after two cycles of testing. After one more test cycle the oxide growth in the faying surface had buckled the skin to the point where it was splitting open at several locations. This bukcling and cracking became so severe that deflection measurements were no longer meaningful after 7 test cycles. The specimen is shown in Figure 73 after 11 test cycles had been completed.

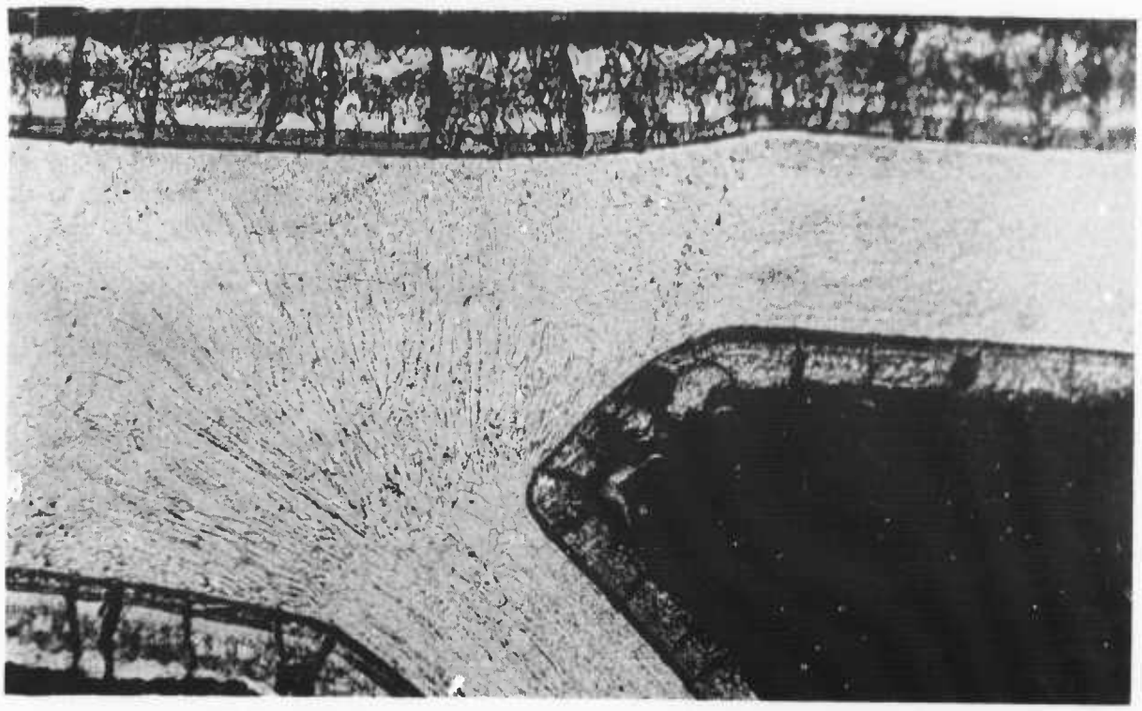

100X

Figure 70 Joint Area Of Vee Corrugation Stiffened Panel After 29 Flights In An External Pressure Environment

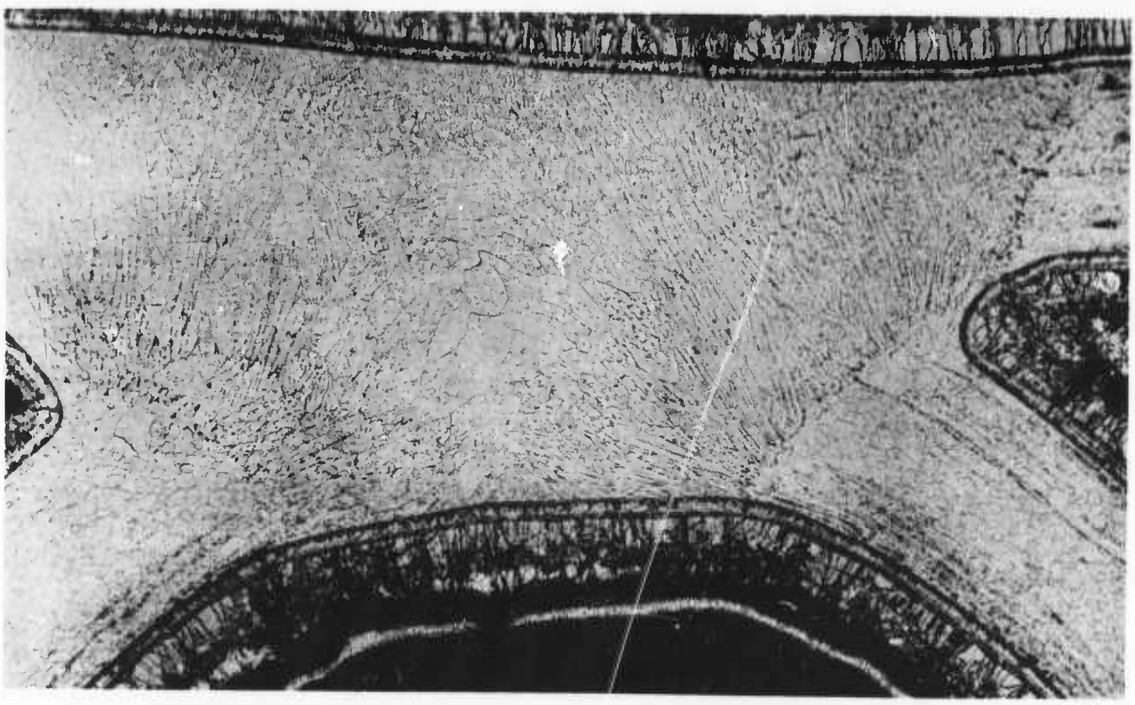

100x

Figure 71 Joint Area Of Vee Corrugation Stiffened Panel After 32 Flights In An Internal Pressure Environment

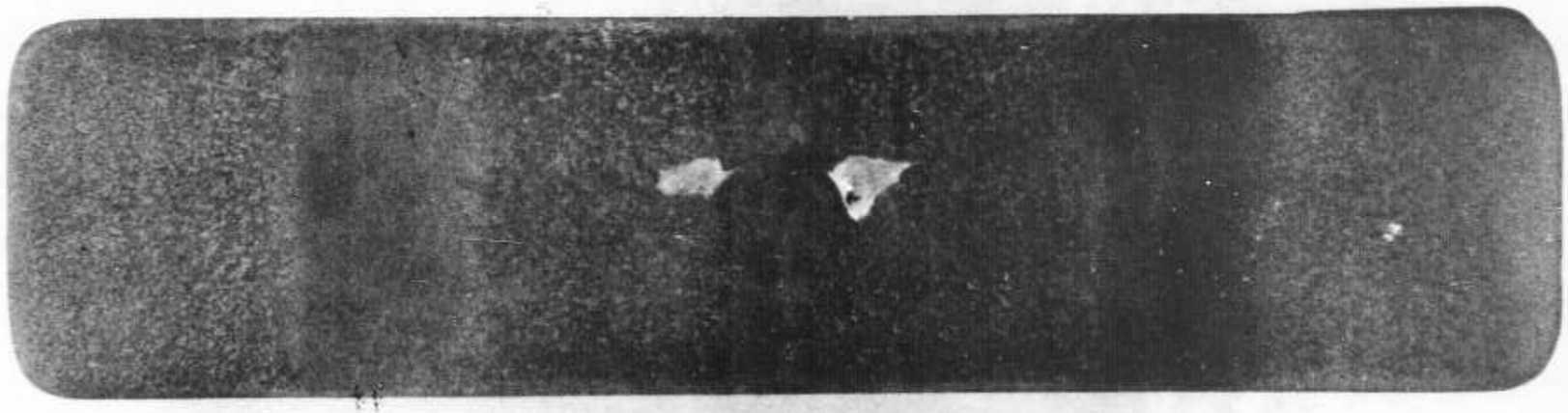

Figure 72 Zee Stiffened Heat Shield After 22 Simulated Flights In An External Pressure Environment (Note The Columbium Oxide In The Center Of The Panel)

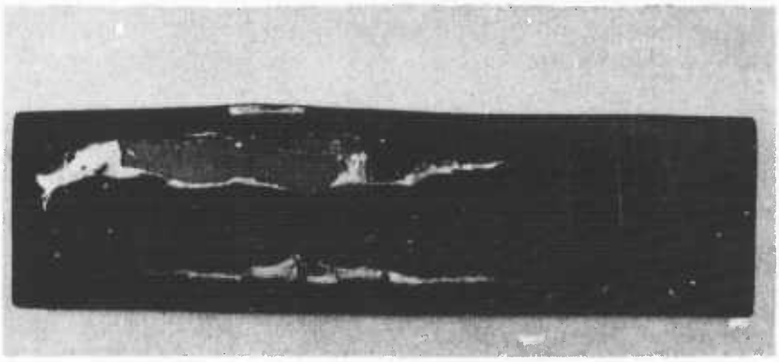

Figure 73 Rivet Heat Shield After 11 Simulated Flights In An External Pressure Environment

Testing continued until 26 cycles or simulated flights had been completed, at this time structural integrity was lost. The fact that this specimen maintained structural integrity after extensive base metal oxidation was surprising. Apparently the specimen lost its rigidity during the last few test cycles due to the consumption of columbium by oxidation and readily deflected elastically so that the scissors loading fixture straightened out and could no longer fully load the specimen.

The riveted channel specimen which was exposed to the internal pressure environment required 52 flights to produce 40 mils of deflection. After test the specimen, quite unlike the panel tested in the external pressure environment, was intact and showed no visible signs of oxidation. Metallographic examination revealed considerable contamination in the faying surface between the skin and channel stiffener. This contamination is shown in Figure 74 in an area adjacent to one of the rivets.

The riveted panel configuration produces a faying surface between the skin and stiffener which is eight-tenths of an inch wide. As determined by testing in the internal and external pressure environment this faying surface cannot be protected by the R-512E coating when applied after assembly. That is after the skin and stiffener had been joined together by riveting. Therefore, a riveted heat shield panel which was prepared by a different assembly coating sequence was tested. The details (skin, stiffener, and rivets) were coated with R-512E coating prior to assembly. The details were then joined by inserting and squeezing the rivets. The coating on the rivets was damaged during this operation and was repaired by locally applying R-512E slurry on each rivet and refiring per the normal coating process (1 hour-2580^{o}F). The heat shield specimen was then exposed to controlled temperature, air pressure, and stress simultaneously per the high stress and external pressure profile conditions shown in Figure 19 of Section II. No coating failures were observed and structural integrity was maintained for 51 cycles of exposure. A cross section photomicrograph of a rivet and adjoining area after exposure to the 51 cycles as shown in Figure 75. The damage to the coating on the ends of the adjoining sheet from the riveting operation was minimal. The reapplied coating on the ends of the rivet sufficiently sealed the rivet shank and adjoining areas and prevented oxidation in this area. The riveted specimen which was coated after assembly and was tested under high stress-external pressure profile conditions survived only two cycles before oxidation in the faying surface was visually detectable.

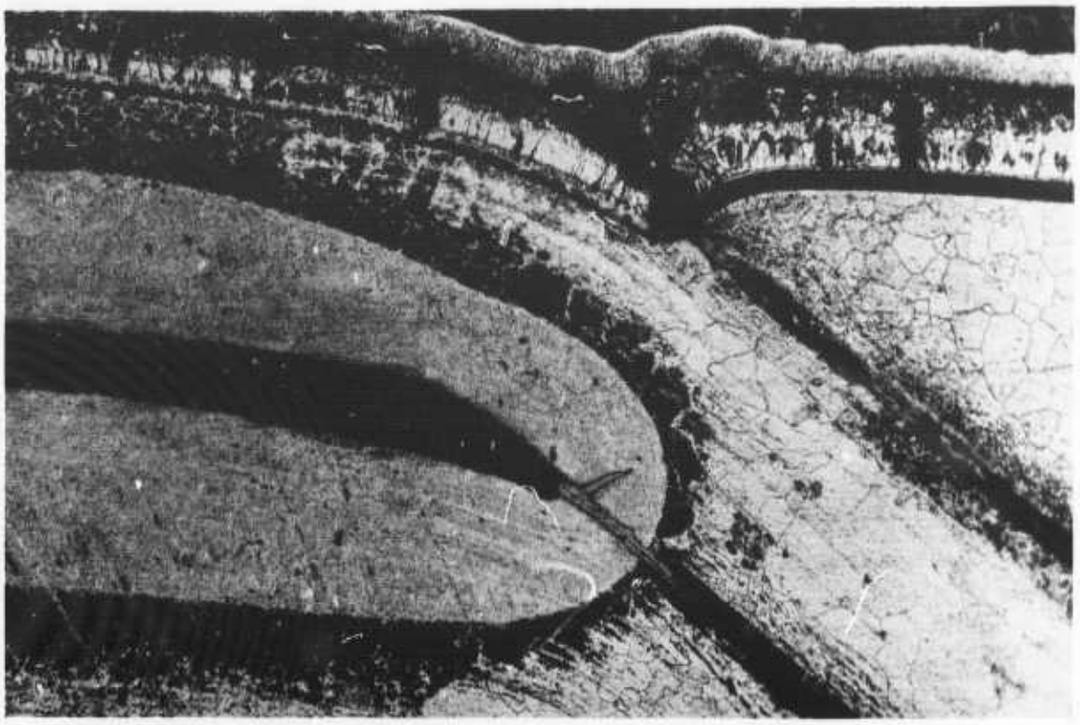

Figure 74 Riveted Heat Shield Specimen After 52 Flights In An Internal Pressure Environment

100X

In order to obtain maximum performance from the R-512E coating on faying surfaces of large widths, which are formed by thin gauge material and are exposed to bending stresses in an external pressure environment, positive means of coating the faying surfaces must be employed.

The influence of specimen design or configuration had no effect on coating performance, as judged by visual observation or by loss of structural integrity in the internal pressure-high stress reentry environment. This is due to a low rate of columbium oxidation with no gross columbium oxide formed at the low internal pressures. Post test destructive evaluation did reveal some base metal contamination in the faying surface of the flat corrugation stiffened design where the coating had not completely penetrated or sealed the joint. It can be assumed that the faying surfaces of the zee and riveted configurations also had base metal contamination in the faying surfaces after exposure in the internal pressure environment, because these faying surfaces are of much greater area than those on the electron beam welded flat corrugation panel. However, the structural integrity was maintained for 52 or more flights for the riveted construction which has the greatest faying surface area.

The testing of all the different heat shield configurations in the external pressure environment did allow the determination of a discernible influence of specimen design or configuration on coating performance. This discernible influence was evidenced by columbium oxide growth in the faying surface. It must be remembered that testing of joints and faying surfaces areas in the external pressure environment is not truly representative of the actual flight environment exposure for joints and faying surfaces. Typically joints and faying surfaces in actual flight see internal type pressures. The

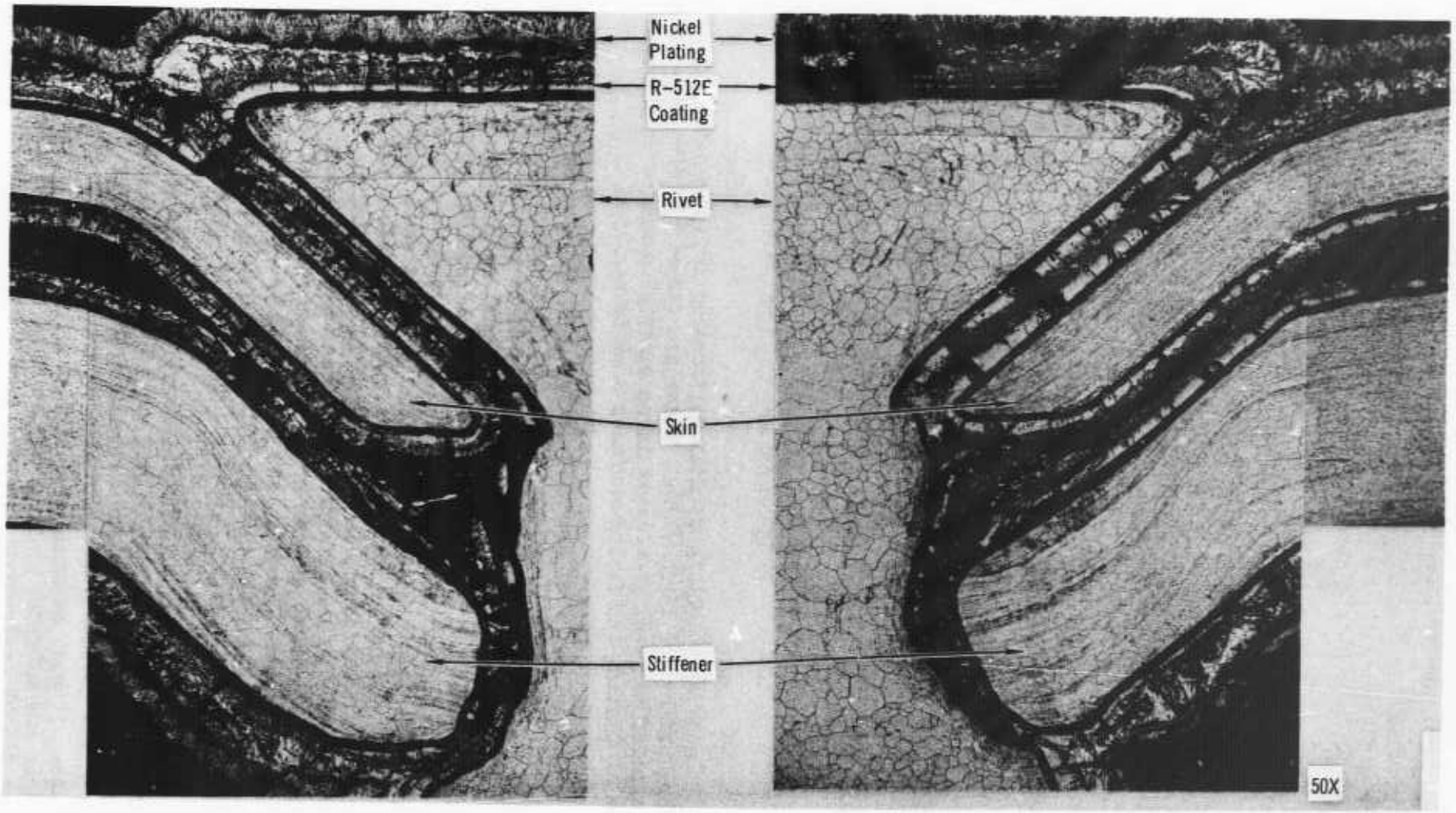

Figure 75 Rivet and Adjoining Area from Riveted Heat Shield Panel Exposed to 51 Simulated Reentries at External Pressure/High Stress Conditions

specimens with the largest faying surface area (riveted construction) showed the earliest coating failures. The specimens with the second largest faying surface area (zee stringer stiffened) showed coating failures next, etc., all the way down to those specimens which have no faying surfaces. The specimens which have no faying surfaces showed no failures in the external pressure environment for exposures up to 61 flights.

3. EFFECTS OF LOCAL COATING REMOVAL

The effect of local coating damage or loss on the structural integrity of coated refractory metal hardware is an important consideration in any actual flight program and one which has been largely overlooked to date. As coated refractory metal structures are required to perform multi-missions, the ability to judge structural adequacy in relation to local coating damage becomes even more important.

With respect to coating damage or loss effects on the structural integrity of columbium alloys, two main points must be considered. The first is the contamination of the columbium substrate with oxygen and nitrogen and the embrittlement which this causes. The initial effect is strengthening of the substrate with an accompanying loss of ductility, followed by deterioration of the strength. The second consideration is the oxidation of columbium leading to a reduction in the load bearing cross section. The first consideration, contamination, is the most important aspect in a reduced pressure environment. The loss of columbium cross section due to gross oxidation is small compared to the depth of contamination which is usually several times greater in volume. In both damage considerations, the atmosphere must come in contact with the substrate by passing through the coating or by the coating being totally absent. For this program coating damage was induced by mechanically removing the coating in a local area so that the variable of defect size can be precisely defined.

A method of abrasive blasting with aluminum oxide grit was investigated and procedures developed to produce the desired coating removal. Apparatus was assembled, showin in Figure 76, which allows the specimen to be held firmly in place a fixed distance (1.5 mm) from the abrasive blasting nozzle. The nozzle movement is controlled in the vertical and horizontal directions so that exact alignment with a predetermined area can be attained. The nozzle diameter is 20 mils which allows a coating damage area of 30 mils in diameter to be induced. Aluminum oxide grit used is -200 mesh. Surface and edge defects induced by this method are shown in Figures 77 and 78 respectively. The coating was completely removed down to the base metal.

Discussed in this section are the effects of local coating removal on baseline stress oxidation specimens and on heat shield panel specimens.

a. Baseline Specimens

A summary of baseline stress oxidation specimens which were tested is shown in Table XIII. Baseline stress oxidation specimens (tensile type) which had coating removal sites (30 mils in diameter) were exposed to the 2400°F maximum temperature-high stress-external pressure profile environment. Each specimen had one coating damage site located either on the edge or on a surface.

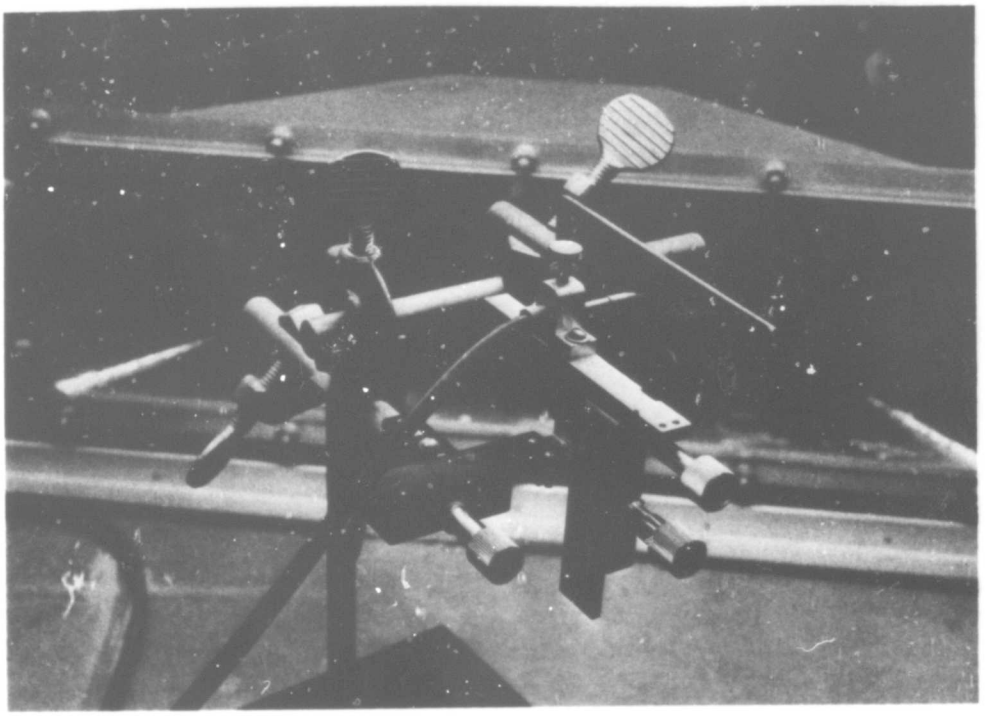

Figure 76 Set-up for Inducing Coating Damage

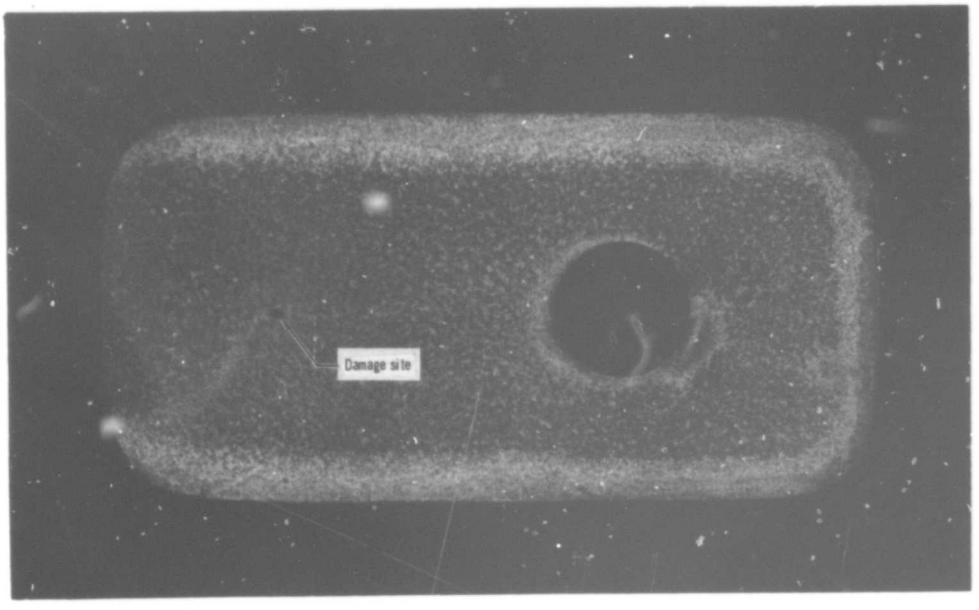

Figure 77 Small (30 Mil Diameter) Surface Coating Damage Site

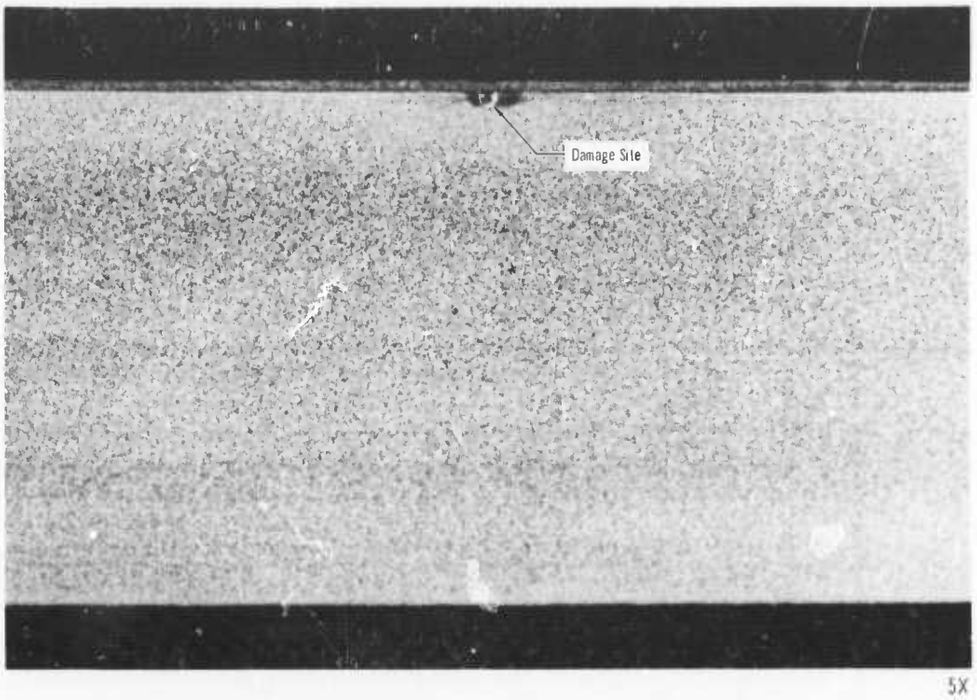

Figure 78 Small (30 Mil Diameter) Edge Coating Damage Site

Two tensile specimens which had coating damage sites located on one surface equidistance from each edge ruptured through the damage site during the initial loadings of the eleventh and twelfth cycles. The tensile specimen with the damage site on the edge ruptured through the damage site during the initial loading of the twelfth cycle.

A large coating damage area (.375 inch in diameter) was induced on one of the baseline stress oxidation specimens which in turn was exposed to the 2400°F maximum temperature-high stress-external pressure profile conditions. Rupture occurred through the damage site during the 6000 psi stress peak in the middle of the fifth cycle. It is encouraging to know that structural integrity is retained for this length of time with a coating damage area that spans 75 percent of the specimen width on a specimen which had only 9 mils of base metal thickness after coating.

For comparison baseline stress oxidation specimens without coating damage areas had rupture times from 35 to 60 plus cycles in the high stress-external pressure environment. Therefore local coating damage had a significant detrimental effect on the performance of R-512E coated Cb-752 specimens under tensile stress in the external pressure environment. Coating damage size also was significant. However, the size (width) of the specimen must also be considered; even tho 30 mil damage site represents a significant fraction of total coating cross section.

Baseline stress oxidation specimens (tensile type) which had coating damage sites were exposed also to the 2400°F maximum temperature-high-stress-internal pressure profile environment. Each specimen had one coating damage site. Two of the specimens had small (30 mils in diameter) damage sites, one on a surface and one on an edge. The other specimen had a large (.375 inch in diameter) damage site. The specimen with the small surface damage site ruptured during the initial loading of the fiftieth cycle. Failure did not

Table XIII
Coating Damaged Tensile Specimens

No.	Test cond.*	No. of cycles tested	Coating damage	Remarks
1	E.P./H.S.	1	Small damage on edge	Terminated test after 1 cycle, no apparent oxidation
2	I.P./H.S.	60	Small damage on edge	Fracture on initial load 61st cycle
3	E.P./H.S.	3	Small damage in center	Terminated after 3 cycles, no apparent oxidation.
4	I.P./H.S.	49	Small damage in center	Fracture on initial load 50th cycle
5	E.P./H.S.	11	Small damage in center	Fracture on initial load 12th cycle
6	I.P./H.S.	61	Large damage (3/8" dia.) in center	Fracture on initial load 62nd cycle
7	E.P./H.S.	10	Small damage in center	Fracture on initial load 11th cycle
8	E.P./H.S.	4 1/2	Large damage (3/8" dia.) in center	Fracture on mid load 5th cycle
9	E.P./H.S.	11	Small damage on edge	Fracture on initial load 12th cycle

*E.P./H.S. – External pressure high stress

I.P./H.S. – Internal pressure high stress

occur through the damage site. The specimen with the small edge damage site ruptured through the damage site during the initial loading of the sixtieth cycle. The specimen with the large damage site ruptured during the initial loading of the sixty-second cycle. Again failure did not occur through the damage site. A photomicrograph of the specimen tested with the large damage site is shown in Figure 79. Contamination has occurred but no gross oxidation has occurred. Local coating damage or removal does not appear to have any significant effect on the performance of R-512E coated Cb-752 specimens under tensile stress in the internal pressure environment. Damage size does not influence the structural integrity under these conditions.

With respect to damage site location, there does not appear to be any significant effect on structural performance when the damage area is on the surface or on the edge. However, all specimens with edge damage fractured through the damage site, while the specimens with surface damage sites did not follow this pattern. This indicates that a notch effect is created by the edge damage sites.

b. Heat Shield Panels

Heat shield specimens with the small (.030" dia.) and large (.375" dia.) coating damage sites were evaluated. The 2400°F maximum temperature high stress and external pressure profile was used primarily. Specimens were tested to an accumulated creep deflection of 40 mils. The external pressure environment as was determined by the baseline tensile tests.

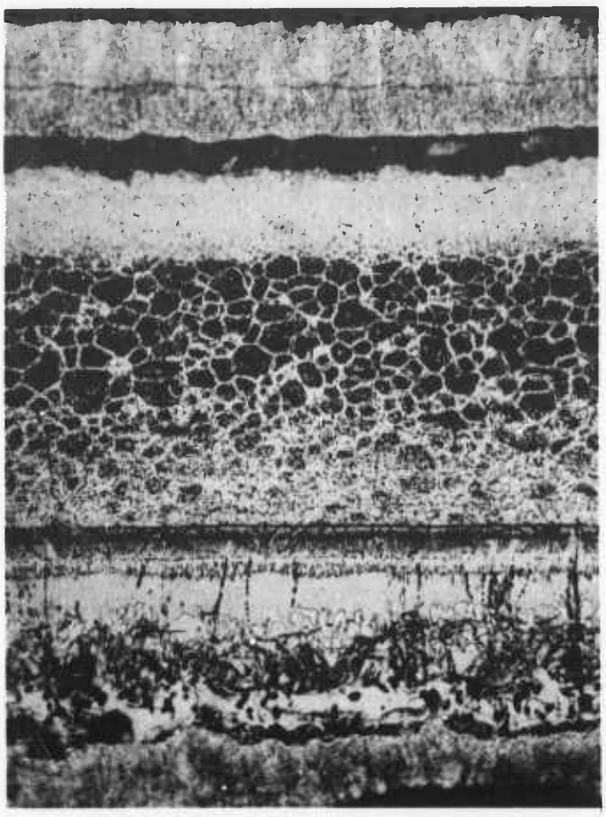

Figure 79 Section Through Large Damaged Area (.375" Dia.) After 61 Cycles In An Internal Pressure – 2400°F Environment

Since only the external surface of a heat shield panel will experience external pressures, damage sites were induced on the external surface and edge of the heat shield panel skins. A summary of the results of testing heat shield specimens having coating damage is shown in Table XIV.

Figure 80 shows the performance of spot welded flat corrugation stiffened type panels with and without a damage site when exposed to the high stress-external pressure conditions. The damage site was located directly on a spot weld in the center of the panel and was 30 mils in diameter. There is an indication of a strengthening effect due to contamination in the base metal, as 21 cycles or simulated reentries was required to produce 40 mils of deflection as compared to 13 cycles for the undamaged panel. It should be remembered that the skin of the panel is experiencing compressive stresses and loss of strength would be caused only by loss of load bearing material. After eight or nine cycles the oxide growth in the faying surface, which became evident, probably had an over-shadowing effect. After 19 cycles the oxide growth was becoming rather severe as the skin was buckling and cracking. As can be seen from the increase in deflection rate, the structural integrity was becoming affected in the last couple of cycles.

Table XIV
Summary Of Damaged Heat Shield Specimen Results

Type	No.	Test Cond.	No. of cycles tested	Coating damage	Remarks
Spot welded flat corrugation	4	E.P./H.S.	10	Small damage on weld	Terminated with .040" deflection
	10	E.P./H.S.	22	Small damage off weld	Terminated with .040" deflection
	11	E.P./H.S.	16	Small damage on edge	Terminated with .033" deflection, overload on cycle 17
	12	E.P./H.S.	23	Small damage off weld	Terminated with .040" deflection, cracking of skin
E.B. welded flat corrugation	7	E.P./H.S.	13	Small damage on edge	Terminated with .040" deflection
	11	E.P./H.S.	6	Small damage on weld	Terminated with .018" deflection, overload on cycle 7
	13	E.P./H.S.	4	Small damage on weld	Malfunction of loading mechanism
	16	E.P./H.S.	11	Small damage off weld	Terminated with .040" deflection
	18	E.P./H.S.	5	Small damage on edge	Malfunction of loading mechanism
E.B. welded Vee corrugation	10	E.P./H.S.	41	Small damage off	Terminated with .040" deflection
	11	E.P./H.S.	37	Small damage on weld, repaired	Terminated with .040" deflection
	12	E.P./H.S.	49	Small damage on weld	Terminated with .040" deflection
	16	E.P./H.S.	22	Large damage (3/8" diameter)	Oven temperature on cycle 7 terminated because of substrate consumption by oxidation
Zee stiffened	8	E.P./H.S.	20	Small damage on weld	Terminated with .040" deflection
Rib stiffened	5	E.P./H.S.	58	Small damage on weld	Terminated with .040" deflection
	6	E.P./H.S.	57	Large damage (3/8" diameter)	Fractured due to substrate consumption by oxidation

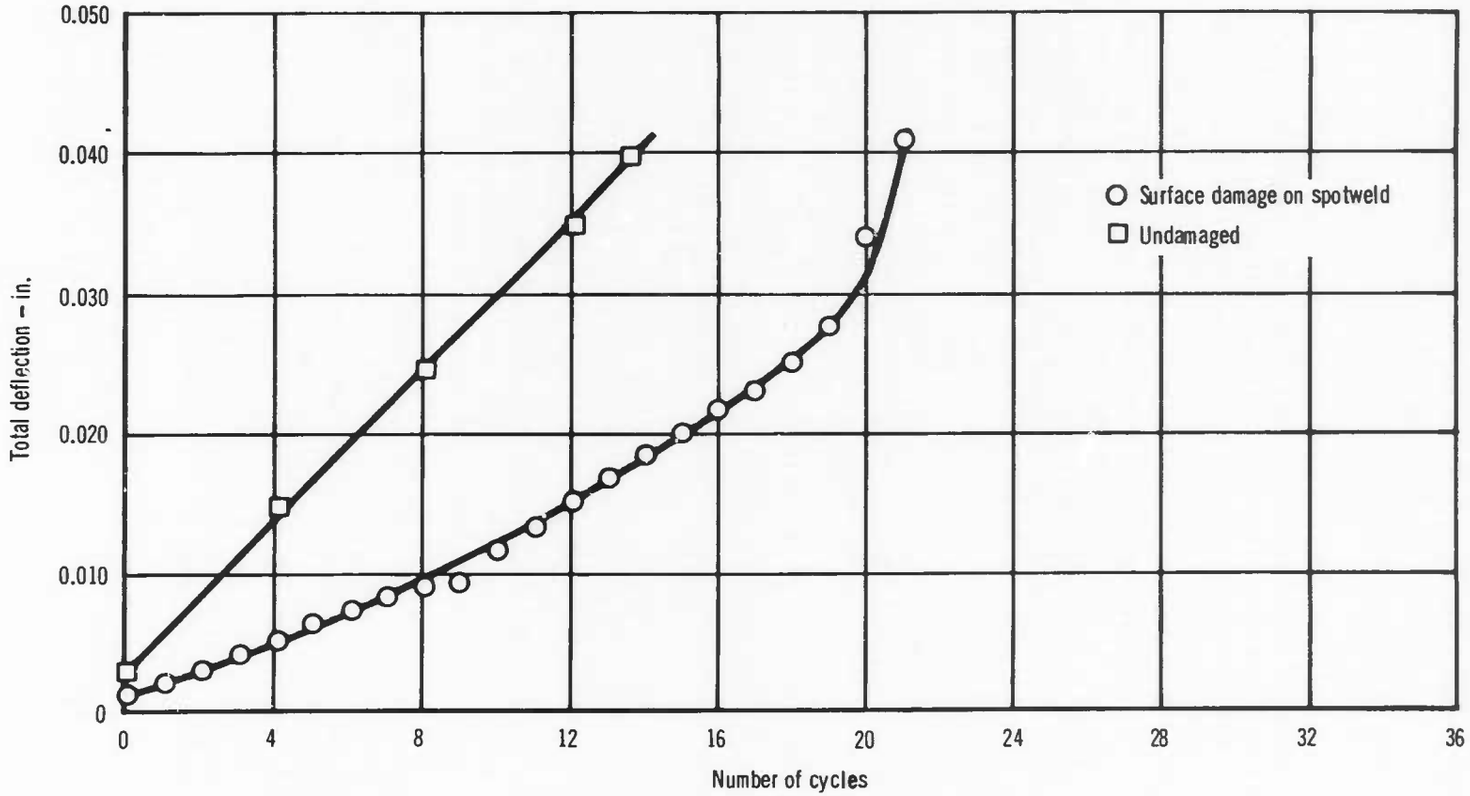

Figure 80 Total Deflections of Undamaged and Surface Damaged Spotwelded Flat Corrugation Stiffened Panels Tested at External Pressure/High Stress

Figure 81 shows the performance of a spot welded panel with an edge coating damage site located centrally between the ends of the panel on the skin. Structurally the skin on the edge of a panel that extends beyond the skin-corrugation joint contributes very little for it is essentially free to buckle or to bend. As can be seen, the damage site on the edge had essentially no effect on the structural performance of the panel.

Electron beam welded single faced vee corrugation stiffened heat shield specimens were evaluated with small (30 mil diameter) coating damage areas. Damage areas were located directly on a weld and between welds or corrugations. Forty one (41) cycles were required to produce 40 mils of deflection in the panel with the damage area located between welds. Forty nine (49) cycles were required for the panel with the damage area on a weld. Vee corrugated panels without damage areas required 30 cycles to produce 40 mils of deflection. Apparently the coating damage is allowing an amount of contamination of the columbium significant enough to change the creep properties. A microsection through the small damage area of the panel that was tested for 49 flights is shown in Figure 82. Columbium oxide (Cb_2O_5) can be seen in the area where the coating was removed. Oxygen and nitrogen have diffused into the metal (skin and corrugation) to the points where the dark bands are present. This degree of oxidation and contamination did not have any effect on the structural integrity of the panel. The oxide was visibly detectable after the second or third flight simulation. In the internal pressure environment where the amount of oxygen is much less a corresponding lesser amount of oxidation and contamination takes place.

A large damage area (.375 inches in diameter) was induced on the skin side of a vee corrugated panel and exposed in the external pressure environment. The panel survived through six cycles without any noticeable effect except oxide growth on the damage area. During the seventh cycle the furnace overheated to 2800°F and the oxide on the damage area became molten, reacted and consumed the skin beneath the damage area leaving a hole in the skin. Testing was continued at 2400°F and the panel maintained structural integrity for 15 more cycles. The panel actually never ruptured but consumption by oxidation had progressed to the point where the panel was deforming elastically and the loading fixture could no longer apply the desired stress.

A spotwelded zee stringer stiffened single faced heat shield panel with a small (30 mil diameter) coating damage area located on the skin side, directly on a spotweld, was evaluated. Twenty two (22) cycles were required to produce a deflection of 40 mils. This compares to the 21-24 cycles required to produce 40 mils of deflection in the undamaged panels tested under the same conditions. As has been mentioned previously columbium oxide growth in the faying surfaces of this type of construction over-shadows or hides the effect of the small coating damage area.

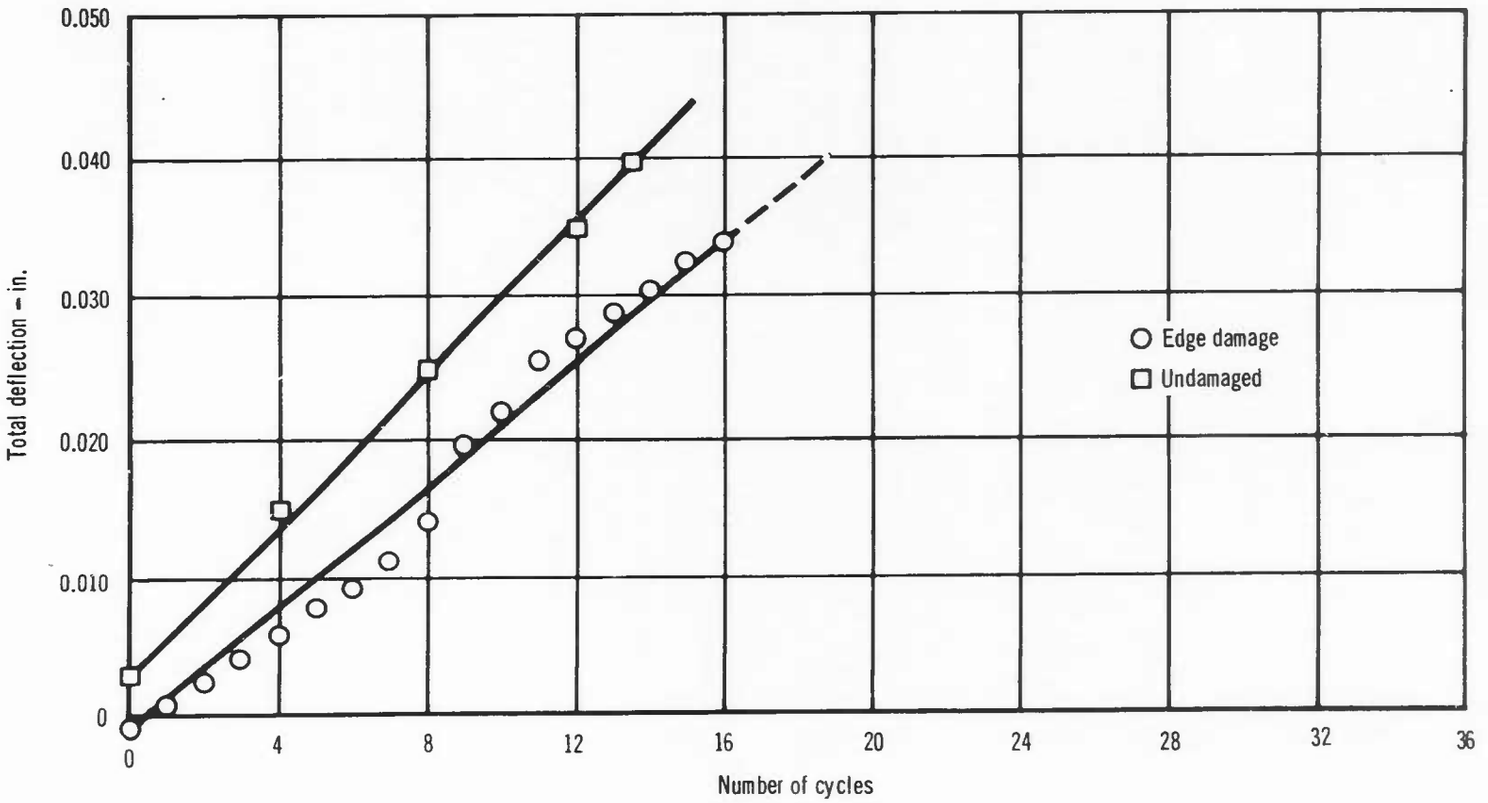

Figure 81 Total Deflections of Undamaged and Edge Damaged Spotwelded Flat Corrugation Stiffened Panels Tested at External Pressure/High Stress

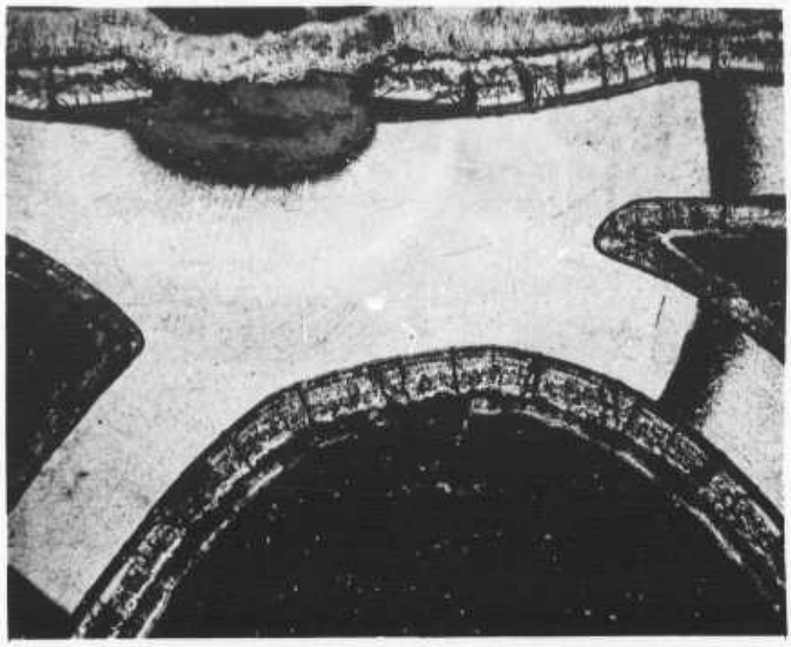

50X

Figure 82 Microsection Through .030" Diameter Coating Removal After 49 Flights Under External Pressure – 2400°F Profile Conditions

A rib stiffened heat shield with a small coating damage area located on the skin side directly on the weld which joins the skin to one of the rib stiffeners was evaluated. Fifty-eight cycles was required to produce a deflection of 36 mils. Fifty to fifty-five cycles were required to produce 40 mils of deflection on the undamaged rib stiffened panels. The rib stiffener which was directly above the small damage area became contaminated more and more as testing progressed and prevented the panel from bending uniformly. This is because the contamination causes a strengthening of the columbium. Testing was terminated because the loading fixture could not function properly with this warped panel.

A rib stiffened heat shield panel with a large (3/8" diameter) coating damage area on the skin side was evaluated. Oxidation, contamination and stress caused the columbium metal directly beneath the coating damage to be destroyed. Actually it just popped-out as a 3/8" diameter plug of contaminated metal. This occurred during the seventh cycle. As testing progressed the hole grew larger and on the initial loading of the 57th cycle the panel broke or fractured. It is quite apparent the metal (Cb-752) can tolerate a considerable amount of contamination before it can no longer function as a structural material.

Depending upon size, the loss of coating effectiveness on external panel surfaces can reduce the reuse capability of the heat shield. The small (.030" diameter) areas of coating removal had no effect on the reuse capability. With a large damage area (3/8" diameter) the small heat shield panel failures were slow and required a number of flights. Coating failures on external surfaces can be readily detected by visual examination due to the distinct yellowish coloration of the Cb_2O_5 formed at the failure site. In general, the structural integrity of coated columbium is very tolerant of the local absence of coating or the local loss of coating effectiveness.

4. REPAIR COATINGS

Field type repair coatings were evaluated to determine if local coating damage could be effectively repaired and returned to normal service. A glass sealed flame sprayed ceramic oxide type repair coating was evaluated. Sealed flame spray repair coatings consist of flame spraying the damaged area with an oxide coating and overcoating, by brushing or spraying, with a glass slurry which has a fairly low melting point but which retains a high viscosity at high temperatures. Thus the glass is held in the porous flame sprayed coating and a self-healing quality is achieved due to the mobility of the viscous glass. Small (.030" dia.) and large (.375" dia.) coating damage sites were induced on R-512E coated Cb-752 coupons. The small damage sites at edges and on surfaces were coated with just the glass slurry and tested at 2500°F -one atmosphere air. Protection was afforded for 29 one hour cycles. In order to obtain protection on the large damage sites a pre-coating of flame sprayed Al_2O_3 was required before the glass slurry is applied. Without the flame sprayed pre-coating, the glass spalls due to the rapid heating and cooling associated with the cyclic conditions of testing. With the glass sealed flame spray repair coating, oxidation protection was obtained for 20 hours at 2500°F.

Two baseline stress oxidation tensile specimens, one with a small surface damage site and one with a small edge damage site were repair coated with the brush-on glassy type repair coating prior to testing. The specimen with the repaired surface damage ruptured during the initial loading of the thirty-fifth cycle and the specimen with the repaired edge damage site ruptured during the initial loading of the thirty-sixth cycle. This compares to eleven and twelve cycles for unrepaired specimens. The specimen with the repaired surface damage site did not rupture through the damage site, while the specimen with the repaired edge damage site did, again indicating some notch effect due to edge coating damage. Repair coatings were not investigated under internal pressure conditions.

The deflection versus number of cycles or flights is shown in Figure 83 for a spotwelded panel which had a repair coated damage site. The damage site was located directly on a spotweld. The repair coating prevented any significant amount of contamination from occurring,for the structural performance was very similar to the undamaged panel.

A photomicrograph through a small damage area on a vee corrugation panel that has been repair coated with the brush-on glassy repair is shown in Figure 84 after 37 flights in the external pressure environment. A considerable amount of contamination is present but there is not formation of the bulky Cb_2O_5, as was observed in Figure 82. The repair glass doesn't appear to have completely filled the coating damage site. Had the damage site been filled with the glass, no doubt the repair would have been more effective. Undamaged vee corrugation panels normally took 30-32 cycles or flights to attain 40 mils of deflection while this repaired one required 37 flights.

5. NON-DESTRUCTIVE TESTING (NDT)

Discussed in this section is the non-destructive measurement of coating thickness.

Non-destructive test techniques were utilized to determine coating thickness before testing, between cyclic exposures, and after oxidation tests.

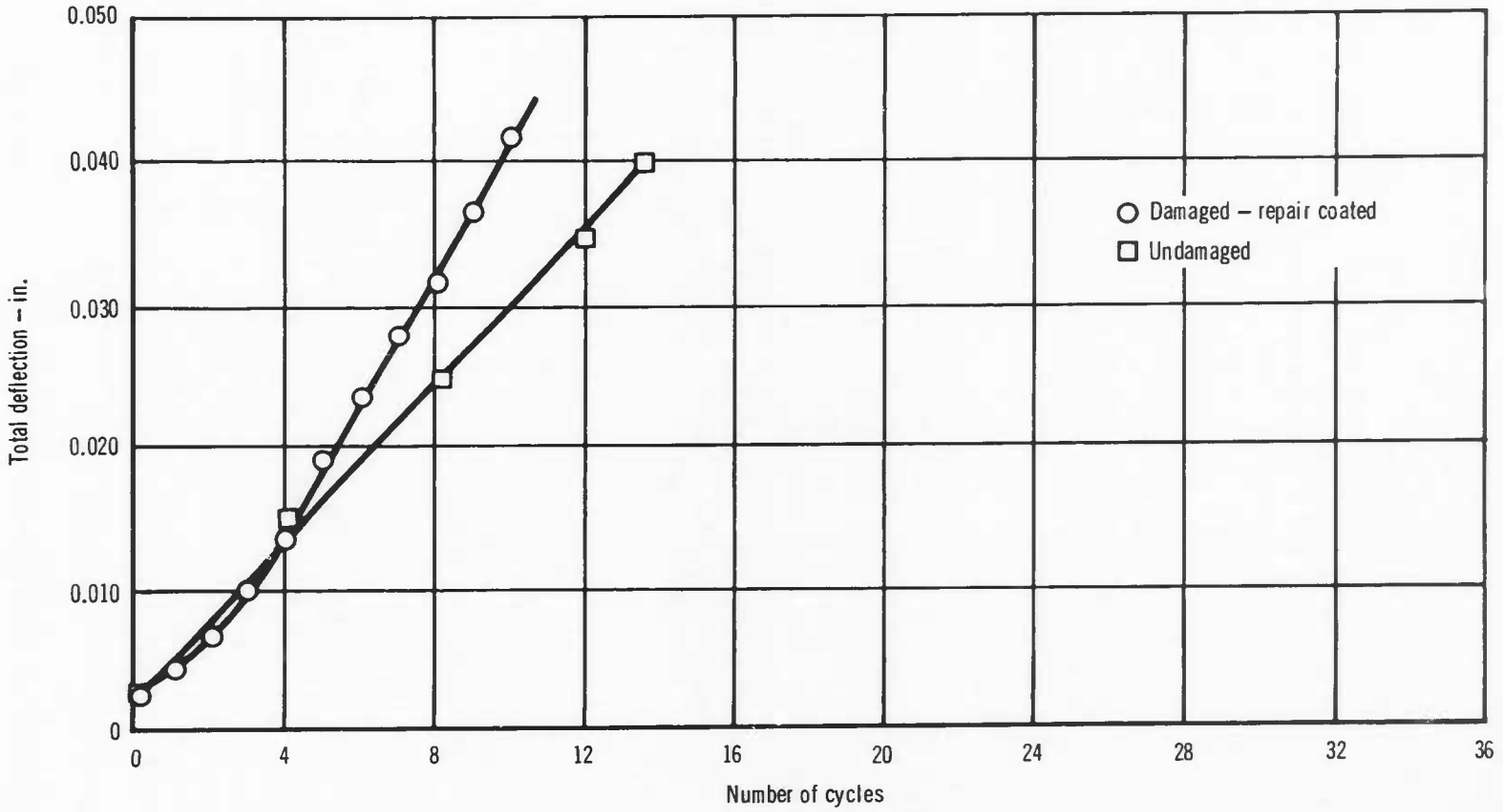

Figure 83 Total Deflections of Undamaged and Damaged – Repair Coated Spotwelded Flat Corrugation Stiffened Panels Tested at External Pressure/High Stress

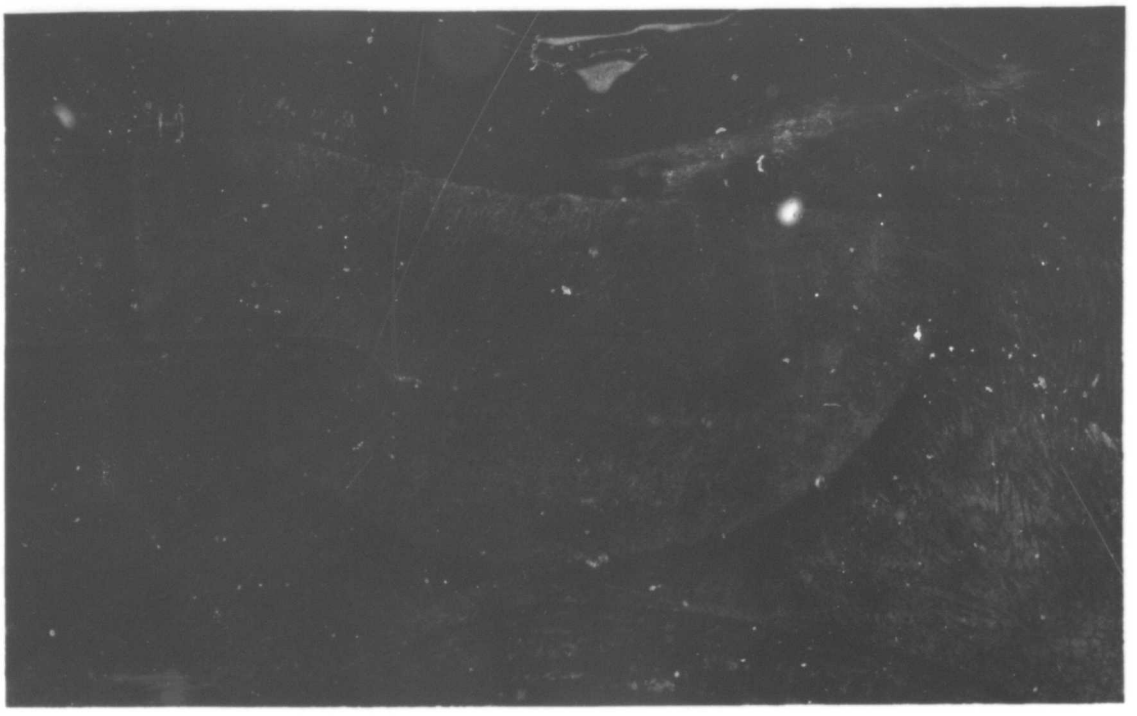

100X

Figure 84 Microsection Through Repaired Damage Site After 37 Flights In An External Pressure Environment

AVCO Corporation had determined that the most prominate mode of coating failures in the R-512E/Cb-752 system is related to thin coated edges (References 14 and 15). A thermo-electric device which works on the Seebeck principle was used to measure coating thickness on edges and/or surfaces of "as coated" specimens. The thermo-electric device requires electrical continuity to function therefore cannot be used on coatings after they have been exposed to oxidation because of the non-conductive oxide film which forms on the surface. A dermitron or eddy current device was used to measure coating thickness on flat surfaces of coated specimens before and after exposure to oxidizing environments.

Baseline oxidation tests which were conducted include static, slow cycle, reduced pressure profile, and reduced pressure-stress profile. All specimens used in the baseline tests were surveyed with the thermoelectric device, with particular attention given to the edges (See Appendix III Table XXX). The standard oxidation type specimens (1-1/2" x 3/4") had top edge (with respect to dipping orientation) thicknesses that were only 1/6 to 1/3 of the surface coating thickness (3-3.5 mils). The thinnest coating found on each specimen was always on the top edge. As a result all coating failures were edge failures. Coating lives obtained were not, however, considered low.

observed were on the thinly coated top edges. No correlation of failure could be made with change in coating thickness because this is an area where changes in thickness could not be monitored.

Dermitron coating thickness measurements were made on specimens (See Appendix III, Table XXXI) tested in the external pressure environment after every 5 cycles up to 50 cycles. There was a noticeable increase in coating thickness ranging from .8 mils to 1.4 mils per side. This is explained by coating oxide growth and diffusion zone growth.

Dermitron coating thickness measurements were made on temperature-pressure-stress oxidation test specimens which were exposed to internal and external pressures at 2600°F and 2400°F $T_{max.}$ profiles (see Appendix III, Tables XXXII and XXXIII respectively. The 2600°F still showed thickness decreases in the internal pressure environment and increases in the external pressure environments. At 2400°F a slight thickness decrease was detectable in the internal pressure environment with practically no change in coating thickness in the external pressure environment. The location of failure or fracture of these stress oxidation specimens could not be correlated with any of the coating thickness measurements made. Visual detection of columbium oxide on edges were definite indications of where fracture would occur. Fracture would occur 2 to 5 cycles after the oxide was detected.

Dermitron and thermoelectric coating thickness measurements were made on all heat shield panels tested. The Dermitron measurements proved to be of little value over what had been learned on the baseline test specimens. Thermoelectric coating thickness measurements on three panels of each of the five configurations (see Appendix III, Tables XXXIV, XXXV, XXXVI, XXXVII, and XXXVIII) were examined and compared. Thickness measurements on the skin, edges, and stiffeners were examined. Coating thickness uniformity on all configurations was excellent. Edge thicknesses approached those on the flat surfaces. Careful examination of the measurements does however, reveal the dipping direction for each panel. The lower edge coating thickness is slightly thicker. The corrugation stiffened panels (flat and vee shaped) show an average coating thickness increase of approximately .4 mils per side over the other configurations. This can only be explained by a geometry/drainage effect.

SECTION IV

EMITTANCE STUDIES

The total normal emittance of Sylvania's R512E coated columbium Cb-725 alloy was measured from 1600 to 3000°F, at reduced pressures and under simulated flight profile conditions, using an integral cavity emissometer.

The objectives of the emittance study were to calibrate the emissometer and to measure the emittance and emittance variations of fused slurry silicide coated columbium. The emittance of the coated columbium was determined at various conditions to include the temperature range of 1600 to 3000°F, various pressures, slow heating and cooling, and at time-temperature-pressure profiles representative of lifting reentry. The effect on emittance of variations in the coating processing was determined also. An important task was the determination of emittance under simulated flight conditions for up to 20 flights.

The emissometer (Reference 18) used was developed about four years ago, and it has been used extensively for high temperature emittance measurements at various pressure conditions and for both rapid and slow specimen heating. Reentry vehicle time-temperature-pressure profiles have been closely simulated. The emissometer utilizes an inductively heated specimen in a controlled atmosphere enclosure, having a reference radiation cavity integral with the specimen, collects the radiation emitted by the specimen and the reference cavity with a precision optical system, and accurately measures the radiation intensities.

Most techniques of measuring radiative properties require the utilization of a separate blackbody or reference cavity and a specimen, the temperatures of both set equal and the spectral or total radiance compared. However, it is extremely difficult to use this technique when the specimen temperature must be changed rapidly and frequently as required in a simulated reentry profile. Our solution to this problem was to integrate the reference cavity into the specimen so that both are at the same true temperature and are viewed through the same optical system so that any contamination of optical components will be compensated for. The major problem in using an integral reference cavity is making sure that it has stable and reproducible radiative properties at high temperature and in a chemically active environment. This problem was effectively solved by fabricating the reference cavity from dense high purity aluminum oxide whose radiative properties are well-known and are stable at high temperatures. The reference cavity was studied analytically to determine the magnitude of the longitudinal temperature gradients and the resultant emittance of the cavity as a function of temperature. In addition, the reference cavity was evaluated experimentally by comparing it to a primary blackbody whose emittance was accurately known ($\varepsilon = 0.997 \pm 0.002$). The overall accuracy of the emissometer was verified by measuring the emittance of polished platinum, tungsten and graphite.

1. DESCRIPTION OF THE EMISSOMETER

The specimen was in the form of a 0.5" diameter cylinder, as shown in Figure 85, having a small aluminum oxide reference cavity mounted in the front face and supported by an aluminum oxide rod attached to an adjustable specimen holder. Each reference specimen cavity was fabricated to maintain a cavity length to radius ratio of 5.00.

Emittance measurements were made, at a specific temperature, by comparing the emitted radiation from the reference cavity to that from the specimen area adjacent to the aperture of the cavity. This was accomplished by the optical system shown in Figure 86. Temperature of the reference cavity was measured with an optical pyrometer which was calibrated by a NBS secondary brightness temperature standard (tungsten strip lamp) placed at the specimen position. The temperature uncertainty associated with the standard was $\pm$ 16 degrees at 3100°F. The emitted radiation was chopped and the signal generated by the thermopile detector measured with a lock-in amplifier.

The specimen was heated by a 15 kva radio frequency generator operating at a frequency of 450 kHz. The induction coil was external to the sample chamber as illustrated in Figure 87. The sample housing consisted of a quartz sample chamber, equipped with a back flow inlet for controlled gas flow capabilities, and copper, water-cooled end supports. One end of the support connected to the vacuum system, and the other contained a calcium fluoride window for sample observation.

The vacuum system consisted of a mechanical fore pump which was coupled to the specimen chamber through a cold trap to prevent oil vapor backstreaming. A pressure of 1 to 360 torr could be maintained with this system.

Variations in chamber pressure required for reentry simulation was accomplished by introducing air through a small inlet in front of the specimen so that the air flowed past the specimen before leaving the chamber. The pressure range of the system was from 1 to 360 torr which was adequate for simulation requirements. The air inlet was equipped with a calibrated flow meter.

A high temperature emissometer apparatus is shown in Figure 88. Emitted radiation from the heated specimen exits through a calcium fluoride window in the specimen housing, is mechanically chopped (13 Hertz), and then falls on a plane scanning mirror which is manually rotated between limiting stops. This permits observation of first the specimen and then the specimen reference cavity. The radiation is then collimated and refocused by a pair of off-axis parabolic mirrors, the radiation beam is partially reflected by an infrared beam splitter which transmits visible and reflects infrared radiation. The transmitted portion reaches the disappearing filament, microoptical pyrometer, thus enabling in situ specimen observation as well as temperature measurement. The reflected portion of the beam falls on the receiver of a thermopile detector placed at the focal point of the second off-axis parabolic mirror. The detector is a Reeder RP-5W

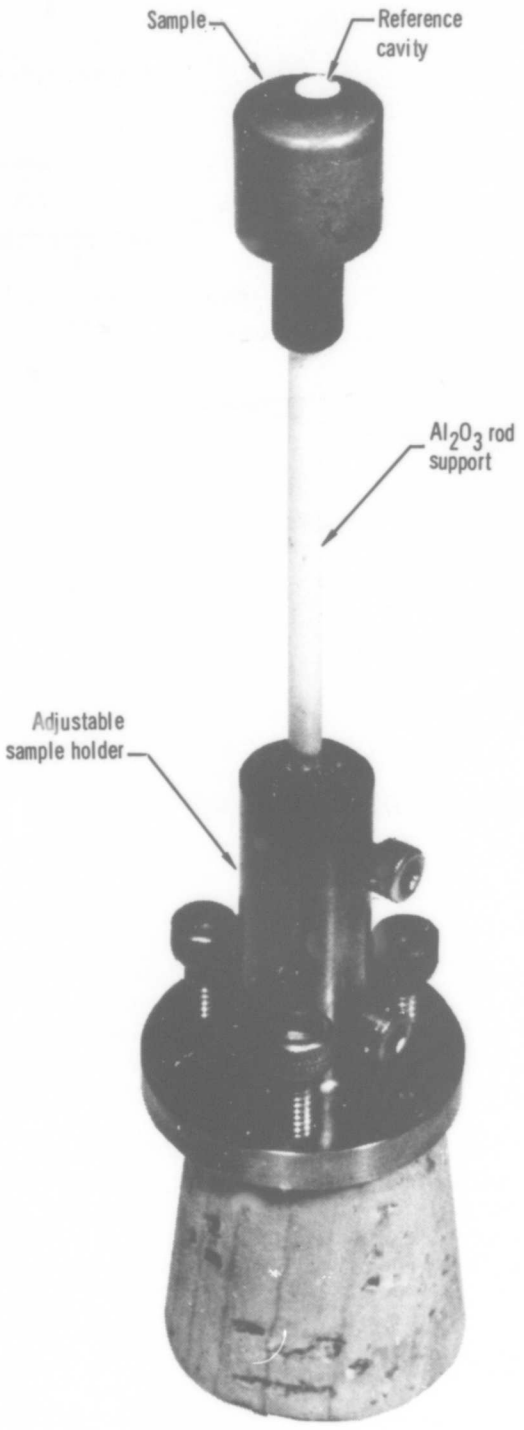

Figure 85 Sample and Adjustable Holder

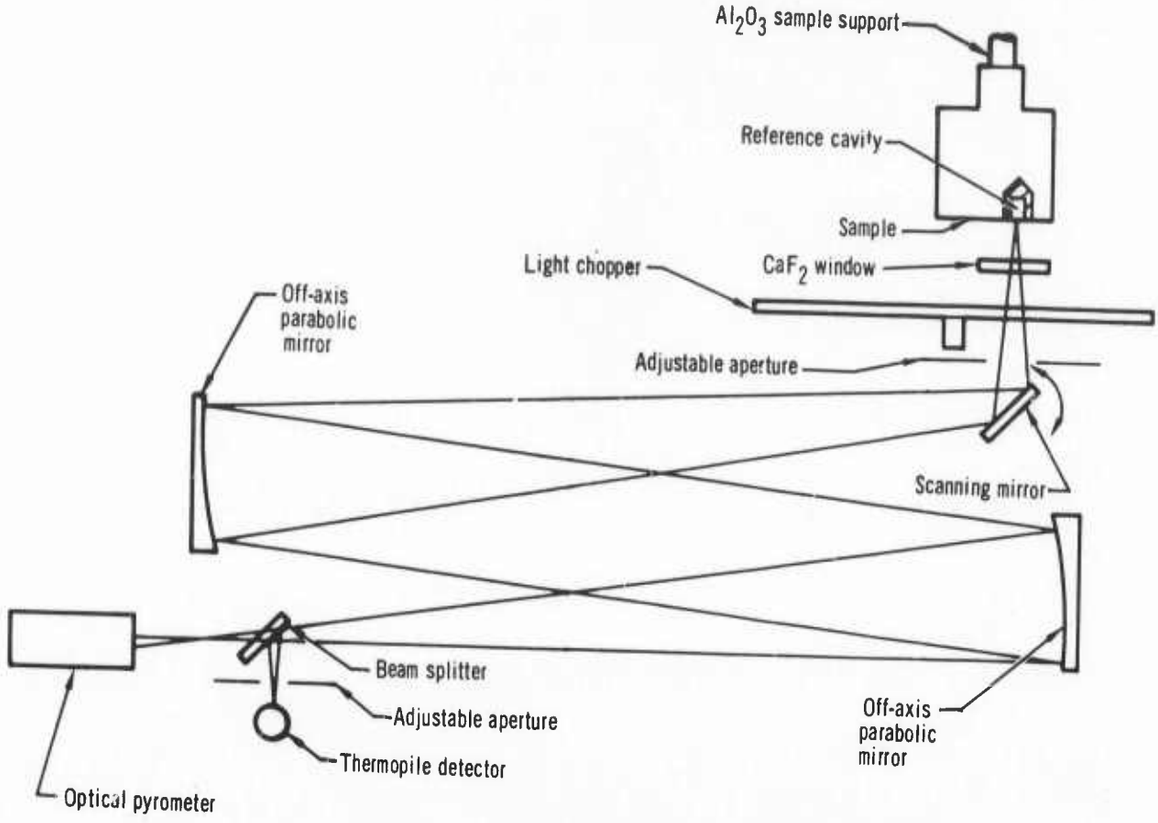

Figure 86. Optical Arrangement

type with a 0.2 x 2 mm receiving area in an evacuated casing having a potassium bromide window. The signal from the thermopile detector is measured with a lock-in amplifier. Background radiation is determined by blocking the optical path with a mirror facing the thermopile. This background mirror slides manually in and out of the optical path (Figure 87).

For ease of optical alignment of the emissometer system, a helium-neon laser was used as shown in Figure 90. The optical path of the radiation was readily observable because of the high intensity and collimation of the laser light, and adjustments of optical components are easily made. The optical pyrometer was calibrated for optical system losses with a tungsten filament strip lamp.

(a) Analytical Treatment

A brief analytical description of the basic principles involved for the emissometer used are as follows:

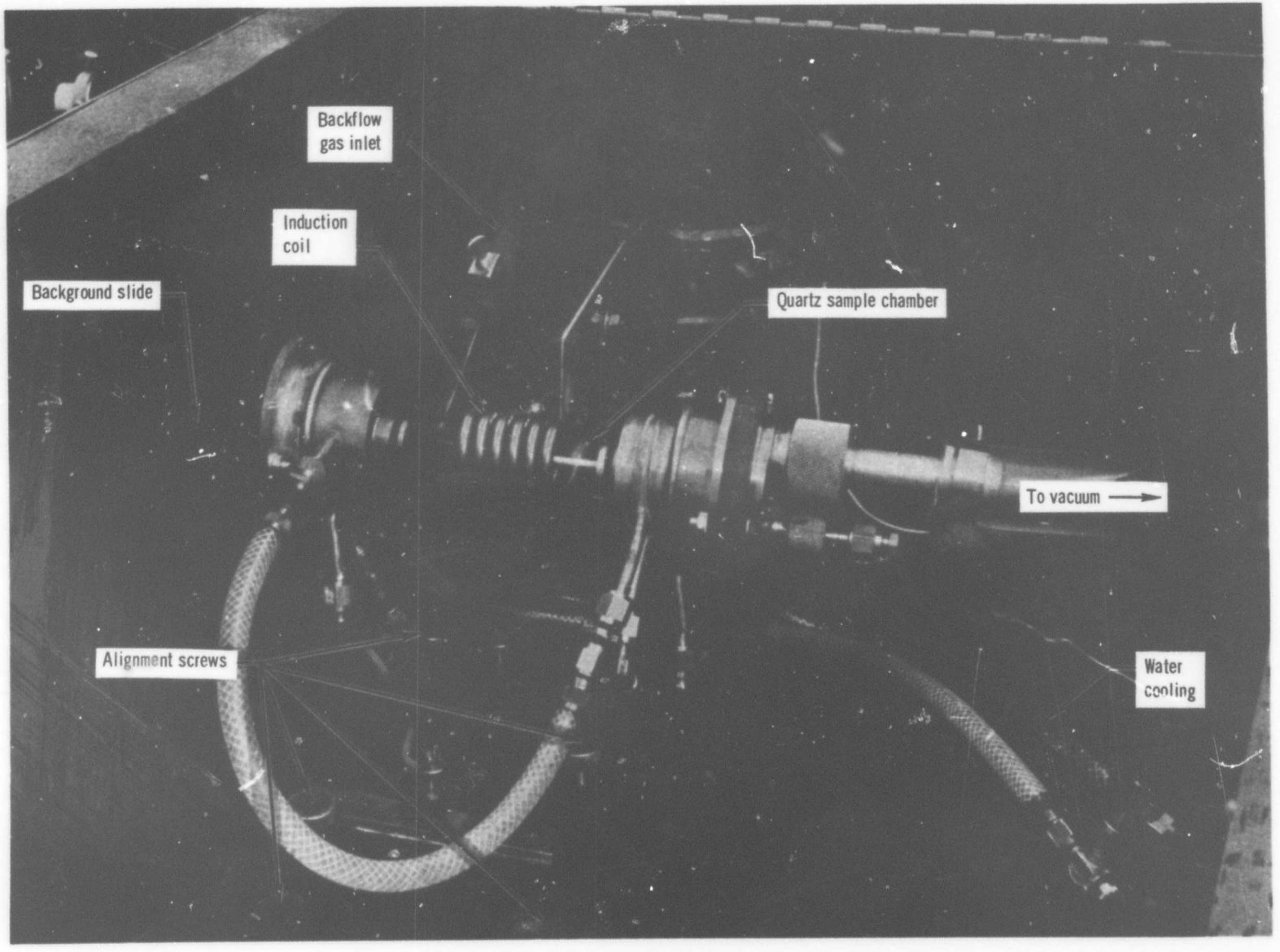

Figure 87 Sample Housing

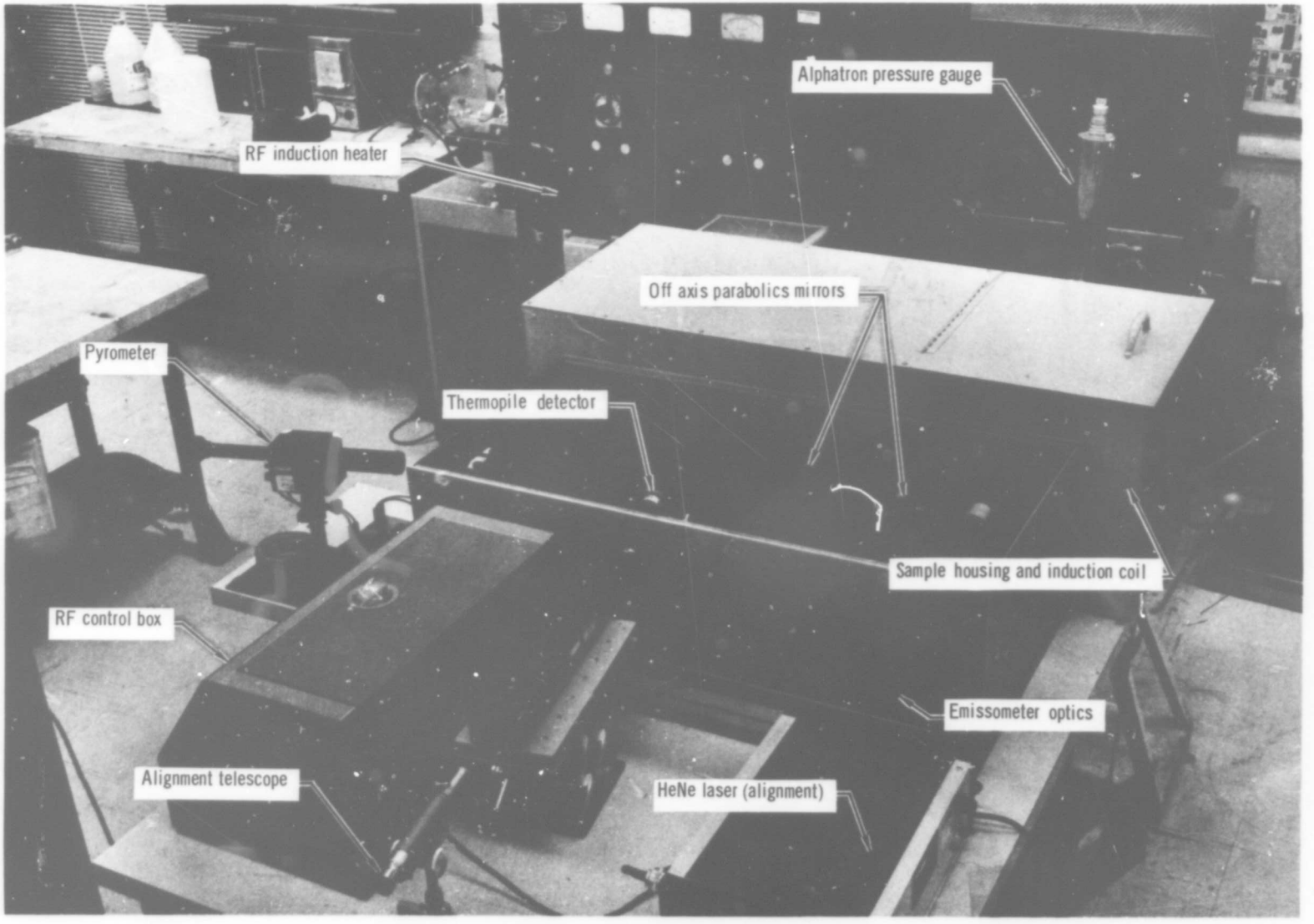

Figure 88 High Temperature Emissometer Apparatus

The spectral radiance of a blackbody, for randomly polarized radiation is given by Planck's equation:

$$N^{o}_{\lambda} = C_1 \lambda^{-5} \left[e^{C_2 / \lambda T_1} - 1 \right]^{-1} \qquad (1)$$

where:

C_1 = Planck's first radiation constant (3.740×10^{-12} watt cm^2)

C_2 = Planck's second radiation constant (1.438 cm degree Kelvin)

T_1 = Albsolute blackbody temperature (°K)

The total sample radiance, J, can be computed by integrating the spectral radiance, as given by Equation 1, over all wavelengths:

$$J = \int_{o}^{\infty} N^{o}_{\lambda} \, d\lambda = \sigma T_1^{4}$$

where:

σ = Stefan-Boltzan constant (5.67×10^{-12} watt cm^{-2} $°K^{-4}$)

J_1 = Total radiance (watt cm^{-2})

Cavity temperature uniformity	0.1% of set temperature
Cavity temperature range	1832 to 5432°F
Cavity temperature stability	0.1% of set temperature
Cavity emissivity	0.99 ± 0.01
Cavity diameter	1/2 inch
Aperture diameter (inches)	0.2, 0.1, 0.05, 0.025, 0.0125
Window material (removable)	calcium fluoride
Window spectral response	0.2 to 11 microns
Field of view	10 degrees – nominal
Sensing probe	silicon photovoltaic detector
Type of control	continuous, electronic proportional control
Warm-up time (to 5432°F)	1-1/2 hours (91°F/min)

Figure 89 Specifications EO Model 146
Blackbody Radiation Source

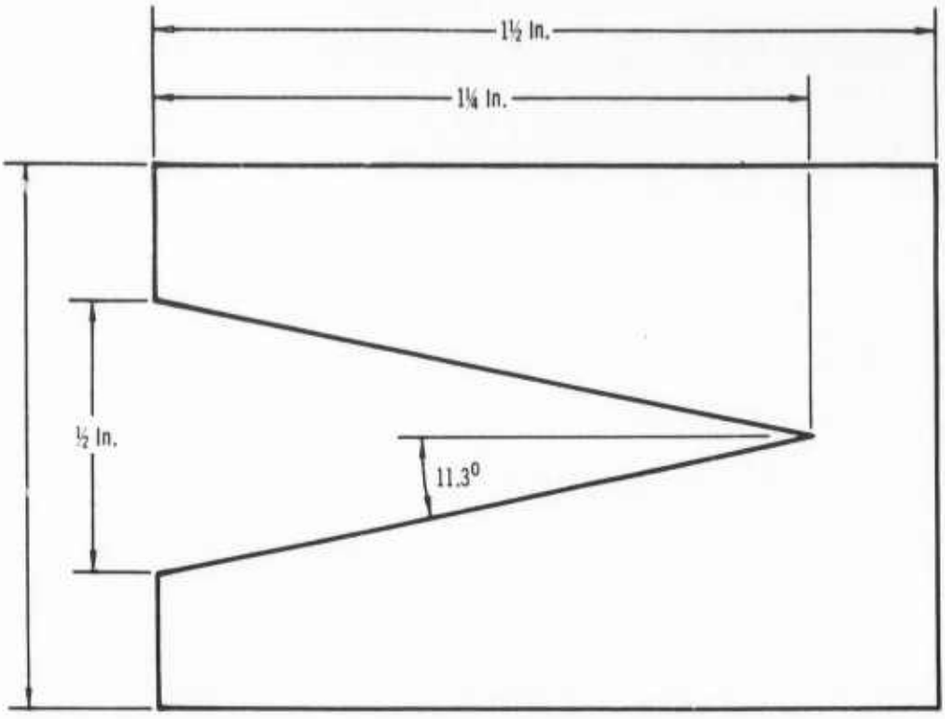

Figure 90 Cavity Geometry of EO Model 146 Blackbody Radiation Source

This is known as the Stefan Boltzmann equation and is the basic relation used for total emittance measurements. The emittance of a sample is defined as the ratio of its spectral radiance to that of a blackbody at the same absolute temperature, wavelength and viewing gemetry. Mathematically this is given by:

$$\epsilon_{TN} = \frac{\int_{\lambda_1}^{\lambda_2} \epsilon\,(\lambda,\theta)\, N_\lambda^\circ\, d\lambda}{\int_{\lambda_1}^{\lambda_2} N_\lambda^\circ\, d\lambda}; \quad \theta = 0$$

where:

ϵ_{TN} = Total normal emittance

λ_1, λ_2 = Limiting wavelength as defined by the optical components of the emissometer

$\epsilon(\lambda,\theta)$ = Directional, spectral emittance of the sample

The total brightness of the sample, B, is given by:

$$B = \frac{J}{\pi}$$

and is expressed in watts cm^{-2} steradian $^{-1}$.

If a sample, having a given brightness, B_2, is observed through an imaging optical system, which collects the radiation emitted by the sample over a solid angle, ω, and a finite sample area, A, the total irradiance, H, at the image plane of the optical system is:

$$H = \frac{\tau B \omega A}{m^2}$$

where:

τ = Mean transmittance of the optical system over the wavelength interval defined by λ_1 and λ_2.

m = Lateral magnification of the optical system.

It should be noted that the effects of optical aberrations have not been considered since the optical system utilizes off-axis parabolic mirrors. If a detector is positioned such that its receiver is at the image plane, a voltage, V, will be generated which is proportional to the total irradiance incident on the receiver:

$$V = KH$$

where:

K = Proportionality constant

In the case of the integral cavity emissometer, both the reference cavity and adjacent sample are observed under the viewing conditions and at the same absolute temperature so that the resulting background corrected signals for these two sources are as follows:

$$\text{Sample: } V_2 = K_2 H_2 = K_2 \tau_2 \epsilon_2 \sigma T_2^4 \omega_2 \Big/ m_2^2 \pi$$

$$\text{Reference Cavity: } V_3 = K_3 H_3 = K_3 \tau_3 \epsilon_3 \sigma T_3^4 \omega_3 \Big/ m_2^2 \pi$$

Taking the ratio of the preceding voltages:

$$\frac{V_2}{V_3} = \frac{K_2 H_2}{K_3 H_3} = \frac{K_2}{K_3} \frac{\epsilon_2}{\epsilon_3}$$

This equation shows that if the proportionality constant, K, is independent of irradiance, i.e., linear, then the ratio of the background corrected signal voltages can be used to measure the emittance ratio of the reference cavity and the sample. If the emittance of the cavity is known, then the emittance of the sample can be determined.

2. CALIBRATION OF THE EMISSOMETER

(a) Primary Blackbody Calibration - The primary radiation cavity used for calibrating the specimen reference cavity was purchased from Electro-Optical Industries, Inc., of Santa Barbara, California. The specifications and cavity geometry are shown in Figures 91 and 92 respectively. A complete block diagram of the system is shown in Figure 93. Evaluation of the primary blackbody was necessary because it was utilized to calibrate the aluminum oxide reference cavity.

The primary blackbody consisted of a conical cavity having an apex angle of 25° 50' and a depth of 1.125 inches. It is fabricated from high purity graphite and can be operated at temperatures up to 4940°F when protected with an inert gas environment. The manufacturer states that the emittance of the conical cavity is 0.99 ± 0.01.

The emittance of this cavity was analytically computed using analytical techniques developed by Gouffee (Reference 19), Kelly and Sparrow. (Reference (20), (Reference (21). In order to facilitate these computations the following assumptions were made:

- The conical cavity emits and reflects radiation in a perfectly diffuse manner.
- The walls of the cavity emit radiation in a graybody manner.

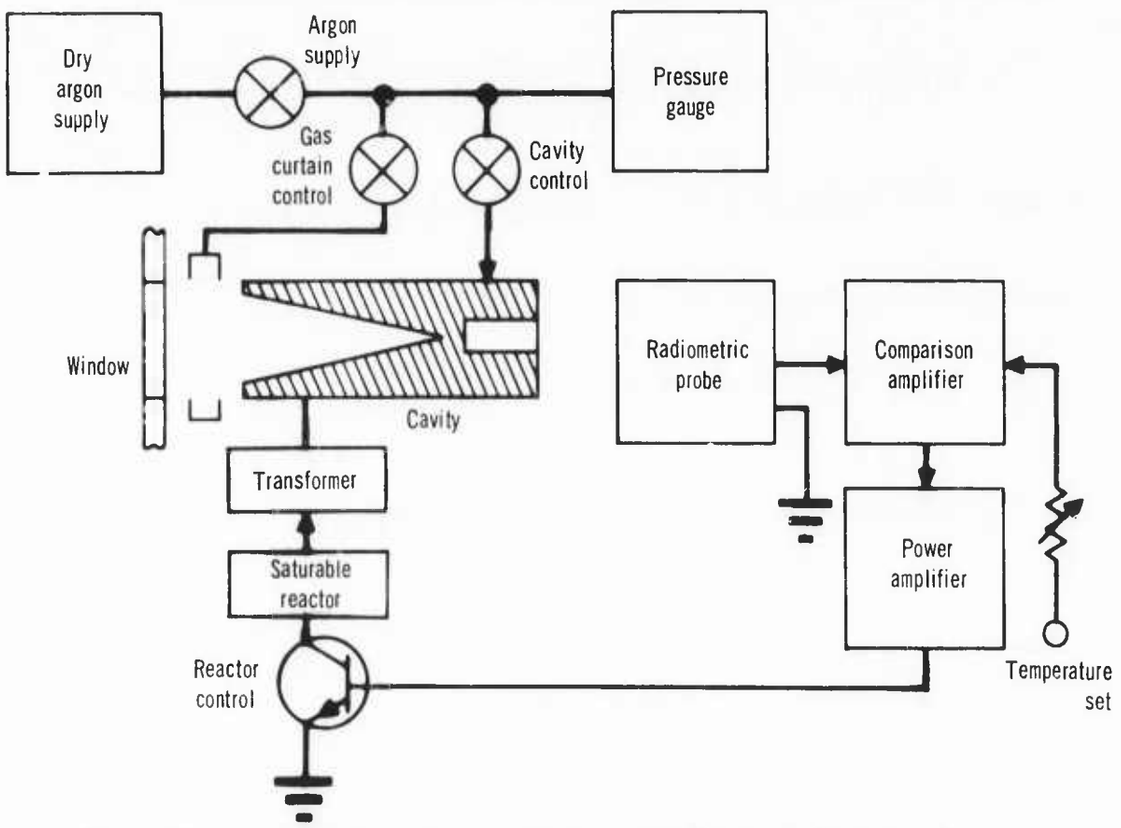

Figure 91 Simplified Block Diagram EO Model 146 Blackbody Radiation Source

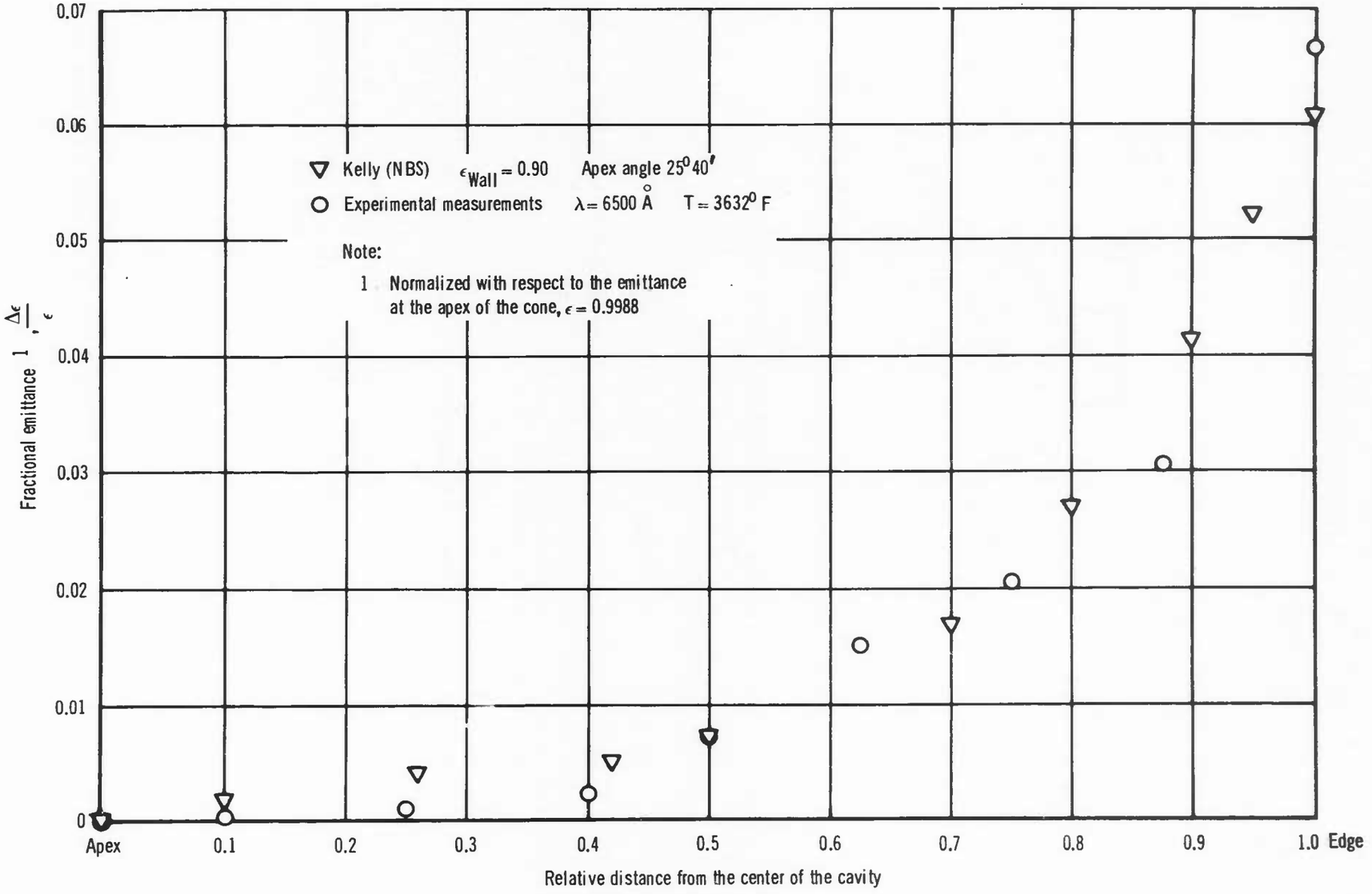

Figure 92 Primary Cavity Survey

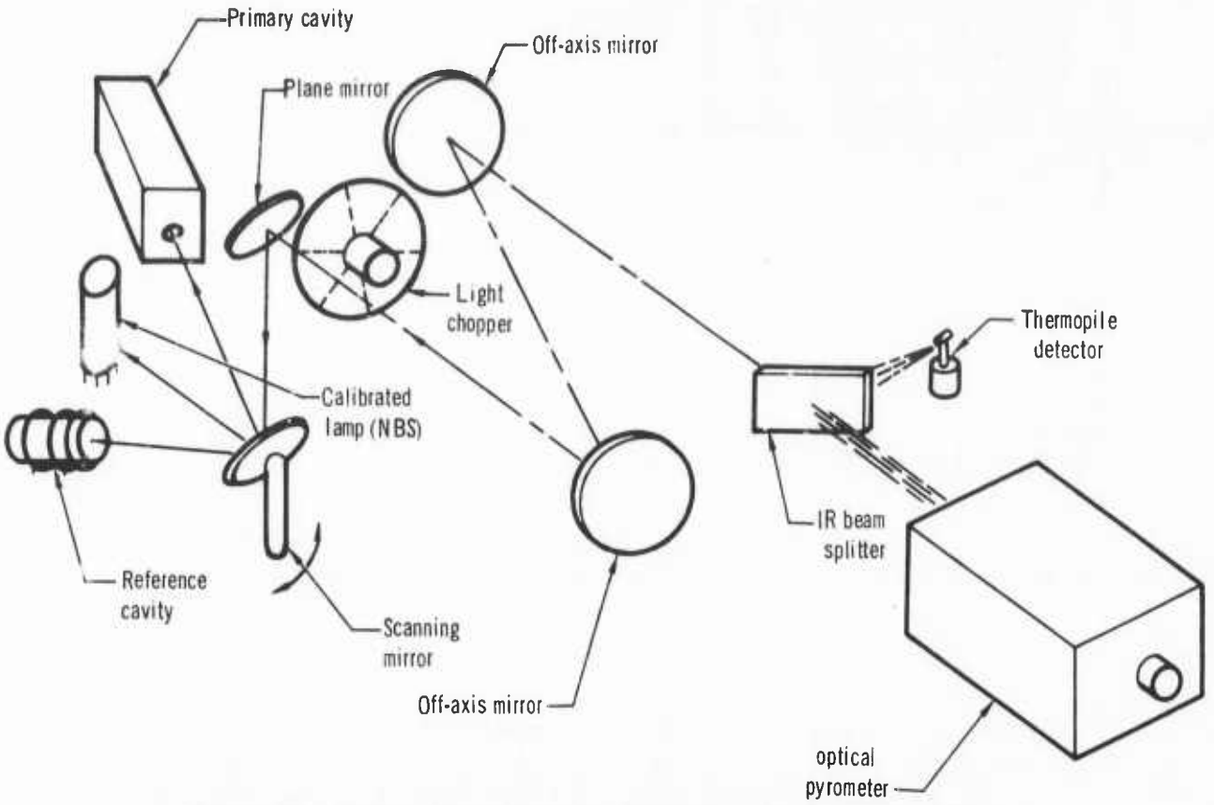

Figure 93 Optical Arrangement for Calibrating the Reference Cavity

- The cavity is isothermal.
- Flux entering the cavity from the local environment is negligible.

The computed emittance, based on Gouffe's equations, was 0.995 for a graphite wall emittance of 0.9. Next, the method developed by Kelly was used to compute the local apparent hemispherical emittance over the aperture of the cavity. The results of these computations gave a maximum value of 0.998 at the appx (center) of the cone to 0.938 at the edge. These anlaytical computations were verified experimentally by measuring the spectral radiance over the exit aperture of the cavity. The spectral radiometric measurements were made with a grating spectrometer at a wavelength of 6500A and a bandwidth of 8A using a photomultiplier to measure the radiation from the spectrometer. The results of these measurements are shown in Figure 92 and are in good agreement with the analytical computations. The most important results of these computations and measurements are that only the central area of the cavity, defined by the apex and a slant height of 0.2L, where L is the total slant height of the cavity, should be used if the emittance uncertainity is to be minimized.

A temperature survey of the Primary cavity indicated that temperature gradients are equal to or less than 0.1%.

(b) Reference Cavity Calibration - The optical arrangement for comparing the primary blackbody and the reference is shown in Figures 93 and 94. This optical system is similar to the one used in the emissometer except that an additional plane mirror has been added. This additional mirror permits the primary cavity, reference cavity or NBS calibrated lamp to be observed simply by rotating the plane scanning mirror. It should be noted that the radiation from any of the three sources travels the same optical path so that absorption effects tend to cancel.

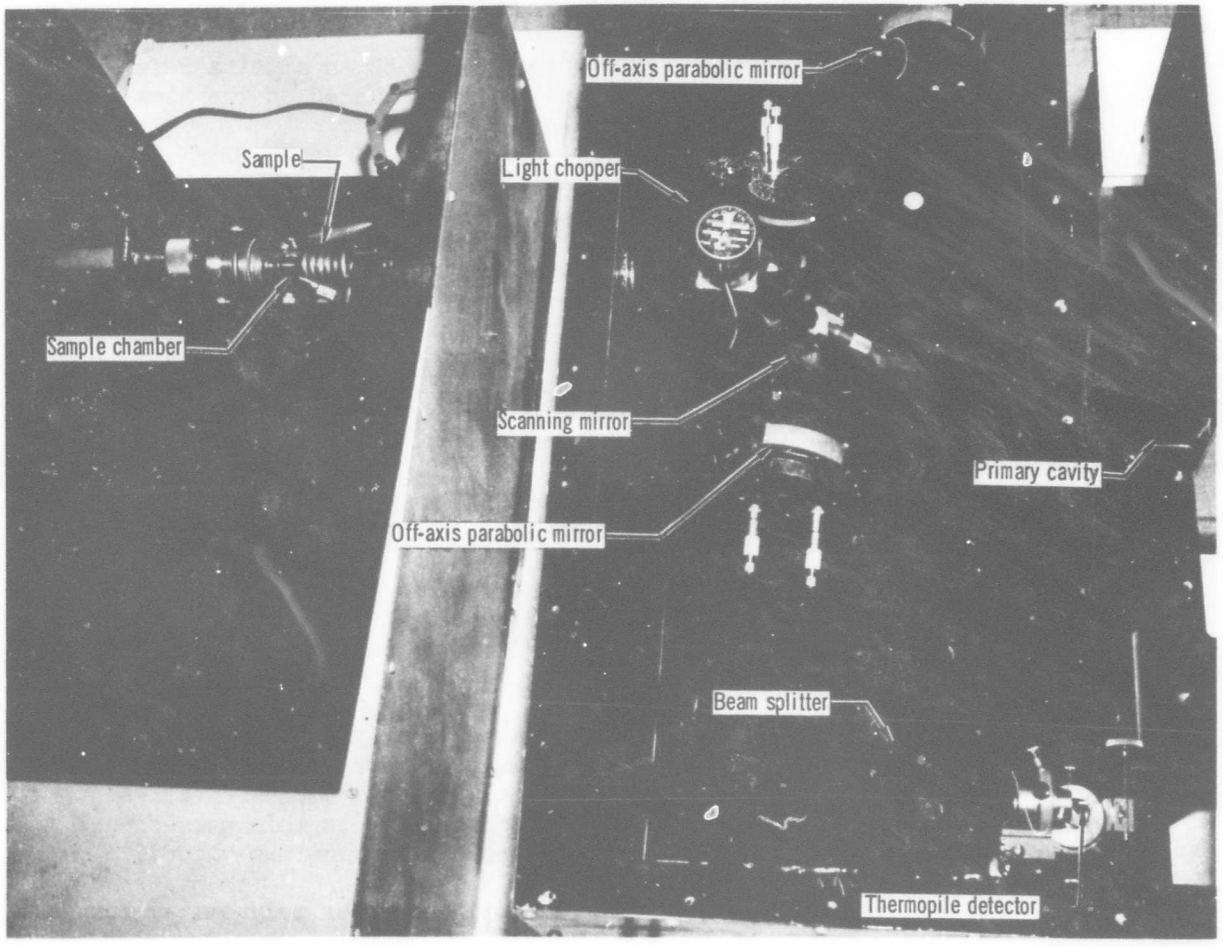

Figure 94 Optical System for Calibrating the Reference Cavity

The emittance of the aluminum oxide reference cavity was experimentally measured by comparing it to the primary blackbody, at the same true temperature and viewing geometry. This comparison was made using the previously described optical system. Prior to the comparison, the combined optical pyrometer-emissometer was calibrated using a tungsten filament lamp as a secondary brightness temperature standard. The calibration of this lamp is traceable to the National Bureau of Standards. The resulting calibration curve is shown in Figure 95. After completion of the temperature calibration, the reference cavity was compared to the primary blackbody. The measurement sequence used for this comparison was as follows:

1. The specimen (tungsten specimen equipped with an alumina reference cavity) and the primary blackbody was placed on the viewing circle and the optical system aligned.

2. The temperature of the primary blackbody was set at a predetermined temperature and allowed to stabilize. The final temperature was measured with the optical pyrometer and the total radiance was measured with a thermopile detector.

3. The temperature of the specimen was set to correspond to that of the primary blackbody and it was allowed to stabilize. The temperature was measured with the optical pyrometer and the total radiance of the aluminum oxide reference cavity was measured with the thermopile detector.

4. This sequence was repeated at specific temperatures over the temperature range of the emissometer.

5. The emittance, at the indicated temperatures, was calculated by taking the ratio of the background corrected voltage signals from the reference cavity and primary blackbody and correcting for the emittance of the primary blackbody.

The results of these measurements are shown in Figure 96. The emittance of 5 cavities was measured. The 5 cavities were chosen at random from the 270 cavities fabricated by Coor's Porcelain. All of the cavities were heated to a temperature of 2500°F for 60 hours prior to this measurement to stabilize the thermal and radiative properties of the aluminum oxide.

The measured values were curve fitted to a 2nd order polynomical curve i.e.

$$T_N = A - B + CT^2 \ (°K)$$

where $A = 1.0849$
$B = 2.3854 \times 10^{-4}$
$C = 9.4133 \times 10^{-8}$

The standard error in estimating the emittance using the above equation is ± 0.01 emittance unit.

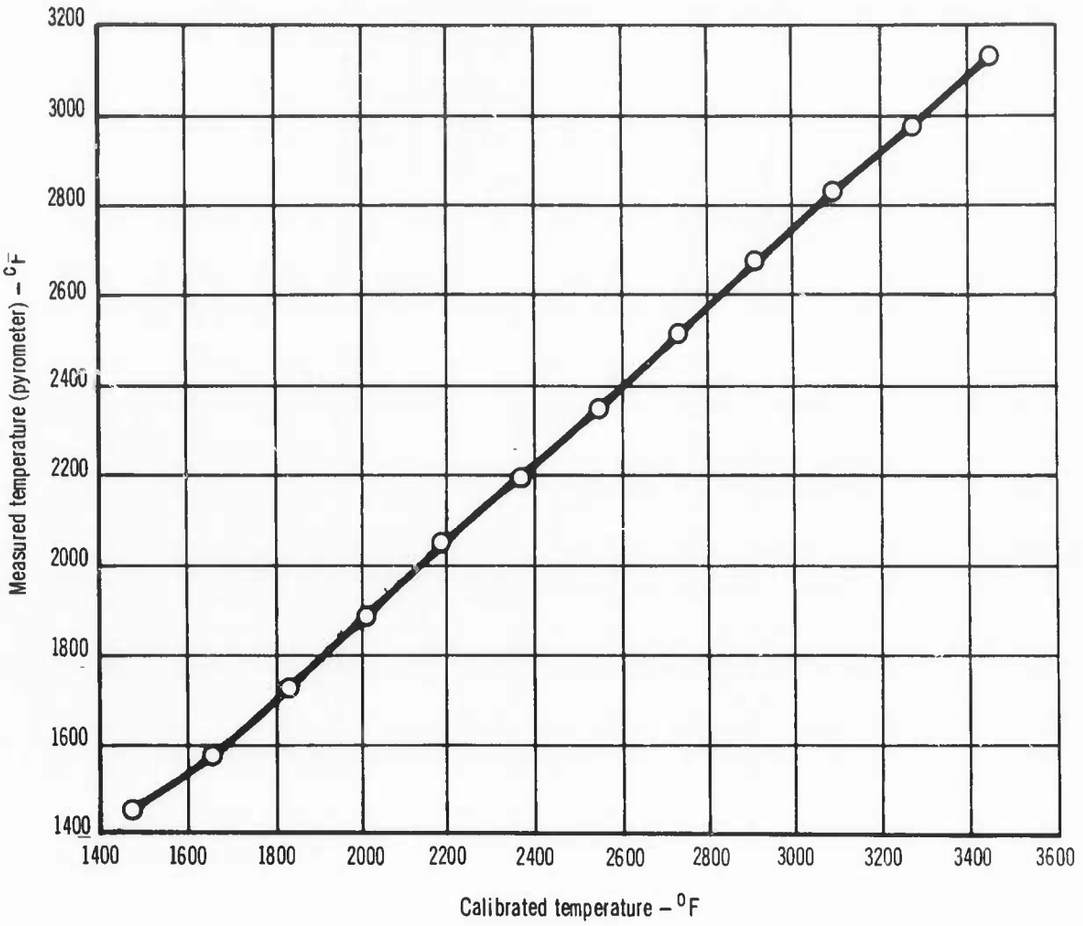

Figure 95 Strip Lamp Calibration of the Emissometer*
Versus
Pyrometer Temperature

*Emissometer with a calcium fluoride window

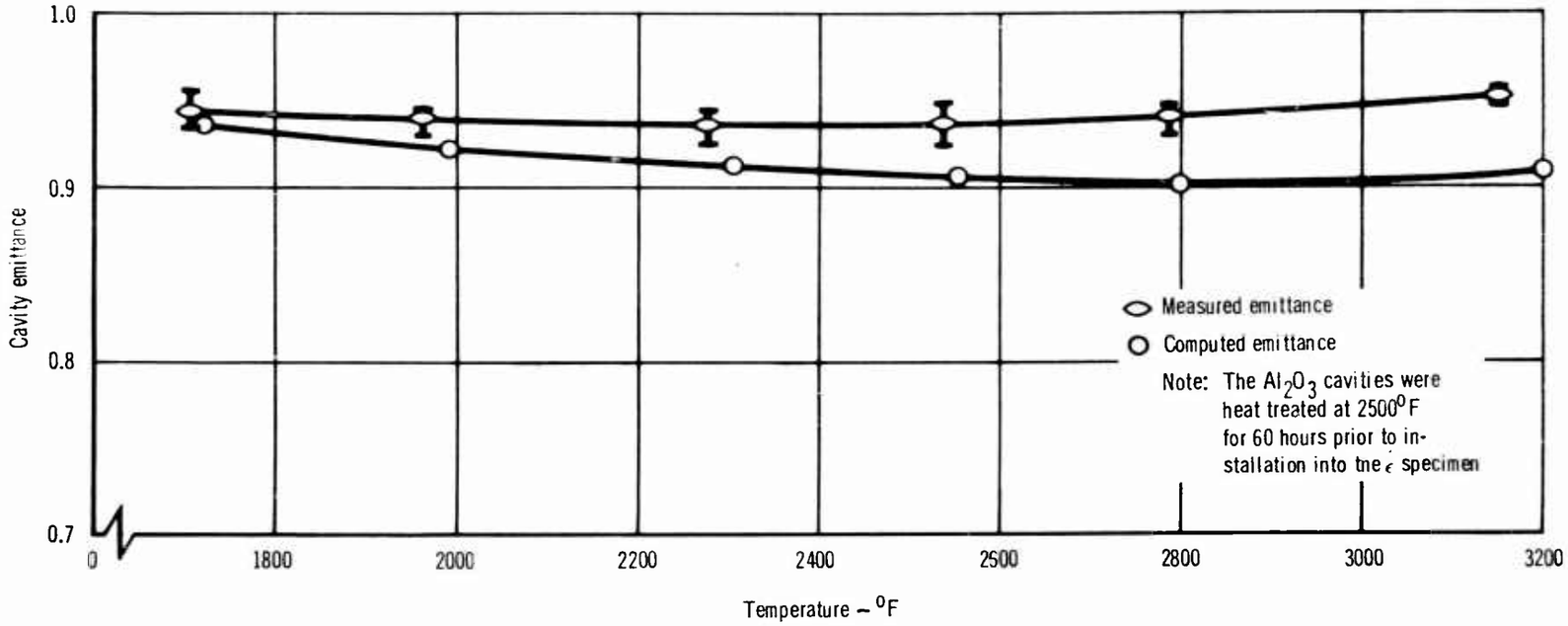

Figure 96 Alumina Cavity Emittance Versus Temperature

The aluminum oxide cavities when compared to a primary blackbody had a higher emittance over the complete temperature range of 1600° to 3200°F. The computed emittance values were based on thermal and radiative properties measured by several investigators. The uncertainties associated with these measurements (thermal conductivity, translucency, emittance, etc.) could account for the difference in the two curves.

The variation in measured emittance from one cavity to another cavity was only ± 0.01. The measured emittance of the aluminum oxide reference cavity determined by comparison to a primary blackbody was used to determine the true temperature of the R-512E coated columbium specimens for emittance measurements from 1600° to 3000°F.

The most important part of the integral cavity emissometer is the aluminum oxide reference cavity since the accuracy of the emittance measurement depends upon how accurately the emittance of the reference cavity is known. Not only must its emittance, as a function of temperature, be accurately known and reproducible but it must be stable at elevated temperatures and in chemically active environments. This problem was solved by fabricating the cavity from pure, dense aluminum oxide. The depth to radius ratio of this activity is 5.0 and it has an outside diameter of 0.19 in. and a length of .37 in.

Since aluminum oxide is translucent and has a low thermal conductivity, an analytical study was conducted (Reference 22) to determine the magnitude of thermal gradients along the cavity wall. The results of this study showed that the thermal gradient can be mathematically represented by:

$$T_1^4 = \frac{k(T_2-T_1)}{\sigma\epsilon_2\epsilon_1 R}\left[\coth(\xi L)-\operatorname{csch}(\xi L)\right]\left[\frac{J_1(\xi R)-Y_1(\xi R)}{J_o(\xi R)-Y_o(\xi R)}\right] + \frac{T_2^4\sin^2\theta_m}{\epsilon_1}$$

where: T_1 = temperature of the cavity wall at the front opening.

T_2 = temperature of the rear wall of the cavity and the temperature along the outside wall of the cavity.

ϵ_1 = total emittance of the cavity wall at temperature T_1

ϵ_2 = total emittance of the cavity wall at temperature T_2

R = radius of the cavity

L = depth of the cavity

θ_m = angle defined by the depth and radius of the cavity

ξR = argument of the Bessel functions

J = Bessel function of the first kind

Y = Bessel function of the second kind

The temperature T_1 was computed for given values of T_2 and are given in Table XV.

The results in Table XVI show that the cavity is nearly isothermal and that Gouffe's (Reference 23) equations for computing the emittance can be used with a high degree of certainity. The results of these computations are shown in Figure 96. Unfortunately both the radiative and thermal properties are not only a function of the intrinsic optical properties of the aluminum oxide but also other extrinsic properties such as initial powder size distributions, sintering temperature and time, etc. so that these preceeding properties must be used with caution in computing the emittance of the cavity.

(c) Linearity

In addition to the calibration of the reference cavity, it was also necessary to determine the characteristics of the optical system of the emissometer. This includes the optical elements, detector, and electronics which are used to compare the radiation emitted by the specimen and the reference cavity.

The linearity of the optical system was experimentally measured by attenuating the radiance of the source by a known amount and measuring the corresponding change in the signal. This was done by placing a mechanical chopper between the specimen and the detector and adjusting the chopping frequency so that it did not interfere with the chopping frequency (14 Hz) used for thermopile measurements. The transmittance of the mechanical chopper is given by the ratio of open to opaque areas. Four individual mechanical choppers were used having transmittances varying from 0.233 to .951. The precision of the measurement was determined by taking the total differential of the following equation:

$$\gamma = \frac{V_1}{V_2}$$

$$\left|\frac{\Delta r}{r}\right| = \left|\frac{\Delta V_2}{V_2}\right| + \left|\frac{\Delta V_1}{V_1}\right|$$

Where ΔV_1 and ΔV_2, are the uncertainities in the voltage measurement. For these measurements $\Delta V_1/V_1 = \Delta V_2/V_2 = \pm .01\%$. The results of these measurements are given in Table XVI.

All of these measurements are within the computed uncertainty of the measurements except at .951 transmittance. These results indicate that the uncertainty due to nonlinearity of the emissometer is equal to or less than $\pm$ 0.6 percent.

(d) Reference Materials

The emittance of several materials with well known radiative properties was measured to verify the overall performance of the emissometer. The materials utilized for these measurements were pure polycrystalline platinum and tungsten, and graphite. The results of these measurements are

Table XV
Temperature Gradients Of The Reference Cavity

T_2 (^{0}F)	T_1 (^{0}F)	% Change
1700	1690	0.50
2060	2040	0.86
2420	2390	1.19
2780	2730	1.67
2960	2890	2.00

Table XVI
Radiometer Linearity

Transmittance (Measured) τ_1	Transmittance (Calculated) τ_2	Difference $\Delta\tau = \tau_1 - \tau_2$	Uncertainity $\Delta\tau$ (Computed)
.233	.227	+.006	±.006
.741	.742	−.001	±.003
.871	.870	+.001	±.003
.951	.946	+.005	±.002

Table XVII
Total Normal Emittance Of Platinum

Temperature ^{0}F	ϵ_{TN} (MDC)	$\Delta\epsilon_{TN}$ (Computed)	ϵ_{TN} (Ref. 1)	$\Delta\epsilon_{TN}$ Measured
1620	.126	±.004	.119	+.007
2000	.145	±.004	.141	+.004
2350	.167	±.005	.159	+.006
2700	.181	±.005	.181	.000
2920	.191	±.006	.193	−.002

shown in Figures 97, 98 and 99. The measurements were curve fitted to a linear function for comparison with other measurements. The results on the platinum were:

(MDC) $\varepsilon_{tn} = 4.681 \times 10^{-2} + 0.908 \times 10^{-4}$ T°K

(Ref.24) $\varepsilon_{tn} = 1.03 \times 10^{-4}$ T (°K)

The emittance values obtained from these two equations are within the quoted uncertainty of ± 5%.

The results on the graphite were:

(MDC) $\varepsilon_{tn} = 0.990 - 1.115 \times 10^{-4}$ T (°K)

(Ref.25) $\varepsilon_{tn} = 1.072 - 1.580 \times 10^{-4}$ T (°K)

The results on the tungsten were:

(MDC) $\varepsilon_{tn} = 7.543 \times 10^{-2} + 1.808 \times 10^{-4}$ T (°K)

(Ref.26) $\varepsilon_{tn} = 6.040 \times 10^{-2} + 1.663 \times 10^{-4}$ T (°K)

The three reference materials were mechanically polished prior to making emittance measurements. The chamber pressure was reduced to 10^{-5} torr using an oil diffusion pump equipped with a cold trap for the tungsten and graphite measurements in order to eliminate surface roughening due to oxidization. However, post examination of the tungsten specimen revealed that some roughening had occurred as is indicated by the increase in emittance at elevated temperatures. Metallographic examination indicated that the surface roughening was due to recrystallization. Of the three reference materials, the results of the platinum are the most meaningful because of the reliability of the published measurements and no surface roughening was observed.

For comparison purposes the computed emittance for specific temperatures are shown in Table XVII.

(e) Uncertainity and Precision:

Analytically, the maximum uncertainty can be estimated by taking the total differential of the equation:

$$\varepsilon_1 = \frac{V_1}{V_2}\,\varepsilon_2$$

which gives:

$$\left|\frac{\Delta\varepsilon_1}{\varepsilon_1}\right| = \left|\frac{\Delta\varepsilon_2}{\varepsilon_2}\right| + \left|\frac{\Delta V_1}{V_1}\right| + \left|\frac{\Delta V_2}{V_2}\right|$$

where $\frac{\Delta\varepsilon_2}{\varepsilon_2}$ represent the uncertainty of the reference cavity

and $\frac{\Delta V_1}{V_1}$ and $\frac{\Delta V_2}{V_2}$ are the uncertainites in measuring the voltage signals.

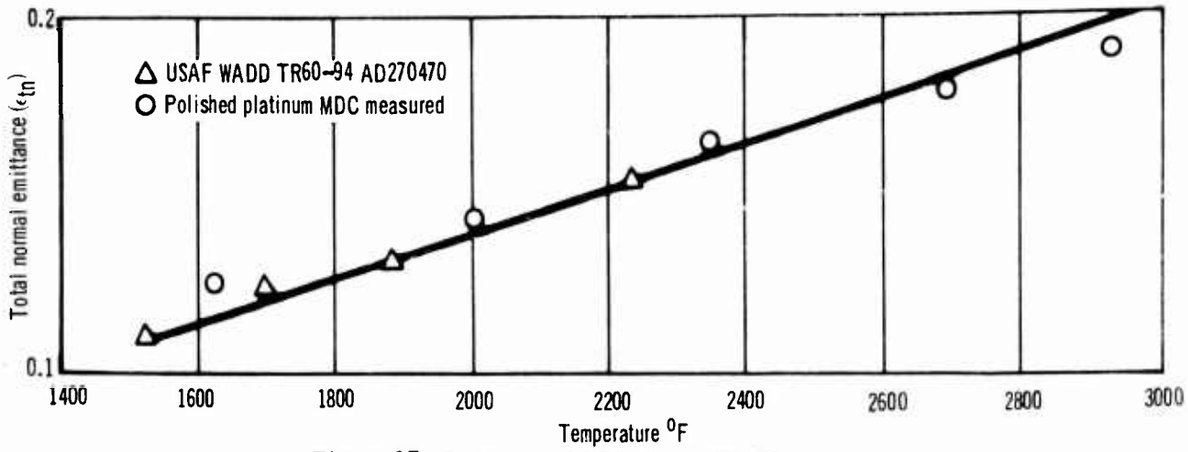

Figure 97 Emittance Of Platinum VS Temperature

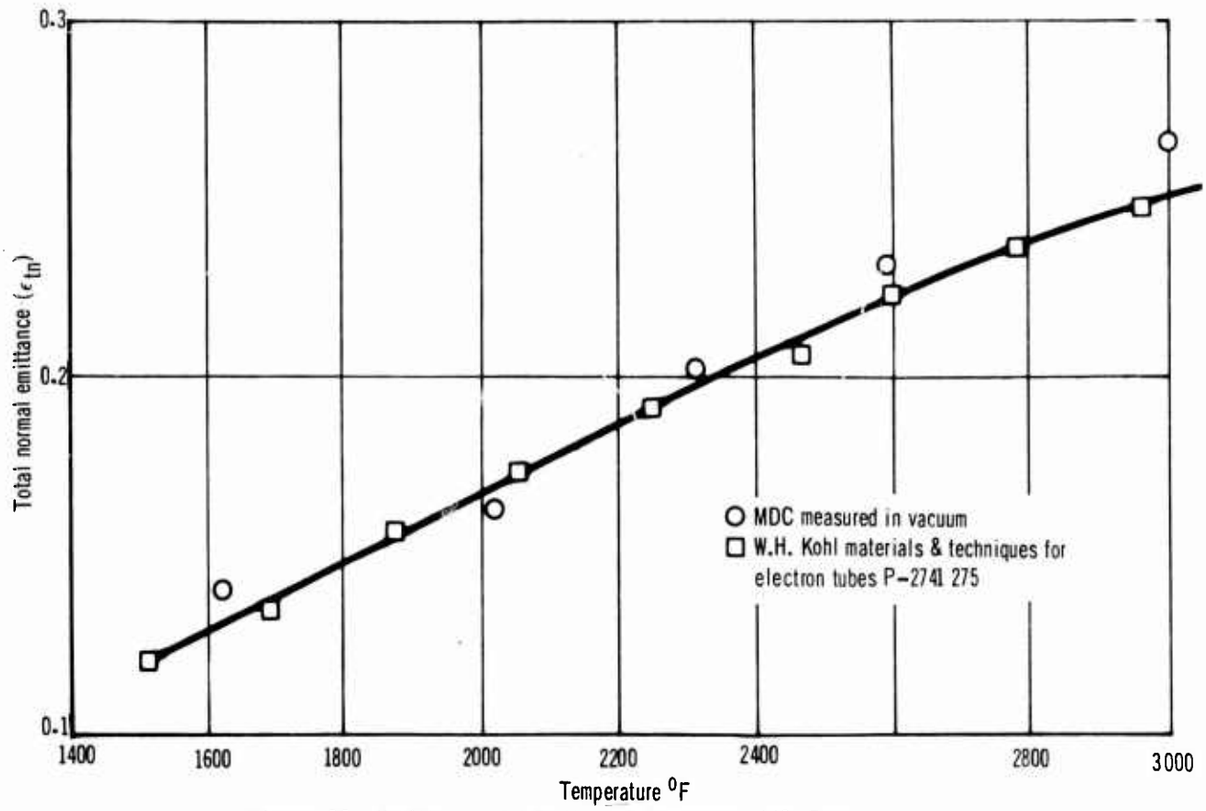

Figure 98 Emittance Of Polished Tungsten VS Temperature

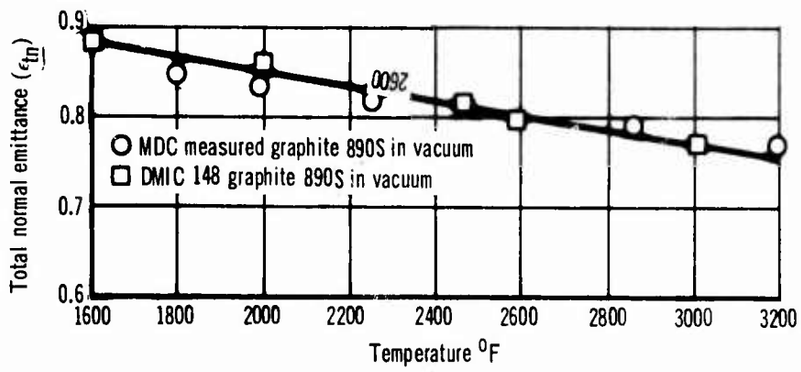

Figure 99 Emittance Of 890S Graphite VS Temperature

The results of the reference cavity calibration showed that $\Delta\varepsilon_2/\varepsilon_2 = \pm 0.01$ and from the linearity measurements $\frac{V_1}{V_1} = \frac{\Delta V_2}{V_2} = \pm 0.01$, substituting into the equation of the total differential:

$$\frac{\Delta \varepsilon_2}{\varepsilon_2} = \pm 0.03$$

The uncertainty was used to compute the ε values listed in column 3 of Table XVII and there is good agreement with the measured differences as given in column 5.

The precision of the measurements is estimated to be ± 1% based on repeated measurements on the same reference cavity.

3. EMITTANCE MEASUREMENTS

(a) Specimen Preparation

A total of fifty four (54) Cb-752 columbium emittance specimens were fabricated and then coated with the R-512E coating by Sylvania Electric Products, Inc. Twenty seven (27) of these specimens received the R-512E (60% Silicon, 20% Iron and 20% Chromium) coating with an applied coating weight of 25 ± 2 mg/cm^2 or a coating thickness of 3.5 ± 0.2 mils/side. Nine (9) additional specimens were processed with the same coating weight, 25 ± 2 mg/cm^2, but in a separate batch to evaluate the effect of batch-to-batch variations on emittance. Nine (9) specimens received the R-512E coating with an applied coating weight of 12.5 ± 2 mg/cm^2 or a coating thickness of 1.75 ± 0.2 mils/side. Thus the effect of coating thickness could be determined.

Nine specimens received a modified R-512E coating (40% silicon, 30% chromium and 30% iron) with a coating weight of 25 ± 2 mg/cm^2 or a coating thickness of 3.5 ± 0.2 mils/side. This enabled the determination of coating compositional effects on emittance.

Also, several additional modified versions of the R-512E coating were tested to 2400°F to determine the effect of chemistry variation on the emittance.

(b) Test Conditions

The total normal emittance of three (3) R-512E coated columbium specimens was measured for each of three pressure levels (1.0, 15 and 30 torr) from 1600 to 3000°F, with measurements at approximately 200°F increments during heating and cooling. This testing was repeated for five cycles per specimen and air was flowed past the specimens at all times during testing. The total normal emittance of two (2) R-512E coated columbium specimens was measured from 1600° to 2400°F and one (1) additional specimen from 1600° to 2600°F per a simulated time-temperature-pressure reentry profile (Figure 100), with emittance measurements made at approximately 500°F increments during heating and cooling.

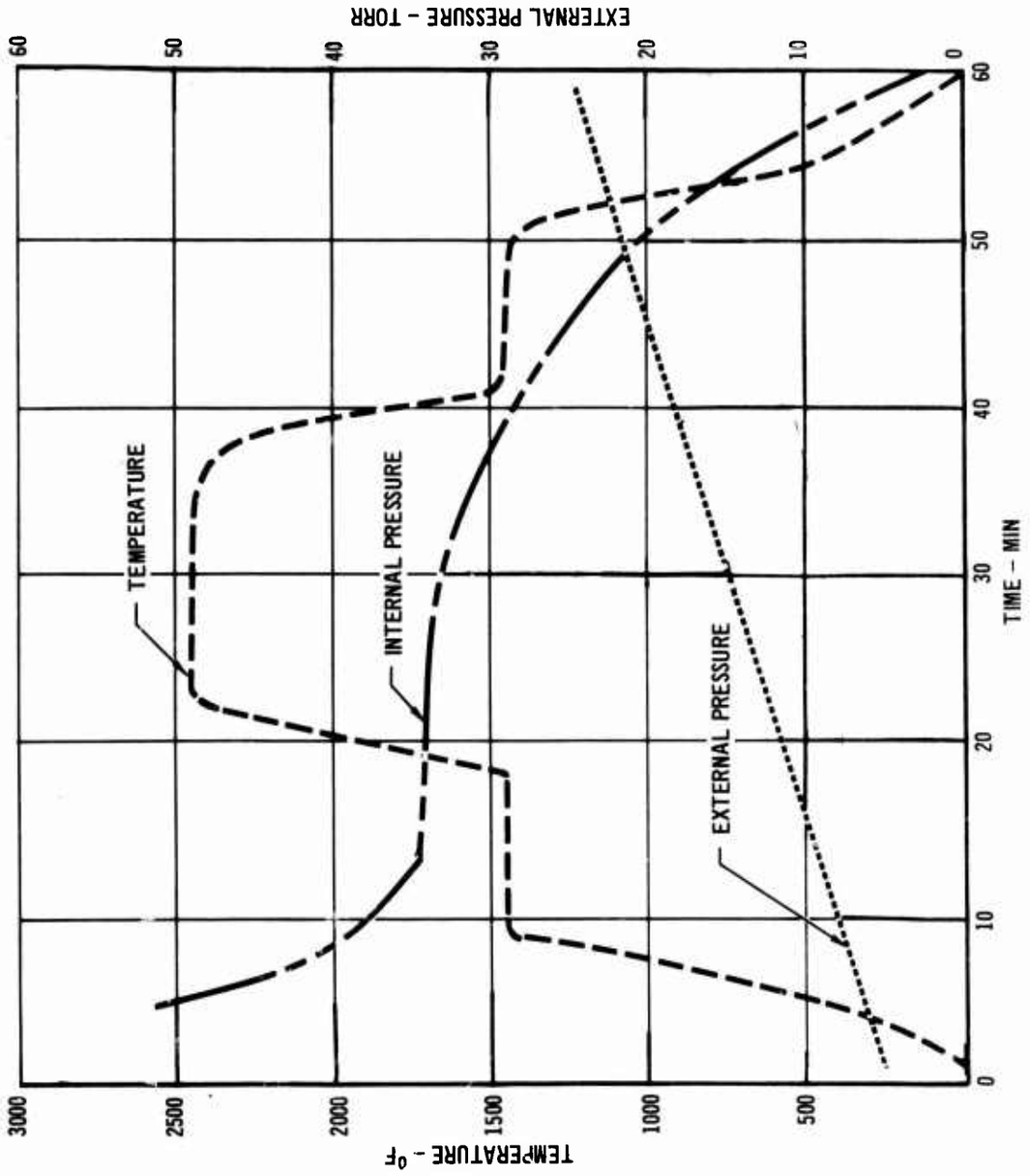

Figure 100 Profile Test Conditions Of Temperature, Pressure

The total normal emittance was measured from 1600° to 3000°F for the R-512E coated columbium with variations in coating thickness (2.0 mils vs. 3.5 mils), batch-to-batch processing and coating composition. The test conditions were as follows: (1) slow heating from 1600° to 2800°F or with emittance measured at 200°F increments during heating and cooling and the testing repeated for five cycles per specimen for the 2800°F maximum temperature; (2) simulated profile heating to 2400° and 2600°F, with emittance measured during heating and cooling at 1600°, 2100° and 2400° or 2600°F. Thermal cycling was performed in a controlled time-temperature-pressure environment for up to 20 cycles, with emittance measured during the 1st, 2nd, 3rd, 5th, 10th, 15th and 20th cycles.

The emittance test parameters for the different conditions of R-512E coated columbium are given in Table XVIII.

(c) Reuse Effects

Recycling the R-512E coated columbium from ambient temperature to 2400°F for 20 times following a simulated reentry time-temperature-pressure profile decreased the total normal emittance from 0.89 to 0.66 at 1600°F and from 0.80 to 0.75 at 2400°F.- (Figure 101). The largest decrease in emittance occurred between the first and second cycle because the largest amount of surface oxidation of the intermetallic coating occurred during the first heating. The emittance change gradually decreased with increased cycling, and after 10 cycles to 2400°F the emittance remained relatively constant (within the accuracy of the emissometer, $\pm$ 0.03).

Another batch of R-512E coated columbium, processed using a new batch of slurry material, and designated as a separate batch was profile cycled 20 times to 2400°F (Figure 102). The emittance between 1600° and 2400°F behaved in a similar manner to the original batch. Both the original and separate batch had a greenish yellow color during and after testing to 2400°F. This color was different from the dark brown heat shield specimens profile cycled to 2400°F in a reduced pressure Astro furnace. The only difference in the test environment between emissometer and the Astro furnace was the flow rate across the specimen during thermal cycling. The emissometer had a flow rate of approximately 1 to 2 liters of air per minute, while the Astro furnace had a different flow rate of approximately 0.3 to 3.73 liters of air per minute. An emittance specimen (FSS-17) from the original batch of material was thermal cycled to 2400°F at a lower flow rate, .3 to .5 liters per minute. The lower flow rate more closely matched the flow rate of the Astro furnace (.3 to 3.73 liters/minute) where the heat shield specimens were tested. The exact flow rate could not be matched because of the limitations of the flow meter being used in connection with the emissometer. This specimen (FSS-17) was cycled 4 times to 2400°F and the color of the specimen was brownish green with one area of the specimen (which faced the setter during coating processing) having a distinct different color (dark gray). Therefore, an emittance specimen (FSS-16) was tested in the Astro furnace at 2400°F for 4 cycles, and the same color phenomenon occurred as with specimen No. FS-17. This established that the flow rate difference was not the important factor for the difference in color of the emittance specimens and the heat shield panels tested at 2400°F. But since a lower flow rate, while maintaining the

Table XVIII
Specimen Parameters

Specimen Number	Batch	Maximum Temp. °F	Air Pressure Torr	Air Flow Liters/ Min.	Number of Cycles	Comments – Post–Test Conditions
FSS–1	(1) Original	3000	15	2	3	Blisters appeared at 3000°F during the 1st cycle; gross, oxidation after the 3rd cycle.
–2	"	2800	15	2	5	Few blisters after 2nd cycle to 2800°F; gross oxidation around the Al_2O_3 reference cavity after the 5th cycle.
–3	"	2800	15	2	5	Same as FSS–2.
–4	"	3000	1	0.8	5	Crusty coating after 1st cycle; the crust fell off at 2000°F during the the 2nd cycle; gross oxidation and scaling occurred for all 5 cycles.
–5	"	2800	1	0.8	5	Specimen black, minute blisters on the surface.
–6	"	2800	1	0.8	5	Specimen black, some oxidation at the leading edge.
–7	"	3000	30	2	1	Specimen black, minute blisters on the surface; specimen in very good condition.
–8	"	2800	30	2	5	Specimen black, gross oxidation at the leading edge.
–9	"	2800	30	2	5	Specimen brownish black, minute blisters on the surface; specimen in very good condition.
–10	"	3000	15	2	1	Specimen greenish black, minute blisters on the surface; gross oxidation at the leading edge.
–11	"	3000	1	0.8	1	Gross oxidation of the entire specimen.
–12	"	2400	8–22	1.2–2	20	Specimen greenish yellow and in very good condition.
–13	"	2400	8–22	1.2–2	20	Specimen greenish yellow and in very good condition.
–14	"	2400	8–22	1.2–2	20	Specimen greenish yellow and in very good condition.
–18	Original	2600	8–22	1–2	20	Specimen grayish black and in very good condition.
–17	"	2400	8–22	.05–.37	4	Specimen brownish green on the surface and dark grayish green around the setter area – specimen in very good condition.
–16	"	2400	8–22	.3–3.73	4	Specimen heated in astro furnace. Specimen was brownish green on the surface and a dark grayish green around the setter area, specimen in very good condition
FSS–28	(2) Separate	3000	15	2	1	Specimen grayish black with gross oxidation around the leading edge and the Al_2O_3 reference cavity.
–29	"	2800	15	2	5	Specimen grayish black with gross oxidation around the Al_2O_3 reference cavity.
–30	"	2800	15	2	5	Specimen grayish black with gross oxidation around the Al_2O_3 reference cavity and minute blisters on the surface.
–31	"	2400	8–22	1–2	20	Specimen greenish yellow and in very good condition.
–32	"	2400	8–22	1–2	20	Specimen greenish yellow and in very good condition.
–35	"	2600	8–22	1–2	20	Specimen brownish black with gross oxidation around the Al_2O_3 reference cavity and minute blisters on the surface.

Table XVIII (Continued)

Specimen Parameters

Specimen Number	Batch	Maximum Temp. °F	Air Pressure Torr	Air Flow Liters/ Min.	Number Of Cycles	Comments – Post–Test Conditions
FSS–37	Thin (3)	3000	15	2	1	Specimen grayish black, gross oxidation over the leading face.
–38	"	2800	15	2	3	Specimen bluish black, gross oxidation over the entire specimen.
–39	"	2800	15	2	4	Specimen bluish black, gross oxidation over the entire specimen.
–40	"	2400	8–22	1–2	20	Specimen greenish yellow and in very good condition.
–41	"	2400	8–22	1–2	20	Specimen grayish yellow and in very good condition.
–42	" (4)	2600	8–22	1–2	18	Specimen grayish black, gross oxidation over the entire specimen.
FSS–46	Modified	2400	8–22	1–2	20	Specimen brownish black and in very good condition.
–47	"	2800	15	2	1	Specimen grayish black, gross oxidation around the Al_2O_3 reference cavity.
–48	"	2800	15	2	5	Specimen grayish black, gross oxidation over the entire specimen.
–49	"	2800	15	2	5	Specimen grayish black, gross oxidation over the entire specimen.
FSS–50	"	2400	1–22	1–2	20	Specimen brownish black and in very good condition.
–52	"	3000	15	2	1	Specimen grayish black, minute blisters over the entire specimen and gross oxidation around the Al_2O_3 reference cavity.
–53	"	2600	8–22	1–2	20	Specimen grayish black, minute blisters over the entire specimen.

(1) R512E (20% F_e, 20% C_r, 60% Si) coated CB–752 columbium 25 mg/cm^2 coating weight (coating thickness approximately 3.5 mils).

(2) R512E (20% F_e, 20% C_r, 60% Si) coated CB–752 columbium 25 mg/cm^2 coating weight coated with a different batch of R512E.

(3) R512E (20% F_e, 20% C_r, 60% Si) coated CB–752 columbium 12.5 mg/cm^2 coating weight (coating thickness approximately 2.0 mils).

(4) Modified R512E (30% F_e, 30% C_r, 40% Si) coated CB–752 columbium 25 mg/cm^2 coating weight.

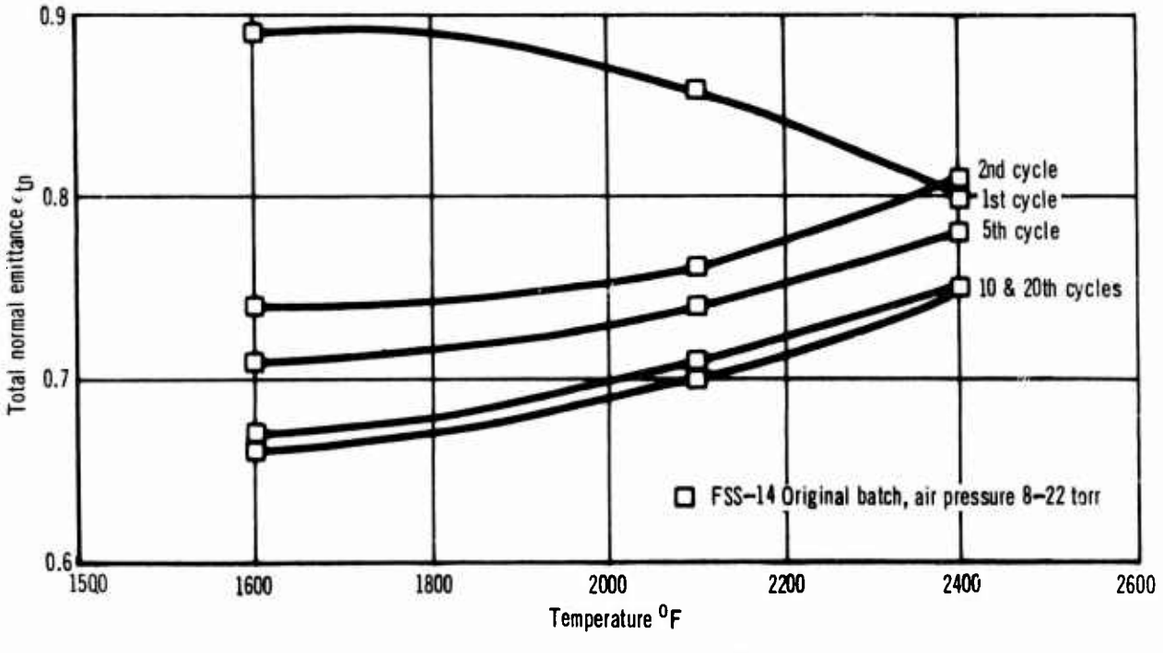

Figure 101 Emittance Of R–512E Coated Columbium (Original Batch) Vs Temperature (2400°F Max.)

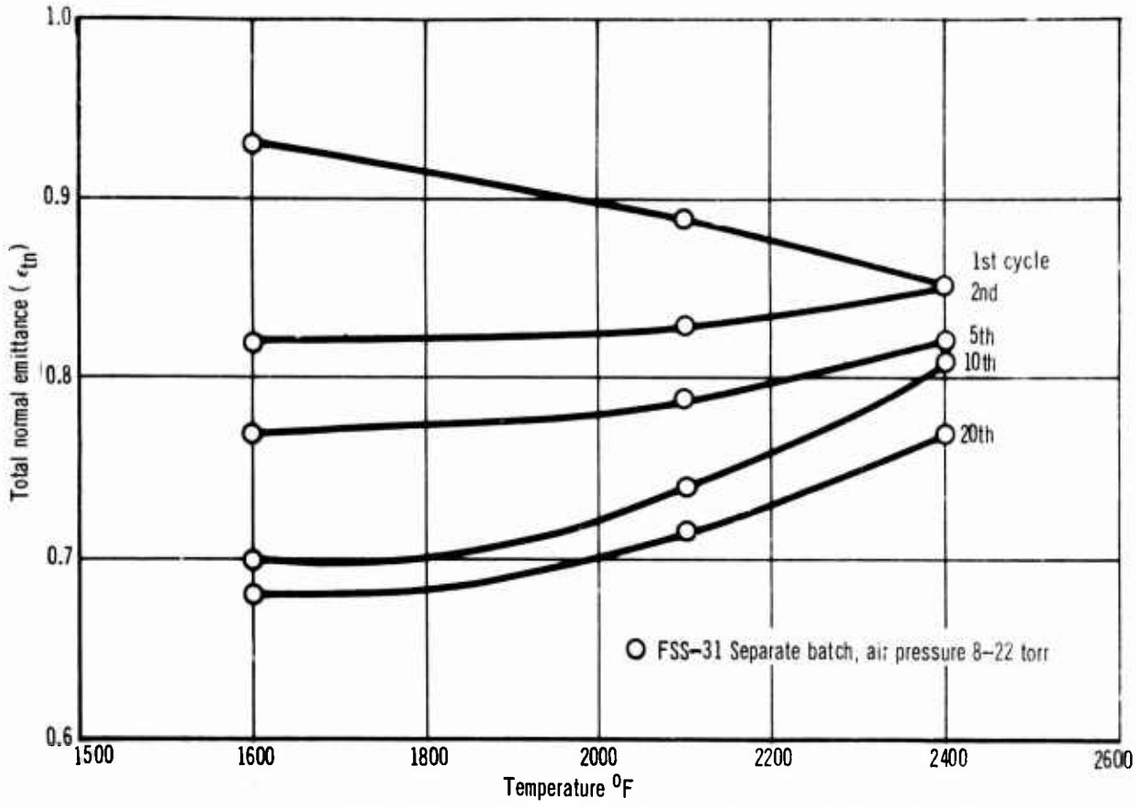

Figure 102 Emittance of R-512E Coated Columbium (Separate Batch) Versus Temperature (2400°F Max)

same pressure, did produce a higher emittance at 2400°F (Figure 103) and a slightly darker specimen (brownish green), a study of the effect of different flow rates on emittance may be warranted.

Sylvania was contacted to determine if there could be any possible contamination in their furnace during the coating of the emittance specimens, because the area of the specimen shaded by the specimen holder during processing had a dark brown appearance similar to the heat shield panels. Sylvania stated that the R-512E coated emittance specimens in the orignal batch did not have as great a weight loss (due primarily to chromium vaporization) during the coating cycle as is normal for batches of R-512E coating. Therefore, the emittance specimens may have had an excessive amount of chromium, thereby producing a chromia-rich oxide layer on the surface that is different from the heat shield panels when exposed to elevated temperatures in an oxidizing atmosphere. This discoloration phenomenon can possibly be corrected through better quality control during the coating process and/or by a slight change in formulation of the coating to eliminate the excess chromium on the surface.

The original and separate batches of the R-512E coated columbium had a coating weight of 25 mg/cm^2 (thickness of approximately 3.5 mils). To determine the effect of coating thickness on emittance during reuse, a batch of specimens with a coating weight of 12.5 mg/cm^2 (thickness of approximately 2.0 mils) was evaluated. The 12.5 mg/cm^2 coating thickness was designated as a thin coating batch.

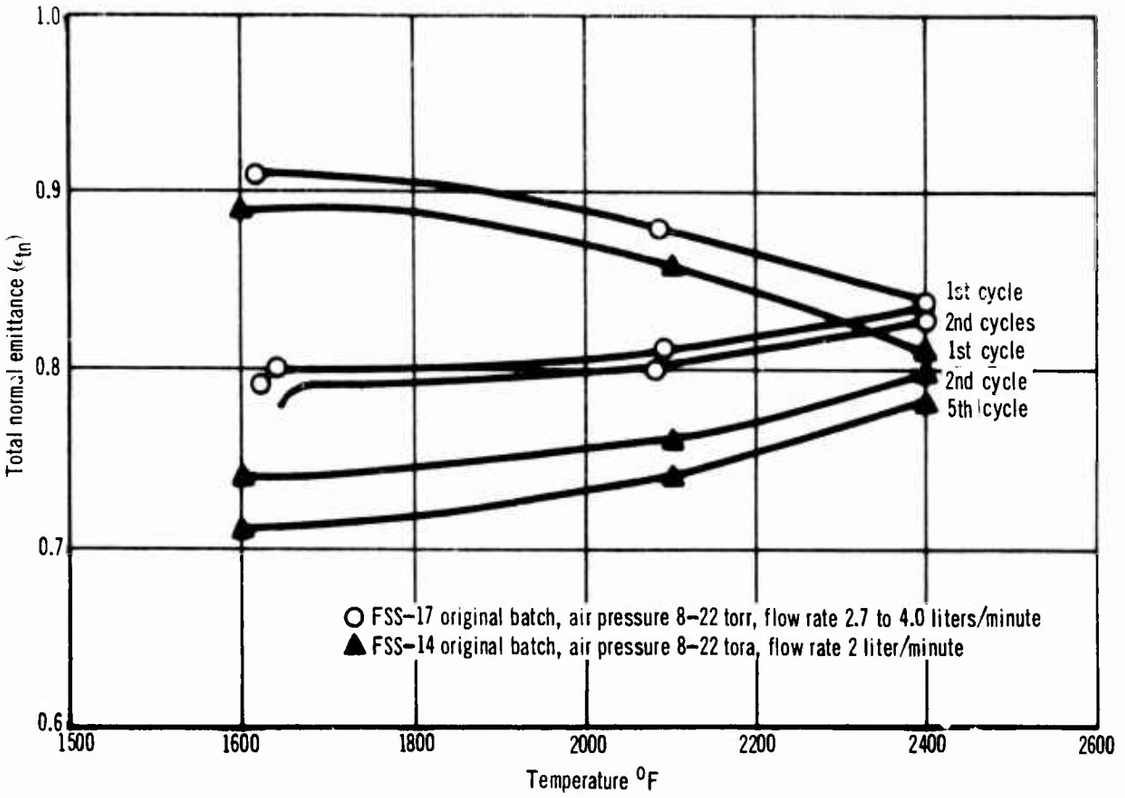

Figure 103 Emittance of R-512E Coated Columbium (Different Flow Rates) Versus Temperature (2400°F Max)

The emittance of the thin batch during profile testing to 2400°F also decreased (Figure 104) with thermal cycling, but not to the extent of the original or separate batches. The emittance decreased from 0.88 to 0.84 at 2400°F and from 0.94 to 0.80 at 1600°F after 20 simulated reentry profiles. The thin specimen, FSS-41, had a darker grayish green appearance during and after profile testing to 2400°F.

To determine the effect of a different coating chemistry on the emittance, a modified R-512E (40% Si, 30% Fe, 30% Cr) was evaluated having a coating weight of 25 mg/cm^2. The emittance of the modified R-512E (FSS-50) remained between 0.85 and 0.89 over the temperature range 1600 to 2400°F during all 20 simulated reentry cycles, (Figure 105). The modified coating remained a dark grayish black color during and after the 20 cycles to 2400°F. Although the modified R-512E had a much higher and a more stable emittance than the unmodified R-512E coating, the oxidation protection of the modified coating was not determined. Therefore, this may not be the optimum formulation to produce a higher and more stable emittance during reuse.

Figure 106 shows the emittance versus temperature and cycling for up to 20 cycles for the four different conditions of R512E coated columbium evaluated. This plot of data shows the emittance during the heating and cooling portion of the cycle. A hysteresis in the emittance data occurred during the 1st cycle to 2400°F and to a lesser extent on the succeeding cycles.

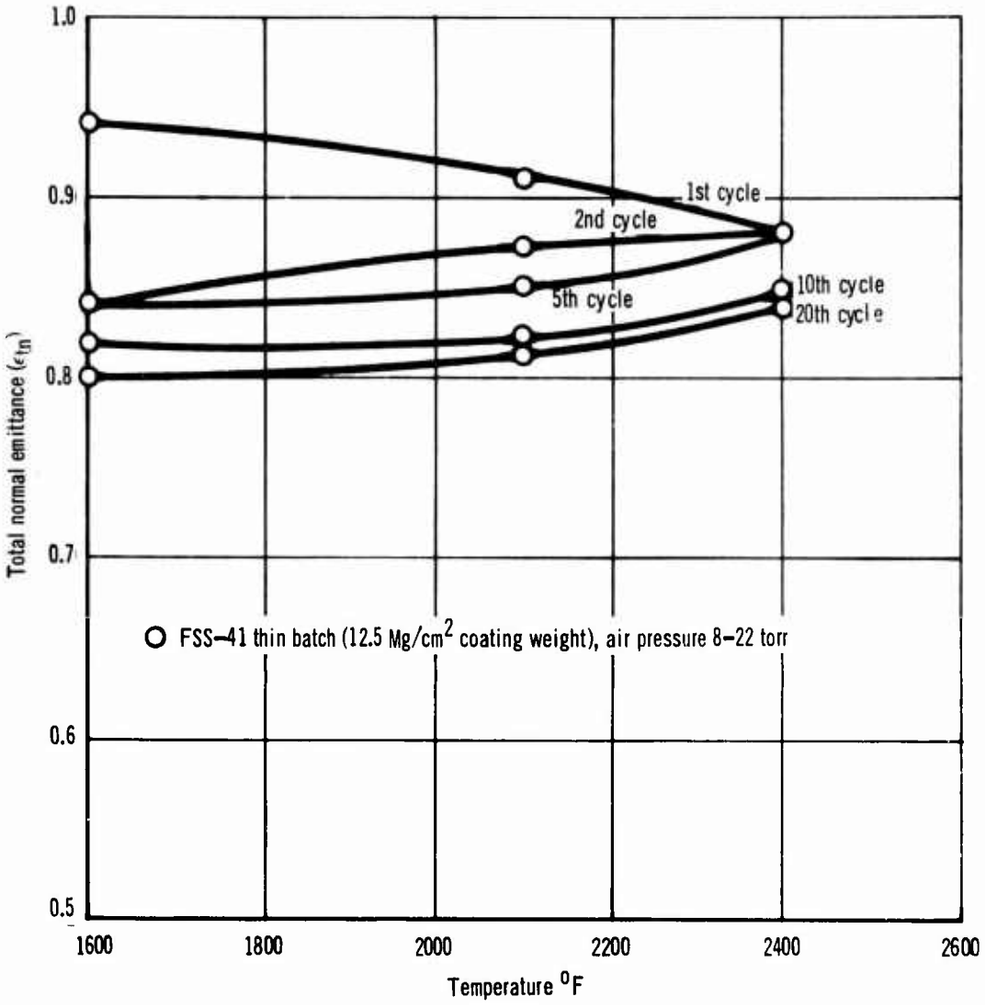

Figure 104 Emittance Of R-512E Coated Columbium (Thin Batch) Versus Temperature (2400^{o}F Max.)

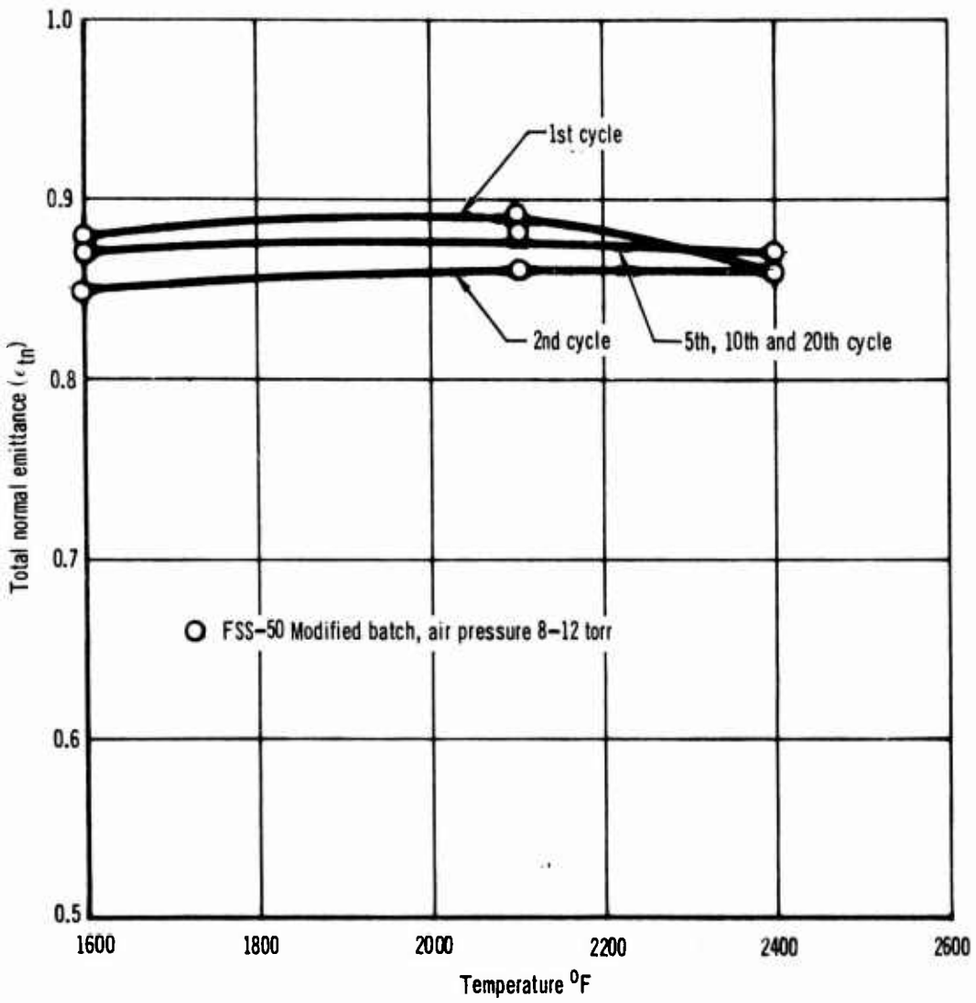

Figure 105 Emittance Of Modified R-512E (40% Si, 30% Cr 30% Fe) Coated Columbium Versus Temperature (2400°F Max.)

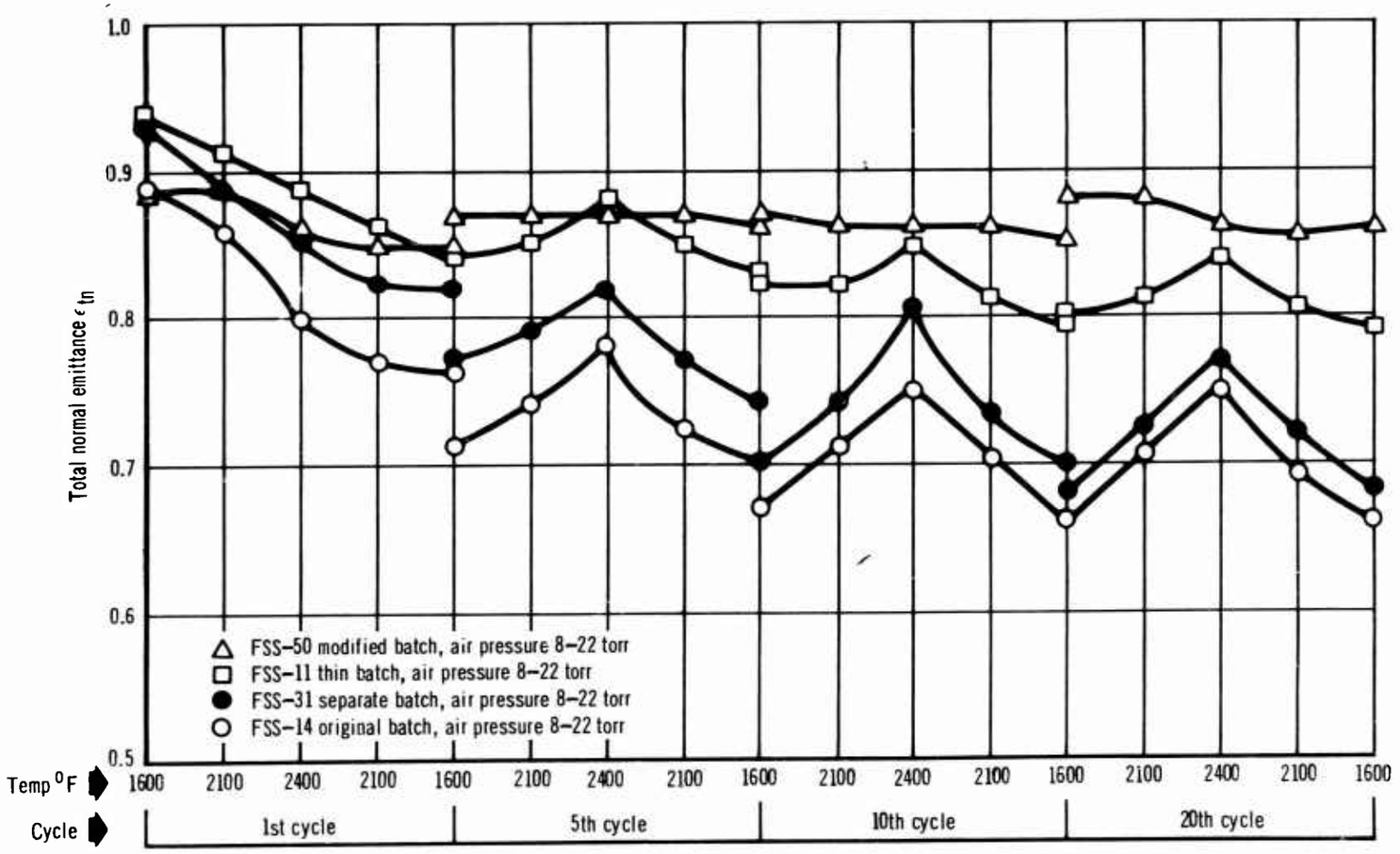

Figure 106 Emittance Of R-512E Coated Columbium (Four Different Batches) Versus Temperature (2400°F Max) and Cycles

Increasing the maximum temperature during simulated reentry profile testing to 2600°F for the original batch of R-512E coated columbium resulted in a further decrease in emittance after the 10th cycle to 2600°F. The emittance at 2600°F (FSS-18, Figure 107)decreased with thermal cycling similar to results obtained for the 2400°F maximum temperature profile (FSS-14, Figure 95) except after the 10th cycle the emittance at 2600°F continued to decrease. The emittance decreased from 0.85 to 0.70 at 2600°F compared to an emittance drop of 0.80 to 0.75 at 2400°F after 20 time-temperature-pressure profile cycles.

The separate batch (FSS-35) test at 2600°F for 20 cycles resulted in a complete reversal in the emittance trend with thermal cycling. The emittance (Figure 108) decreased similar to previous specimens during the 1st cycle to 2600°F, but as cycling continued the emittance increased until after 20 cycles the emittance had increased from 0.79 to 0.85 at 2600°F.

The thin coating also had the same trend as the separate batch in that the emittance increased with cycling after the 1st cycle to 2600°F, Figure 109. This specimen, FSS-42, failed due to gross oxidation after the 18th cycle to 2600°F, therefore, the test was terminated at this point.

All specimens tested to 2600°F had a dark greyish black appearance during and after testing. The modified R-512E coating maintained a high emittance (0.85 to 0.90) during all 20 cycles to 2600°F, Figure 110.

The plot of emittance versus temperature and thermal cycling, Figure 111, shows that the separate batch had a much higher emittance than the original batch during thermal cycles to 2600°F. This data then differs from the emittance trend at 2400°F maximum test temperature (Figure 106) whereby the original and separate batch had similar values.

Thermal cycling to 2800°F (up to 5 cycles) was accomplished at a constant pressure of 15 torr with emittance measured at approximately 300°F increments during both heating and cooling. No time-temperature profile was followed during these measurements and it normally took approximately 30 minutes to complete the emittance measurements during heating and cooling from 1600 to 2800°F.

The emittance of the original batch of R-512E coated columbium Figure 112, increased between the 2nd and 5th cycle after exhibiting the normal decrease in emittance during the 1st cycle as previously observed at lower maximum temperature (2400 and 2600°F) profile tests.

The separate batch, Figure 113, had the initial decrease in emittance during the 1st cycle and a slight decrease on the 5th cycle at 2800°F from 0.83 to 0.77.

The emittance of the thin batch during the 2800°F test started out lower at 1600°F (ε = 0.82) and gradually increased with increasing temperature, Figure 114. The emittance peaked out at 2600°F (= 0.89), then decreased at 2800°F (ε = 0.85). During the 2nd cycle to 2800°F, the emittance decreased to 0.75 at 2800°F. The coating failed due to gross oxidation in the 3rd cycle and the test was terminated.

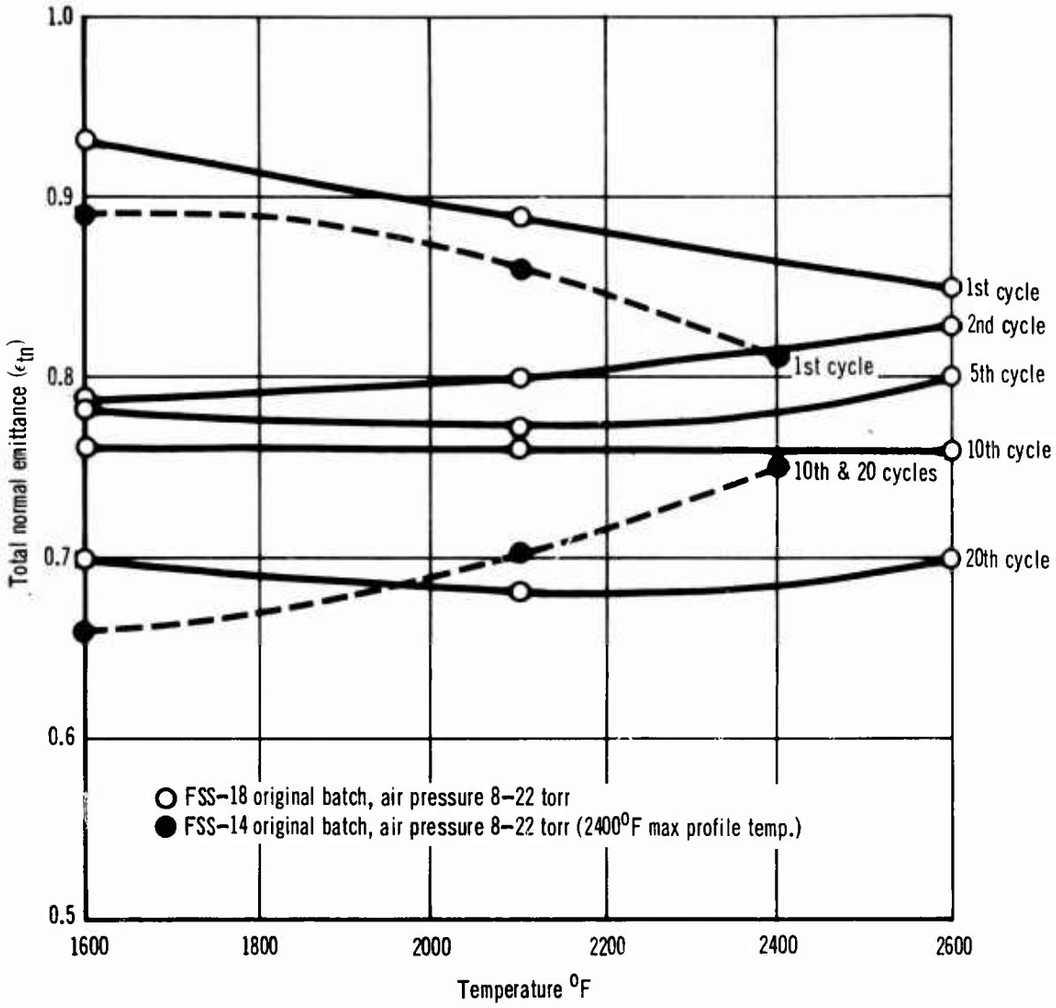

Figure 107 Emittance of R-512E Coated Columbium (Original Batch) Versus Temperature (2600°F Max)

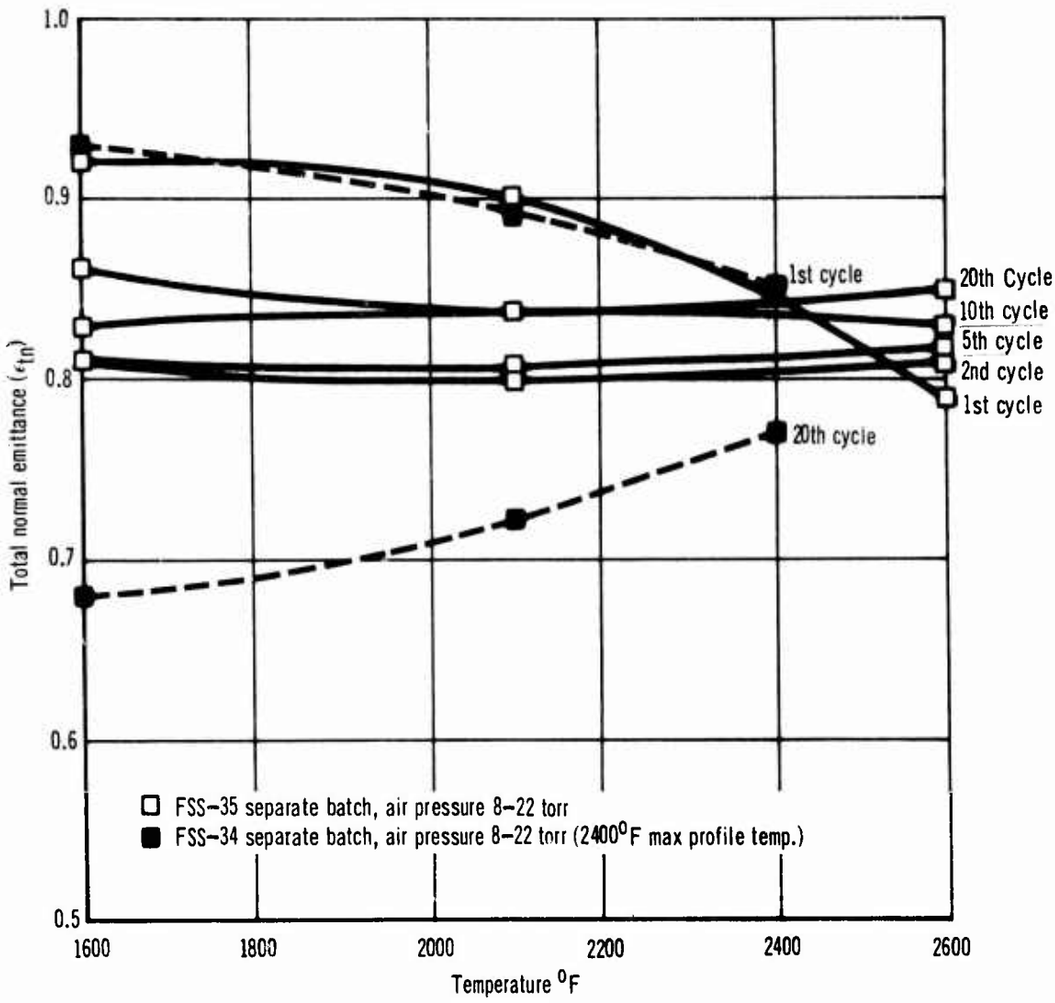

Figure 108 Emittance of R-512E Coated Columbium (Separate Batch) Versus Temperature (2600°F Max)

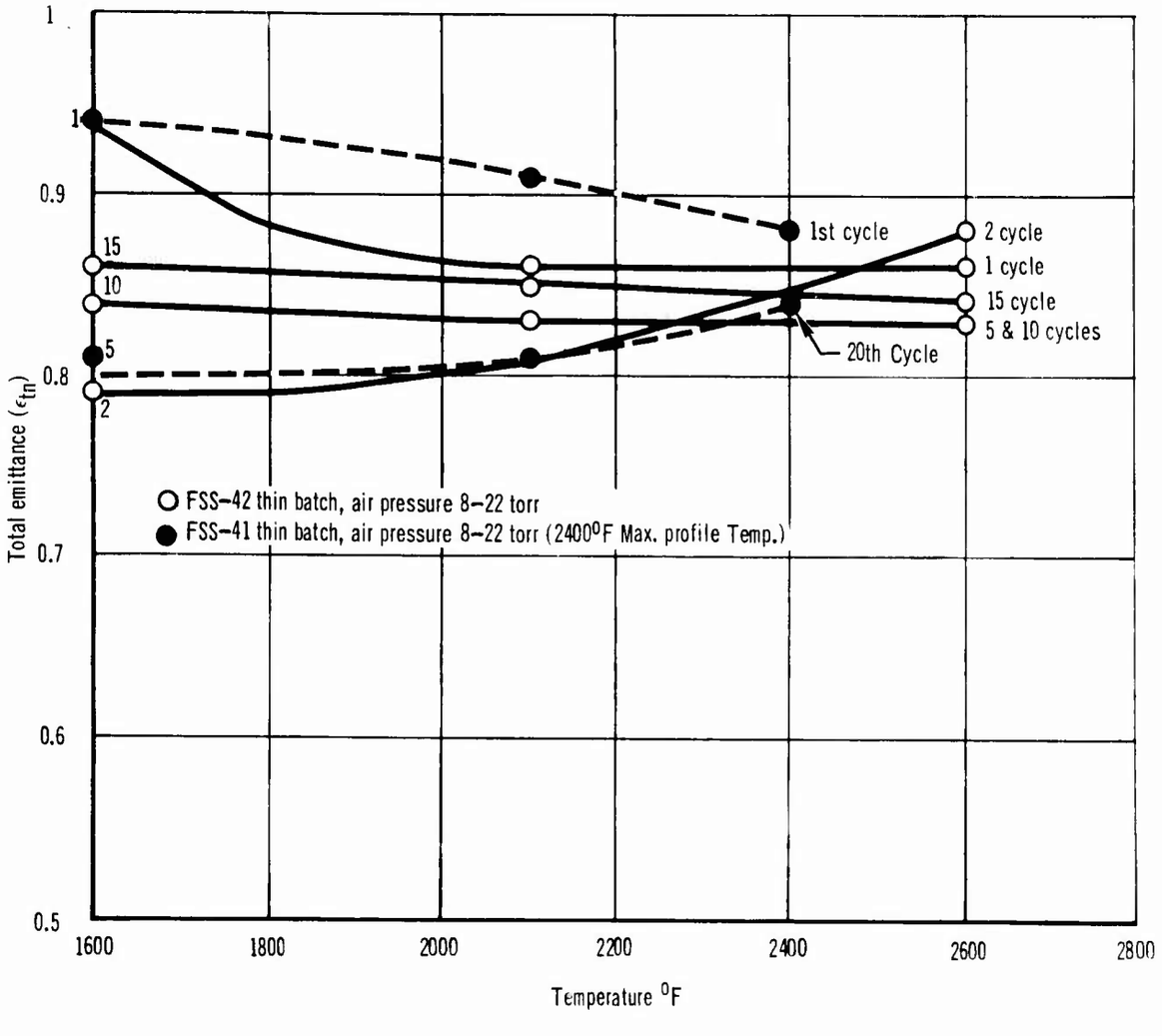

Figure 109 Emittance Of R-512E Coated Columbium (Thin Batch) Versus Temperature (2600°F Max.)

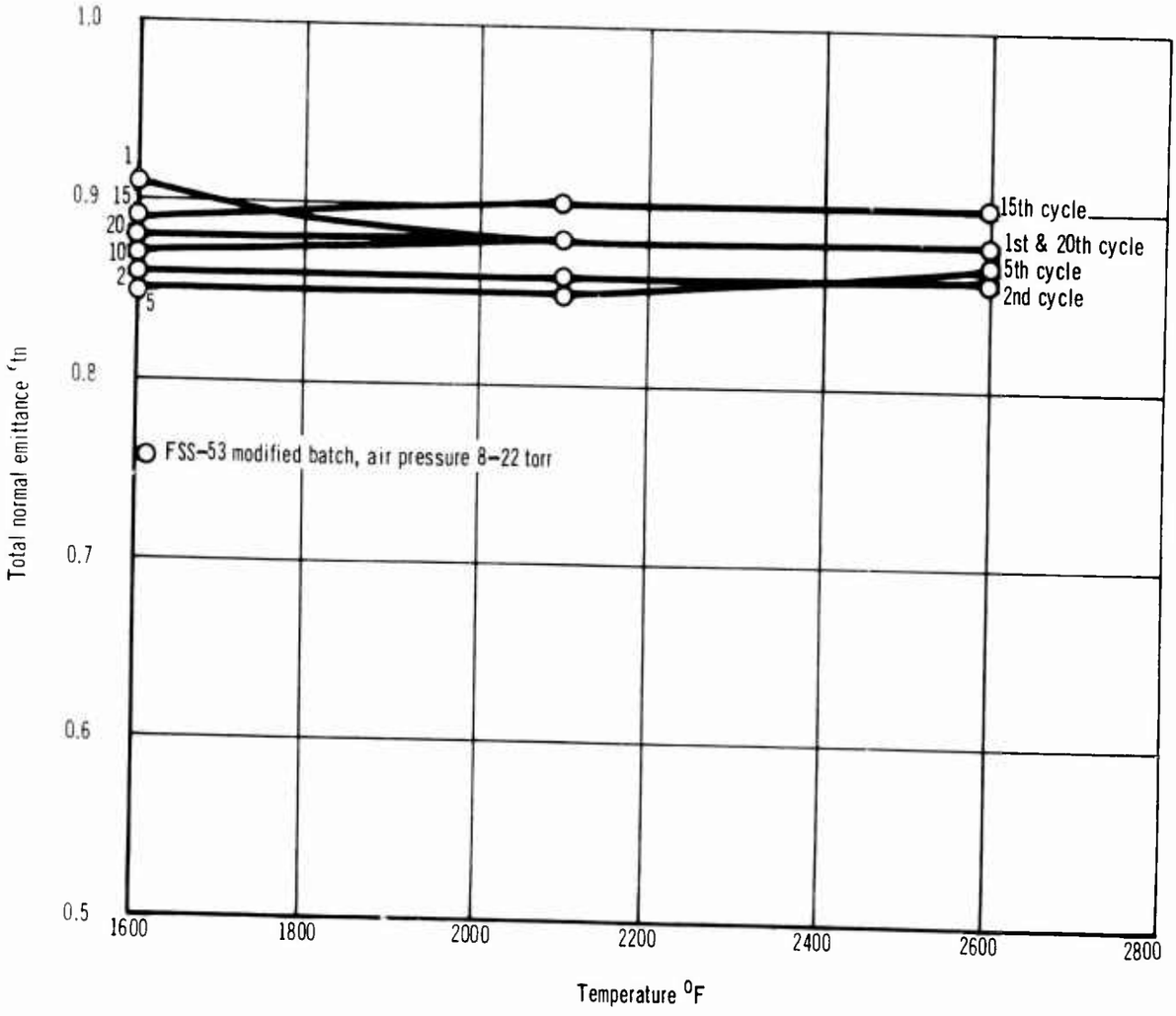

Figure 110 Emittance Of R-512E Coated Columbium (Modified Batch) Versus Temperature (2600°F Max.)

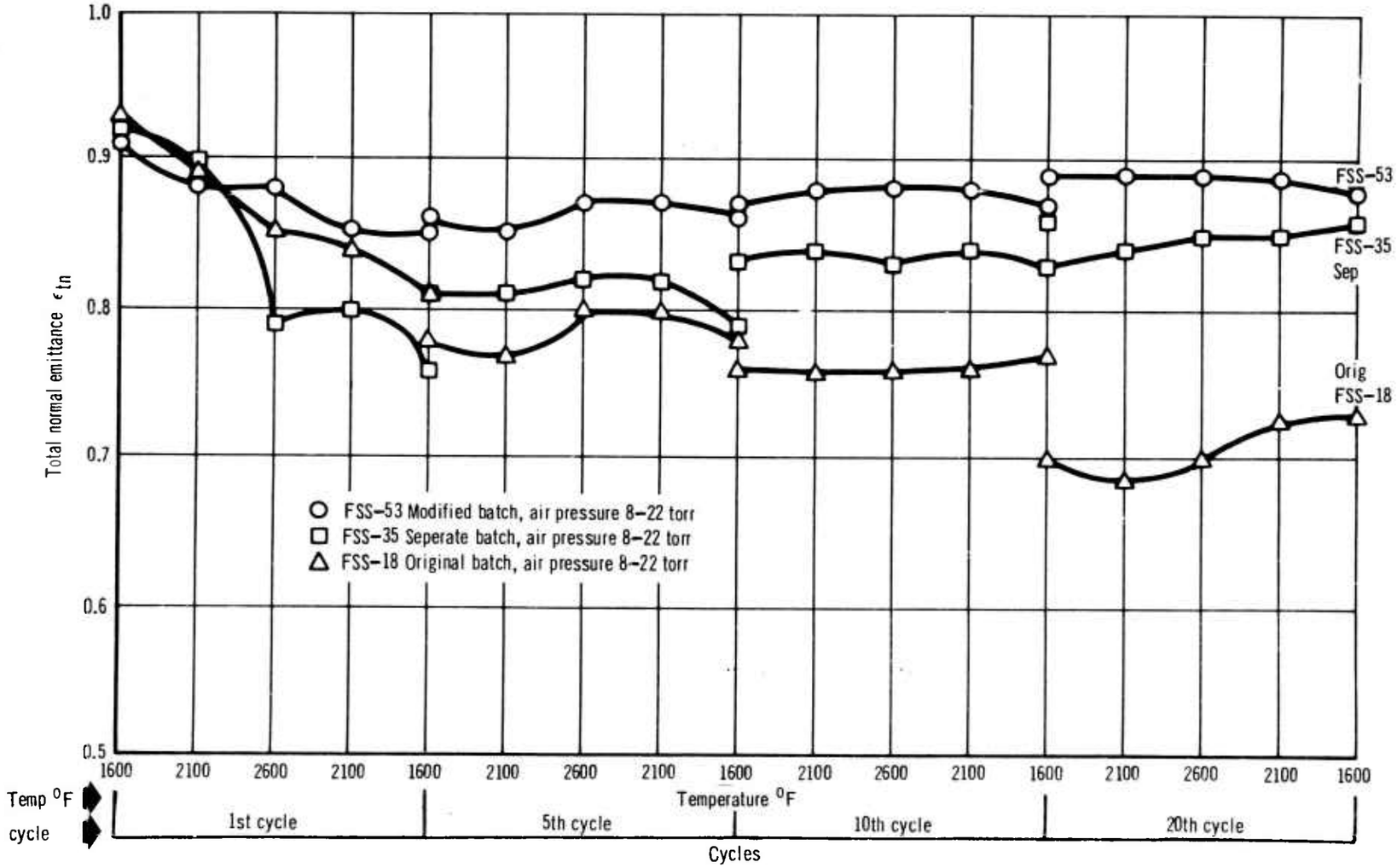

Figure 111 Emittance Of R–512E Coated Columbium (Three Different Batches) Versus Temperature (2600°F Max.) And Cycles

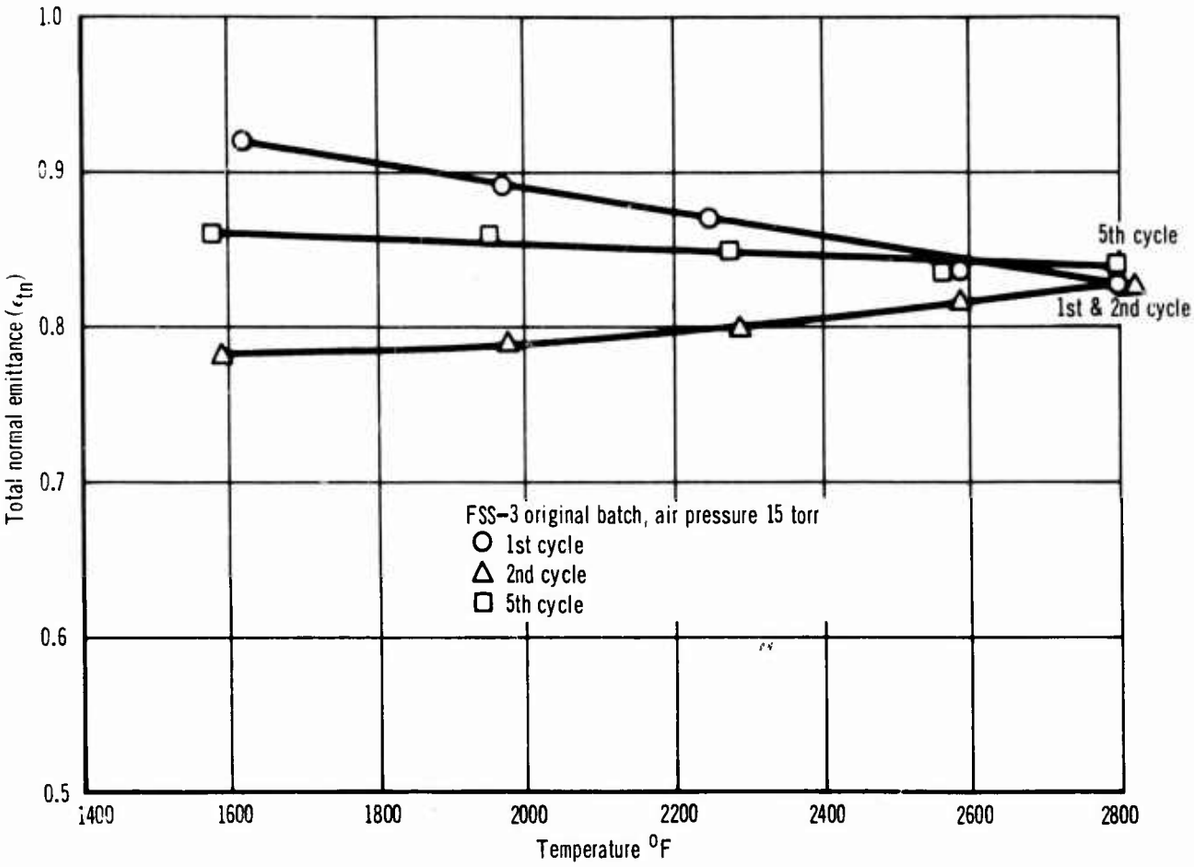

Figure 112 Emittance Of R-512E Coated Columbium (Original Batch) Versus Temperature (2800°F Max.)

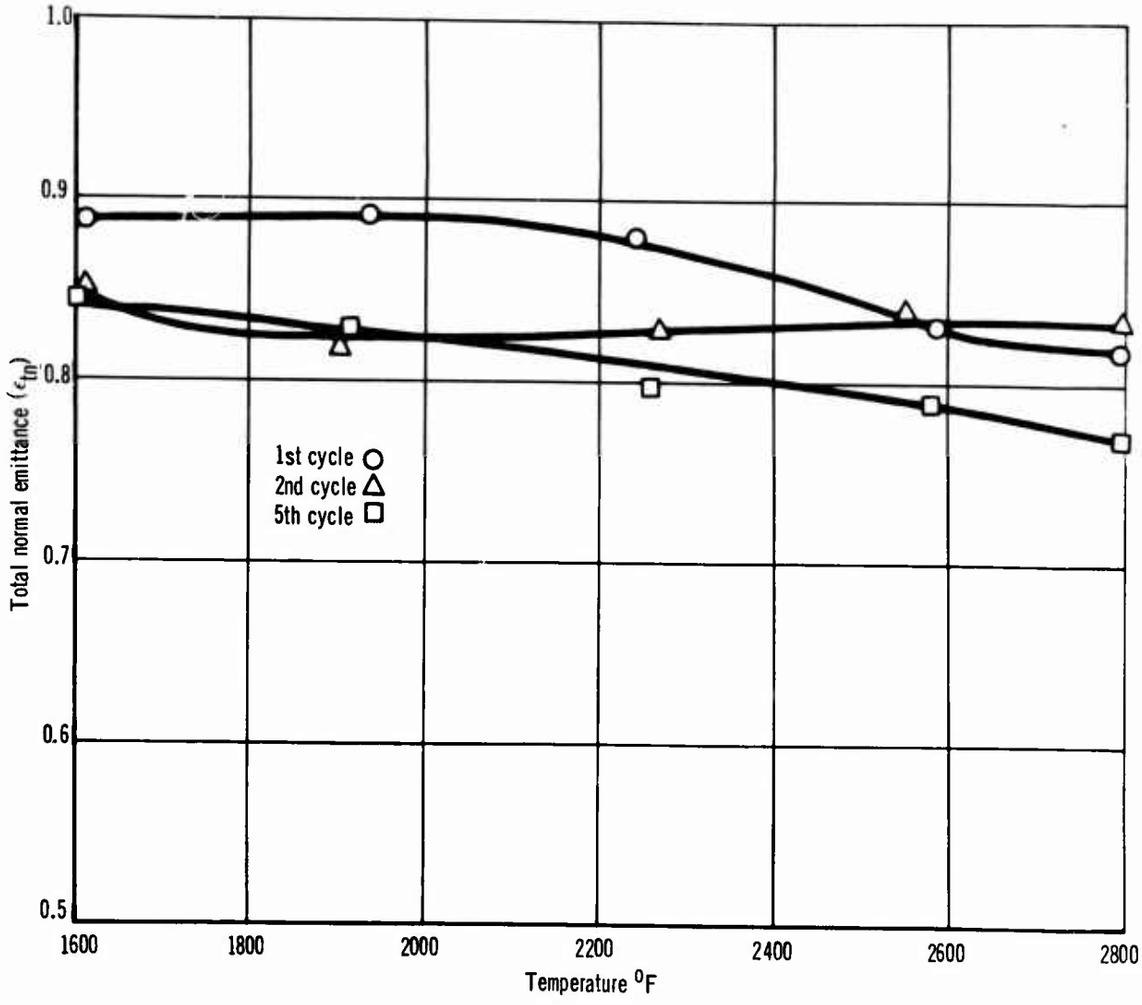

Figure 113 Emittance R–512E Coated Columbium (Seperate Batch) Versus Temperature (2800°F Max.)

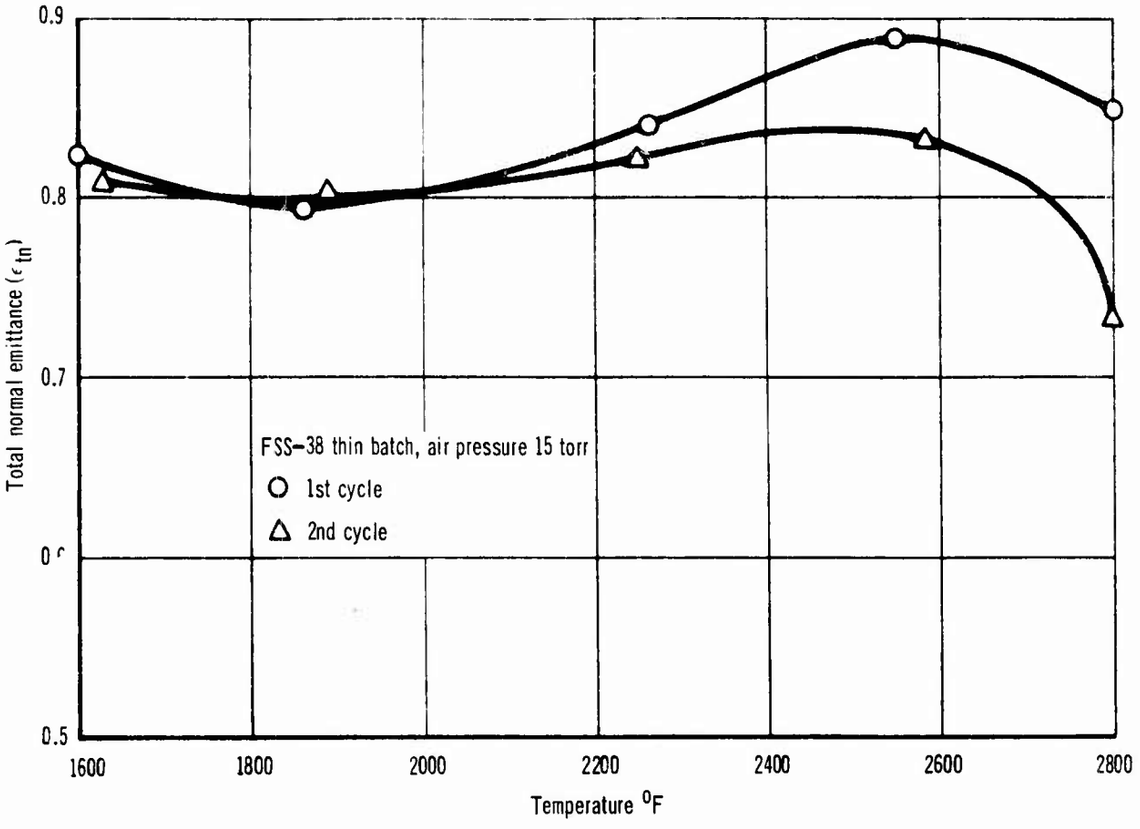

Figure 114 Emittance Of R-512E Coated Columbium (Thin Batch) Versus Temperature (2800°F Max.)

The modified R512E coating maintained a high emittance during all five cycles to 2800°F, Figure 115. The emittance was approximately 0.84 to 0.90 between 1600 and 2800°F for the five cycles. The coating failed due to gross oxidation between the 2nd and 5th cycle. The gross oxidation around the Al_2O_3 reference cavity was very predominant. It was concluded that for temperatures above 2600°F, the Al_2O_3 reacted with the R512E coating.

(d) Pressure Variations

The original batch specimens (FSS 1, 7 and 11) were thermal cycled to 3000°F using three different constant pressures (1, 15 and 30 torr). These different pressures had very little effect on the emittance especially above 2400°F, Figure 116. For temperatures below 2400°F, there was a maximum of 0.1 emittance units difference between specimens for the temperature range of 1600 to 2400°F. The emittance in general tended to decrease from 1600 to 2600°F (ϵ = 0.80) and then increased slightly at 3000°F (ϵ = 0.87).

At a constant pressure of 15 torr, the emittance at 3000°F in the first cycle (only 1 cycle performed) was in close agreement for all the different coating combinations tested, Figure 117. The separate and original batch both had a slight decrease in emittance at 2600°F.

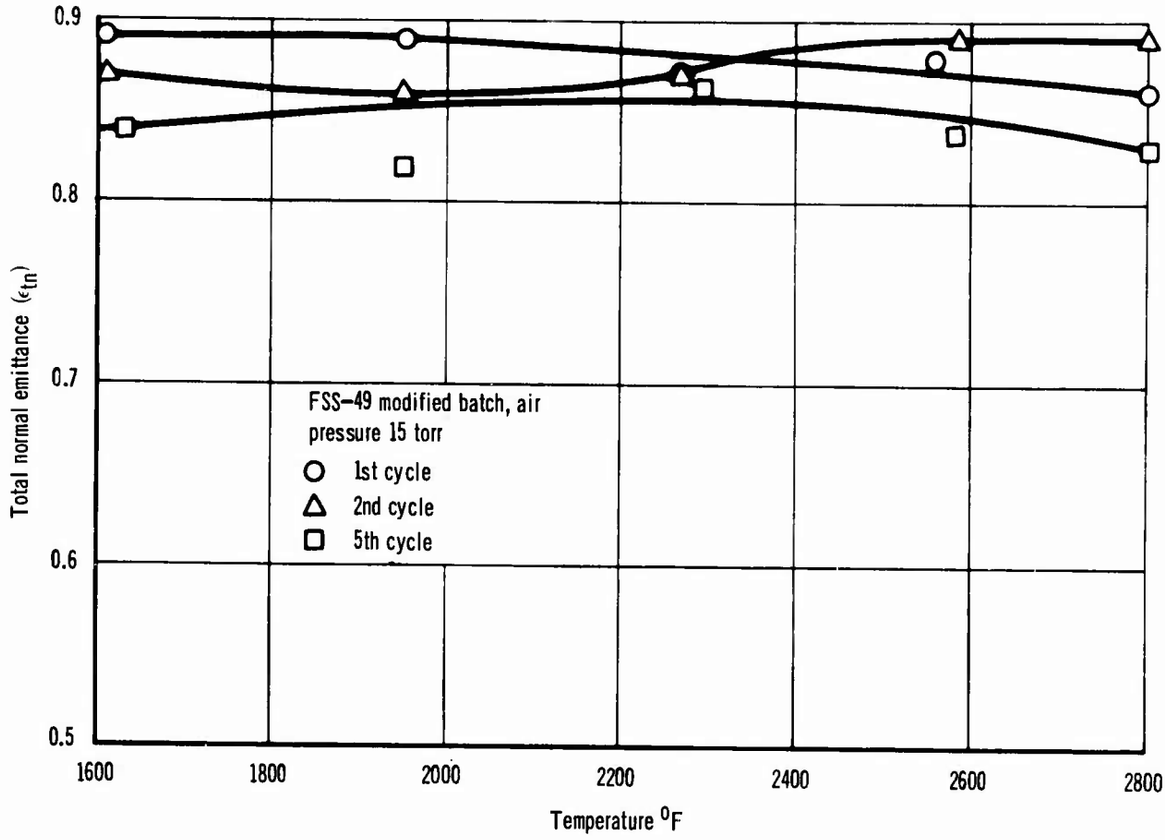

Figure 115 Emittance Of R–512E Coated Columbium (Modified Batch) Versus Temperature (2800°F Max)

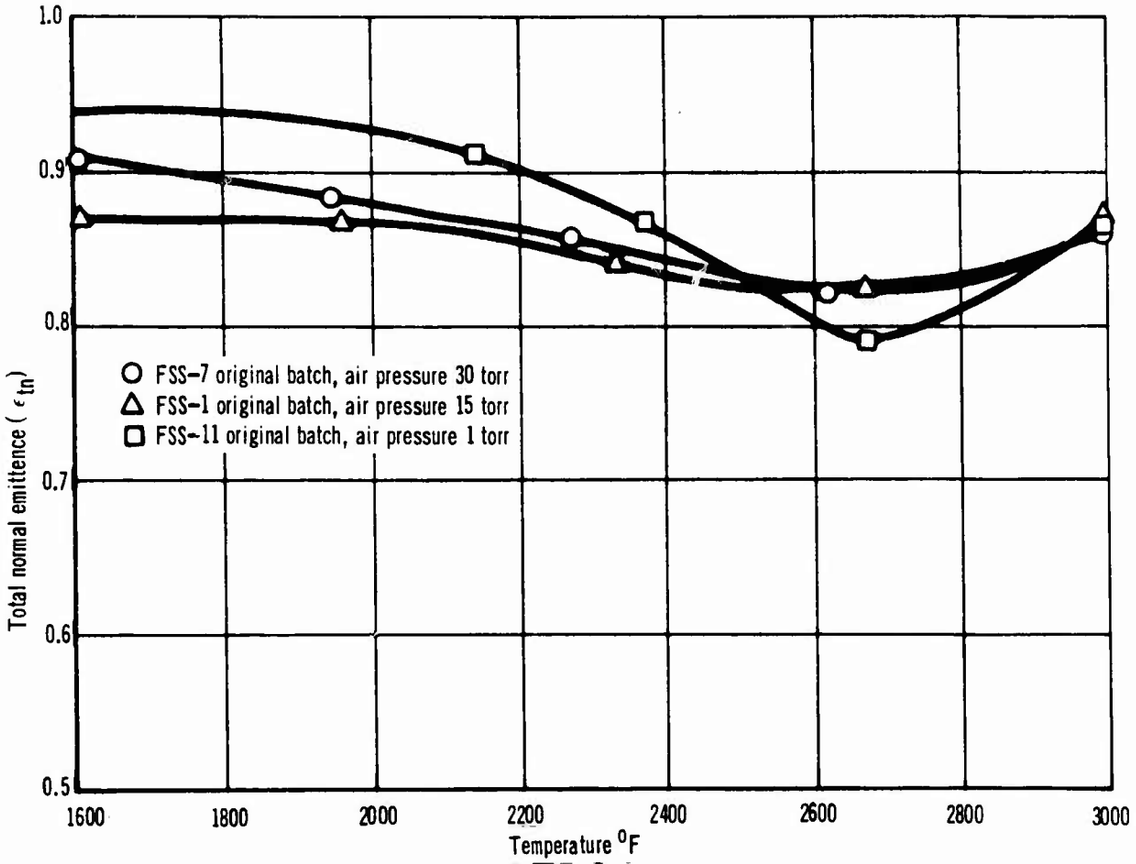

Figure 116 Emittance Of R-512E Coated Columbium (Original Batch) Versus Temperature (3000°F Max)

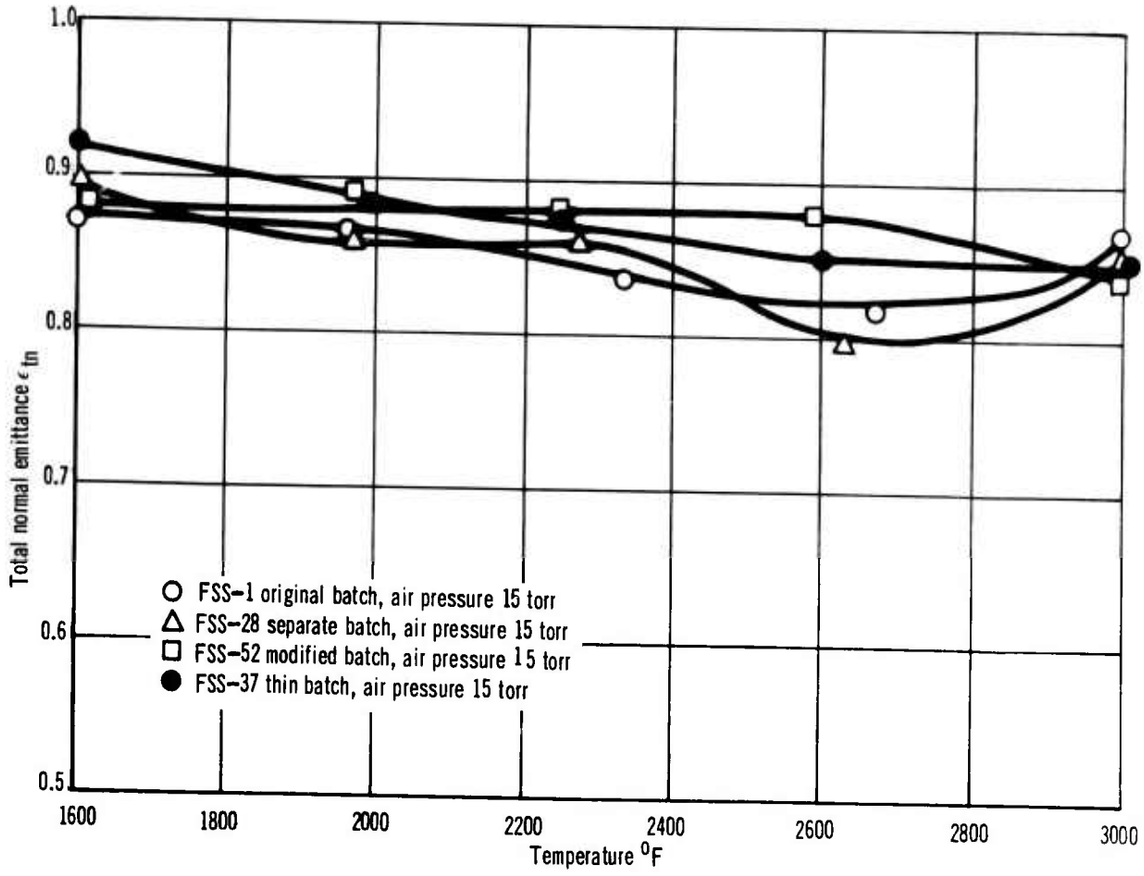

Figure 117 Emittance Of R-512E Coated Columbium (Four Different Batches) Versus Temperature (3000°F Max.)

(e) Specimen to Specimen Variations

Specimen to specimen variation in emittance was determined by measuring 2 or 3 specimens under the same test conditions from each batch and comparing the values. The emittance of the original batch, Figure 118, shows that a maximum variation of 0.12 emittance units was measured at 1600°F during profile testing to 2400°F for 20 cycles. This largest variation occurred at the 20th cycle to 2400°F, while at the 10th cycle only a difference of approximately 0.04 emittance units was measured. This was within the accuracy of the emissometer which is $\pm$ .03.

The separate batch, Figure 119 and the thin batch, Figure 120 had a much closer agreement between specimens from the same batch when heated to 2400°F following a time-temperature-pressure profile. The greatest difference in emittance was 0.04.

Increasing the maximum temperature to 2800°F for the original batch did improve the specimen to specimen variations in emittance. After five cycles to 2800°F the greatest difference in emittance was .06 on the 5th cycle, Figure 121. The separate batch at a maximum temperature of 2800°F had a maximum difference in emittance of .05, Figure 122.

(f) Batch to Batch Variations

The average emittance values for the original (3 specimens) and separate (2 specimens) batches are plotted in Figure 123 for the 2400°F maximum test temperature. The emittance difference for the 2400°F maximum temperature cycle varied by 0.075 emittance units at 1600° after the 1st cycle to 2400°F, but after the 20th cycle only an emittance difference of .05 was measured.

Increasing the temperature to 2600°F during profile testing accentuated the batch-to-batch variations, a difference of 0.13 was measured during the 20th cycle, Figure 111.

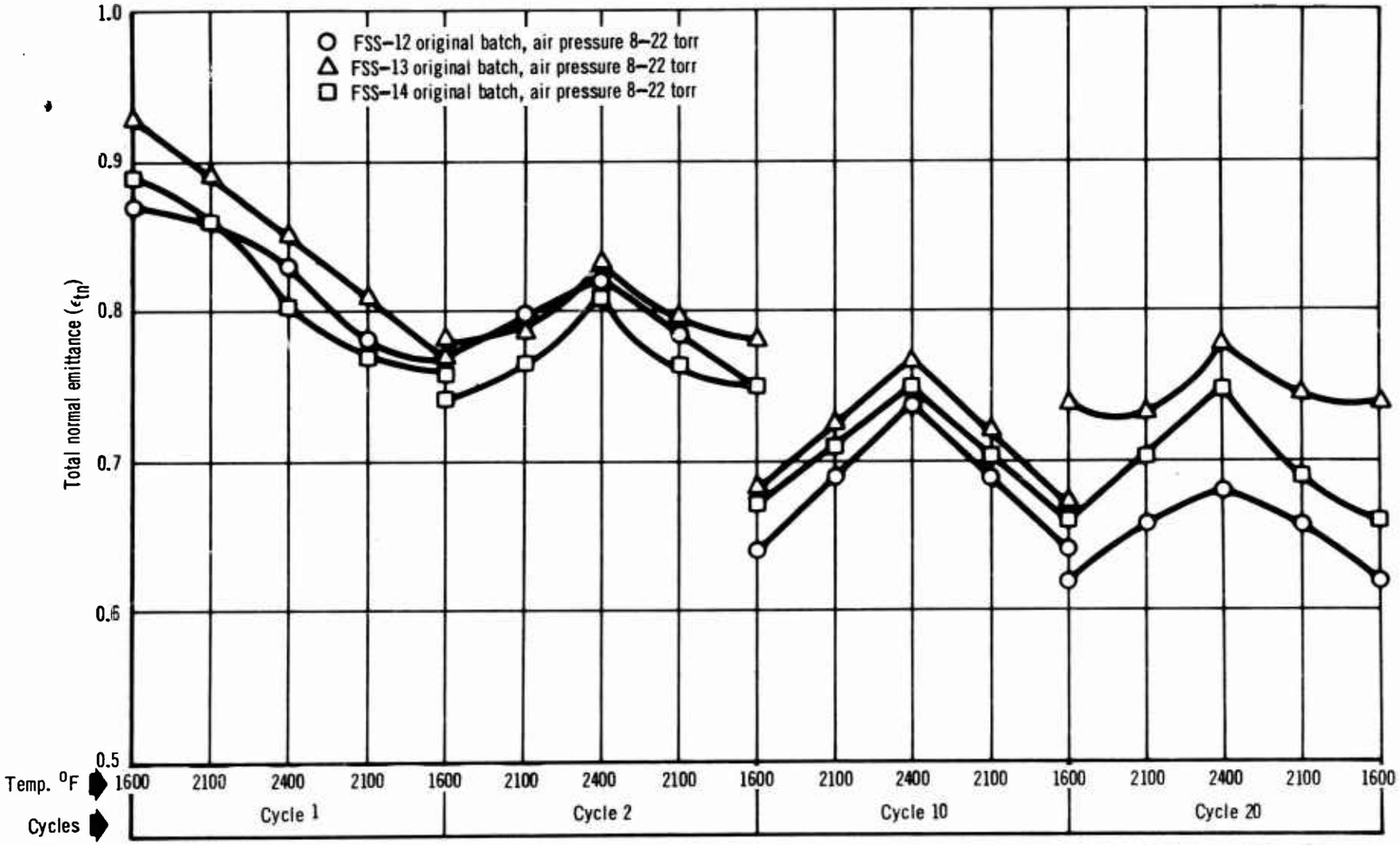

Figure 118 Emittance Of R-512E Coated Columbium (Original Batch) Versus Temperature (2400°F Max) & Cycles

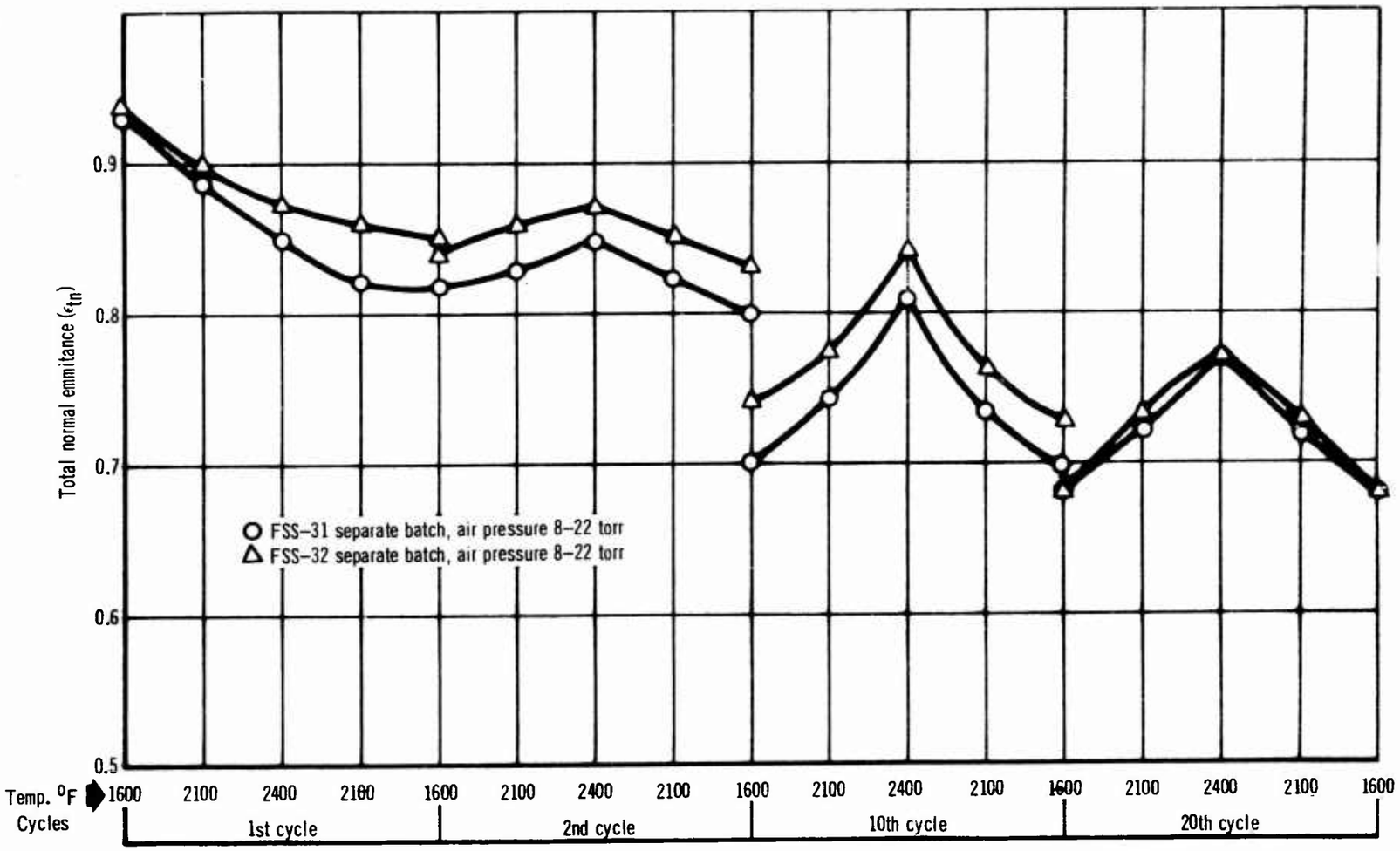

Figure 119 Emittance of R–512E Coated Columbium (Separate Batch) Versus Temperature (2400°F Max.) & Cycles

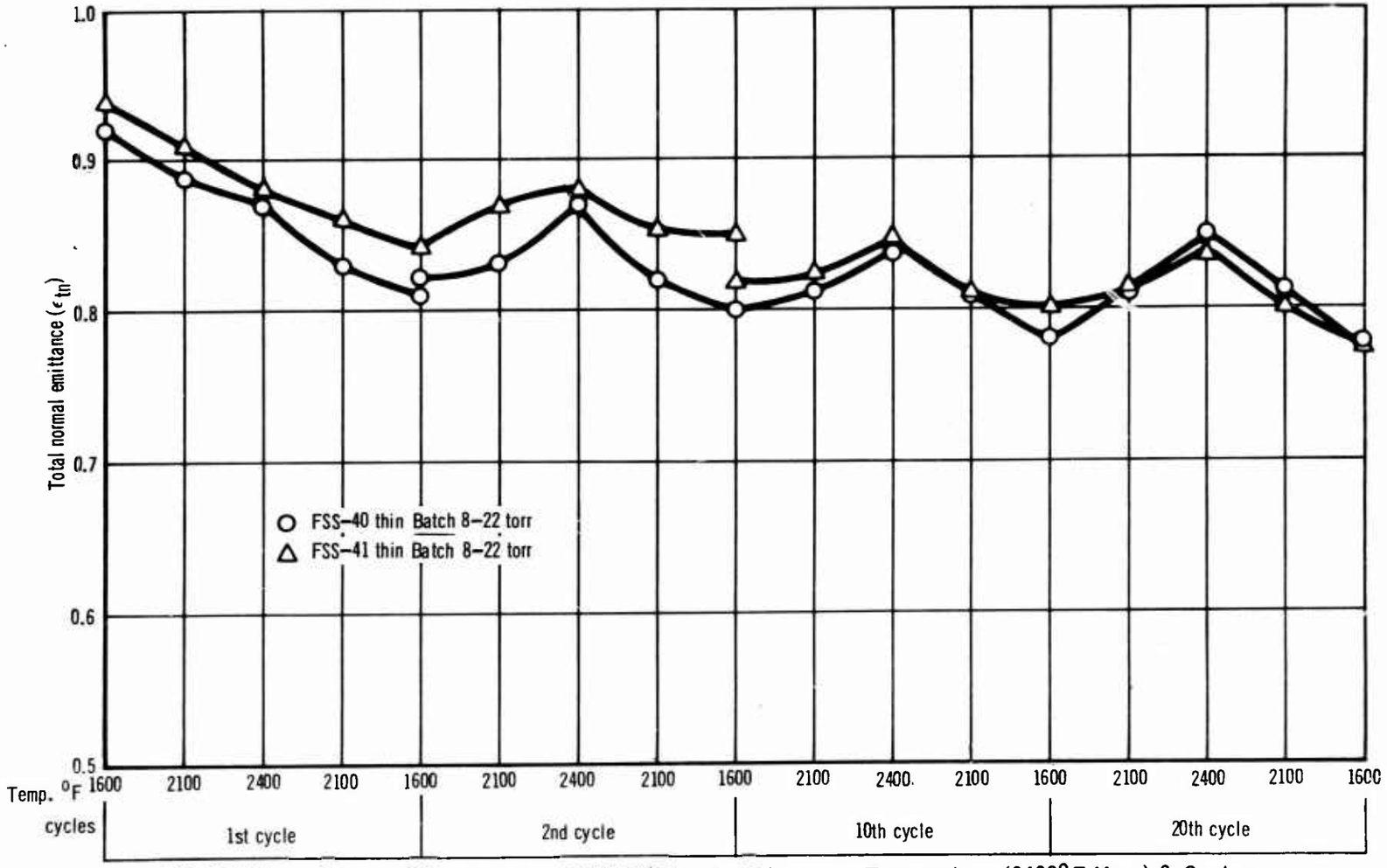

Figure 120 Emittance Of R-512E Coated Columbium (Thin Batch) Versus Temperature (2400°F Max.) & Cycles

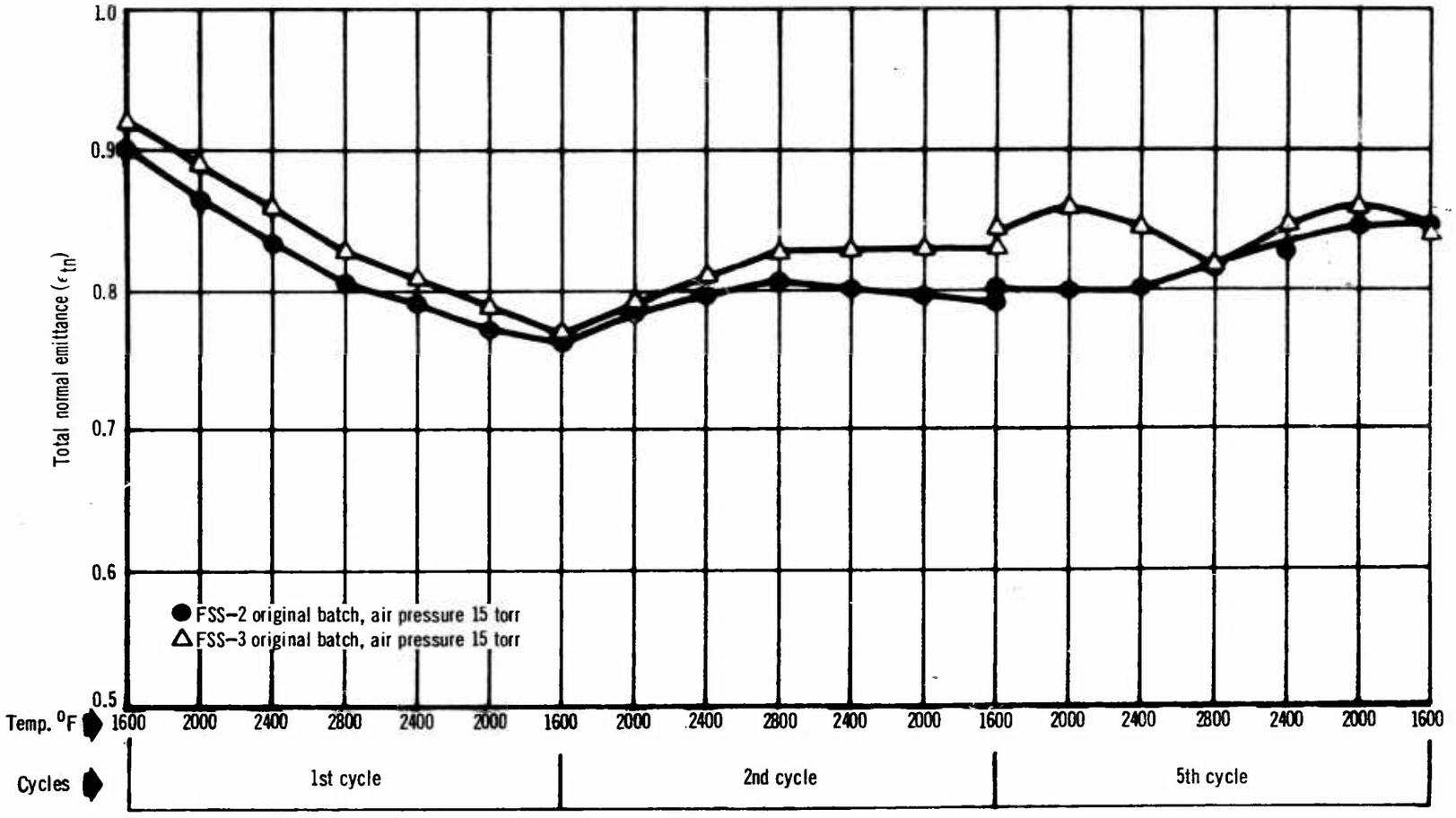

Figure 121 Emittance of R–512E Coated Columbium (Original Batch) Versus Temperature (2800°F Max.) & Cycles

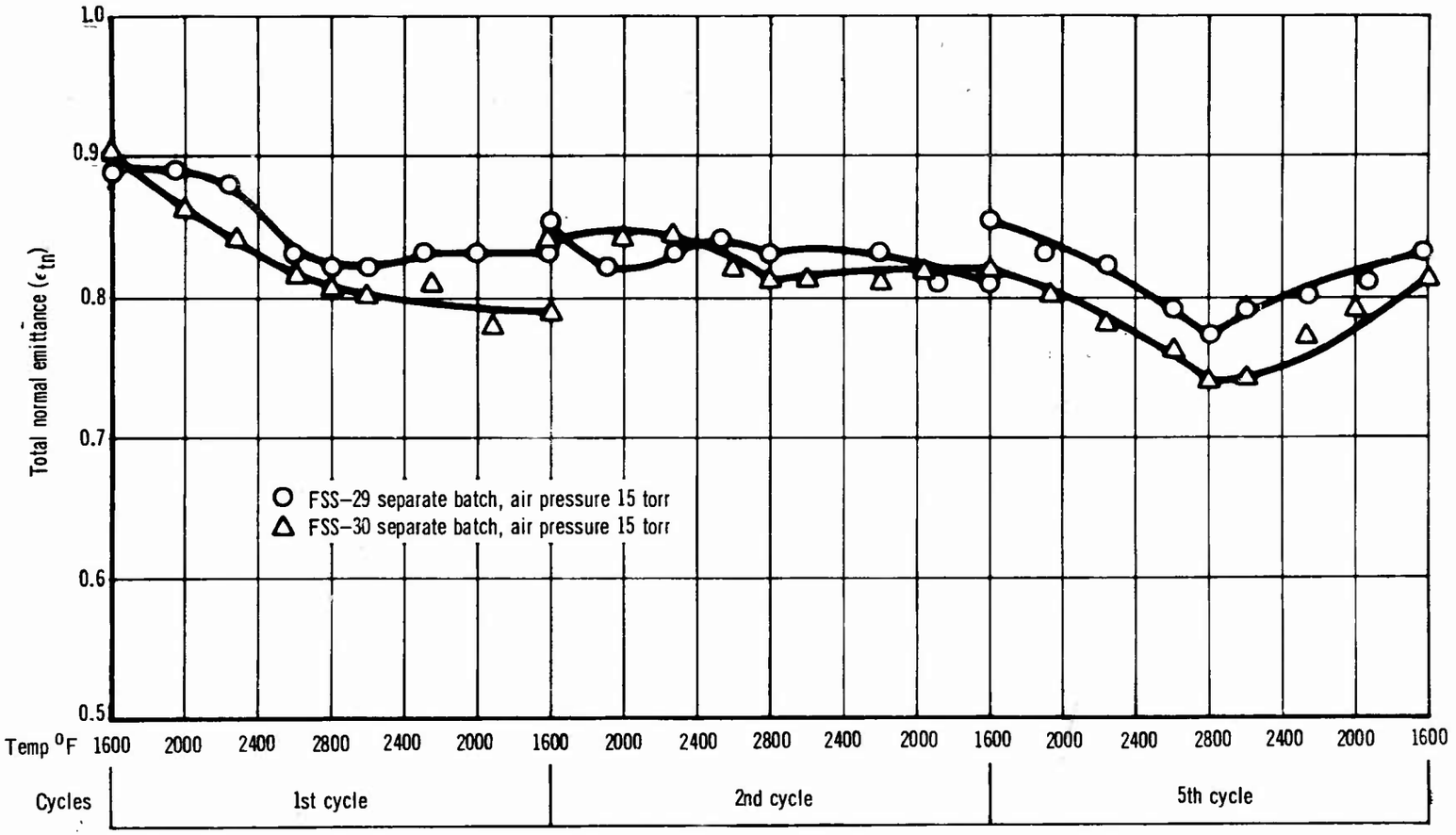

Figure 122 Emittance Of R–512E Coated Columbium (Separate Batch) Versus Temperature & Cycles

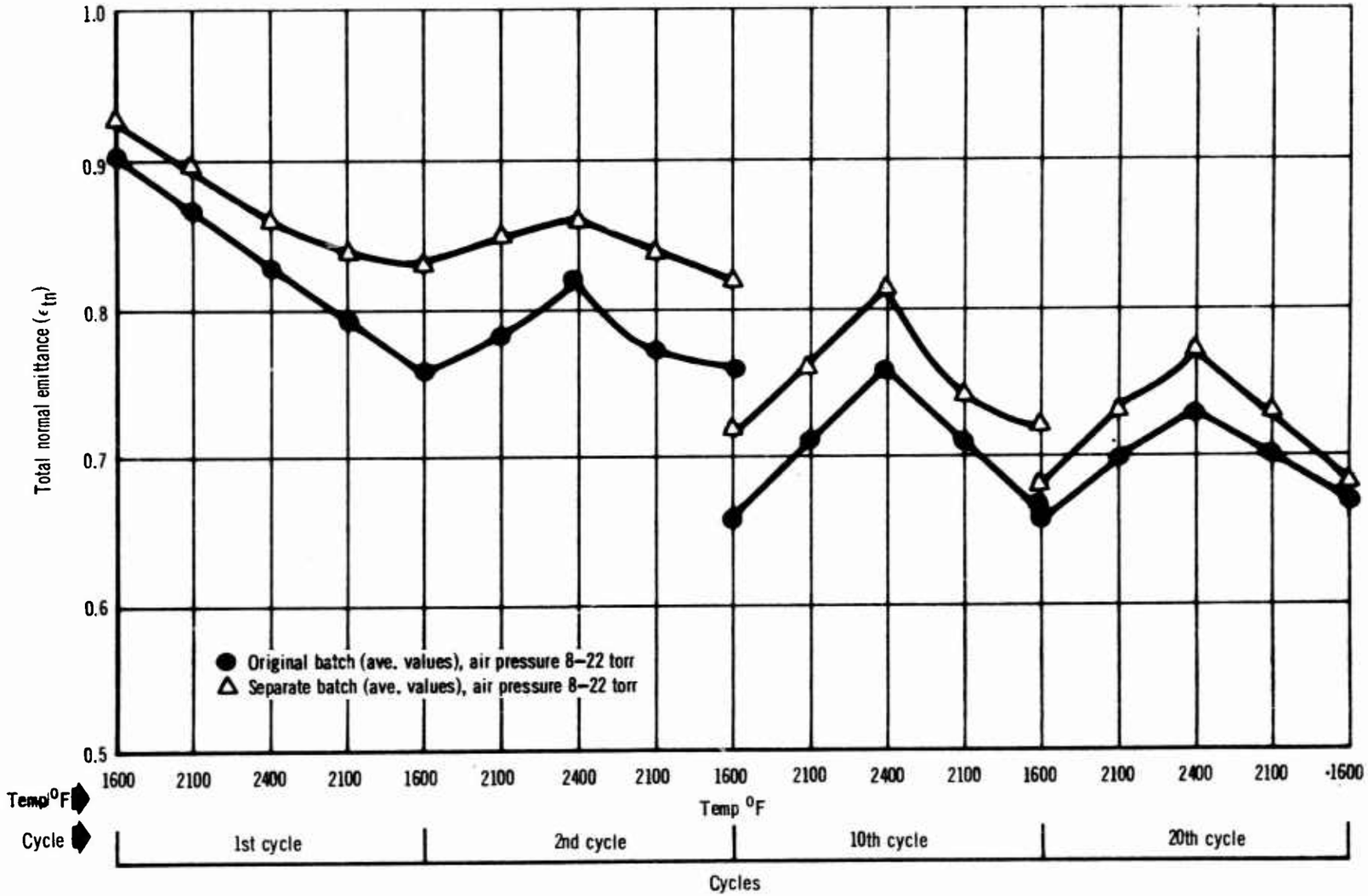

Figure 123 Emittance Of R–512E Coated Columbium (Original & Separate Batches) Versus Temperature (2400°F Max.) And Cycles

(g) Thickness Variations

The emittance of the R-512E coated columbium having a normal coating weight of 25 mg/cm^2 was compared with a coating weight of 12.5 mg/cm^2. Thermal cycling to 2400°F, following a reentry profile, showed that the average emittance value of the thin batch were considerably higher than the original batch in the temperature range of 1600° to 2400°F for up to 20 cycles, Figure 124. As much as a 0.125 emittance unit difference was measured between the two difference thicknesses at the same temperature. This increase in emittance for the thinner coating was apparently due to differences in intermetallic coating formed at elevated temperatures. The thinner coating by appearance had a darker surface coating and may not be as rich in chromium at the surface as the original batch of coating.

Increasing the maximum test temperature to 2600°F did not decrease the difference in emittance between the thin batch (ε = 0.84 after 15 cycles) and original batch (ε = 0.73 after 15 cycles), Figure 125.

The thin coating failed due to gross oxidation on the 18th cycle to 2600°F. The oxidation started around the leading edge of the specimen where the induction field may cause localized heating and premature coating failure. Further tests should be run in the Astro furnace to determine the effect of coating thickness on the coating life.

(h) Chemistry Variations

The R-512E coating (Si-20Cr-20Fe) was modified by changing the ratios of the three ingredients. The Modified R-512E (Si-30Cr-30Fe) coating evaluated through all phases of this program had a higher emittance at all temperatures (1600 to 3000°F) and at all pressures. The emittance results of the original R-512E and the modified R-512E after 20 cycles to 2400°F are compared in Figure 126.

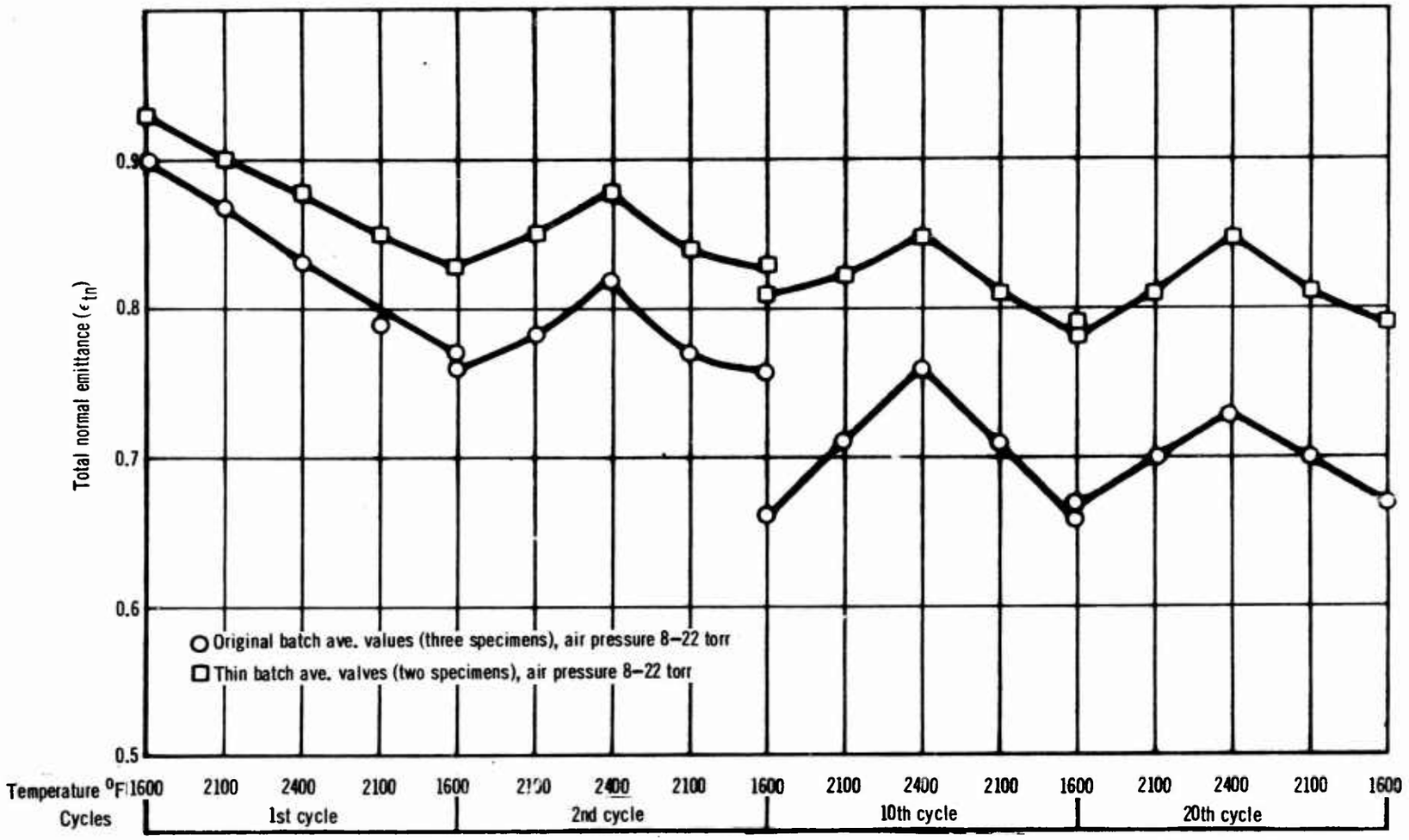

Figure 124 Emittance Of R–512E Coated Columbium (Original & Thin Batch) Versus Temperature (2400°F Max.) & Cycles

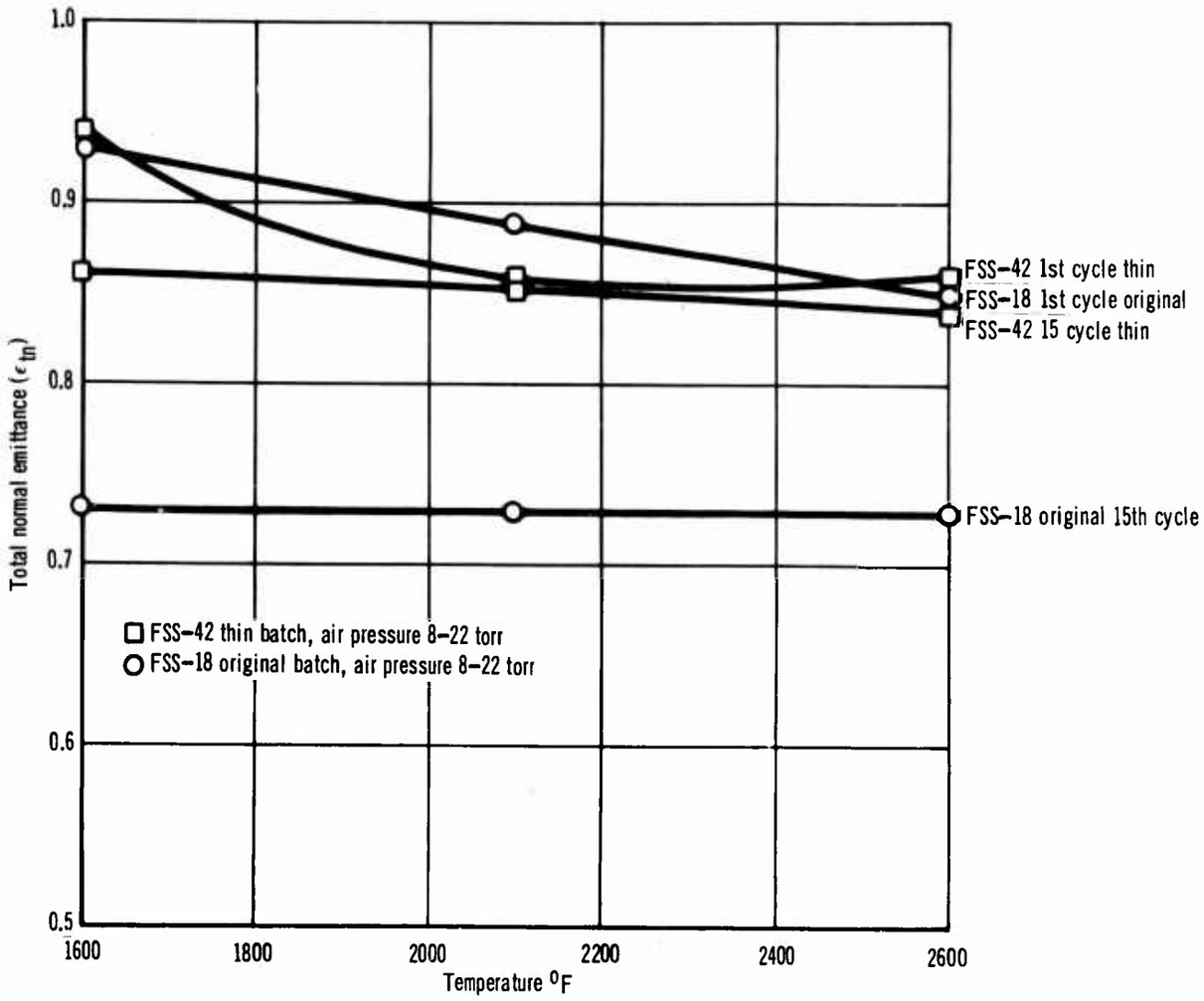

Figure 125 Emittance Of R-512E Coated Columbium (Original & Thin Batch) Versus Temperature (2600°F Max.)

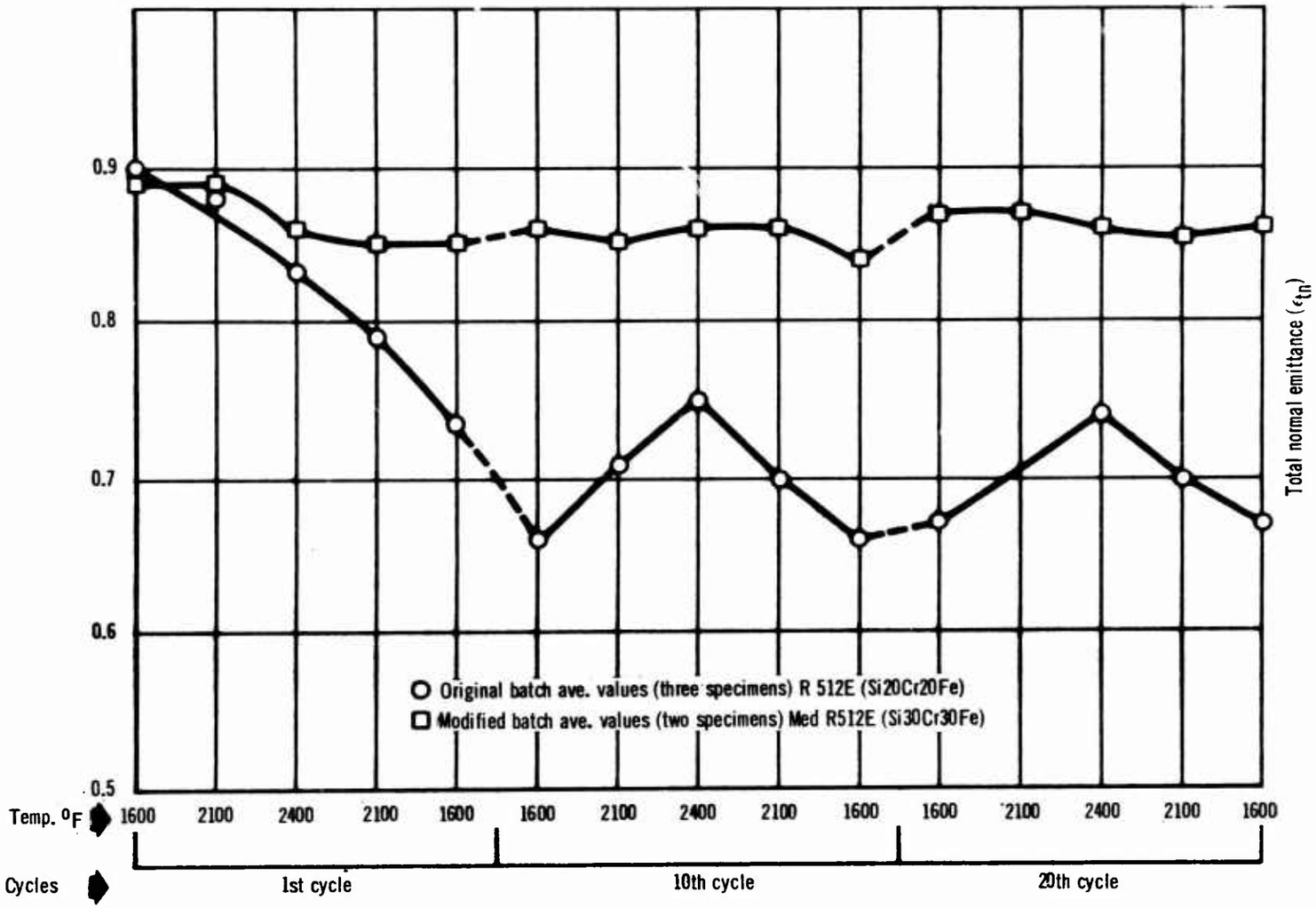

Figure 126 Total Normal Emittance Of R–512E Coated Columbium
VS
Temperature (2400°F Max.) And Cycles

Additional modifications of the R-512E coating were evaluated for 5 cycles to 2400°F, Table XIX. The emittance of all of these specimens, with the exception of the original R-512E, remained at approximately 0.87 after 5 cycles to 2400°F.

The original and the modified (Si-30Cr-30Fe) were coated early in the program and the specimens were laid on their side (cylinder side facing the specimen holder) during coating at Sylvania. The side facing the holder turned a darker color than the other areas, including the surface where the emittance was measured. The other specimens with different chemistries were coated at a later date and the specimens were coated with the face of the cylinder (area where emittance is measured) facing the holder. This area facing the holder remains a darker color during emittance measurements and that may be the reason for the close agreement in emittance after 5 cycle to 2400°F for all the different chemistries, Table XIX.

Table XIX

Emittance of Several Modified R512E Coated Columbium

Specimens	1st Cycle			5th Cycle		
	1600	2100	2400	1600	2100	2400
FSS-75 R-512 (Si-15 Cr-15 Fe)	.89	.92	.86	.81	.85	.89
FSS-73 R-512 (Si-17 Cr-20 Fe)	.85	.86	.83	.82	.85	.88
FSS-70 R-512E (Si-20 Cr-20 Fe)	.85	.86	.86	.82	.86	.87
FSS-14 R-512E Original	.89	.86	.80	.71	.74	.77
FSS-74 R-512 (Si-22 Cr-20 Fe)	.84	.86	.85	.84	.86	.88
FSS-71 R-512H (Si-25 Cr-25 Fe)	.91	.88	.87	.80	.81	.81
FSS-50 R-512 Mod (Si-30 Cr-30 Fe)	.88	.89	.86	.87	.87	.87

(i) Summary of Emittance Measurements

The Cb752 columbium emittance specimens coated with Sylvania's R-512E coating were classified into four (4) different batches: (original, 25 mg/cm^2, separate, thin (12.5 mg/cm^2), and modified (40% Si, 30% Fe, 30% Cr)).

The 2400°F emittance of the original batch of R-512E coating decreased from 0.85 to 0.75 after thermal cycling to a maximum temperature of 2400°F for twenty (20) simulated flight time-temperature-pressure profiles. Increasing the maximum temperature to 2600°F during profile testing also caused a decrease in the 2600°F emittance (from 0.85 to 0.70) after 20 cycles.

The separate batch had about the same emittance as the original batch at 2400°F after 20 cycles. The largest difference in the emittance between the original and the separate batch during cycling to 2400°F was 0.12 emittance units (at 1600°F). This difference in emittance occurred during the 1st and 10th cycles to 2400°F. The separate batch after 20 cycles to 2600°F had a higher emittance $\varepsilon = 0.85$ versus $\varepsilon = 0.70$ for the original batch. At 2600°F and after 20 reentry profile cycles some gross oxidation was observed, especially around the Al_2O_3 reference cavity. This may be due to a reaction between the Al_2O_3 reference cavity and the R-512E coating. Coating failure around the edges may be due to either a thinner coating or excessive surface heating of this edge when heated with the induction heater.

The thin batch (12.5 mg/cm^2) in all cases had a higher emittance (approximately 0.13) than the original batch at 2400°F and 2600°F.

A modified R-512E coating with a higher iron and chromium content (30% Fe - 30% Cr) maintained an emittance of 0.85 or higher when profile tested 20 times from 1600°F to 2400°F or 2600°F. The modified R-512E specimens had the normal grayish black color the same as observed during testing of the heat shield panels. The original and separate batches of R-512E coatings turned a medium green color, except where the specimen faced the setter during the coating operation, when tested under a simulated time-temperature-pressure profile to 2400°F at reduced pressures ranging between 8-22 torr. This color phenomenon occurred when testing in both the induction heated emissometer and in the Astro furnace. The area that faced the setter during the coating operation turned a darker grayish green color; this area covered about 1/3 of the cylinder surface but not the face of the specimen where emittance measurements were made. Emittance specimens tested at higher temperatures 2600° to 3000°F in the emissometer turned a grayish black color similar to the heat shield panels and the modified R-512 coating. Therefore, it was postulated that the original and separate batches may have had an excess amount of chromium, thereby producing a yellowish green color at 2400°F.

The R-512E coating maintained a high emittance ($\varepsilon = 0.85$) when the temperature was increased to 2800°F at a constant pressure of 1, 15, or 30 torr, altho the specimens had gross oxidation around the Al_2O_3 reference cavity and at the

leading edge. All specimens did not exhibit gross oxidation when tested to 2800°F; the few specimens which did not, exhibited black granular substance on the surface.

The emittance specimens were heated for only 1 cycle to 3000°F and the emittance of the original batch was approximately 0.87 for the three different constant pressures of 1, 15 and 30 torr (air pressure). The emittance at 2000°F (determined on the same specimens that had been cycled to 3000°F) was about the same ($\varepsilon = 0.87$) for the separate, thin, and modified batches at a constant air pressure of 15 torr.

A summary of the emittance data follows:

	T-T-P Cycles @ 2400°F		T-T-P Cycles @ 2600°F		Effect of Pressure @ 3000°F			Effect of Pressure @ 2000°F		
Coating	1st Cycle	20th Cycle	1st Cycle	20th Cycle	1 Torr	15 Torr	30 Torr	1 Torr	15 Torr	30 Torr
Original	.80	.75	.85	.70	.87	.87	.86	.93	.87	.88
Separate	.87	.77	.79	.85		.85			.86	
Thin	.88	.85	.86	___*		.85			.88	
Modified	.86	.86	.88	.89		.84			.88	

* Gross oxidation after the 18th cycle and the test was terminated.

SECTION V

CONCLUSIONS

Because of the fused slurry silicide coating is formed from an aggressive molten phase, it has great potential for reproducible coating of complex parts, including areas of limited accessibility. The R-512E coating has no significant de·-imental effects on the mechanical properties of the single annealed Cb-752 al y. Neither coating or coating processing had any adverse affect on weld strength. When designing columbium alloy structures for reuse capabilities, complete characterization of the properties of the specific lot of material from which the component will be fabricated is essential for optimum performance.

The temperature and primarily the pressure environment, which a coated columbium structure will encounter in flight, must be considered in order to obtain maximum efficiency. With respect to coating life alone, internal pressure environment is more severe than external pressure environment at 2600°F test temperature. However, superimposed stress tends to reverse this trend. Life of the R-512E coated columbium is significantly decreased by superimposed stress at high temperature. Levels of stress applied in this test program accelerated the time to produce coated columbium tensile specimen failure at 2600°F by at least 25% under internal pressure and 40% for external pressure conditions.

It is possible for coated columbium structures with bare faying surfaces to be used in multiple missions without loss of structural integrity if the internal air pressure is sufficiently low. However, positive means of coating faying surfaces should be employed when using thin gauge material in external pressure environments; the R-512E coating cannot reliably protect faying surfaces for appreciable times if the coating is applied after creation of the faying surface, i.e., after assembly.

The structural integrity of R-512E coated Cb-752 is very tolerant of local loss of coating in typical reentry pressure environments at temperatures up to 2400°F. The effect of local loss of coating on structural integrity should be determined under closely simulated conditions for the particular flight profile being considered. Tmperatures and especially pressures drastically effect the coating damage tolerance. Deliberately damaged coated panels maintained structural integrity through reuse up to 15 times at 2400°F even after accidental exposure to such extreme temperature as 2800°F. Large damage sites (3/8 inch diameter) in coatings resulted in extensive substrate contamination, but panels endured continued testing to 2400°F without loss of structural integrity for up to 50 cycles thereafter.

R-512E coated Cb-752 heat shield specimens have an extensive reuse capability of greater than 100 one hour reentry flights to peak temperatures of 2400°F. The effects of design on reuse are directly related to the pressure environment. Flight simulation profile testing to maximum temperature of 2600°F produced exceissive creep deflections within four cycles, but no coating failures occurred even after 12 profiles, using spot welded flat corrugation panels. Thus, coating reusability at 2600°F appears to be at least 10 flights.

The total normal emittance of the R-512E coated columbium (Cb-752) gradually decreased with reentry simulation cycling to 2400°F through the first 10 cycles and then remained relatively stable through 20 cycles. Increasing the peak temperature to 2600°F during reentry profile testing caused a gradual decrease in emittance for the original batch, but the separate batch had a gradual increase in emittance after the first cycle to 2600°F. Batch to batch variation in emittance was evident.

Pressure in the range of 1 to 30 torr did not affect the emittance when tested at a peak temperature of 3000°F. The thin R-512E coating (12.5 mg/cm^2) had a higher emittance at 2400 and 2600°F than the original batch (25 mg/cm^2).

A modified version of R-512E (Si-30% Fe-30% Cr) had a higher emittance, greater than 0.35, for all temperatures (1600 to 3000°F) and for all test conditions.

SECTION VI

RECOMMENDATIONS FOR FUTURE WORK

1. Explore other alloy/coating systems for reuse capability and damage tolerance.

2. Testing of larger heat shield panels for better representation.

3. Add acoustic and vibration testing to the sequential simulation of critical flight conditions.

4. Thoroughly explore the benefits of repair coating damaged areas after various exposures to oxidizing conditions.

5. Pursue development of NDT methods for detecting contaminated base metal beneath intermetallic coating for post flight examination.

6. Measure the total normal emittance of the R-512E coating under simulated time-temperature-pressure profile conditions for up to 100 cycles and for peak temperatures of 2400°F.

7. Investigate the effects of different R-512E coating compositions on the oxidation protection afforded columbium alloys and on emittance.

8. Determine the effect of air flow rate on the emittance of the coated columbium.

9. Study the effect of processing variables on the emittance properties of the R-512E coated columbium.

Appendix I
MECHANICAL PROPERTY DATA

Presented in this appendix are the data of the mechanical property tests conducted on bare and R-512E coated single annealed Cb-752 columbium alloy.

Table XX

Room Temperature Bend Test Data

Specimen	Surface condition of material	Mandrel radius (in.)	Die throat ⚠1 opening (in.)	Remarks
14 16 17 15	Bare	0.031	0.099	Passed
1 2 3 4	Coated	0.031	0.117	Passed (Coating cracked)

⚠1 Die throat opening=2R + 2.5t
R = Radius of Mandrel
t = Thickness of material

Table XXI
Tensile Test Data

Specimen	Surface Condition of Material	Test Temperature ^{o}F	Fty (KSI)	Ftu (KSI)	Elongation (%)
68	Bare	R.T.	63,100	80,200	29
69			62,500	79,300	30
70			63,400	80,500	30
Average			63,000	80,000	30
71	Bare	1300	35,700	51,200	19
73			37,000	52,500	18
74			36,700	52,100	16
Average			36,500	51,900	18
75	Bare	1800	31,100	41,800	36
76			28,000	40,400	34
77			30,000	42,900	35
Average			29,700	41,700	34
78	Bare	2400	20,100	20,600	94
1			18,600	19,300	93
2			19,600	19,700	98
Average			19,450	19,900	95
3	Bare	2600	15,300	15,600	BOG [1]
5			14,300	14,500	103
6			14,700	14,900	98
Average			14,760	15,000	100
7	Coated	R.T.	60,340	83,050	19
8			60,560	83,100	20
9			59,780	82,090	19
Average			60,230	82,750	19
10	Coated	1300	34,120	59,120	9
11			39,720	60,850	10
12			39,430	61,140	11
Average			37,760	60,370	10
13	Coated	1800	39,050	50,560	15
14			36,740	49,270	11
15			33,660	49,440	13
Average			36,480	49,760	13
18	Coated	2400	23,460	25,280	62
19			23,540	26,110	51
20			24,240	24,650	61
Average			23,750	25,350	58
21	Coated	2600	10,970	11,940	107
22			11,600	11,770	108
23			12,430	12,640	98
Average			11,670	12,120	104

[1] BOG – Broke out of gage.

Table XXII
Notch Tensile Test Data

Specimen	Surface Condition of Material	Test Temperature (^{0}F)	Notch Radius (In.)		Notch Tensile Strength (PSI)	Average NTS (PSI)
			R1 [1]	R2 [2]		
6	Bare	R.T.	0.0005	0.0010	76,580	77,600
9			0.0005	0.0007	78,110	
19			0.0005	0.0006	78,130	
7	Bare	1300	0.0010	0.0010	52,620	52,850
8			0.0008	0.0005	53,510	
24			0.0006	0.0007	52,430	
18	Bare	1800	0.0007	0.0008	45,370	44,080
22			0.0007	0.0008	44,150	
23			0.0007	0.0008	42,730	
15	Coated	R.T.	0.0006	0.0008	78,130	79,990
16			0.0007	0.0007	84,030	
17			0.0005	0.0009	77,800	
14	Coated	1300	0.0010	0.0010	52,580	53,950
13			0.0005	0.0007	54,610	
12			0.0007	0.0007	54,660	
11	Coated	1800	0.0007	0.0008	44,380	44,670
10			0.0007	0.0006	44,530	
4			0.0007	0.0006	45,110	

[1] Notch radii determined prior to coating

[2] See Figure 19 on page 27 for notch radii after coating.

Table XXIII
Welded Lap Shear Data

Specimen	Surface Condition of Material	Type of Weld	Test Temperature (^{o}F)	Ultimate Load (Lb)	Average Ultimate Load (Lb)
11 12	Bare	E.B.	R.T.	1205 1270	1237
11 12		Spot		683 737	710
13 14	Bare	E.B.	1300	716 (1) 615 (1)	660
13 14		Spot		342 513	427
16	Bare	E.B.	1800	592	592 (2)
16		Spot		401	401
15 17	Bare	E.B.	2400	289 287	288
15 18		Spot		157 165	161
18 19	Bare	E.B.	2600	201 219	210
17 19		Spot		133 142	137
1 2	Coated	E.B.	R.T.	1315 1315	1315
1 2		Spot		705 679	692
3 4	Coated	E.B.	1300	674 (1) 768 (1)	721
3 4		Spot		518 523	521
5	Coated	E.B.	1800	752	752 (2)
5		Spot		454	454
6 7	Coated	E.B.	2400	404 417	411
6 7		Spot		320 333	327
8 9	Coated	E.B.	2600	246 220	233
8 9		Spot		205 221	213

(1) Failed in grip area

(2) Only one specimen of each type was tested at 1800^{o}F

Table XXIV
Creep Summary for Uncoated Cb–752

Specimen No.	Temperature (°F)	Stress (ksi)	2% Creep (Hr)	Test Duration	Final Elongation (%)
48	2400	3.0	11.0	30.0	6.5
49	2400	4.0	7.6	19.4	4.5
50	2400	5.0	5.4	14.9 (a)	5.1
51	2400	6.0	3.1	13.2	9.9
52	2400	7.0	2.4	15.2	2.3
53	2400	8.0	1.7	14.7	16.2
54	2400	5.5	5.4	15.8	7.0
55	2400	2.0	24.0	81.3	4.8
56	2400	9.0	1.3	39.6	42.3
57	2600	1.5	11.2	140.7	10.4
59	2600	2.5	5.6	86.5	10.0
60	2600	1.0	8.8	91.8	9.9
63	2600	2.0	4.0	40.5	13.3
64	2600	3.0	2.2	15.4	11.9
65	2600	4.0	0.9	18.4	29.1
66	2600	5.0	0.9	15.7	17.5
67	2600	6.0	0.6	6.1 (a)	70.0
62	2600	3.5	3.0	15.5	10.0

(a) Specimen failed. All others were removals.

Table XXV
Creep Data for Bare Specimens at 2600°F

Time (hr)	Specimen Number & Percent Creep								
	57	59	60	63	64	65	66	67	62
0.1	0.05	0.15	0.02	0.02	0.08	0.15	0.22	0.30	0.06
0.2	0.15	0.18	0.03	0.12	0.15	0.32	0.44	0.56	0.16
0.3	0.17	0.26	0.06	0.18	0.25	0.62	0.63	0.87	0.24
0.4	0.17	0.31	0.08	0.22	0.32	0.80	0.85	1.27	0.31
0.5	0.20	0.35	0.14	0.26	0.43	1.08	1.11	1.56	0.42
0.6	0.26	0.35	0.15	0.29	0.51	–	1.35	1.93	0.45
0.7	0.29	0.42	0.17	0.32	0.62	–	1.42	2.21	0.52
0.8	0.31	0.45	0.20	0.38	0.71	–	1.81	2.64	0.58
0.9	0.35	0.48	0.22	0.45	0.80	–	2.06	3.00	0.66
1.0	0.42	0.57	0.28	0.51	0.91	2.15	2.29	3.44	0.74
1.5	0.57	0.74	0.42	0.77	–	–	3.56	5.63	1.06
2.0	0.62	0.92	0.54	1.03	1.84	3.85	4.97	–	1.35
2.5	0.74	1.08	0.66	1.28	–	–	6.40	–	1.69
3.0	0.82	1.23	0.80	1.52	2.72	5.46	–	–	2.00
3.5	0.91	1.37	0.92	1.75	–	–	–	–	2.32
4.0	0.97	1.58	1.00	2.00	3.49	6.85	–	–	2.58
4.5	1.06	1.69	1.08	2.28	–	–	–	–	2.92
5.0	1.12	1.86	1.23	2.49	4.37	8.28	–	–	3.18
6.0	1.26	2.14	1.46	2.92	5.07	9.26	–	–	3.80
7.0	1.42	2.40	1.69	3.24	5.85	11.20	–	–	4.42
8.0	1.55	2.62	1.85	3.66	6.63	12.90	–	–	5.04

Table XXVI
Creep Data for Bare Specimens at 2400°F

Time (hr)	Specimen Number & Percent Creep								
	48	49	50	51	52	53	54	55	56
0.1	0.08	0.01	0.09	0.03	0.08	0.22	0.01	0.02	0.12
0.2	0.12	0.07	0.13	0.12	0.15	0.31	0.04	0.02	0.25
0.3	0.18	0.11	0.14	0.16	0.23	0.46	0.07	0.03	0.38
0.4	0.22	0.13	0.17	0.22	0.31	0.55	0.09	0.04	0.53
0.5	0.25	0.15	0.21	0.29	0.38	0.63	0.15	0.06	0.62
0.6	0.28	0.18	0.25	0.36	0.46	0.69	0.17	0.08	0.85
0.7	0.31	0.24	0.29	0.43	0.53	0.77	0.22	0.08	0.93
0.8	0.32	0.25	0.31	0.48	0.62	0.92	0.24	0.11	1.08
0.9	0.35	0.29	0.35	0.55	0.69	0.98	0.29	0.12	1.28
1.0	0.37	0.32	0.40	0.62	0.77	1.12	0.32	0.14	1.42
1.5	0.46	0.45	0.62	0.95	1.20	1.80	0.40	0.18	2.38
2.0	0.49	0.56	0.82	1.27	1.73	2.42	0.68	0.23	3.46
2.5	0.58	0.71	0.93	1.58	2.28	3.16	0.86	0.29	5.23
3.0	0.62	0.84	1.10	1.92	2.82	3.97	1.04	0.37	6.23
3.5	0.68	0.98	1.27	2.28	3.42	4.76	1.26	0.39	–
4.0	0.74	1.09	1.54	2.63	4.04	5.70	1.42	0.45	–
4.5	0.82	1.30	1.68	3.02	4.69	6.70	1.64	0.53	–
5.0	0.92	1.44	1.85	3.42	5.35	7.78	1.81	0.60	–
6.0	1.12	1.68	2.08	4.17	6.78	10.01	–	0.69	–
7.0	1.28	1.88	2.48	4.93	–	12.29	–	0.77	–
8.0	1.49	2.12	2.81	5.68	–	14.81	–	0.85	–

Table XXVII
Creep Summary for Silicide Coated Cb–752

Specimen No.	Temperature (°F)	Stress (ksi)	2% Creep (Hr)	Test Duration	Final Elongation (%)
24	2400	3.0	16.0	41.2	4.3
25	2400	4.0	9.8	24.3	4.3
26	2400	5.0	6.3	20.8	6.1
27	2400	3.5	11.5	38.6	5.1
28	2400	8.0	2.4	4.8	4.5
29	2400	9.0	2.2	15.7	16.7
30	2400	6.0	4.2	17.3	7.6
31	2400	7.0	3.1	16.2	11.3
32	2400	2.0	28.7	68.7	3.9
34	2600	3.0	2.4	39.4	13.8
35	2600	2.0	4.4	122.2	11.0
37	2600	1.0	9.0	167.1	7.0
38	2600	4.0	1.7	14.6	13.4
39	2600	5.0	1.4	18.9	23.8
40	2600	6.0	0.3	2.5 (a)	43.8
41	2600	1.5	7.3	41.8	4.1
42	2600	2.0	4.5	39.7	8.9
44	2600	2.5	3.5	18.5	6.3

(a) Specimen failed. All others were removals.

Table XXVIII
Creep Data for Coated Specimens at 2600°F

Time (hr)	Specimen Number & Percent Creep								
	34	35	37	38	39	40	41	42	44
0.1	0.03	0.00	0.03	0.20	0.20	0.78	0.03	0.03	0.03
0.2	0.15	0.06	0.06	0.35	0.35	1.54	0.08	0.14	0.06
0.3	0.28	0.15	0.14	0.51	0.48	2.34	0.12	0.15	0.17
0.4	0.35	0.18	0.15	0.60	0.66	3.24	0.15	0.20	0.25
0.5	0.43	0.22	0.17	0.69	0.77	4.05	0.20	0.18	0.29
0.6	0.51	0.28	0.22	0.82	0.89	4.94	0.22	0.25	0.35
0.7	0.62	0.29	0.23	0.85	1.02	5.87	0.28	0.34	0.45
0.8	0.71	0.35	0.28	1.06	1.11	6.78	0.32	0.35	0.51
0.9	0.80	0.38	0.31	1.08	1.23	7.87	0.35	0.40	0.55
1.0	0.86	0.46	0.32	1.15	1.39	8.65	0.37	0.45	0.58
1.5	1.29	0.71	0.46	1.75	2.12	13.3	0.54	0.74	0.89
2.0	1.69	0.95	0.62	2.37	2.79	–	0.66	0.95	1.20
2.5	2.08	1.20	0.72	2.92	3.43	–	0.78	1.10	1.46
3.0	2.43	1.42	0.80	3.54	3.96	–	0.95	1.34	1.72
3.5	2.76	1.65	1.03	4.15	4.59	–	1.09	1.55	1.95
4.0	3.08	1.89	1.14	4.79	5.26	–	1.23	1.77	2.24
4.5	3.37	2.09	1.25	5.35	5.96	–	1.35	2.00	2.48
5.0	3.70	2.31	1.35	5.92	6.60	–	1.46	2.17	2.66
6.0	4.28	–	1.51	6.85	8.06	–	1.69	2.50	3.02
7.0	4.77	–	1.70	7.46	9.60	–	1.92	2.72	3.40
8.0	5.19	–	1.85	8.25	10.80	–	2.10	3.08	3.74

Table XXIX
Creep Data for Coated Specimens at 2400°F

Time (hr)	Specimen Number & Percent Creep								
	24	25	26	27	28	29	30	31	32
0.1	0.02	0.04	0.00	0.00	0.14	0.14	0.08	0.07	0.02
0.2	0.04	0.08	0.00	0.01	0.22	0.19	0.08	0.08	0.02
0.3	0.06	0.09	0.08	0.02	0.32	0.27	0.15	0.15	0.03
0.4	0.08	0.12	0.08	0.03	0.39	0.35	0.16	0.23	0.04
0.5	0.10	0.14	0.16	0.05	0.46	0.42	0.22	0.30	0.07
0.6	0.12	0.15	0.17	0.06	0.54	0.51	0.26	0.35	0.08
0.7	0.13	0.18	0.20	0.07	0.62	0.62	0.31	0.42	0.09
0.8	0.14	0.22	0.28	0.09	0.71	0.73	0.38	0.47	0.10
0.9	0.15	0.24	0.32	0.11	0.84	0.85	0.45	0.53	0.11
1.0	0.15	0.25	0.39	0.13	0.92	0.90	0.47	0.59	0.12
1.5	0.19	0.34	0.47	0.22	1.27	1.32	0.70	0.92	0.18
2.0	0.28	0.40	0.55	0.35	1.73	1.76	0.95	1.24	0.23
2.5	0.36	0.46	0.76	0.46	2.10	2.24	1.19	1.60	0.29
3.0	0.45	0.50	1.00	0.59	2.53	2.77	1.39	1.96	0.34
3.5	0.53	0.65	1.04	0.74	2.99	3.23	1.68	2.31	0.38
4.0	0.60	0.75	1.15	0.90	3.42	4.15	1.85	2.66	0.43
4.5	0.68	0.87	1.39	1.06	3.88	4.31	2.14	3.08	0.48
5.0	0.76	1.00	1.61	1.20	–	4.84	2.58	3.42	0.54
6.0	0.84	1.28	1.86	1.46	–	5.92	3.06	4.20	0.62
7.0	0.96	1.46	2.26	1.62	–	7.08	3.56	4.92	0.68
8.0	1.09	1.64	2.59	1.73	–	–	3.97	5.69	0.76

Appendix II

PANEL DEFLECTIONS VERSUS FLIGHT

Presented in this appendix are the total deflection versus number of cycles for R-512E coated Cb-752 heat shield panels of various configurations.

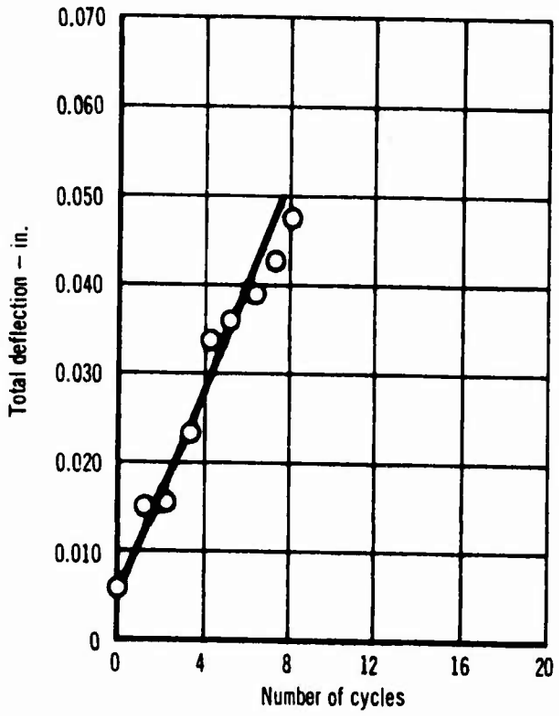

Figure 127 Spot Welded Flat Corrugation No. 2
Internal Pressure High Stress

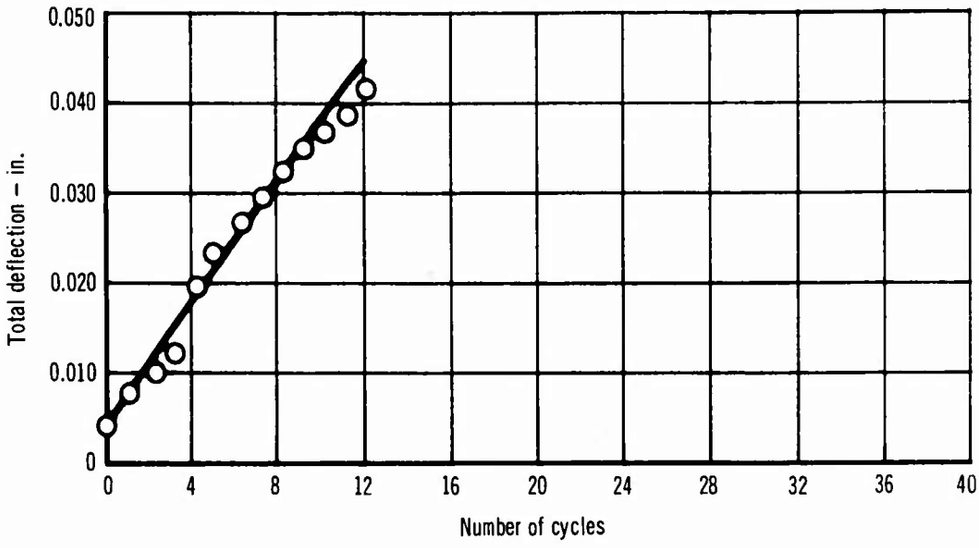

Figure 128 Spot Welded Flat Corrugation No. 7
Internal Pressure High Stress

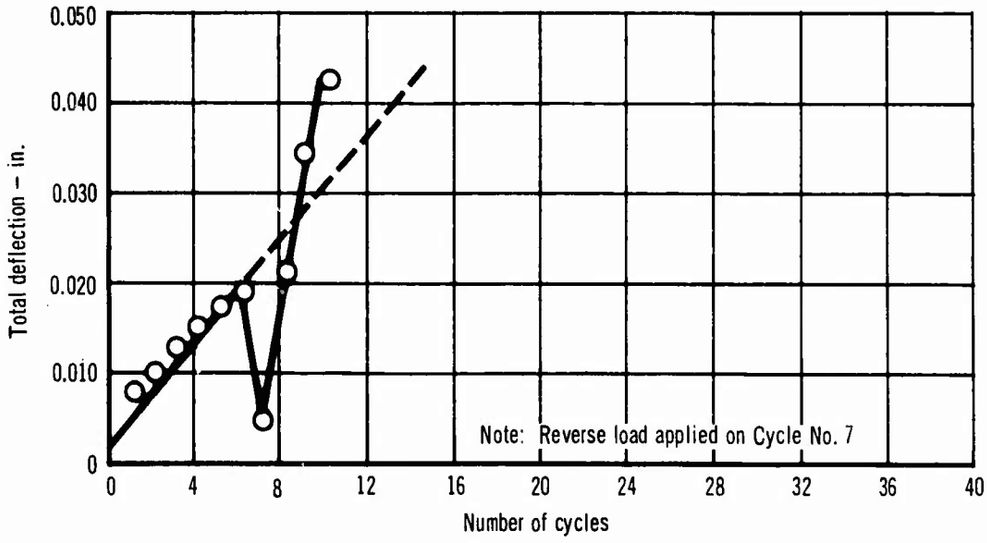

Figure 129 Spot Welded Flat Corrugation No. 9
External Pressure High Stress

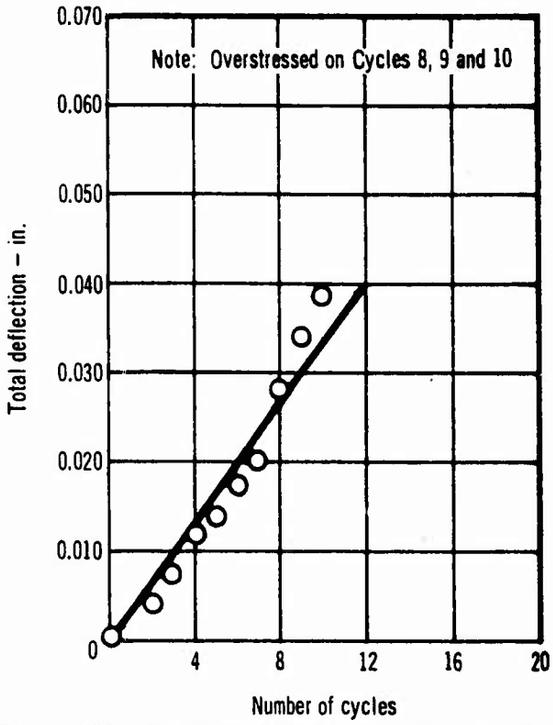

Figure 130 EB Welded Flat Corrugation No. 3
Internal Pressure High Stress

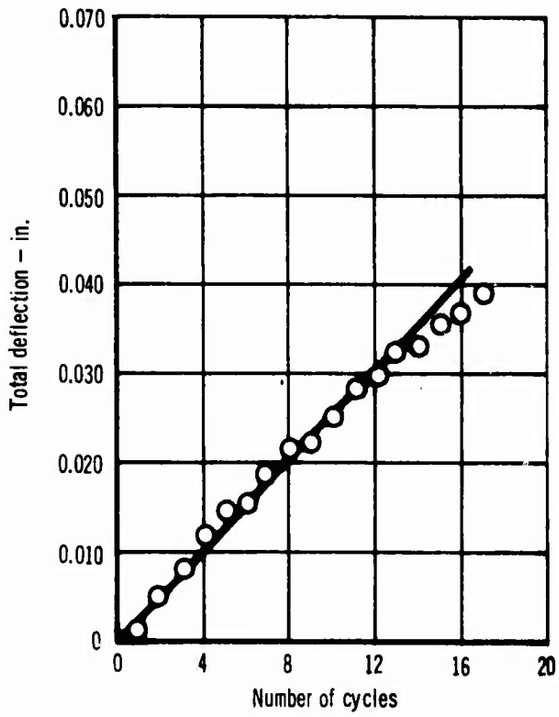

Figure 131 EB Welded Flat Corrugation No. 5
Internal Pressure High Stress

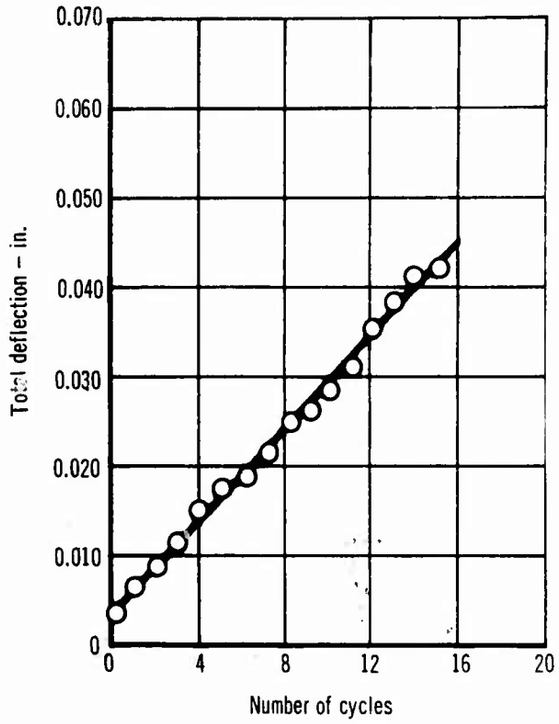

Figure 132 EB Welded Flat Corrugation No. 6
External Pressure High Stress

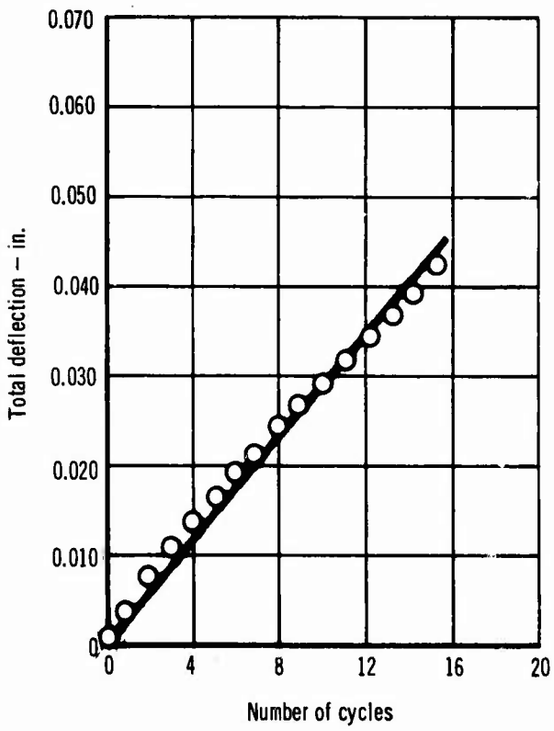

Figure 133 EB Welded Flat Corrugation No. 10
Internal Pressure High Stress

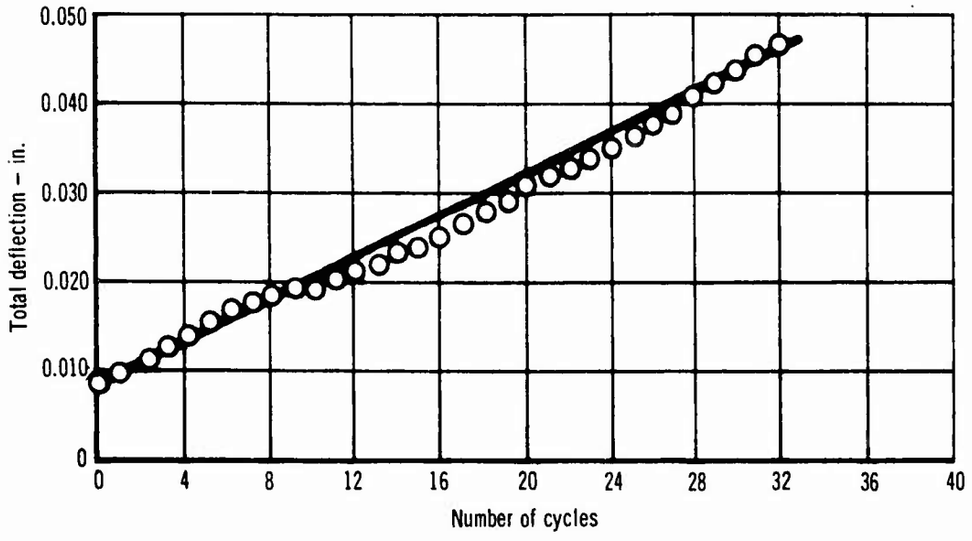

Figure 134 Vee Corrugation No. 1
Internal Pressure High Stress

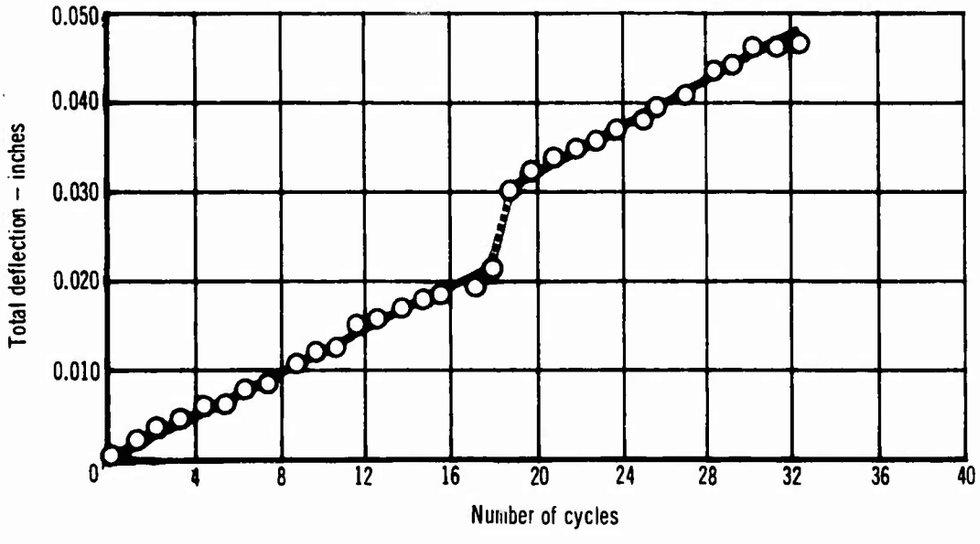

Note: Overload on cycle no. 18

Figure 135 Vee Corrugation No. 2 Internal Pressure High Stress

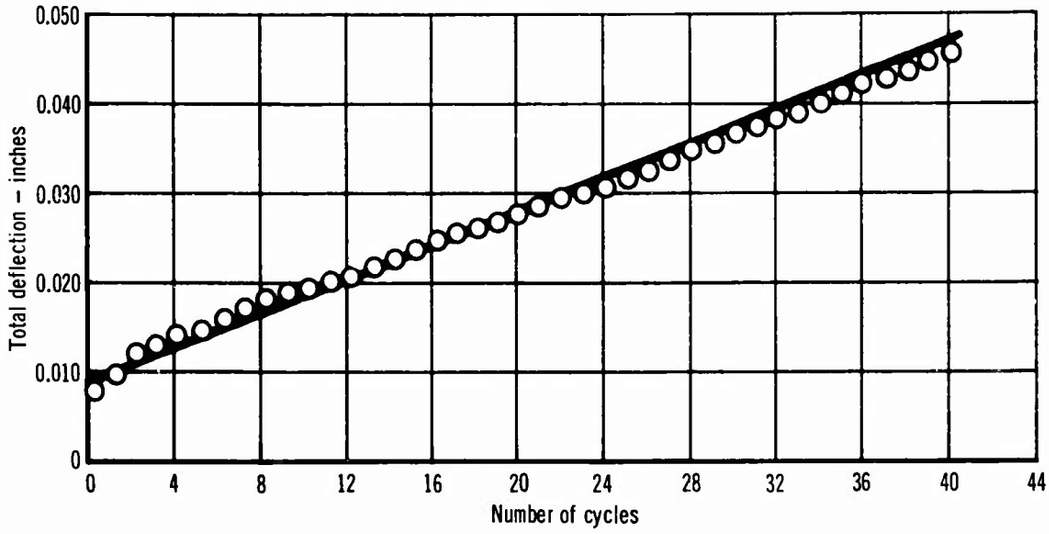

Figure 136 Vee Corrugation No. 3 Internal Pressure Low Stress

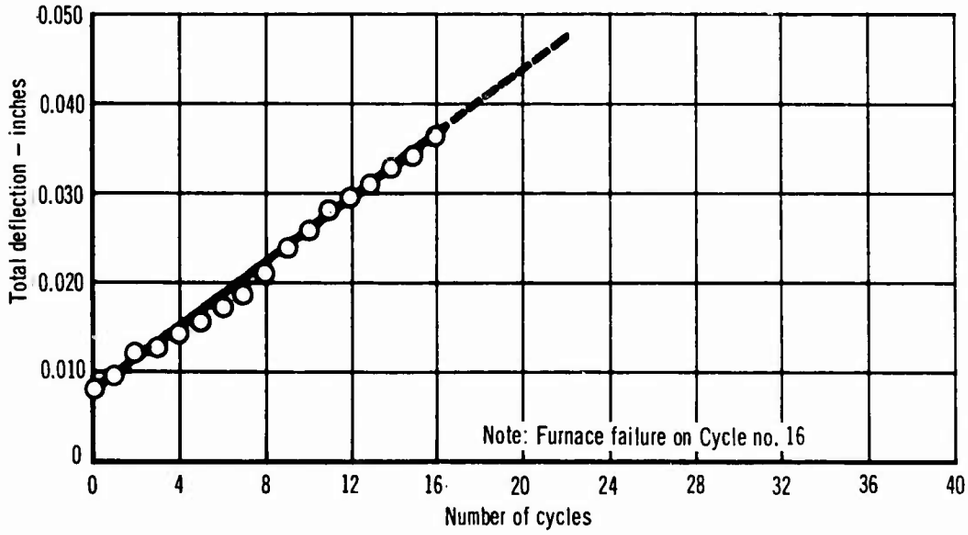

Figure 137 Vee Corrugation No. 5 Internal Pressure High Stress

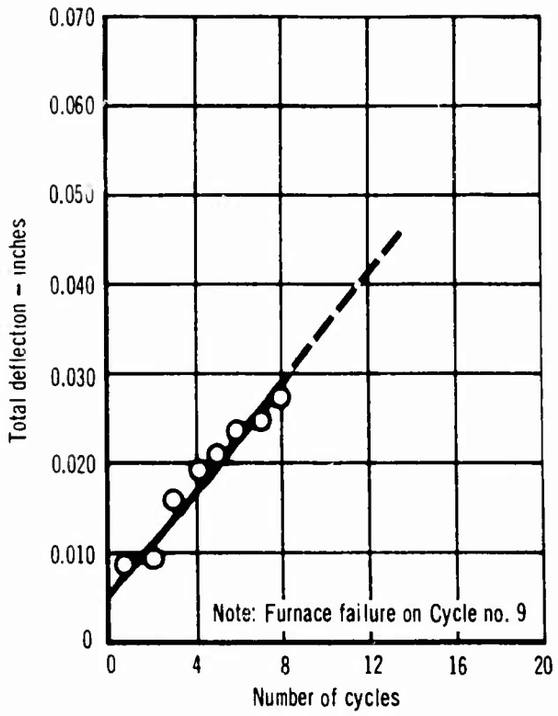

Figure 138 Vee Corrugation No. 7
External Pressure High Stress

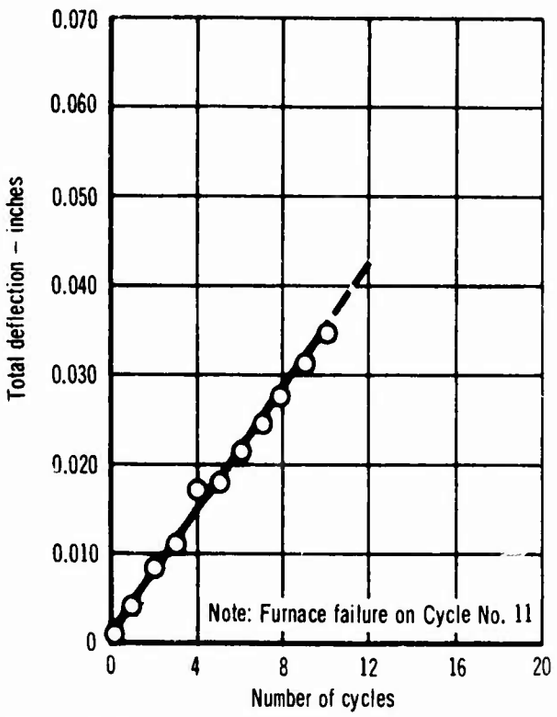

Figure 139 Vee Corrugation No. 9
External Pressure High Stress

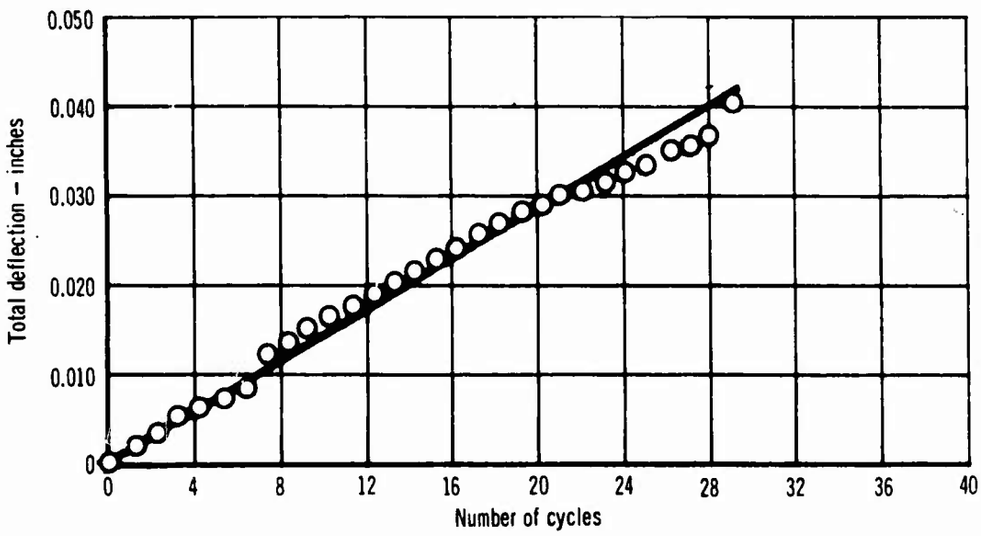

Figure 140 Vee Corrugation No. 13 External Pressure High Stress

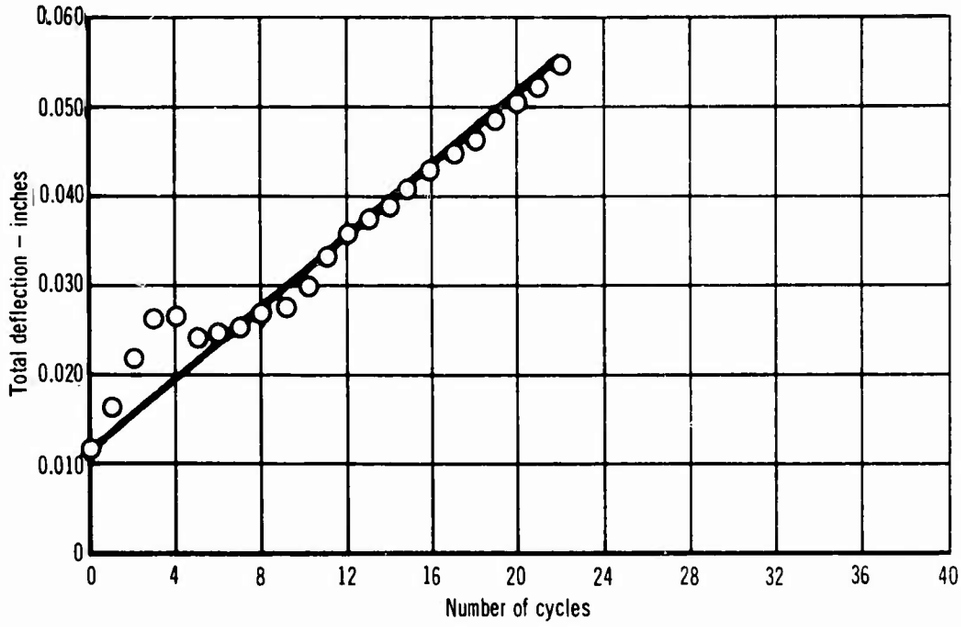

Figure 141 Zee Stringer No. 1 Internal Pressure High Stress

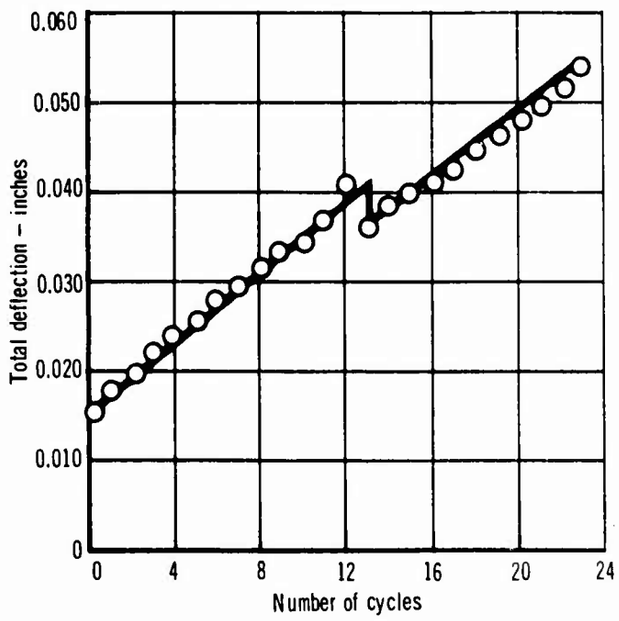

Figure 142 Zee Stringer No. 2 Internal Pressure High Stress

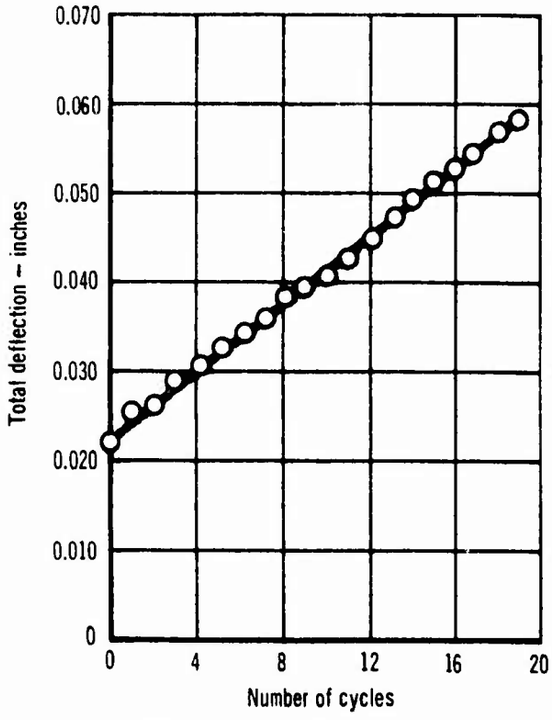

Figure 143 Zee Stringer No. 4 Internal Pressure High Stress

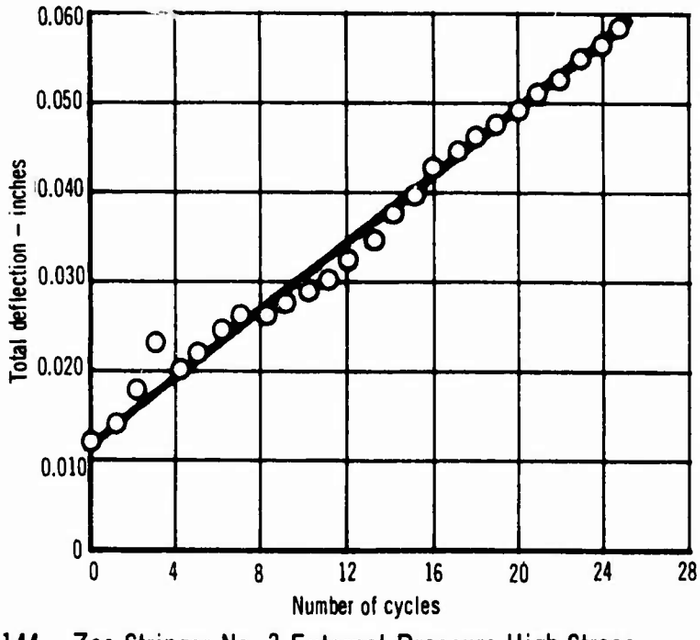

Figure 144 Zee Stringer No. 3 External Pressure High Stress

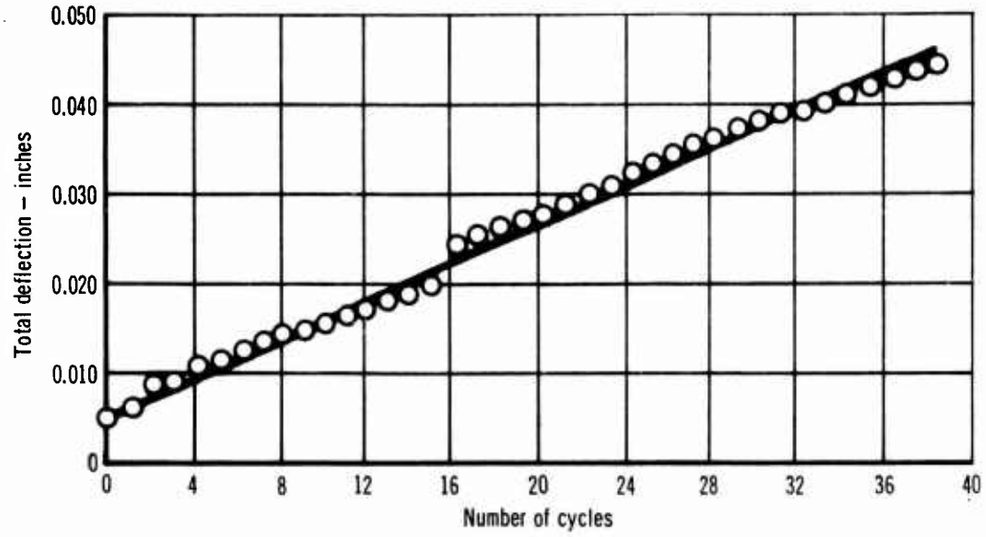

Figure 145 Rib Stiffened No. 1 Internal Pressure High Stress

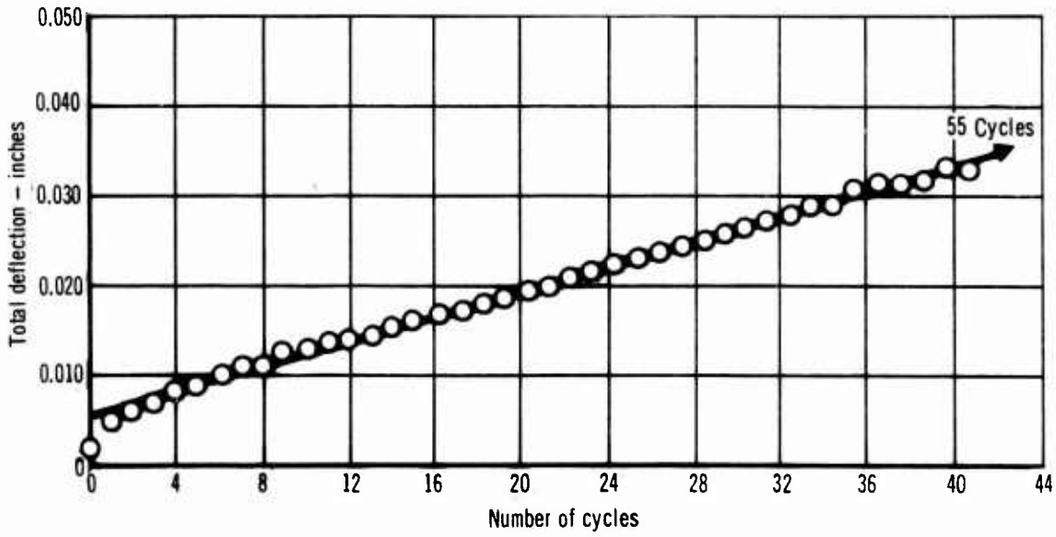

Figure 146 Rib Stiffened No. 2 Internal Pressure High Stress

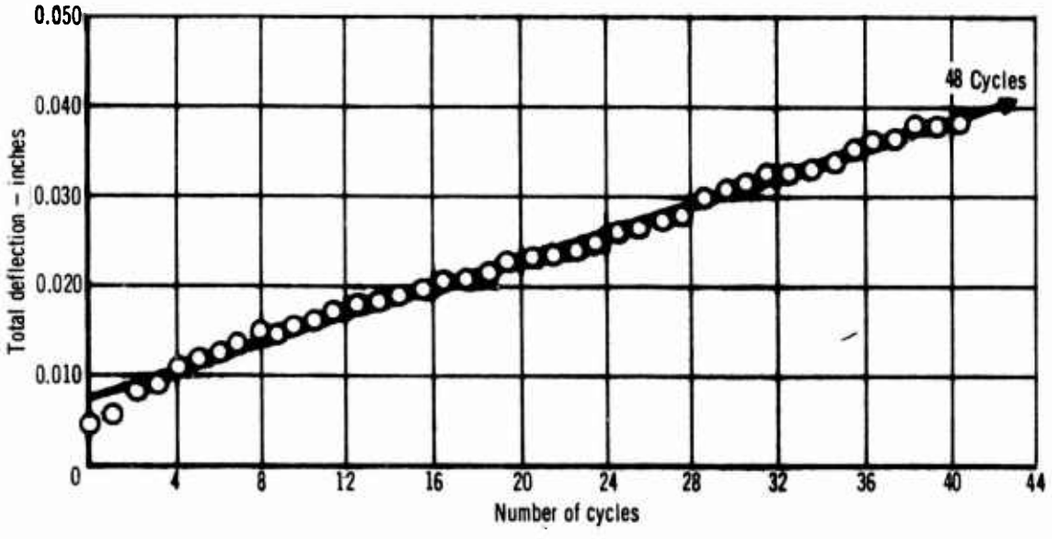

Figure 147 Rib Stiffened No. 3 Internal Pressure High Stress

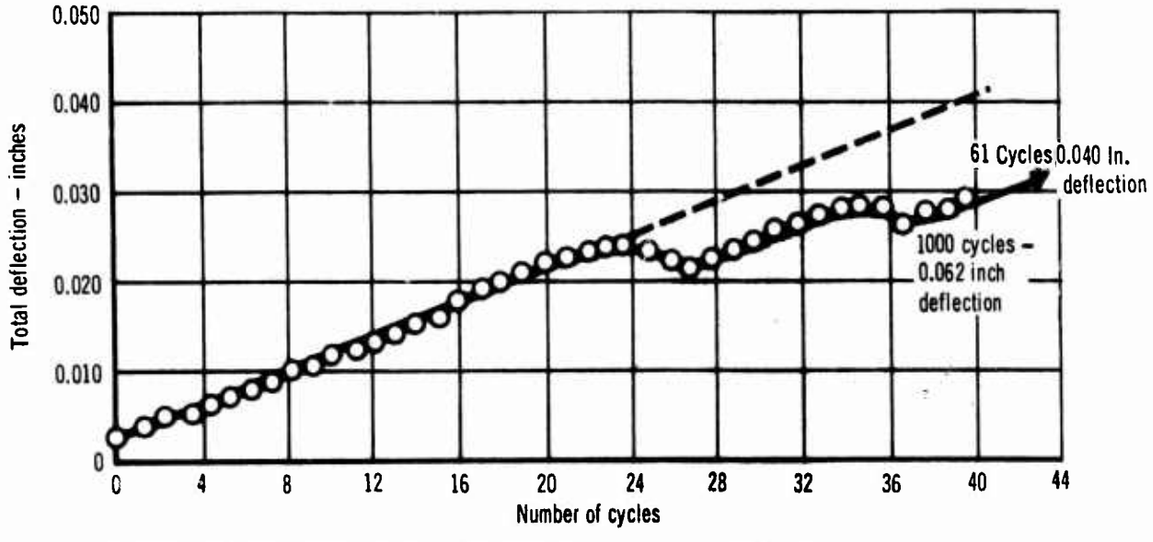

Figure 148 Rib Stiffened No. 4 External Pressure High Stress

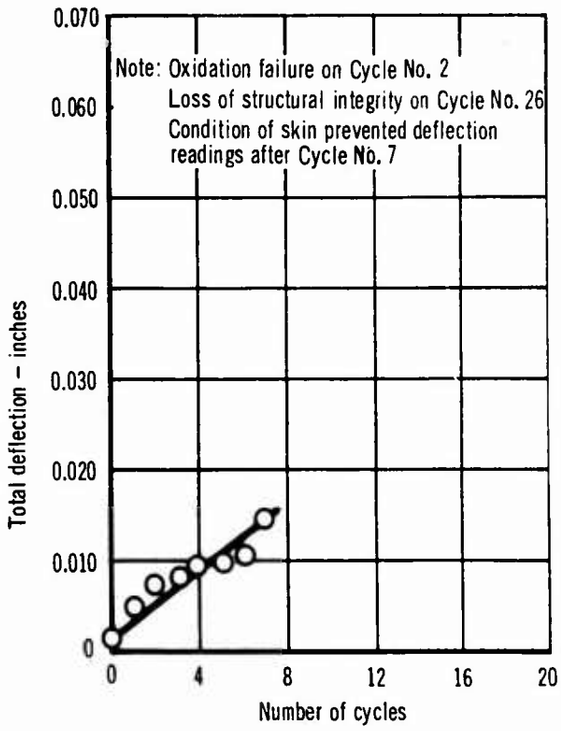

Figure 149 Riveted Flat Channel No. 8 External Pressure High Stress

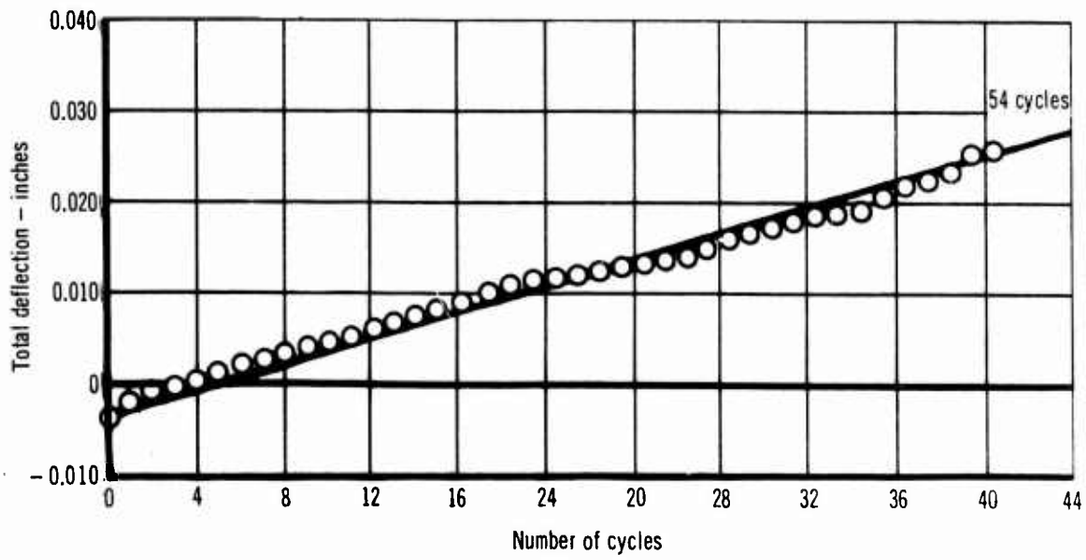

Figure 150 Riveted Channel No. 10 Internal Pressure High Stress

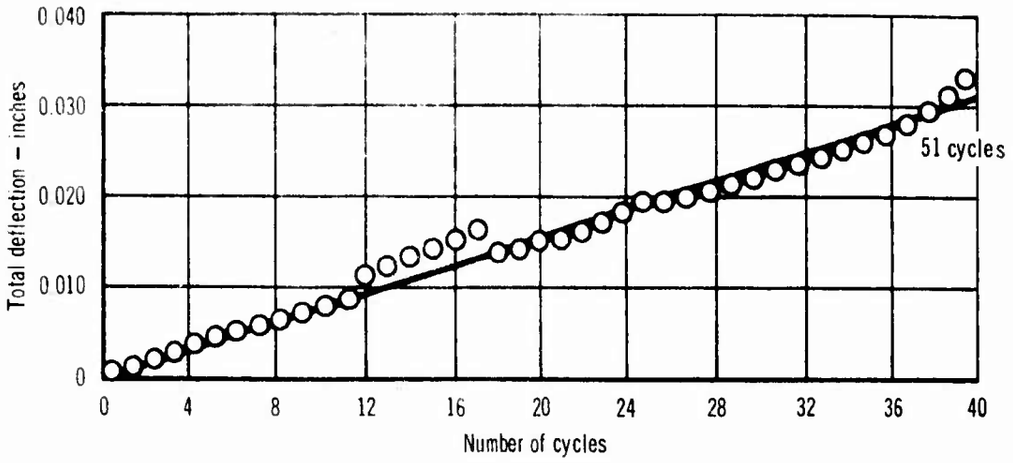

Figure 151 Riveted Channel No. 2 External Pressure High Stress

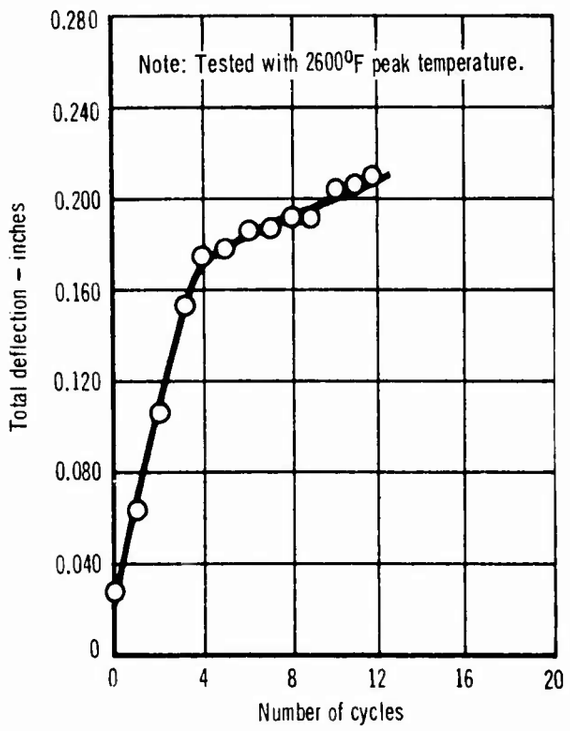

Figure 152 Spot Welded Flat Corrugation No. 3
Internal Pressure High Stress

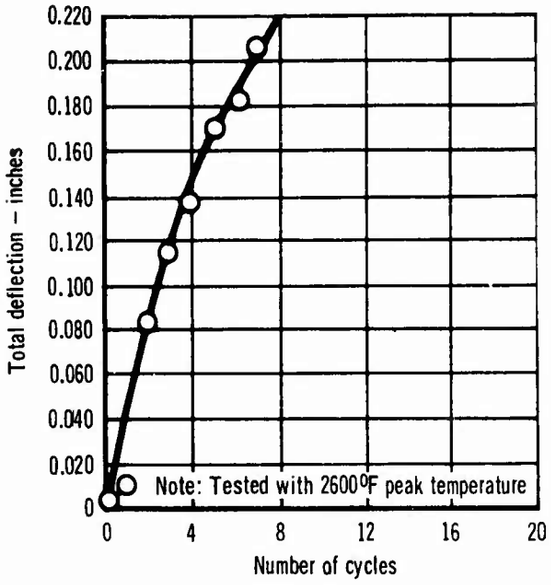

Figure 153 Spot Welded Flat Corrugation No. 5
Internal Pressure High Stress

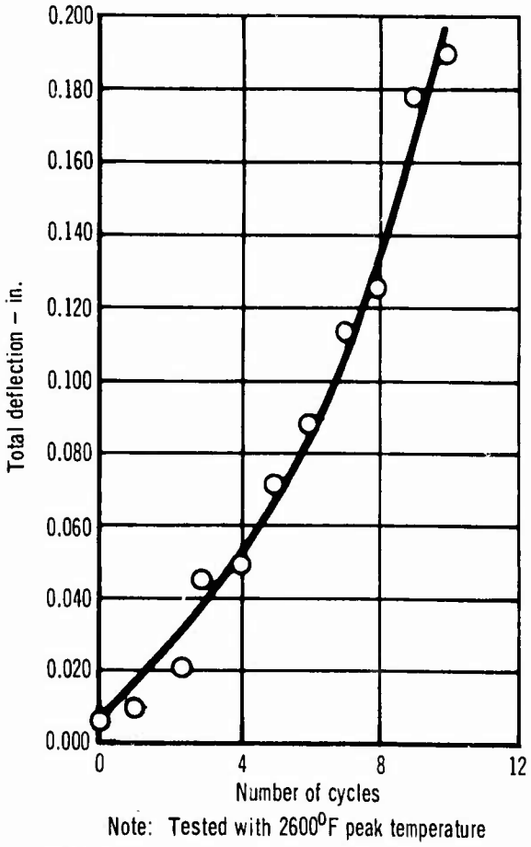

Figure 154 Spot Welded Channel No. 6
Internal Pressure High Stress

Appendix III

NDT DATA - COATING THICKNESS

Presented in this appendix are the NDT coating thickness determinations made on R-512E coated Cb-752 baseline and heat shield specimens with the Dermitron and thermo-electric devices.

Table XXX Coating Thickness Distribution of Oxidation Test Specimens

Specimen Number	Thermoelectric Coating Thickness (mils)			
	Surface	Top Edge	Bottom Edge	Side Edges
1	3.4	0.9	3.3	1.4
2	3.2	1.4	5+	1.5
3	3.3	1.0	4.3	1.9
4	3.2	1.0	3.8	1.6
5	3.2	1.3	3.4	1.3
6	3.2	1.0	3.4	1.9
7	3.1	0.6	5+	1.4
8	3.3	0.6	3.8	1.2
9	3.3	1.0	3.5	1.5
10	3.2	0.6	3.5	1.1
11	3.2	1.0	3.4	1.5
12	3.2	1.3	3.5	1.2
13	3.2	1.3	3.4	1.6
14	3.3	1.0	3.5	1.4
15	3.4	1.0	3.5	1.4
16	3.3	1.3	3.4	1.3
17	3.2	1.0	3.4	1.6
18	3.2	0.6	3.3	1.2
19	3.2	1.0	4.7	1.4
21	3.2	1.0	3.8	1.4
22	3.3	1.0	3.5	1.9
23	3.3	1.3	3.4	1.5
24	3.0	1.3	3.3	1.0
25	3.3	1.0	3.5	1.0
27	3.2	1.3	3.3	1.3
28	3.3	1.0	3.5	2.0
29	3.2	1.3	3.3	1.6
30	3.3	1.0	3.4	1.6
31	3.4	1.3	4.3	1.5
32	3.4	0.6	3.4	1.0
33	3.4	1.3	3.4	1.2
34	3.3	1.0	3.4	1.6
35	3.4	1.3	4.3	1.3
36	3.4	1.3	3.9	1.6
37	3.3	1.6	3.6	1.7
38	3.4	1.3	3.8	1.7
39	3.2	1.0	3.4	1.2
40	3.3	1.0	3.5	1.1

Table XXXI NDT Coating Thickness Measurements
Temperature (2600°F) – Pressure Profile Tests

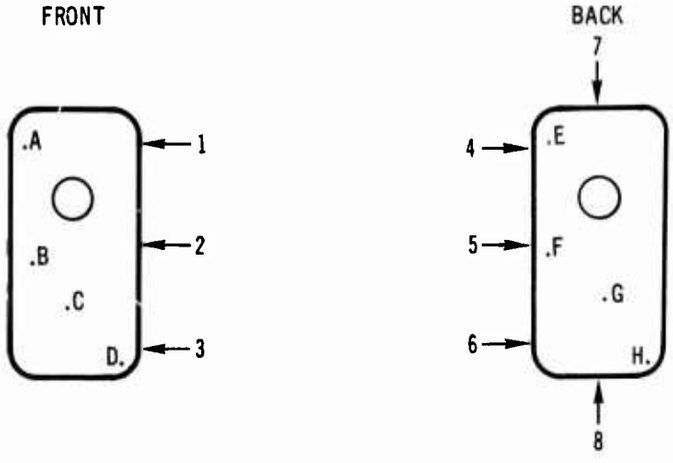

SPECIMEN NO. 28
INTERNAL PRESSURE PROFILE

Cycles	Dermitron								Thermoelectric							
	A	B	C	D	E	F	G	H	1	2	3	4	5	6	7	8
0	2.40	2.90	3.10	3.25	2.45	2.75	2.95	3.25	2.6	2.4	2.8	1.9	1.3	1.3	1.0	3.2
5	2.40	2.95	3.00	3.30	2.30	2.65	2.90	3.20								
10	2.25	2.95	3.60	3.40	2.35	2.65	2.80	3.20								
15	2.25	2.90	3.50	3.30	2.30	2.55	2.65	3.15								
20	2.25	2.90	3.00	3.10	2.60	2.70	2.90	3.30								
25	2.25	2.95	2.95	3.15	2.50	2.75	2.95	3.25								
30	2.20	2.70	2.95	3.10	2.70	2.80	3.20	3.40								
35	2.20	2.75	3.15	3.10	2.45	2.80	2.95	3.25								
40	2.05	2.90	3.00	3.10	2.10	2.90	2.75	3.05								

SPECIMEN NO. 19
EXTERNAL PRESSURE PROFILE

Cycles	Dermitron								Thermoelectric							
	A	B	C	D	E	F	G	H	1	2	3	4	5	6	7	8
0	2.05	2.50	2.90	2.95	2.45	2.50	2.70	2.90	1.9	1.6	1.9	1.3	1.3	1.3	1.0	4.4
5	2.30	3.35	3.75	3.80	2.65	3.55	3.70	3.60								
10	2.70	3.50	3.75	3.70	2.90	3.50	3.75	3.75								
15	2.70	3.55	3.70	3.80	2.75	3.40	3.65	3.70								
20	2.90	3.85	4.10	4.25	3.35	3.80	4.00	4.15								
30	2.70	3.95	4.10	4.15	3.10	4.00	4.15	4.40								
35	2.75	4.50	3.80	4.05	3.00	3.70	3.85	3.90								
40	3.00	3.85	4.10	4.10	3.00	3.80	3.85	4.00								
45	3.40	3.90	4.10	4.05	3.10	4.05	4.30	4.35								
50	3.25	3.90	3.95	4.15	3.25	3.90	4.00	4.05								

Table XXXII NDT Coating Thickness Measurements

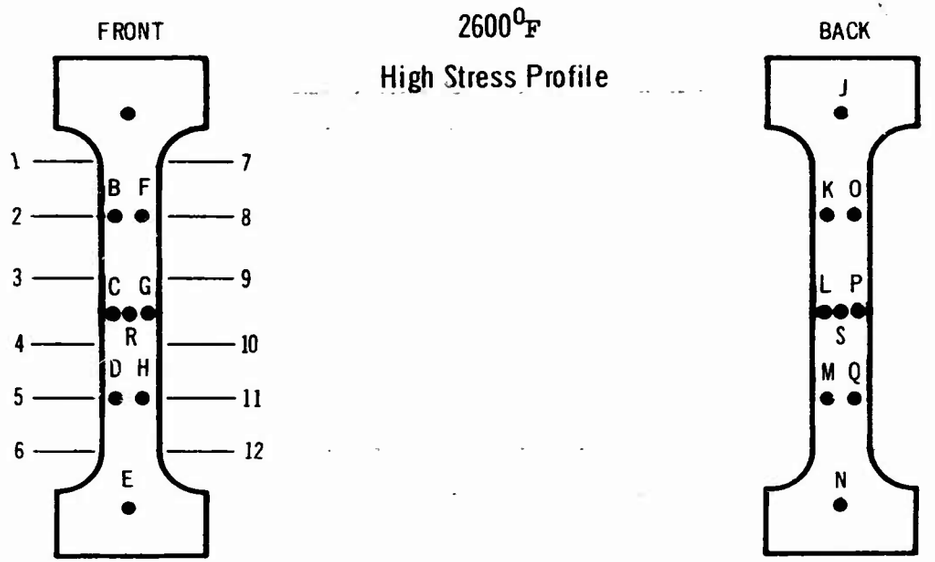

SPECIMEN NO. 16
INTERNAL PRESSURE

Cycles	Dermitron																	Thermoelectric											
	A	B	C	D	E	F	G	H	J	K	L	M	N	O	P	Q	R	S	1	2	3	4	5	6	7	8	9	10	11	12
0	3.00	3.00	3.10	3.20	3.10	3.10	3.00	3.10	2.70	2.80	3.05	3.05	2.15	3.05	3.05	3.05			1.9	2.2	2.2	1.9	1.9	2.2	1.9	1.6	2.4	2.2	2.2	1.9
5	3.85	4.05	4.00	3.85	3.90	3.90	3.90	3.80	3.65	3.70	3.40	3.75	3.70	4.10	3.70	3.65														
10	2.95	2.95	3.15	3.10	2.65	2.95	3.30	3.10	2.95	2.80	2.90	3.20	2.70	2.95	2.90	2.65	2.60	2.60												
15	2.75	2.95	2.70	2.70	2.70	3.00	2.95	2.90	3.00	3.00	3.20	3.10	2.60	2.95	2.80	2.70	2.60	2.65												
20	2.65	2.95	3.10	2.45	3.15	3.00	3.30	2.40	2.75	2.95	3.15	2.75	2.60	3.15	2.95	2.65														
25	2.90	2.70	2.65	2.35	2.70	2.50	2.50	2.05	2.50	2.90	2.80	2.55	2.40	2.90	2.65	2.45														

SPECIMEN NO. 13
EXTERNAL PRESSURE

Cycles	Dermitron																Thermoelectric											
	A	B	C	D	E	F	G	H	J	K	L	M	N	O	P	Q	1	2	3	4	5	6	7	8	9	10	11	12
0	5.00	4.06	4.24	4.42	4.06	4.33	4.33	3.97	3.88	3.79	3.79	3.70	4.24	3.79	3.40	3.61	2.4	2.2	1.6	2.2	2.6	2.2	1.9	2.3	2.0	1.5	1.8	
5	3.60	3.15	3.35	3.35	3.10	3.30	3.30	3.50	3.20	3.35	3.15	3.05	3.35	2.95	3.15	2.75												
10	4.35	3.85	3.70	3.75	3.85	3.80	3.75	3.65	3.40	3.70	3.60	3.35	3.65	3.60	3.30	3.35												
15	3.00	3.20	3.15	3.20	2.80	3.15	3.15	3.10	2.95	3.15	3.00	3.30	3.05	3.10	2.65	3.10												
20	4.4	4.3	4.3	4.6	4.5	4.25	3.95	4.85	4.15	4.10	3.95	4.10	4.35	4.15	4.30	3.85												

Table XXXIII NDT Coating Thickness Measurements

2400°F

High Stress Profile

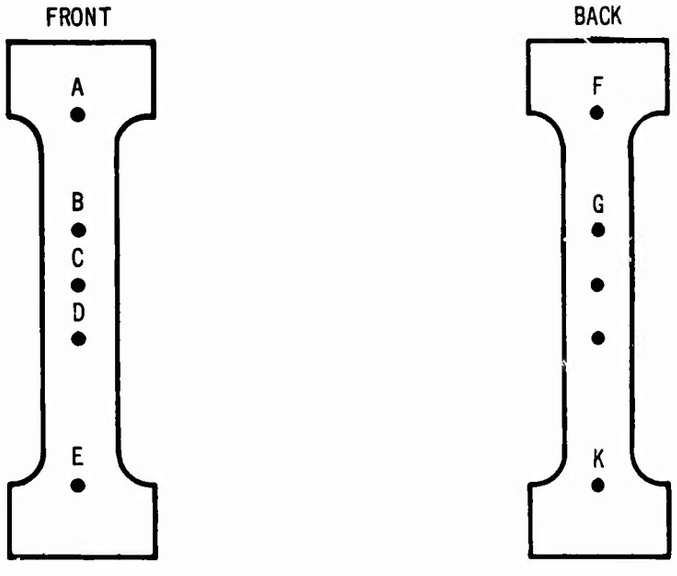

SPECIMEN NO. 22
INTERNAL PRESSURE

Cycles	Dermitron									
	A	B	C	D	E	F	G	H	J	K
0	2.60	2.65	2.90	2.90	2.95	2.60	2.65	2.55	2.45	2.50
10	2.60	2.60	2.55	2.50	2.55	2.45	2.55	2.50	2.50	2.45
25	3.00	3.20	3.00	2.90	2.90	2.95	3.05	3.05	3.05	2.70
32	2.95	2.55	2.80	2.60	2.75	2.95	2.55	2.50	2.65	2.80
37	3.15	3.00	2.90	3.05	3.05	2.95	3.30	3.20	3.20	2.90
46	2.95	2.55	2.45	2.50	2.65	2.70	2.55	2.55	2.55	2.70
53	2.55	2.20	2.25	2.15	2.65	2.55	2.15	2.05	2.25	2.35
60	2.50	2.15	2.10	2.15	2.70	2.55	2.25	2.10	2.20	2.50

SPECIMEN NO. 26
EXTERNAL PRESSURE

Cycles	Dermitron									
	A	B	C	D	E	F	G	H	J	K
0	3.05	2.90	2.80	2.75	2.65	2.65	2.70	2.70	2.70	2.65
7	2.95	2.65	2.60	2.70	2.80	2.90	2.65	2.55	2.60	2.70
14	2.60	2.55	2.45	2.45	2.55	2.50	2.50	2.45	2.45	2.50
25	2.80	2.60	2.55	2.55	2.60	2.75	2.55	2.50	2.55	2.60
31	2.75	2.65	2.55	2.55	2.60	2.60	2.55	2.55	2.55	2.65
41	2.80	2.65	2.55	2.60	2.65	2.65	2.55	2.55	2.60	2.70
53	2.75	2.75	2.60	2.55	2.60	2.65	2.75	2.60	2.70	2.65

Table XXXIV Thermoelectric NDT Coating Thickness Measurement Locations
Flat Corrugation Heat Shield Specimens

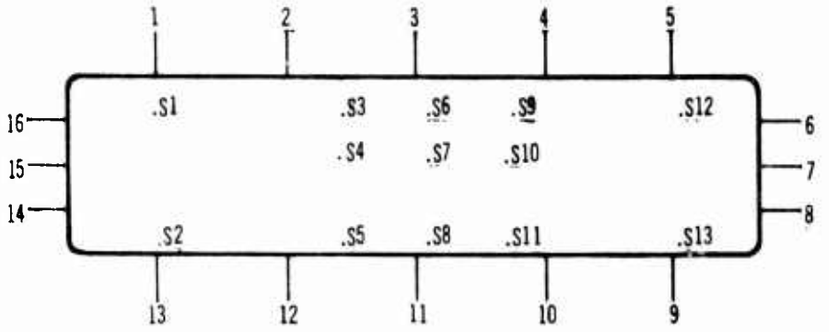

Skin side

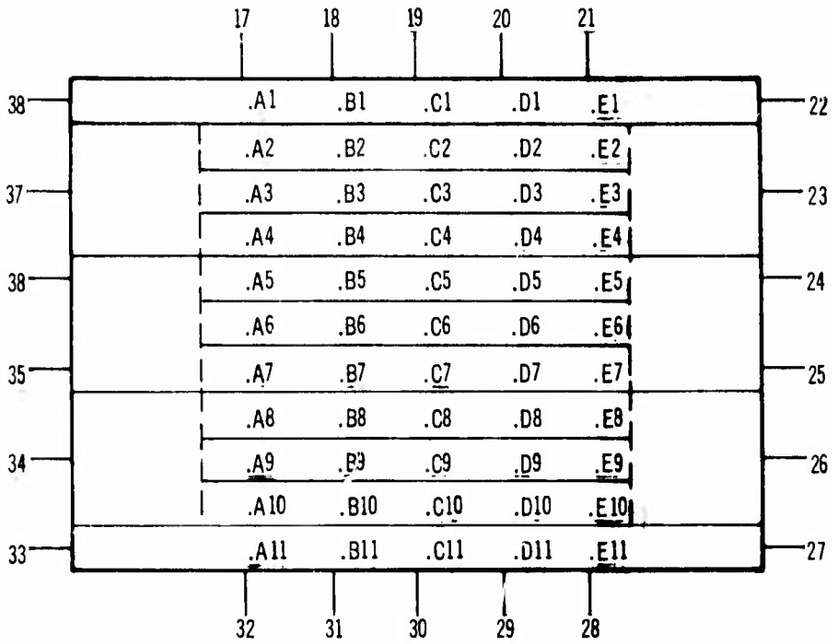

Stretched-out stiffener side

Table XXXIV (Continued)
Thermoelectric NDT Coating Thickness Measurements
Flat Corrugation Heat Shield Specimens
Before Testing

SKIN

Specimen No.	Locations													Av. Coating Thickness
	S1	S2	S3	S4	S5	S6	S7	S8	S9	S10	S11	S12	S13	
3	2.7	2.9	3.3	2.9	2.8	2.8	3.3	3.3	3.0	3.3	3.2	2.8	1.0	3.0
5	3.0	3.1	3.1	3.0	2.9	3.2	3.3	3.1	3.0	3.2	3.2	3.1	3.2	3.1
10	3.1	3.2	3.2	3.0	2.8	3.0	3.1	3.1	2.7	3.1	2.6	3.0	3.2	3.1

EDGES (SKIN)

Specimen No.	Locations																Av. Coating Thickness
	1	2	3	4	5	6	7	8	9	10	11	12	13	14	15	16	
3	3.2	3.3	3.5	3.3	2.9	3.3	3.2	3.1	3.3	3.0	3.3	3.3	3.2	3.4	3.2	3.4	3.2
5	2.9	3.2	2.7	3.2	2.9	3.6	3.0	3.7	3.3	3.3	3.4	3.1	3.2	3.0	3.3	3.1	3.2
10	2.8	3.1	3.2	3.2	3.3	3.3	3.2	3.5	3.7	3.5	3.5	3.3	3.2	2.8	2.9	2.8	3.2

EDGES (STIFFENERS)

Specimen No.	Locations																						Av. Coating Thickness
	17	18	19	20	21	22	23	24	25	26	27	28	29	30	31	32	33	34	35	36	37	38	
3	1.4	2.4	1.8	1.8	2.0	3.2	3.1	3.4	3.3	3.2	3.3	3.2	3.3	3.1	2.8	2.8	2.1	2.0	2.3	2.4	2.0	2.1	2.6
5	2.0	2.1	2.4	1.8	2.6	3.7	2.7	2.1	3.0	3.3	3.7	2.4	2.7	2.7	2.1	2.6	2.1	2.0	2.6	2.1	2.1	1.8	2.5
10	2.7	3.1	3.1	3.1	3.3	3.7	3.6	3.6	3.7	3.5	3.3	2.6	2.7	2.4	2.3	2.3	2.7	2.6	2.1	2.1	3.0	3.3	2.9

STIFFENERS

Column/ Specimen No.	Location										
	1	2	3	4	5	6	7	8	9	10	11
A3	2.8	3.0	3.3	3.3	3.2	2.7	3.0	2.9	3.3	3.2	2.6
B3	3.0	3.1	2.7	3.2	2.7	2.9	2.8	3.1	2.9	3.0	2.7
C3	3.3	3.3	2.9	3.1	2.8	2.8	2.6	3.2	3.2	3.7	3.7
D3	3.2	3.2	3.1	3.7	2.7	2.7	3.0	3.0	3.2	3.3	2.8
E3	3.2	3.2	3.3	3.2	2.7	2.7	2.4	2.8	3.3	3.3	2.9
A5	3.2	3.0	3.2	3.0	2.7	2.7	3.2	2.9	3.3	3.2	2.7
B5	3.4	3.0	3.1	2.9	2.8	3.2	3.1	2.8	3.4	3.1	2.6
C5	3.2	2.8	2.9	2.8	3.0	3.0	2.8	2.7	3.2	2.9	3.0
D5	3.1	3.1	3.2	2.8	2.8	3.0	2.9	2.7	3.0	3.1	2.4
E5	3.2	2.9	3.2	3.1	3.0	3.0	2.6	2.8	2.9	3.2	2.3
A10	3.1	3.0	3.0	3.2	3.1	2.8	2.9	3.2	3.2	3.2	2.8
B10	3.3	3.3	3.2	3.2	3.2	2.7	2.6	3.2	3.2	2.1	2.7
C10	3.2	3.6	3.3	3.0	3.3	2.7	2.7	3.0	3.3	3.2	3.2
D10	3.1	3.1	3.2	3.1	3.3	2.9	2.1	3.2	2.9	2.4	2.9
E10	3.1	3.3	3.1	3.2	3.1	2.8	2.4	3.3	2.7	3.5	2.6

STIFFENERS

Specimen No.	Av. Coating Thickness
3	2.8
4	3.0
5	3.1

Table XXXV

Themoelectric NDT Coating Thickness Measurement Locations

"ZEE" Stringer Heat Shield Specimens

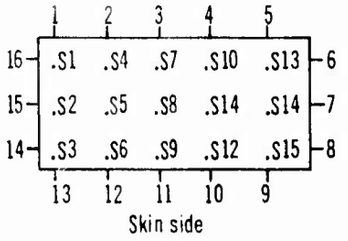

Skin side

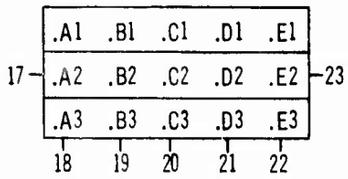

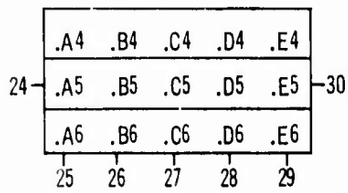

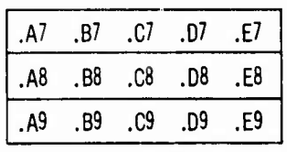

Strectched-out stiffener side

Table XXXV (Continued)
Thermoelectric NDT Coating Thickness Measurements
"Zee" Stringer Heat Shield Specimens
Before Testing

SKIN

Specimen No.	Locations														Av. Coating Thickness
	S1	S2	S3	S4	S5	S6	S7	S8	S9	S10	S11	S12	S13	S14	S15	
4	2.7	3.1	2.6	2.8	2.8	2.9	2.7	2.9	3.1	2.6	2.5	2.7	2.9	2.8	3.0	2.8
5	2.8	3.0	2.7	3.0	2.8	2.6	3.0	2.8	2.9	2.6	2.6	2.5	2.7	2.7	3.0	2.8
6	2.9	2.9	2.8	3.1	3.0	2.6	2.9	2.7	2.7	2.5	2.6	2.3	2.5	2.4	2.6	2.7

EDGES (SKIN)

Specimen No.	Locations																Av. Coating Thickness
	1	2	3	4	5	6	7	8	9	10	11	12	13	14	15	16	
4	2.4	2.2	2.7	2.5	2.6	3.3	3.2	3.2	2.9	3.2	3.0	2.8	2.7	2.4	2.5	2.7	2.8
5	2.7	2.8	3.1	2.7	3.3	3.0	3.3	3.3	3.4	3.0	2.8	2.8	2.7	2.7	2.4	2.6	2.9
6	2.8	2.6	2.7	2.8	2.5	3.2	3.2	3.3	3.1	2.8	3.0	2.9	2.8	2.4	2.8	2.9	2.9

EDGES (STIFFENERS)

Specimen No.	Locations														Av. Coating Thickness
	17	18	19	20	21	22	23	24	25	26	27	28	29	30	
4	2.0	2.4	2.0	1.8	1.8	2.1	3.2	2.1	2.3	2.0	2.1	2.0	1.8	3.2	2.3
5	1.8	2.6	2.3	2.0	2.0	2.8	2.8	2.0	1.9	2.0	2.0	2.1	1.8	2.9	2.1
6	2.3	2.4	2.0	1.8	1.6	1.8	3.0	2.1	2.3	2.1	1.6	2.0	1.8	2.7	2.1

STIFFENERS

Column/ Specimen No.	Locations								
	1	2	3	4	5	6	7	8	9
A4	2.6	2.8	2.4	2.5	2.9	3.1	2.5	2.0	2.7
B4	2.7	2.6	2.6	2.4	2.4	2.8	2.4	2.2	2.6
C4	2.5	2.7	2.7	2.3	2.2	2.4	2.0	2.2	2.5
D4	2.6	2.9	2.9	2.6	2.2	2.6	2.3	2.3	2.6
E4	2.6	2.8	2.9	2.4	2.1	2.8	2.3	2.1	2.3
A5	2.3	2.4	2.6	2.2	2.5	2.7	3.0	2.3	2.2
B5	2.4	2.6	2.7	2.3	2.4	2.7	2.4	3.1	2.1
C5	2.5	2.5	2.8	2.2	2.2	2.6	2.9	2.3	2.3
D5	2.5	2.6	2.6	2.2	2.3	2.9	2.8	2.4	2.3
E5	2.6	2.7	3.0	3.1	2.4	3.0	2.8	2.7	2.4
A6	2.6	3.2	3.0	2.7	2.1	3.0	2.4	2.1	2.7
B6	2.7	3.1	3.1	2.4	2.3	3.0	2.7	2.1	2.8
C6	2.7	3.0	3.0	2.6	2.1	2.6	2.6	2.3	3.1
D6	2.6	2.9	2.9	2.6	2.0	2.7	2.4	2.1	3.2
E6	2.8	2.8	2.8	2.7	2.3	2.8	2.4	2.4	3.0

STIFFENERS

Specimen No.	Av. Coating Thickness
4	2.5
5	2.5
6	2.7

Table XXXVI

Thermoelectric NDT Coating Thickness Measurement Locations

Rib Stiffened Heat Shield Specimens

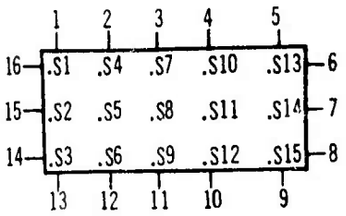

Skin side

.A1	.B1	.C1	.D1	.E1
.A2	.B2	.C2	.D2	.E2

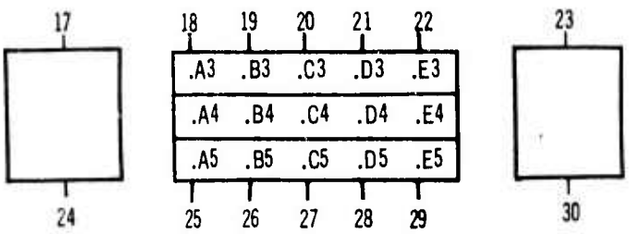

.A6	.B6	.C6	.D6	.E6
.A7	.B7	.C7	.D7	.E7

Stretched-out stiffener side

Table XXXVI (Continued)
Thermoelectric NDT Coating Thickness Measurements
Rib Stiffened Heat Shield Specimens
Before Testing

SKIN

Specimen No.	Locations															Av. Coating Thickness
	S1	S2	S3	S4	S5	S6	S7	S8	S9	S10	S11	S12	S13	S14	S15	
1	3.2	3.0	2.6	3.0	3.2	2.8	3.3	3.0	3.2	3.1	3.0	2.8	3.4	3.2	3.2	3.1
2	3.2	2.9	3.1	3.0	2.9	2.7	3.0	2.8	2.6	2.6	2.7	2.6	3.4	3.2	3.0	2.9
3	3.2	2.9	3.1	3.1	2.9	3.0	3.2	3.0	2.8	3.3	3.1	3.0	3.7	3.4	3.8	3.1

EDGES (SKIN)

Specimen No.	Locations																Av. Coating Thickness
	1	2	3	4	5	6	7	8	9	10	11	12	13	14	15	16	
1	2.3	2.1	2.6	2.7	3.0	4.3	3.8	4.0	3.1	2.7	2.5	2.4	2.3	2.2	2.6	2.3	2.8
2	2.1	2.0	2.4	2.3	2.6	3.7	4.3	3.4	2.9	2.7	2.7	3.1	2.3	2.4	2.4	1.6	2.6
3	2.1	1.8	2.0	1.8	2.4	4.0	3.9	4.0	2.7	2.0	2.3	1.8	2.0	1.8	2.1	2.0	2.4

EDGES (STIFFENERS)

Specimen No.	Locations														Av. Coating Thickness
	17	18	19	20	21	22	23	24	25	26	27	28	29	30	
1	2.0	2.3	2.6	2.7	2.6	2.4	3.4	2.2	2.1	2.3	2.0	2.1	2.6	3.6	2.5
2	1.9	2.3	2.1	1.8	2.0	2.1	3.6	2.0	2.6	0.8	2.0	2.5	2.1	3.7	2.3
3	1.9	2.3	2.2	2.1	2.3	1.8	3.7	1.7	2.8	2.6	2.5	2.6	2.4	4.3	2.5

STIFFENERS

Column/ Specimen No.	Locations						
	1	2	3	4	5	6	7
A1	3.2	3.0	2.9	3.1	3.1	2.7	3.0
B1	2.8	3.2	3.3	3.0	2.9	2.8	3.1
C1	3.3	3.0	3.1	3.3	3.3	3.1	3.2
D1	3.2	3.0	2.8	3.2	2.9	3.0	2.8
E1	3.5	3.1	2.7	3.1	3.0	3.0	3.1
A2	2.7	2.7	3.0	2.7	2.8	2.9	3.1
B2	2.9	2.7	3.1	2.9	2.9	3.3	3.0
C2	2.6	3.1	3.2	2.9	2.6	3.0	3.2
D2	2.7	3.1	3.1	3.2	2.6	3.2	2.9
E2	2.7	2.9	2.7	2.8	2.7	2.8	3.2
A3	2.8	2.7	3.3	3.1	3.1	2.7	3.2
B3	2.7	3.0	3.2	2.8	3.0	3.3	3.3
C3	2.7	3.2	3.3	2.9	3.3	3.0	3.2
D3	2.8	2.9	2.7	2.8	2.9	3.2	3.0
E3	2.9	2.6	2.8	3.0	2.8	3.2	2.7

STIFFENERS

Specimen No.	Av. Coating Thickness
1	3.1
2	2.9
3	3.0

Table XXXVII

Thermoelectric NDT Coating Thickness Measurement Locations

"VEE" Corrugation Heat Shield Specimens

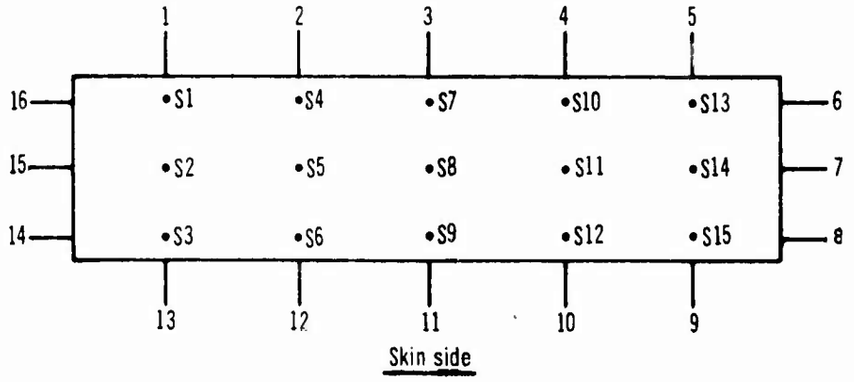

Skin side

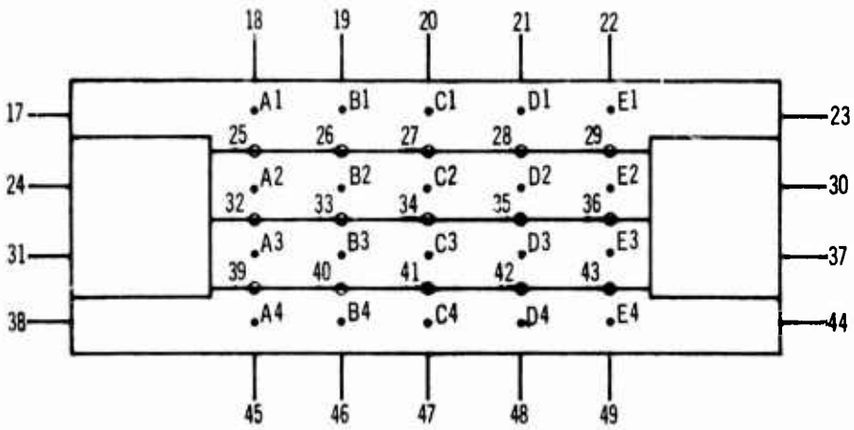

Stretched-out stiffener side

Table XXXVII (Continued)

Thermoelectric NDT Coating Thickness Measurements
Riveted Channel Heat Shield Specimens
Before Testing

SKIN

Specimen No.	Locations																Av. Coating Thickness
	S1	S2	S3	S4	S5	S6	S7	S8	S9	S10	S11	S12	S13	S14	S15	S16	S17	
8	2.7	3.1	2.6	3.2	2.7	2.8	2.6	3.0	3.2	2.8	3.1	3.2	3.1	3.4	3.1	3.2	2.6	3.0
10	2.7	3.2	2.5	3.8	3.0	2.9	2.8	3.0	3.8	2.7	2.7	2.6	2.6	3.6	2.9	3.3	2.6	3.0
11	2.9	3.3	2.7	3.1	2.8	2.9	2.6	2.9	3.6	2.9	3.1	2.9	2.8	3.1	2.6	2.8	2.6	2.9

EDGES (SKIN)

Specimen No.	Locations																		Av. Coating Thickness
	1	2	3	4	5	6	7	8	9	10	11	12	13	14	15	16	17	18	
8	2.6	2.4	2.7	2.6	3.3	3.4	3.2	3.2	2.8	3.6	3.4	3.4	3.3	3.0	2.0	2.3	2.0	2.0	2.8
10	2.8	2.7	3.0	2.8	3.0	3.2	3.3	3.2	3.2	2.7	2.6	2.6	2.7	2.8	2.3	2.7	2.6	2.3	2.8
11	2.8	3.0	3.0	2.8	3.0	3.1	3.4	3.3	3.2	2.7	2.4	2.3	2.3	2.4	2.0	2.4	2.6	1.8	2.7

EDGES (STIFFENERS)

Specimen No.	Locations														Av. Coating Thickness
	19	20	21	22	23	24	25	26	27	28	29	30	31	32	
8	2.4	2.1	2.6	2.4	2.3	2.0	2.4	2.3	2.7	2.8	2.6	2.7	2.4	2.6	2.5
10	2.4	2.6	2.4	2.3	2.4	2.4	3.3	2.5	2.2	2.1	2.6	2.3	2.5	3.2	2.5
11	2.7	2.6	2.1	2.6	2.8	2.4	3.1	2.5	2.3	2.1	2.1	2.0	2.4	3.3	2.5

EDGES (STIFFENERS)

Specimen No.	Locations																	Av. Coating Thickness
	B1	B2	B3	B4	B5	B6	B7	B8	B9	B10	B11	B12	B13	B14	B15	B16	B17	
8	3.2		3.0	3.2	3.7	3.3	3.0	3.5	3.3	3.2	3.7	3.5	3.7	3.1	3.6		3.4	3.4
10	3.1	3.1	3.0	3.9	3.0	3.3	3.1	3.1	3.8	3.2	3.2	3.3	3.2	3.7	3.2	2.9	3.3	3.3
11	3.1	3.0	3.0	3.7	3.2	3.2	3.1	3.2	4.0	2.7	3.3	3.1	2.8	3.7	3.1	3.2	2.9	3.2

Table XXXVIII (Continued)
Thermoelectric NDT Coating Thickness Measurements
"Vee" Corrugation Heat Shield Specimens
Before Testing

SKIN

Specimen No.	Locations															Av. Coating Thickness
	S1	S2	S3	S4	S5	S6	S7	S8	S9	S10	S11	S12	S13	S14	S15	
5	2.7	3.3	3.1	2.7	3.2	3.0	3.1	3.2	3.2	3.3	3.4	3.0	3.2	3.3	3.2	3.1
7	3.0	3.3	3.1	3.3	3.2	3.3	3.2	3.6	3.4	3.2	3.7	3.3	3.5	3.7	3.6	3.4
9	2.8	3.0	3.0	3.0	3.2	3.0	3.0	3.1	3.2	3.0	3.2	2.8	2.8	3.3	3.0	3.0

EDGES (SKIN)

Specimen No.	Locations																Av. Coating Thickness
	1	2	3	4	5	6	7	8	9	10	11	12	13	14	15	16	
5	2.8	3.0	3.1	3.2	3.0	3.0	3.2	3.0	2.8	3.2	3.1	2.9	2.7	2.9	2.7	3.0	3.0
7	2.7	2.8	2.8	2.7	3.1	3.0	3.2	3.0	2.8	2.7	2.7	2.6	2.6	2.3	2.7	2.6	2.8
9	3.0	3.2	3.1	3.0	3.0	3.7	3.7	3.3	3.0	3.1	2.8	2.7	2.6	2.6	2.4	2.6	3.0

EDGES (STIFFENERS)

Specimen No.	Locations																	
	17	18	19	20	21	22	23	24	25	26	27	28	29	30	31	32	33	34
5	2.7	3.1	3.1	3.2	3.4	3.4	3.7	2.1	3.0	3.0	2.8	3.2	3.0	3.7	2.3	2.9	3.0	3.1
7	2.4	3.4	2.6	2.7	2.4	2.6	4.0	2.3	2.8	2.9	2.3	2.9	2.8	4.3	2.0	2.9	3.0	3.0
9	3.1	2.6	2.6	2.8	2.7	2.8	2.8	1.8	2.6	3.0	2.8	2.8	3.2	2.8	1.8	2.8	2.8	3.0

EDGES (STIFFENERS)

Specimen No.	Locations															Av. Coating Thickness
	35	36	37	38	39	40	41	42	43	44	45	46	47	48	49	
5	3.0	2.9	3.2	2.6	3.3	3.2	3.2	2.9	2.8	3.3	3.3	3.2	3.2	3.1	3.2	3.1
7	3.3	3.1	4.3	2.4	2.8	3.0	2.9	3.1	2.7	3.7	2.7	2.8	2.7	2.3	2.4	2.9
9	3.2	3.3	2.7	3.0	3.0	3.1	3.0	2.8	2.9	2.7	2.6	2.6	2.8	2.9	2.8	2.7

Thermoelectric NDT Coating Thickness Measurements
"VEE" Corrugation Heat Shield Specimens
Uncycled

STIFFENERS

Specimen No.		Thermo 1	2	3	4
A	5	3.0	3.3	3.1	2.7
B	5	2.7	3.6	3.4	3.0
C	5	3.5	3.6	3.4	3.5
D	5	3.0	3.3	3.3	3.0
E	5	3.7	3.2	3.1	3.1
A	7	2.8	3.0	3.1	3.3
B	7	3.0	3.3	3.3	3.3
C	7	3.3	3.4	3.3	2.8
D	7	3.0	3.6	3.1	3.3
E	7	2.6	3.3	3.2	3.0
A	9	3.0	2.8	2.9	2.8
B	9	3.0	3.1	2.9	2.8
C	9	3.2	2.9	3.0	2.9
D	9	3.2	3.0	2.8	3.1
E	9	3.0	3.0	2.7	3.0

STIFFENERS

Specimen No.	AV Coating Thickness
5	3.2
7	3.2
9	3.0

Table XXXVIII

Thermoelectric NDT Coating Thickness Measurement Locations

Riveted Channel Heat Shield Specimens

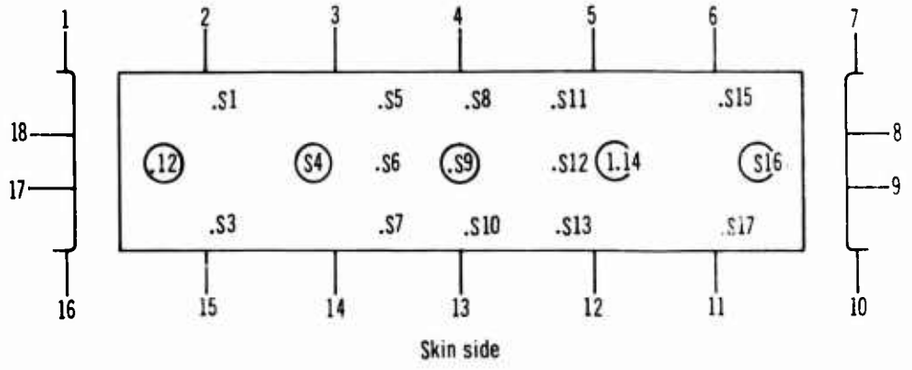

Skin side

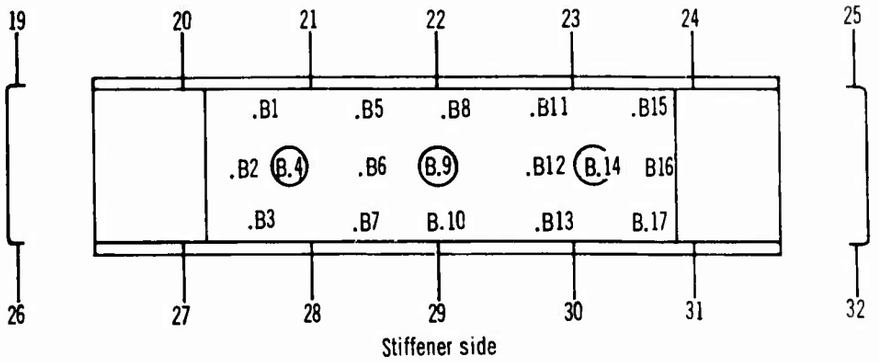

Stiffener side

REFERENCES

1. Beck, E. J. and Schmatzberg, F. R., "Determination of Mechanical Thermophysical Properties of Refractory Metals", **Technical Report** AFML-TR-65-247, July 1965, Martin Company.

2. Aerospace Material Specifications, No. 7851, Issued 15 March 1966.

3. Product Specification No. S-82402-R-0, 29 October 1962, Fansteel Metallurgical Corporation, as cited in Aerospace Structural Metals Handbook, Volume II A Non-Ferrous Heat Resistant Alloys, March 1966.

4. Columbium and Tantalum Alloy Technical Information, Volume II, August 1966, Wah Chang Corporation.

5. Haynes Alloy Cb-752 New Product Data, 1963, Haynes Stellite Company.

6. Gadd, J. D. "Design Data Study for Coated Columbium Alloys" Final Summary Technical Report, NOw 62-0098-C, 21 January 1963, Thompson-Ramo-Wooldridge Inc., as cited in DMIC Report 188.

7. Gentry, W.O. and Michael, A.B., "Properties of Some Columbium Rich Alloys in the Columbium-Tantalum-Tungsten-Zirconium System", Paper presented at AIME High Temperature Matrials Conference in Cleveland on 26-27 April 1961, as cited in DMIC Report 188.

8. Lessmann, G. G., "Effect of 1000 Hour Thermal Exposures on Tensile Properties of Refractory Metal Alloys", Topical Report No. 1, WANL-PR-P-012, NASA Contract NAS 3-2540, 1966 Westinghouse Electric Corporation Astronuclear Laboratory.

9. Yates, L., "Selection of Materials for High L/D Reentry Vehicles", SAE Aeronautic and Space Engineering and Manufacturing Meeting, Los Angeles, October 1966.

10. Hauser, H.A., et al, "Evaluation and Improvement of Coatings for Columbium Gas Turbine Engine Components", AFML-TR-66-186, Part I, July 1966.

11. Cherry, J. A., "Engineering Test Memorandum Number 16", Contract AF33(615)-1312, September 1966.

12. Childers, M. G., "Behavior of Sylcor R512-E Coated Cb-752 Columbium Alloys in a Low Pressure Environment", presented to the Refractory Composites Working Group Meeting, July 1967.

13. Priceman, S. and Sama, L., "Development of Fused Slurry Silicide Coatings for the Elevated Temperature Oxidation Protection of Columbium and Tantalum Alloys", Air Force Contract Number AF33(615)-3272, Progress Report 1 October-31 December 1966.

14. Stinebring, R. C. and Cannon, R., "Development of Nondestructive Methods for Evaluating Diffusion-Formed Coatings on Metallic Substrates", USAF Contract AF33(615)-3877, AFML-TR-67-178, June 1967.

15. Stinebring, R. C. and Sturiale, T., "Development of Nondestructive Methods for Evaluating Diffusion-Formed Coatings on Metallic Substrates", USAF Contract AF33(615)-2855, AFML-TR-66-221, September 1966.

16. Priceman, S. and Sama, L., "Development of Fused Slurry Silicide Coatings for the Elevated Temperature Oxidation Protection of Columbium and Tantalum Alloys", Air Force Contract Number AF33(615)-3272, Progress Report 1 August - 30 November 1967.

17. Priceman, S. and Sama, L., "Development of Fused Slurry Silicide Coatings for the Elevated-Temperature Oxidation Protection of Columbium and Tantalum Alloys," USAF Contract AF33(615)-3272, Progress Report 1 August-30 November 1967.

18. Allen, T. H., Johnson, C. R., Rusert, E. L., "High Temperature Emittance of Coated Refractory Metals" SAMPE National Symposium, 1967

19. Gouffe, A., Rev. Opt. 24 1 (1945)

20. Kelly, F. J., Journal of Applied Optics, 5, 925 (1966)

21. Sparrow, E. M., Johnson, V. R., Journal (pt. Soc., 53, 816 (1963)

22. Allen, T. H., Johnson, C. R., Kemple, T. E. "Procedure for Determining of Total Normal Emittance of an Aluminum Oxide Cavity", McDonnell Douglas Rpt. EN495, Sept. 1966.

23. Gouffe, A., "Correction d'ouverture des Corps - noirs artificiels compete tenu des diffusions multiples internes" 24 No. 1-3 Reoue des Optique

24. Abbott, G. L., Alvares, N. J., Parker, W. J., "Total Normal and Total Hemespherical Emittance of Polished Metals", WADD Rpt. 60-94 Nov. 1961.

25. Kohl, W. H., "Materials and Techniques for Electron Tubes" pp 274-275.

26. Battelli Memo Inst. DMIC 146, Graphite 3903 in Vacuum